BERICHTE
aus dem Fachbereich Geowissenschaften
der Universität Bremen

No. 276

Villinger, H., E. Alexandrakis, P. Alt-Epping, R. Becke, R. Dziadek, K. Enneking, T. Fleischmann, K. Gaida, B. Heesemann, C. Janßen, N. Kaul, T. Pichler, M. Ruiz, F. Schmidt-Schierhorn, A. Schwab, S. Stephan, M. Zwick

Revised Digital Version, July 2011

REPORT AND PRELIMINARY RESULTS OF R/V SONNE CRUISE SO207, CALDERA-CALDERA, 21 JUNE -13 JULY, 2010. SEAMOUNTFLUX: EFFICIENT COOLING IN YOUNG OCEANIC CRUST CAUSED BY CIRCULATION OF SEAWATER THROUGH SEAMOUNTS (GUATEMALA BASIN, EAST PACIFIC OCEAN).

Edited by
Heinrich Villinger, Thomas Pichler and Friederike Schmidt-Schierhorn

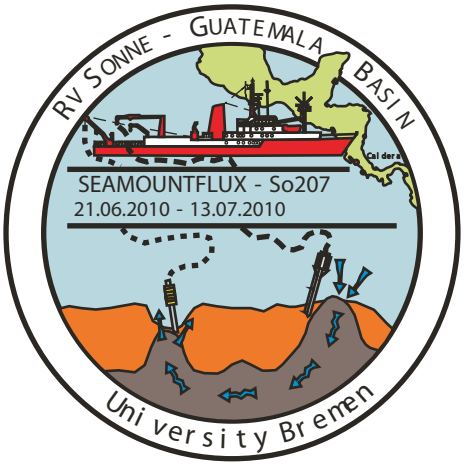

Berichte, Fachbereich Geowissenschaften, Universität Bremen, No. 276, 161 pages, Bremen 2010

ISSN 0931-0800

Contents

July 20, 2011

This is a new, revised version of the cruise report of expedition SO207. Changes have been applied as follows:

- all Parasound profiles are now in the Appendix,
- all Seismic profiles which are in the text are now also in the Appendix,
- a mistake in all the heat flow lists, column Heat Pulse Time is now corrected and
- the nomenclature in maps of seismic profiles was changed for working area GUATB-03, profile GUATB28 (now GUATB29).

The text and all the other figures have not been altered.

Abstract

Expedition SO207 took place from June 21, 2010 until July 13, 2010 at $8°N$ / $90°W$, approximately 360 nm offshore Costa Rica in the eastern Pacific Ocean. On board were scientists with expertise in geophysics and geochemistry from the University of Bremen and the University of Bern.

The scientific goal was to study the exchange of matter and energy between the ocean and the upper lithosphere in the vicinity of unexplained circular depressions in the sediment covered seafloor. A possible model for their formation is the dissolution of calcium carbonate ($CaCO_3$) minerals by upward flowing warm fluids, which are $CaCO_3$ under saturated; hence, the term hydrothermal pits . It is suspected that seamounts act as the entrance point for cold seawater, which then thermally and chemically equilibrates with the basaltic oceanic crust prior to exiting through the hydrothermal pits . Such a processes must affect the thermal structure in and around the pits as well as the geochemistry of the pore water. Therefore, we mapped the pits with acoustic methods (bathymetry, sediment echo sounding and single channel seismic) and conducted heat flow measurements inside and outside. Pore water and sediments samples from inside and outside the pits were collected through gravity coring.

The results can be summarized as follows:

- Acoustic mapping of the pits was very successful; most pits are about 50 to 100 m deep with a diameter of about 1 km. The detailed lithology inside of the pits will be unraveled by combining the results from sediment echo-sounding and seismic profiles.
- Heat flow measurements around seamounts confirm that they act as pathways for cold seawater which leads to a large cooling effect in the vicinity of the seamount with heat values even below 10 mW/m^2. This is a clear indication of strong, efficient and long-lasting flow system.
- All heat flow values inside of the pits show values up to five times higher than background values around the pits. This increase cannot be explained by the observed decrease of sediment thickness inside the pits.
- Gravity coring was highly successful with an average recovered core length of 9 m. In general recovery was significantly less inside the pits, which points to a higher degree of sediment compaction.
- Pore water was extracted and analyzed on board for pH, Eh, Fe^{2+}, NH_4^+, PO_4^{3-} and alkalinity. Differences in Eh were more pronounced between the three different working areas than inside and outside of the pits. Detailed pore water analysis will be done in the laboratory on shore.

We recovered sediment cores with a total length of 191 m and extracted 451 pore water samples. Nine profiles of heat flow values (140 measurements in total) together with about 400 km of seismic profiles will help us to clarify the role of the hydrothermal pits in the context of exchange processes of heat and mass between the ocean and the upper lithosphere.

1 Participants

Table 1: List and affiliation of participants

Name	Title	Position	Expertise	Affiliation
Villinger, Heinrich	Dr.	Prof.	Chief Scientist	University of Bremen
Alexandrakis, Eleni		student	geochemistry	University of Bremen
Alt-Epping, Peter	Dr.	research assistant scientist	geochemistry	University of Bern
Becke, Ronny	M.Sc.	research assistant scientist	geochemistry	University of Bremen
Dziadek, Ricarda		student	geophysics	University of Bremen
Enneking, Karsten		technician	geochemistry	University of Bremen
Fleischmann, Timo		student	geochemistry	University of Bremen
Gaida, Kristin		student	geochemistry	University of Bremen
Heesemann, Bernd	Dipl. Ing.	technician	geophysics	University of Bremen
Janßen, Christoph		student	geochemistry	University of Bremen
Kaul, Norbert	Dr.	research assistant scientist	geophysics	University of Bremen
Pichler, Thomas	Dr.	Prof.	geochemistry	University of Bremen
Ruiz, Maria	Dr.	research assistant scientist	geochemistry	University of Bremen
Schmidt-Schierhorn, Friederike	M.Sc.	research assistant scientist	geophysics	University of Bremen
Schwab, Arne	B.Sc.	student	geophysics	University of Bremen
Stephan, Sebastian	M.Sc.	research assistant scientist	geophysics	University of Bremen
Zwick, Mike		student	geochemistry	University of Bremen

Figure 1: Group photo on board Sonne.

2 Scientific Background and Objectives

(H. Villinger, T. Pichler)

It is known for a long time that heat flow on the Cocos Plate (eastern Pacific ocean) is significantly smaller than the value expected from a conductive lithosphere cooling model (Stein and Stein, 1992; Hutnak and Fisher, 2007). Some of the reasons for this heat deficiency especially close to the ridge are well understood: at mid-ocean ridges and on ridge flanks cold sea water can penetrate into the upper oceanic crust due to completely missing or incomplete sediment cover. In this bare-rock environment permeable oceanic crust allows sea water to enter Layer 2A and permits the exchange of energy and mass between upper crust and ocean. As sediment cover becomes more and more complete as the crust ages the low permeability of marine clay-rich sediments inhibits this exchange of mass and energy and isolates the hydrogeological regime in Layer 2A from the ocean. The sealing age is reached at a crustal age of about 65 Ma where heat flow vs age reaches the predicted values from conductive cooling models (Stein and Stein, 1992).

In areas of complete sediment cover, however, permeable seamounts may provide pathways for the exchange between ocean and upper crust. Cold seawater enters the crust at seamounts and circulates in the upper permeable crustal layers warms up and deposits and/or dissolves minerals. The warm water leaves the system at places like basement highs. The driving force of the circulation is the small horizontal pressure difference between a warm and cold hydrostat (Fisher et al., 1997, 2008). Heat flow observations in the close vicinity of seamounts is often depressed, supporting the idea of inflow of cold seawater into the subsurface and hereby cooling the immediate surrounding of a seamount if this inflow lasts for millions of years even if the flow rates are very small. The outflow of warm seawater is less well supported by observations as it may happen in a diffusive way over large areas and not be confined to an easily identifiable seafloor expression. This hydrogeological circulation model therefore provides a way of exchange of energy and mass between crust and ocean even in the presence of an otherwise complete sediment cover. It is called a hydrothermal siphon after Fisher (2005). It is obvious that not all seamounts are hydrologically active but due to the huge number of them even small flow rates over long period of time will cool a plate significantly on a large scale. Estimates of the energy and mass budget by Harris et al. (2004) show that seamounts play an important role in the exchange between ocean and upper crust. This model is well supported by the numerous heat flow measurements especially on the Cocos Plate (Hutnak and Fisher, 2007; Hutnak et al., 2008).

In the last years different papers were published suggesting an additional mechanism for the efficient cooling of the upper oceanic crust (Bekins et al., 2007; Moore et al., 2007; Michaud et al., 2005). Their ideas are based on comparatively old observations by Mayer (1981). Their model starts with the observation of almost circular depressions in a well-sedimented area with

a diameter of up to a kilometer and a depth of 50 to 100 m. These depressions are mostly associated with basement highs and are named hydrothermal pits by Moore et al. (2007) (Fig. 3). Striking examples of these pits are published by Michaud et al. (2005), which were observed during the SONNE-cruise SALIERI (Fig. 2). Bekins et al. (2007) suggested a model which could explain the formation of the pits (Fig. 4). It is assumed that cold seawater enters the crust through a seamount and is heated up. Due to the temperature increase carbonate is dissipated. Therefore the water circulating in the upper crust is undersaturated in carbonate. When it rises again for example at basement highs and meets carbonate rich sediments it dissolves the carbonate because the circulating water is undersaturated in carbonate. Therefore (Bekins et al., 2007) speculate that the pits are nothing else but dissolution pits , some kind of submarine karst. The authors show that their model is supported by the assumption of known flow rates, driving forces and geochemical reactions. Supporting observations of the model must therefore come from heat flow measurements around and within the pits and the analysis of pore waters inside the pits. The model of Bekins et al. (2007) is controversial as no observations are available at the moment which supports or refutes the hypothesis of dissolution pits. If the model is supported by observations then the chemical budget of the exchange processes may have to be revised as these pits are probably very frequent in the equatorial Pacific and contribute significantly to the budget. Modelling the heat transport based on Hutnak et al. (2008) together with constraints of the pore water geochemistry will allow to characterize the circulation system in a semi-quantitative way.

The currently accepted hypothesis is mainly based on thermodynamic calculations and assumes that cold calcium carbonate saturated seawater is gradually heated while it circulates from one seamount to the next. Due two its retrograde solubility, calcite should precipitate as seawater is heated during downward circulation. The precipitation of secondary calcite was observed in ODP cores (Alt, 2004). Since the upwelling fluid is cooling (either through heat flow or mixing) it becomes under saturated with respect to calcite and thus could cause the dissolution of carbonaceous sediments. The currently used models, however, are not based on direct measurements but rather on estimated values and calculations, which were transferred from the groundwater environment (Bredehoeft and Papadopolous, 1965). In order to go beyond simple estimations, it is necessary to sample pore water and sediments from dissolution pits and use this data in conjunction with heat flow measurements to calculate and model the energy and mass transport. The geochemical models have two approaches (a) the estimation of mass transport (i.e., calcium carbonate dissolution) from the hydrothermal pit using heat flow and pore water data in conjunction with a thermodynamic and kinetic model (this will be done using either the PHREEQC (`http://wwwbrr.cr.usgs.gov/projects/GWC_coupled/phreeqc/`) or GWB code) and (b) the estimation of geochemical reactions along the circulation path in the volcanic basement. This could be done with a coupled reactive transport model such as PHT3D (`http://www.pht3d.org/`).

The planned investigations are focused on the Cocos Plate within the Guatemala Basin where

the thermal regime of the plate is not yet well characterized by marine heat flow measurements but where three areas were well surveyed during site survey investigations for ODP Site 1256 (Teagle et al., 2006a). This also includes ODP Site 844 in the northernmost of the three areas. In both drill holes massive layers of biogenic carbonates were recovered and numerous pits can be identified in the published seismic and bathymetric surveys (Wilson et al., 2003a). These areas therefore provide enough background information for a detailed geophysical and geochemical study of hydrothermal pits.

F. Michaud et al. / Marine Geology 216 (2005) 205–219

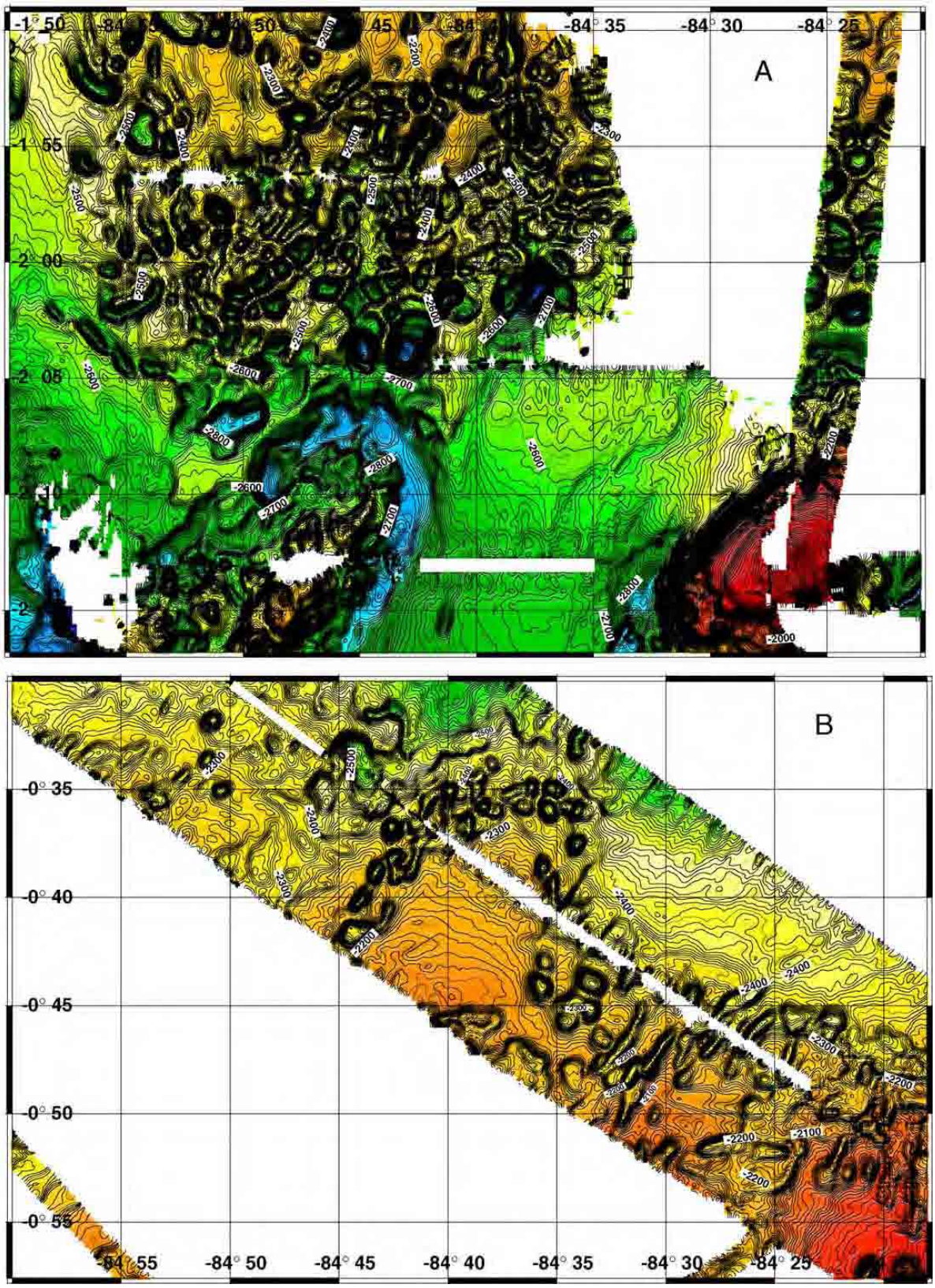

Figure 2: Example of dissolution pits from Michaud et al. (2005).

Fig. 4. Close-up of the southern flank (A) and on the northern flank (B) of the Central Carnegie Ridge showing a densely packed field of circular depressions (grid size 200 m; processed from Caraibes software, IFREMER). Bathymetric interval is 10 m.

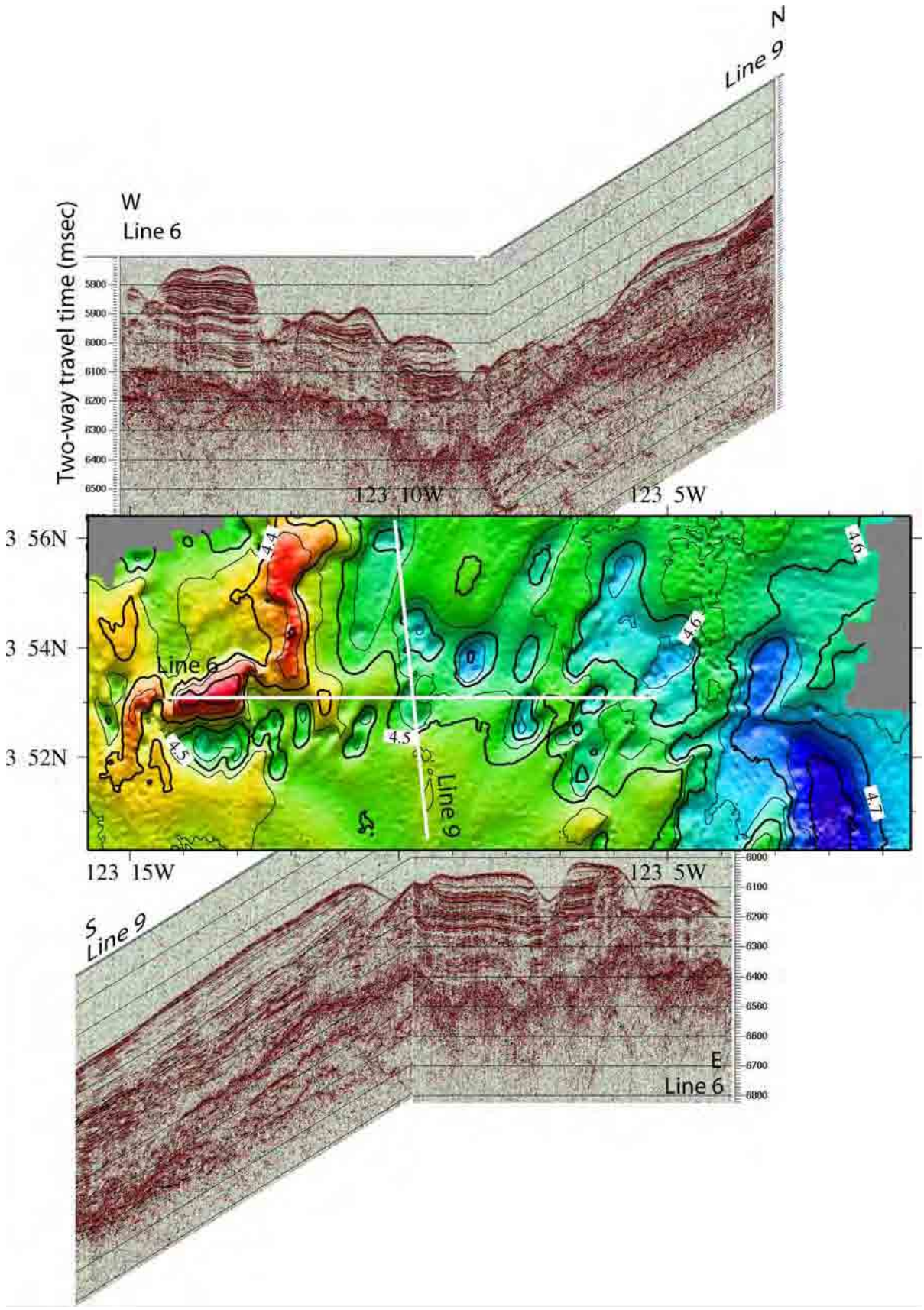

Figure 3: Example of dissolution pits from Moore et al. (2007).

Figure 5

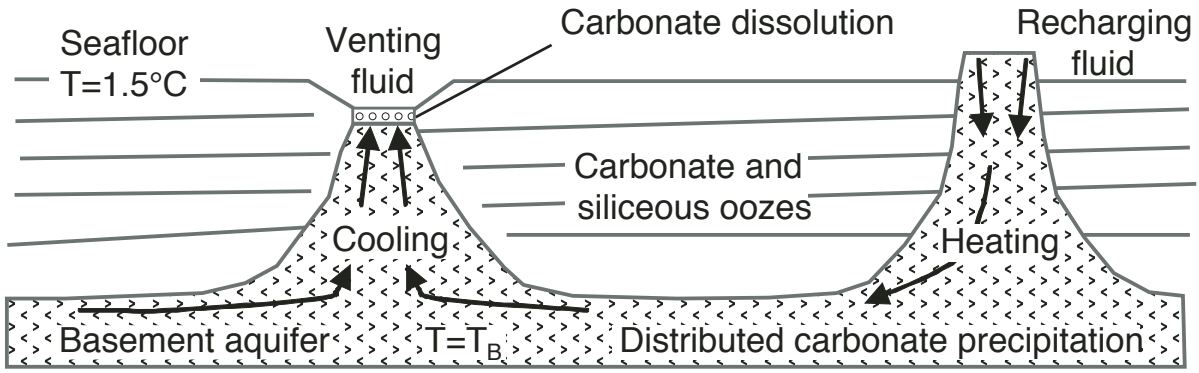

Figure 4: Model of Bekins et al. (2007)

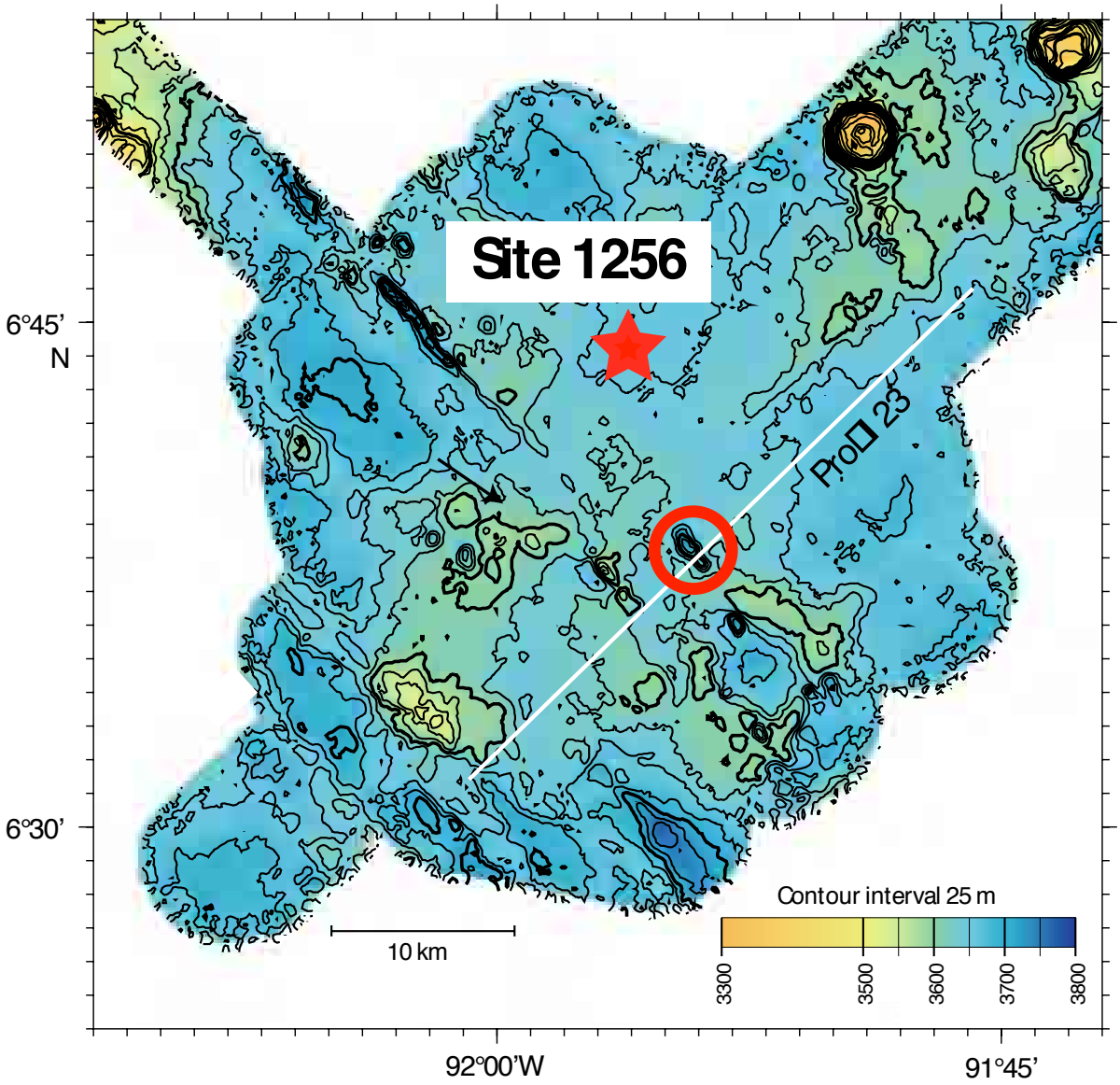

Figure 5: Bathymetry from cruise EW9903 around ODP/IODP drilling site 1256. The red circle marks a depression which can be clearly identified as a dissolution pit in Fig. 6.

Figure F34. Migrated MCS section for lin e 23, grid 3. See Figure F28, p. 34, for location. The upper panel shows part of the same data as the lower panel but plotted at lower gain and greater vertical exaggeration to show detail in the sedimentary section. Distances are measured northeast of the line 26 crossing.

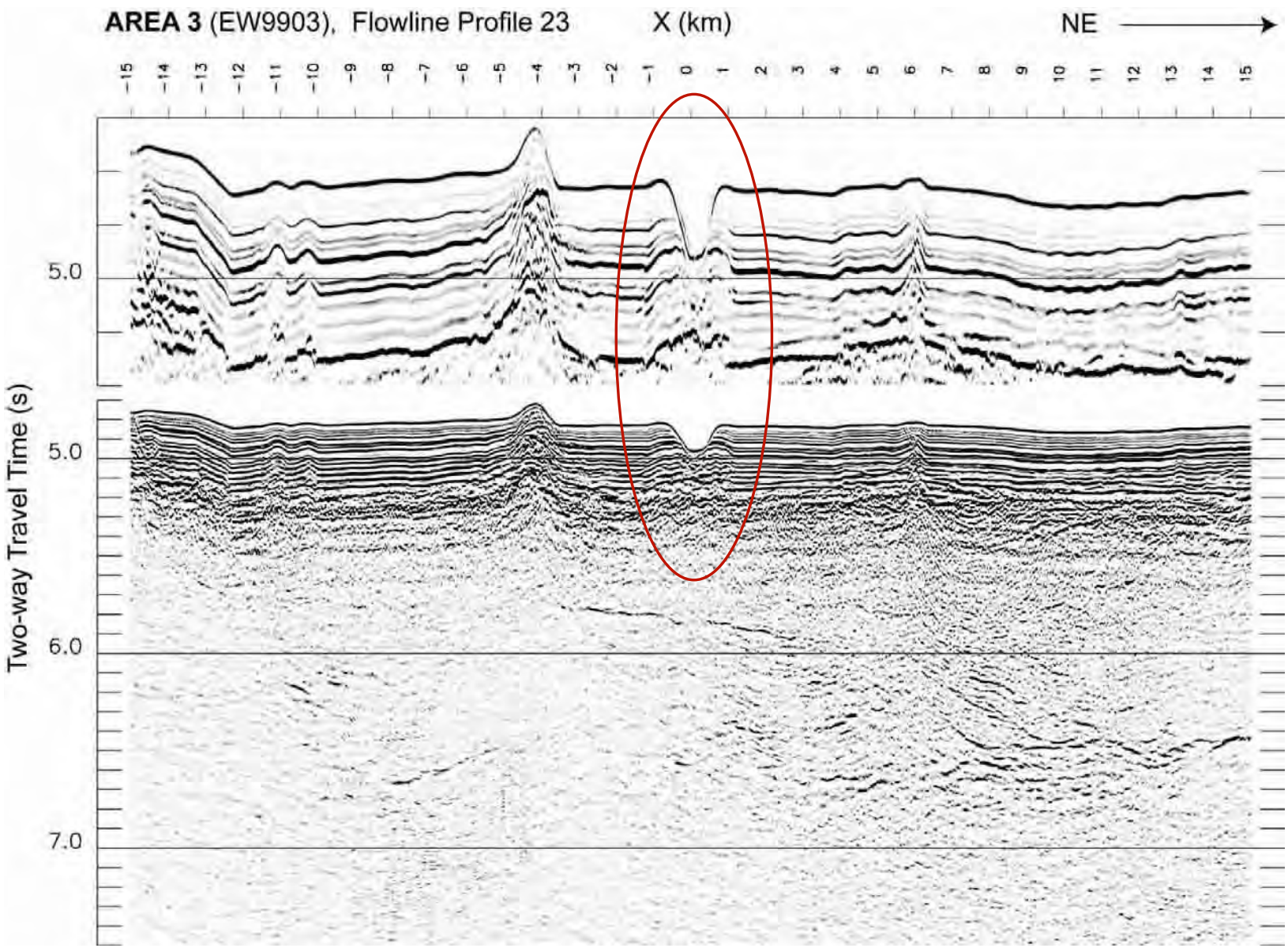

Figure 6: Seismic section of Profile 23 from cruise EW9903 (Wilson et al., 2003a). The upper picture shows the sedimentary coverage with less amplification and higher vertical super elevation than the lower subfigure. This depression is very similar to the dissolution pits presented in Moore et al. (2007).

Abbildung 4: Seismische Sektion des Profils 23 (*Wilson et al.*, 2003) (siehe Abb. 3). Das obere Bild zeigt nur die sedimentäre Bedeckung, dargestellt mit geringerer Verstärkung und größerer vertikaler Überhöhung als das untere Bild. Die Depression (’hydrothermal pit’) sieht im seismi-

3 Narrative of the Cruise

(H. Villinger)

On Monday, June 21, 2010 at 12:30, R/V SONNE left the harbor of Caldera (Costa Rica). Our departure was delayed for half a day due to the late pickup of frozen biological samples from the previous cruise. We had a technician of Atlas Electronic on board who installed new software for the Parasound system which he tested successfully during Monday afternoon off Nicoya Peninsula. We came back to the port of Caldera in the late evening where he was picked up by the pilot boat. Then we finally left and headed west for our first working area which was located about 360 *nm* southwest of Caldera (Fig. 7). During the transit the research groups were very busy to set-up laboratories and test all their equipment. A short test of our seismic equipment on Tuesday morning showed that everything worked well. The science party was introduced to the swath mapping and sediment echosounding system by ship s personal. In a short science meeting on Wednesday evening we familiarized the science party with the science goals of the cruise. Our working strategy was to core during the day and use the nights for seismic and heat flow surveys. Also we intended to get an overview of the three working areas in the first two weeks of our cruise and use the third week to fill in gaps and revisit interesting sites on our way back to Caldera.

We reached the first working area GUATB-1 (Guatemala Basin 1) on Wednesday morning at 8 o clock and started our investigations with a CTD cast in order to get a sound velocity profile which we needed for the calibration of our swath mapping system Simrad EM120. We spent the days until Sunday, June 27 with coring, heat flow and seismic surveys. A visual inspection of the seafloor in and around the seafloor depressions (pits) with the camera system was successful on the one hand as all systems worked but disappointing on the other hand as we did not observe anything highly unusual. The second and third working area (GUATB-2 and GUATB-3) were investigated in a similar fashion and we completed our work in the southernmost area on Monday, July 5th. On the way back we took a heat flow profile close to a very prominent seamount and managed to do heat flow measurements in the caldera and even took a gravity core there. After filling in gaps in working area GUATB-2 and -3 we returned to Caldera where we tied up on July 13 at 8 o clock.

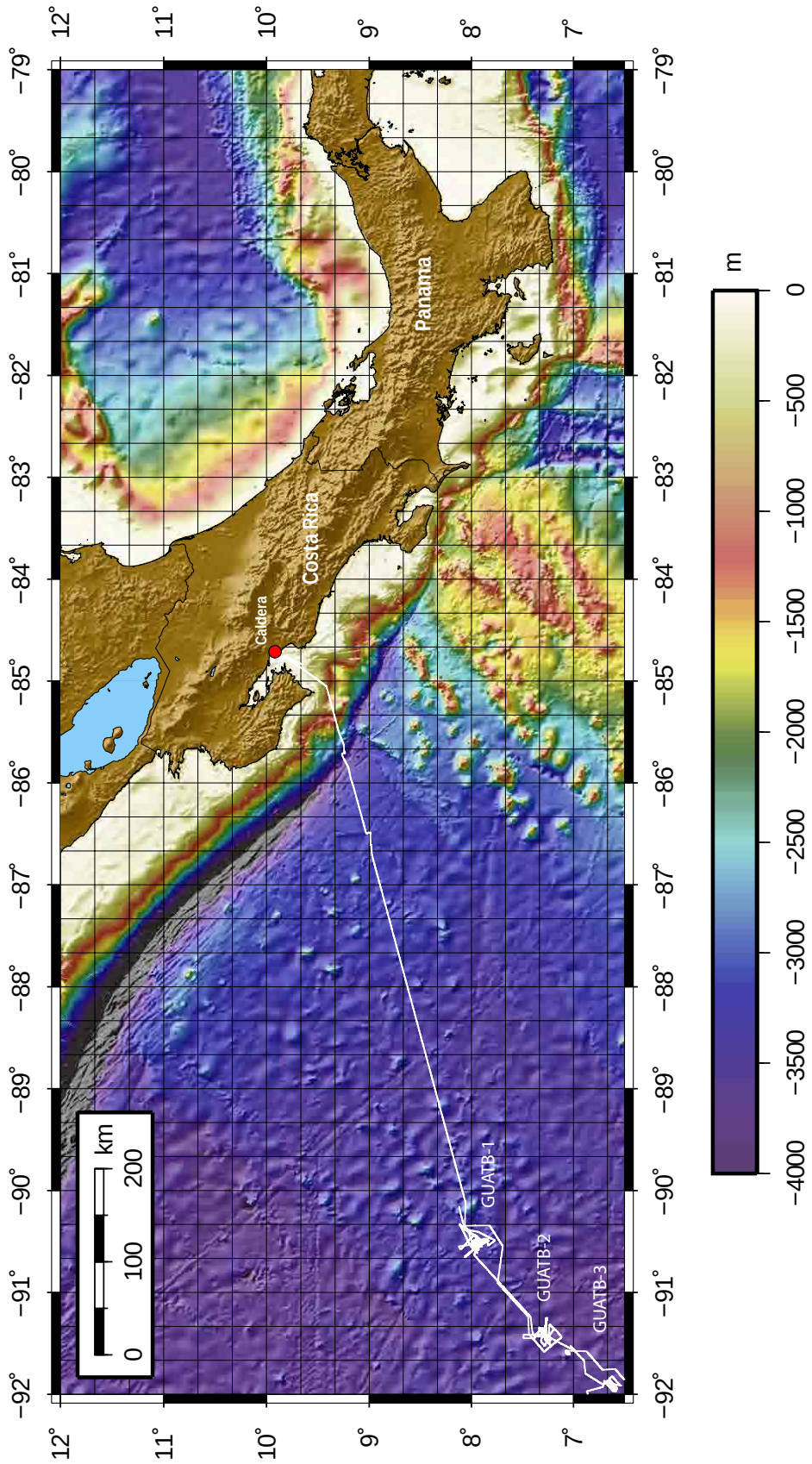

Figure 7: Overview about the SO207 cruise track starting from Caldera, Costa Rica (white) and the three working areas GUATB-1 to GUATB-3.

4 Methods

4.1 Geophysics

4.1.1 Bathymetry Survey

(S. Stephan)

On board Sonne the multi-beam echosounding system (MBES) KONGSBERG EM 120 is used for deep-sea bathymetric surveys. It is mounted on the hull of the research vessel and provides 191 beams with spacings that can be set up equidistant or equiangular. The emission beam can be adjusted to opening angles of up to 130° across-track while the opening angle along-track is fixed to 2°. Resulting footprints for each individual ping depend on water-depth (opening angle 2° along-track and 2° across-track). The echo received from the seafloor consists of 191 reflected beams from frequency coded (11.25 to 12.6 kHz) acoustic signals. For further details see Tab. 2. The absolute water depth can be estimated by using a sound velocity profile (SVP) describing ray-bending in the water column and by knowing the two-way travel time for each beam. Measurement accuracy is achieved by using a combination of phase for the central beams and amplitude for the lateral beams. Raw depth data obtained by the MBES and recorded by Kongsbergs SIS-Software contain along-track distance, across-track distance and depth information. This raw data is already corrected for sound-velocity changes in the water-column by a SVP and for heave/pitch/roll movement by data from the motion reference unit (MRU) and static offsets such as the roll bias. Processing of the MBES-Data is performed by using MB-System Software (Caress and Chayes, 2009) which is distributed over the Internet (`http://www.ldeo.columbia.edu/res/pi/MB-System/`). The raw-data (.asd-files) are converted to the MB-System processing format (.mb57) and are organized in datalists. Manual editing of each beam is performed using `mbedit`, static offsets are set with `mbset`. Processing is done using `mbprocess`. The processed lines (sonnep.mb57) are combined to a grid with `mbgrid` for each working area and the transit areas respectively. For gridding parameters see Tab. 2. Grids for detailed areas are produced with a smaller grid-size. The grid-file is blended on an existing bathymetry (from cruise EW9903 and the GEBCO dataset, latter one downloadable at `http://www.gebco.net/data_and_products/gridded_bathymetry_data/`) using Generic Mapping Tools (Wessel and Smith, 2010).

Table 2: Technical Data of the Kongsberg EM120 and gridding parameters used to process the bathymetry data.

Technical Data KONGSBERG EM 120	
Main Frequency	12 kHz (varying between 11.25 and 12,60 kHz for sector-coding)
Beams	191/Ping
Opening angle	2 x 2°
Beam width	equidistant or equiangular
Coverage	<=130°
Operating depth	20...11000 m
Depth resolution	10...40 cm
Pulse length	2, 5, 15 ms

Gridding parameters (mbgrid)	
Datatype (-A)	2 (positive upwards)
Gridding Algorithm (-F)	5 (Weighted Sonar Footprint)
Empty Cells (-N)	set to NaN (rather to 99999.9)
Interpolation Setting (-C)	3 (interpolation for up to three times cell size)
Speed (-S)	5 (minimum vessel speed for valid beams in km/hr)
Grid Size (-E)	75/75 or 50/50 (grid size x/y in meters)

4.1.2 Sediment Echosounding

(N. Kaul, A. Schwab)

Parasound System

On board RV Sonne, an Atlas PARASOUND P70 System is installed permanently for sediment echo sounding. The main goal of using the PARASOUND System was the selection of suitable sites for sediment sampling and deployments of the heat flow lance. The PARASOUND System is a low-frequency sediment echosounder in combination with a high-frequency narrow beam sounder for water depth. It utilizes the parametric effect that means that two acoustic signals of almost similar frequencies (in our case 18.8 kHz and 19.3 kHz) are emitted simultaneously which produces through nonlinear acoustic interactions a primary signal with 3.5 kHz. This pulse travels within the emission cone of the original high frequency waves, which are limited to an angle of 4.5°. Therefore, the footprint size of 7% of the water depth is much smaller than for conventional 3.5 kHz systems. Vertical and lateral resolution is significantly improved. Since the two-way travel time in the deep sea is long compared to the length of the reception window of up to 266 ms, the PARASOUND System sends out (in deep sea mode) a burst of pulses (0.500 ms length) at 400 ms intervals before the first echo returns. The coverage of this discontinuous mode depends on the water depth and produces non-equidistant shot distances between bursts. On average, one echogram is recorded every second providing a nominal spatial resolution on the order of a 2 to 3 m on seismic profiles at 5 knots. The PARASOUND System is equipped with the digital data acquisition system PARADIGMA, which was developed at the

University of Bremen (Spieß, 1993). The sample frequency of the echogram is 40 kHz with a recording length of approx. 500 ms for a depth window of 400 m. Real part and phase of the envelope from the returned echo signals are saved in the ASD format. Because of the limited penetration of the echosounder signal into the sediment, only a small depth window close to the seafloor is recorded and saved in PS3 format which can be used for post-processing. The PC allows buffering, transfer, and storage of the digital seismograms at very high repetition rates. From the emitted series of pulses, usually the pulse could be digitized and stored, resulting in recording intervals of 800 ms within a pulse sequence.

Processing of Data

Data files in PS3 format are processed employing the software package SeNT (by Hanno Keil, AG Spieß, Univ. of Bremen).

4.1.3 Seismic Survey

(N. Kaul, A. Schwab)

Instrumentation

Seismic Source For seismic signal generation a single GI gun (Landrø, 1992) is used during SO207. GI Guns are pneumatic seismic sources which incorporate two independent air guns within the same body casing. The first gun generates the primary pulse (generator). The second air gun (injector) can be configured in different ways, i.e. to control oscillation of the air bubble produced by the generator. Each gun has its own reservoir, its own shuttle, its own set of exhaust ports, and its own solenoid valve. Volumes of both generator and injector can be adjusted by inserting plastic volume reducers inside respective chambers. During this cruise we operated in Harmonic Mode . No volume reducers are mounted in the injector and generator section. In this case the total air consumption is 2 x 105 in^3 or 3.4 L. Discharge port hole reducer medium is used for the injector ports. In Harmonic Mode , injection is tuned to optimally suppress the oscillation of the bubble by time delay modification. The source field hydrophone signal is not used during this survey. According to the documentation for a source depth of 7 - 8 m a delay time of 40 ms is employed. Compressed air is provided by the ships build-in LMF compressor delivering an actual pressure of 140 bar (2000 psi) The trigger signal is supplied from a dedicated triggerbox (SchwaBox, by Arne Schwab, AG Villinger, Univ. of Bremen) system with a high precision quartz timing base. This system provides trigger pulses for generator and injector valves and for the recording system. During this cruise on Sonne, the seismic source is operated from the starboard side of the stern. The mechanical set up is as follows: one buoy is fixed to the rear eye of the gun hanger with app. 8.5 m of rope. The

seismic source is mounted horizontally 1 m below the gun hanger. An 12 mm steel wire of 20 m fixed length is used as tow wire. It was fastened to the front end of the gun hanger. The towing wire of the umbilical is fixed to the front eye of the hanger. In this configuration, towing force is provided through the steel wire. Position of air gun is 16-17 m behind the vessel and app. 3 m to starboard with regard to the ships center line.

Streamer and data acquisition Reflection seismic data are obtained using a 101 m active length streamer. It is a 16 channel unit built by Teledyne Exploration Co. in 1993. The system comprises five parts, a 101 m active length, a 7 m transformer section, a 25 m stretch section, and a 125 m tow leader, together with a 75 m deck cable (Fig. 8). The active length is separated into 16 groups of 8 hydrophones. Within one group the hydrophones are 0.78 m apart and therefore forming a 6.25 m long unit. Tail rope length is 20 m. The whole streamer is stored and operated from a manual winch and towed on port side from the stern.
The data acquisition was done using a home-made integrated Seismic Acquisition Unit (SAU3, by Arne Schwab, AG Villinger, Univ. of Bremen). It contains the trigger system Schwabox, a filter- and preamplifier section and an A/D-converter (DAQ). The DAQ is a National Instruments 6259 USB OEM system which allows sampling of 16 channels at a maximum rate of 125 μs and a resolution of 16 bit.
Digital seismic data are then transferred to the MaMuCS seismic recording system (Version 1.8.8., by Hanno Keil, AG Spieß, Univ. of Bremen). This system performs display of shot gathers, real time demultiplexing and storing of raw data on disc in SEG-Y format as well as a brutestack. Data are recorded with a record length of 4 s, a sample interval of 250 μs, and a water delay of 3 s since water depth varied very little during the survey. Data are filtered by an analogue input filter of the acquisition system at 1 Hz (high-pass) and at 1000 Hz (antialiasing). The components and setting of the complete seismic systems in use are shown in Table 3.

Table 3: Attributes of the seismic system used during cruise SO207.

Seismic source	GI gun, 3.4 l, harmonic mode, 40 ms delay @ 140 bar
streamer	Teledyne streamer, 16 channels, 6.25 m each, 25 m stretch section, 125 m lead in as receiver
Data acquisition	Home-made seismic acquisition system SAU3 (includes NATIONAL NI “6259 USB OEM” A/D Converter System), MaMuCS recording software
Trigger	Time trigger system SchwaBox
Shot interval	8 sec (equivalent to 16 m shot spacing at 4 kn)
Sample interval	250 µs
Water delay	3000 msec

Processing of Data

The recorded seismic data was processed with VISTA VW PROCESSING 3D (Version 7.010) by GEDCO. All 16 channels were vertically stacked for a first and fast visualization. A bandpass-

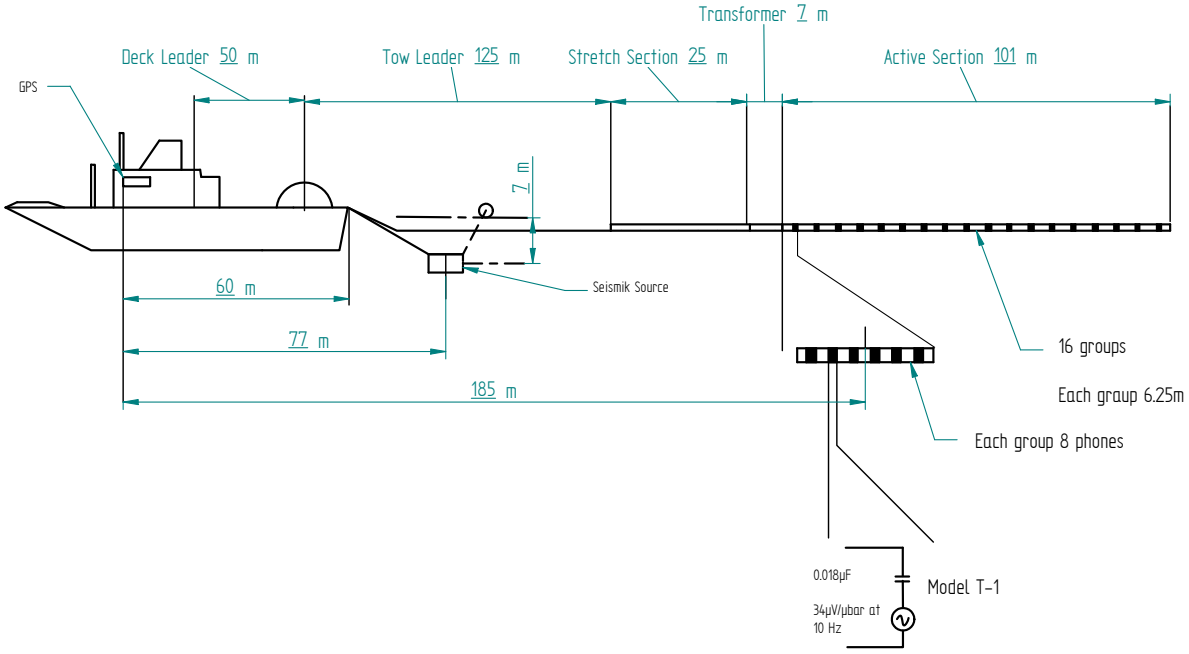

Figure 8: Schematic showing the set-up of the seismic system on board.

filter was applied to remove noise caused by the streamer and the ship (Ormsby 20/25 - 200/250). GPS navigational data files in NMEA-format were additionally stored with the recording software MaMuCS. In order to get a shotpoint - position list, the header data (recording time, shot point number) was exported into a text file. This text file was then processed with the software WinGeoApp (Version: 0.9.5, by Hanno Keil, AG Spieß, Univ. Bremen) which is also able to incorporate the geometry of streamer gun - GPS-antenna and calculate the locations of the common mid-points. For a better traceability of the basement, the amplitude scale was set to $+6dB$.

4.1.4 Heat Flow Survey

(H.Villinger)

Bremen Heat Probe

During the cruise we used exclusively the 6 m long Bremen heat flow probe also called Giant Heat Flow Probe (GHF). The mechanically robust heat probe is designed for the operation in a pogo-style mode with a wide application range from 6000 m deep sea trenches with mostly soft sediments to the upper continental slope where sediments are often sandy and difficult to penetrate. Due to the 6 m length of its temperature sensor string undisturbed temperature gradients can be determined even in shallow water where seasonal bottom water temperature variations are superimposed on the undisturbed temperature field close to the sea floor.

The heat probe (Fig. 9) is constructed in the classical violin bow design (Hyndman et al., 1979; Hartmann and Villinger, 2002), with 21 thermistors distributed over a total length of 6 m in 0.26 m intervals mounted inside an oil filled hydraulic tube (O.D. 14 mm) which is attached to the strength member (O.D. 130 mm). The sensor tube also contains a heater wire for the generation of high energy heat pulses of typically on the order of 800 watts for in situ thermal conductivity measurements (Lister, 1979). Only non-corrosive steel was used for the heat probe, with special high strength non corrosive steel for the strength member and the fins attaching the sensor tube to it. The complete data acquisition unit including power supply (Sea & Sun, Trappenkamp, Germany) is housed in a single 110 mm O.D. x 300 mm long titanium pressure case and mounted inside the probe s weight stand. A second pressure case of the same size houses the batteries for heat pulses. The signal of the temperature sensors is measured with a resolution of 20-bit at a sample rate of 1 sec, resulting in a final temperature resolution of better than 1 mK at ambient seafloor temperatures. A carefully calibrated PT-100 seawater sensor on top of the weight stand allows to measure the absolute bottom water temperature and to check the calibration of the sensor string in deep water with high accuracy. Inclination and acceleration of the probe is measured also with a 1 sec sample rate to monitor the penetration process into the sediments and potential disturbances during the measurement period while the probe sits in the sediment. The complete data set is stored in the probe but also transmitted via coax cable on board in real time where the data are visualized and stored with a PC. The operator always has complete control of the instrument which allows operational decisions during long term deployments of the probe. In addition the heat probe can also be operated in a completely autonomous mode with internal data storage and automated heat pulses if a coax cable is not available. The battery capacity allows for 3 days continuous operation in a pogo-style mode.

Winch speed during payout and retrieval is 1.0 m/s which guarantees full penetration in the sediments of this working area. Time to equilibrate to in situ temperatures is assumed to be 7 to 8 minutes, time for heat pulse decay observation takes another 8 minutes. The mean duration of one measurement including transit of about 1 km is about 1 - 1.5 h per single point of measurement. When possible the heat probe position was monitored using the RV Sonne s Posidonia under water positioning system.

Processing of Data

The penetration of the heat probe into the upper meters of the soft sediments generates a thermal disturbance due to frictional heating and in addition the sensor string has to come into thermal equilibrium with the sediments. This means that the probe stays in the sediment for about 7 to 8 minutes; however it will not have equilibrated at the end of this time. Therefore the temperature decay has to be fitted to a theoretical decay model. In situ thermal conductivity is measured with the heat pulse method (Lister, 1979) where the sensor string is heated up for typically 20 to 30 s and the thermal conductivity is derived from the temperature decay.

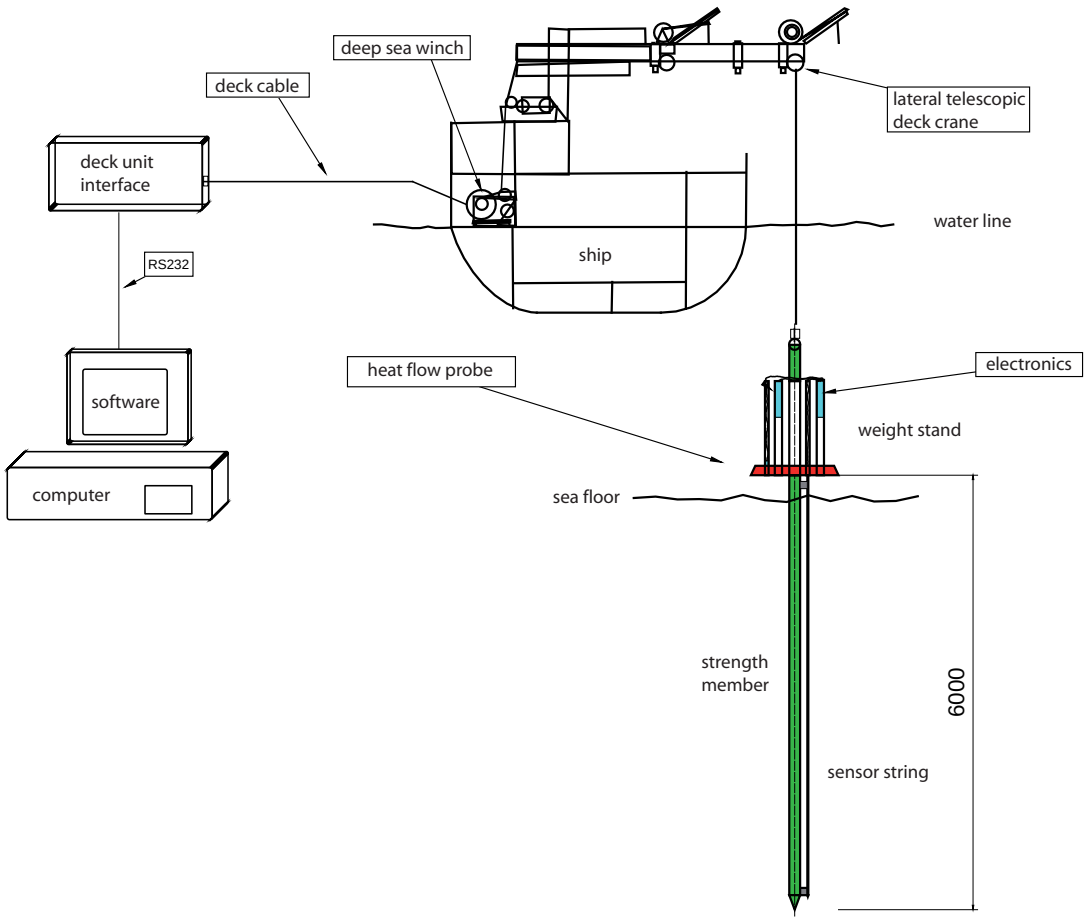

Figure 9: Schematics of heat flow probe setup on R/V Sonne.

Both decays, frictional and heat pulse decay, can be described by the same mathematical model. Figure 11 and 12 show a typical example of a measurement. The basic processing steps of heat flow measurements is outlined in Hyndman et al. (1979) which was then a manual procedure based on the work of Lister (1970) and Lister (1979):

- determine undisturbed sediment temperatures from frictional decay
- correct heat pulse decay for the remaining effect of the frictional decay
- calculate in situ thermal conductivities from heat pulse decay
- fit thermal resistance vs. measured temperatures (Bullard-plot, Bullard (1954)) to derive heat flow

The theoretical background for the analysis of heat flow measurements is discussed in Bullard (1954), Lister (1970), Hyndman et al. (1979), Villinger and Davis (1987) and Hartmann and Villinger (2002). To overcome deficiencies of the processing routine described in Villinger and Davis (1987) and to incorporate platform independent plotting routines, a mathematically sound inversion scheme of observed temperature decays was implemented in a program called HFRED (Villinger and Davis, 1987), using Matlab®.

Figure 10: The 6 m Bremen Heat Flow Probe on deck during cruise SO207.

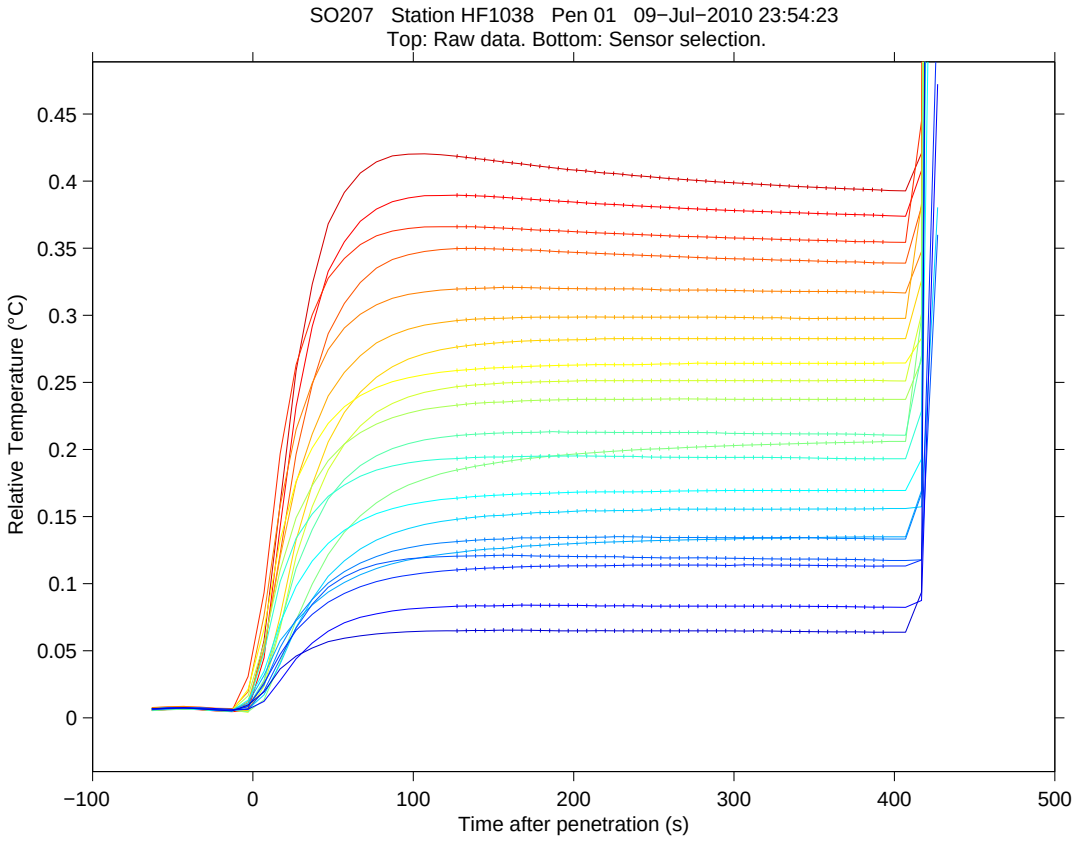

Figure 11: Temperature raw data with time of Profile HF1038, Penetration 1.

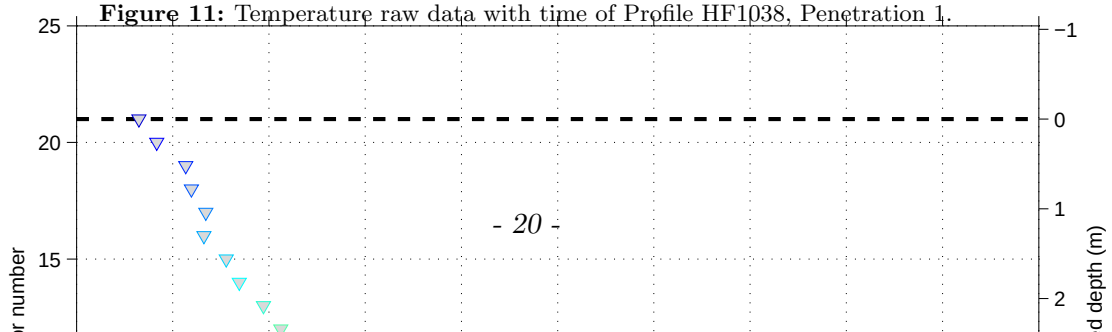

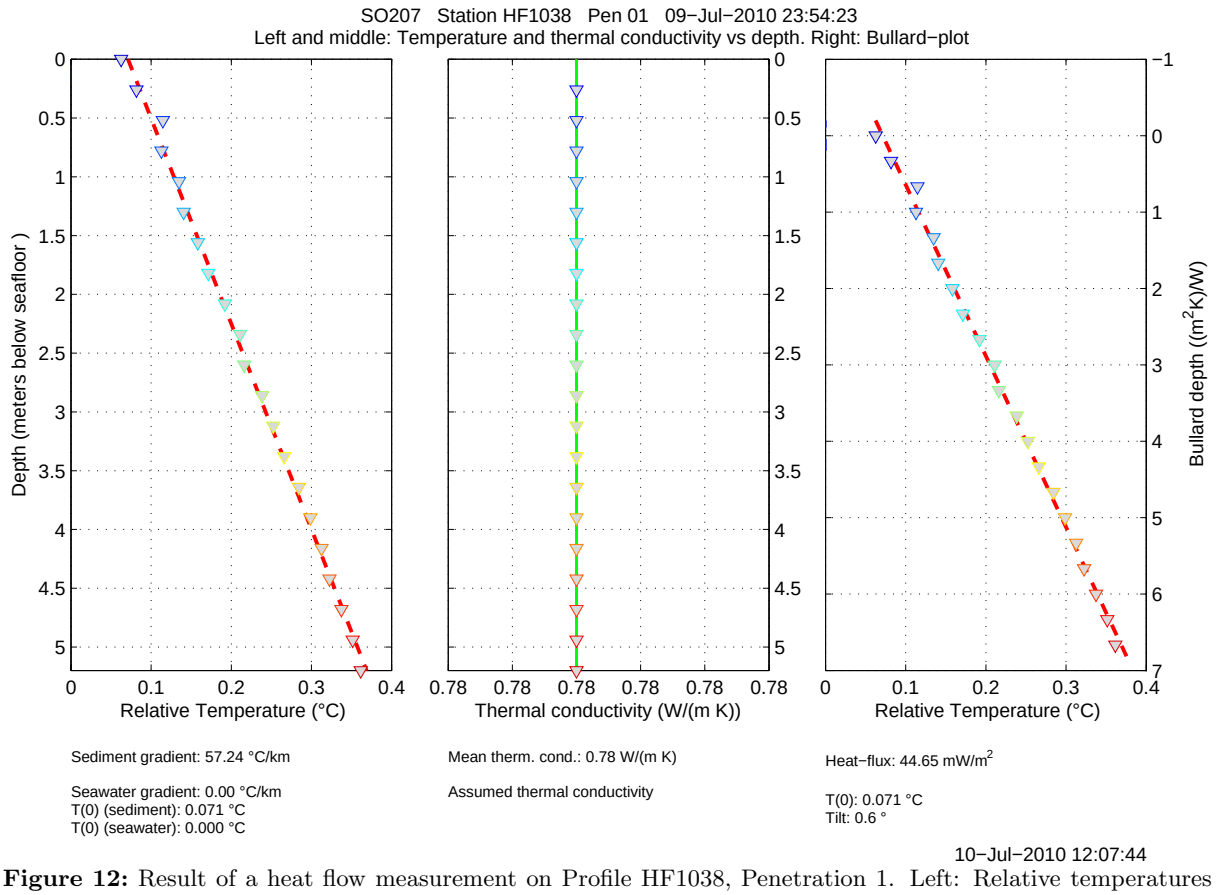

Figure 12: Result of a heat flow measurement on Profile HF1038, Penetration 1. Left: Relative temperatures vs. depth. Middle: In situ thermal conductivity vs. depth. Right: Thermal resistance vs. depth (Bullard-plot).

4.1.5 Thermal Conductivity Measurements

(H. Villinger)

Thermal conductivity measurements were made on split core sections (archive half) with a commercially available thermal conductivity instrument KD2PRO (www.decagon.com) which is based on the needle probe method. The needle used is 60 *mm* long with an outer diameter of 1 *mm*. According to specifications the resulting thermal conductivity has an absolute accuracy of 5%. The split cores were measured after they equilibrated to ambient temperatures in the laboratory. As the sediment was very homogenous only two measurements per core section (normally 1 *m* long) were made. Measurements will be corrected at a later stage for in situ temperature and pressure after Ratcliffe (1960).

4.1.6 Seafloor Penetration Monitoring

(S. Stephan)

Seafloor penetration monitoring has been performed by using the Bremen Lance Insertion Retardation Meter (LIR-Meter, see Fig. 13, Fabian et al. (2008)). The device records acceleration

data at a sampling frequency of 500 Hz and operates autonomously. During this cruise the LIR-Meter was mounted on the weight stand of the 6 m Bremen Heat Probe and thus tethered to the vessel via the wire. The recorded acceleration data can be used to (a) determine the depth of penetration and/or (b) to assess qualitatively and quantitatively the geotechnical parameters of the sea floor like undrained shear strength or bearing capacity.

Figure 13: Left: LIR-Meter in pressure casing; right: electronics

4.2 Sedimentolgy and Geochemistry

4.2.1 Gravity Coring

(M. Zwick)

Sediment cores were retrieved by two means: (a) with gravity corer (GC) for the collection of cores up to 12 m and (b) with a micro corer (MIC) for the collection of seawater-sediment interface. At each site, individual instrument deployments were assigned the site number modified by sequential number suffixes starting with "-1". The gravity corer (GC) was lined with PVC tube and equipped with a stainless steel core catcher. When possible the GC sampling position was monitored using the RV Sonne's Posidonia under water positioning system. During deployment, sediment penetration and retrieval winch speeds were generally 1 $m\ s$. Once retrieved the liner was removed and cut into segments of 1 m length and labeled according to the GeoB-system which consists of cruise no., station no., gear no., range of depth, orientation (Fig. 14). Once

labeled the cores were cut lengthwise and divided into a working and archive half. The archival half was used for onboard sediment description and then put into D-Tubes and stored at a temperature of approximately $4°C$ for transport to the University of Bremen core repository. The working half was used for Eh and pH measurements and sampling of pore waters and sediment material.

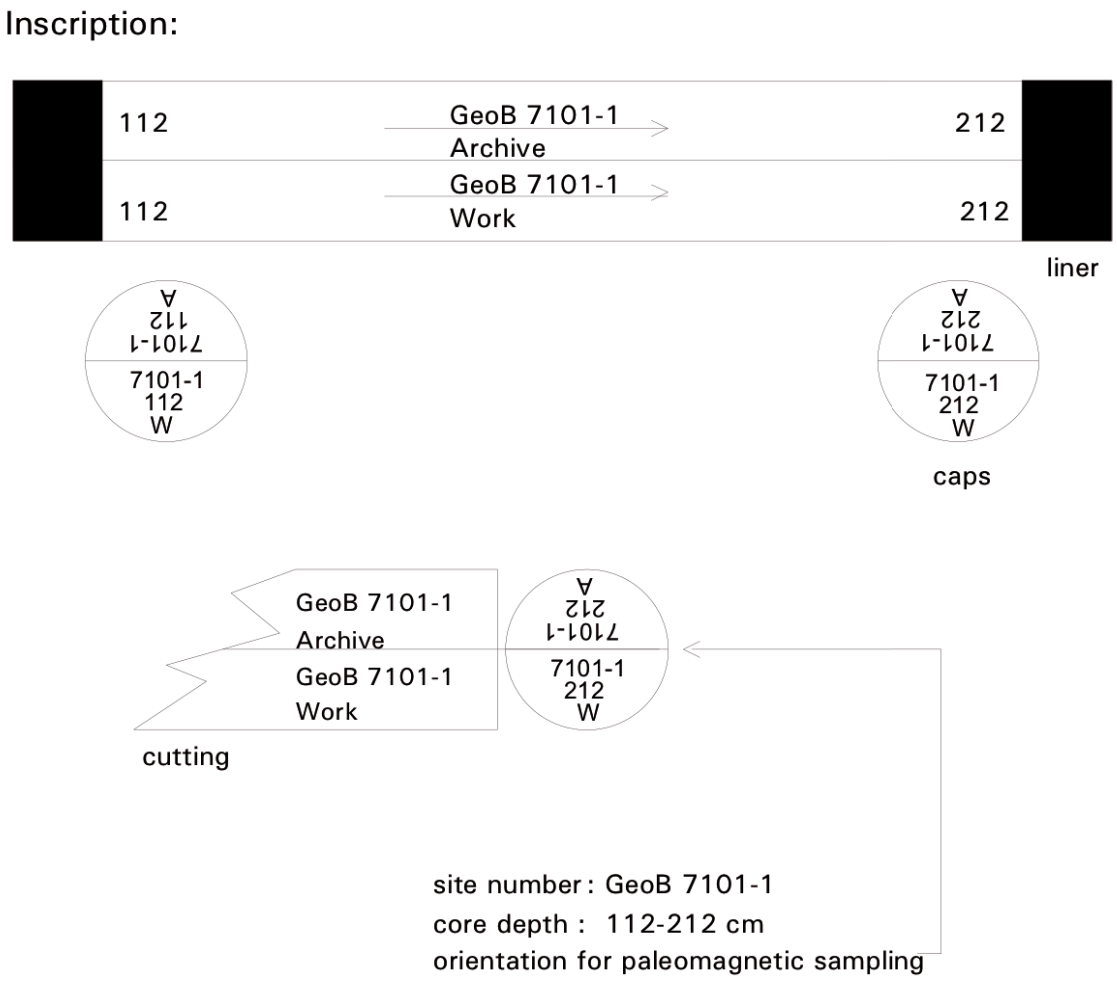

Figure 14: Labeling scheme for the gravity core segments used during the Seamountflux cruise to the Guatemala Basin (SO 207). The actual GeoB numbers were 14600 to 146025.

The MIC was equipped with 4 Plexiglas tubes of 60 *cm* length, which were open during deployment to the seafloor and sediment penetration. Penetration depth was approximately 30 *cm*. Upon retrieval from the sediment the Plexiglas tubes were closed from the top and bottom, thus preserving approximately 30 *cm* of bottom seawater and 30 *cm* of sediment. Once on board sediment samples were obtained by pushing a specially fitted plunger from the bottom up through the Plexiglas tube and collecting sediment every 5 *cm*. Prior to sediment collection Eh and pH were measured. Pore water samples were collected every 5 *cm* through holes which were drilled through the tube prior to deployment and sealed with electrical tape.

4.2.2 Sediment Description

(T. Fleischmann, C. Janssen)

Split gravity cores were described from a largely sedimentological standpoint. Grain size and composition of sediments were determined mainly visually using a simple hand-lens, HCl-testing and analyzing smear slides of dominant lithologies under a cross-polarizing microscope. The size of grains was assessed based on Wenthworth s classification. The color of the material was determined visually on board using Munsell s color chart nomenclature. For each core, a composite one-page core log sheet was compiled, which shows a graphical core log and gives information about the assigned lithological units. A wide variety of features, such as sediment lithology, primary sedimentary structures, bioturbation, soft- sediment deformation, and coring disturbance is indicated by patterns and symbols in the graphic logs. A key to the full set of patterns and symbols used on the barrel sheets is shown in Appendix (Core Logs). The symbols are schematic, but they are placed as close as possible to their proper stratigraphic position.

4.2.3 Pore Water Geochemistry

(K. Gaida)

After splitting the cores, temperature, Eh and pH were measured directly in the sediment of the working half using punch-in electrodes. The location of measurements and sample collection were based on a dual approach, (a) collecting samples at an even spacing in order to cover the whole core and (b) collecting samples in parts of the core where geochemical gradients were indicated by color changes, Eh changes, pH changes. Pore water was extracted with the help of rhizons (pore size 0.1 μm). The sampled pore water amount ranged between 17 and 20 mL. At the same depth where the pore water was extracted sediment samples were taken with 20 mL syringes and stored at $4°C$ in the cooling container for further analysis at the University of Bremen. Onboard pore water analyses consisted of the following parameters: alkalinity, iron (Fe^{2+}), ammonium (NH_4^+) and phosphate (PO_4^{3-}). Dissolved iron (Fe^{2+}) was measured shortly after sampling. Subsamples of 1 mL were taken, immediately complexed with 50 μL of Ferrospektral® , and determined photometrically with Hach DR5000 photometer at 565 nm wavelength. Before measurement the instrument was calibrated with standards ranging from 0.05 to 1.5 mg/L. Phosphate was also measured photometrically. For this 50 μL ammonium molybdate solution and 50 μL ascorbic acid solution were added to 1 mL sample and the resulting blue phospho molibdate complex was measured at 880 nm wave length. Alkalinity analysis was performed volumetrically by titration of 1 mL of sample with 0.01 $MHCl$. For this, an autotitrator and a micro-pH-electrode were used to titrate to pH-endpoint of 3.800. Ammonium was measured on 100 μL of sample using a conductivity method. The sample was diluted with a natrium citrat buffer to reduce ammonium (NH_4^+) to ammoniac (NH_3), which is gaseous. The sample mixture was passed through a reactor where the gas permeated through a teflon-membrane to react with HCl 1 $mmol/L$ causing a conductivity change, which was measured by use of a conductivity

detector. Prior to analysis the ammonium-line was calibrated with standards ranging from 0.5 to 5 mg/L. For further analysis at the University of Bremen aliquots of the remaining pore water samples were diluted 1:10 and acidified with 1% ultrapure HNO_3 for determination of cations (Ca, Mg, K, Ba, S, Mn, Si, B, Li) by ICP-OES. Additionally, samples were preserved for sulfide analysis through adding of 0.6 mL ZnAc solution to 1.5 mL of sample in order to fix hydrogen sulfide as ZnS. For analysis of anions a dilution 1:100 with MilliQ water was performed. 4 mL subsamples were acidified with 1% ultrapure HNO_3 for the analysis of trace elements by ICP-MS. For the analysis of oxygen and hydrogen isotopes 0.5 mL pore water were filled in glass vials and capped. Finally, all sample dilutions and the remaining pore water samples were stored at $4°C$. The samples from the MIC were processed the same way, but the bottom water samples were filtered with a 0.1 μm filter.

4.3 Video survey

(M. Zwick)

To carry out visual observation of the seafloor the RV Sonne s Oceanfloor Observation System (OFOS) was employed. The OFOS allows the visual survey of the seafloor via video camera and still photography with a resolution of up to 10 mega pixels. Cameras, batteries and transponders are attached to a steel frame, which is lowered to approximately 3 m above the seafloor. The system was pulled behind the ship by a rope, which also allowed the positioning of the OFOS within the water column.

5 Preliminary Results

5.1 Bathymetry Survey

(S. Stephan)

The Multibeam Ecosounding System (MBES) EM 120 collected data during Seismic and Parasound surveys. The collected profiles are shown in Tab. 4 and statistics on the collected data is shown in Tab. 5.

The result of the MBES-Survey is shown in Fig. 53 to 57 (see Appendix, section A.1), each figure shows an individual working-area (GUATB-01 to GUATB-03) or transit (GUATB-01_02 or GUATB-02_03). An overview is shown in Fig. 15. The bathymetry obtained during cruise SO207 is blended with a dataset collected during cruise EW9903 in 1999 (Wilson et al., 2003a). The blended bathymetry is shown in Fig. 58 to 62 (see Appendix, section A.1) for a better overview, as this survey was intended to complement and enhance the existing dataset from

1999. Overall the water depth ranges from 4100 m in the south-western part to 3400 m in the north-eastern part of the working-area (see Fig. 15). Minimal water depths of up to 2700 m occurred above seamounts.

Despite the prominent seamounts in each working area or transit, there is very few variation in topography in each area. The depressions which are assumed to be hydrothermal pits are found in area GUATB-01 and GUATB-02 in greater numbers. The seamounts in transit-area GUATB-02_03 have a caldera-like depression on top, which ca clearly be seen in the recorded datasets. The depressions in area GUATB-02 and GUATB-01 are topographic lows in the order of 60 m and 800 m in diameter.

The quality of the MBES-data is good, during preliminary processing onboard SONNE only minor corrections had to be made. Due to similar frequencies and simultaneous use of the Parasound-System and the MBES, erroneous pings with significantly lower or higher water depth occur. These have to be flagged-out during post-processing. The sound-velocity profile obtained from a CTD measurement (see Fig. 16) fits well even to the outer beams so no outer beams had to be removed routinely.

Table 4: Overview about Parasound and bathymetry (Kongsberg Simrad EM120) profiles.

Parasound and Simrad profiles without seismics								
Profile	Date	Start UTC	Position Latitude	Longitude	Date	End UTC	Position Latitude	Longitude
HF1031	2010/06/27	04:32:17	7° 58.7706'	-90° 34.5306'	2010/06/27	06:43:10	7° 55.2588'	-90° 29.5380'
GUATB-06	2010/06/28	01:18:57	7° 58.4568'	-90° 34.2288'	2010/06/28	17:49:00	7° 12.5130'	-91° 20.3292'
HF1033	2010/06/29	12:33:17	7° 13.5432'	-91° 28.0602'	2010/06/29	16:13:32	7° 15.3012'	-91° 25.8522'
GUATB-23	2010/07/02	18:22:24	7° 15.0858'	-91° 26.1036'	2010/07/03	17:32:29	6° 40.2726'	-91° 54.1170'
GUATB-30	2010/07/05	20:00:01	6° 39.7356'	-91° 53.0046'	2010/07/06	00:39:42	7° 01.5816'	-91° 31.6356'
GUATB-31	2010/07/08	01:47:19	7° 21.2940'	-91° 23.8548'	2010/07/08	16:31:23	7° 58.0650'	-90° 36.8238'
GUATB-40	2010/07/11	12:32:54	7° 50.9850'	-90° 28.8384'	2010/07/11	15:47:47	7° 2.86740'	-90° 22.9746'

Table 5: Statistics of the bathymetry survey.

Mapped Area (km²)	5657	5656.96
Number of Profiles (w/o Seismics)	11 (6)	
Number of Working Areas	5	
Median Depth	3600	
Min Depth	2769	
Max Depth	4005	
Region (W/E/S/N)	-92.2195/-90.2822/6.2479/8.1696	
Total Number of Soundings	6562311	

Tab. XX Statistics on Bathymetry Dataset

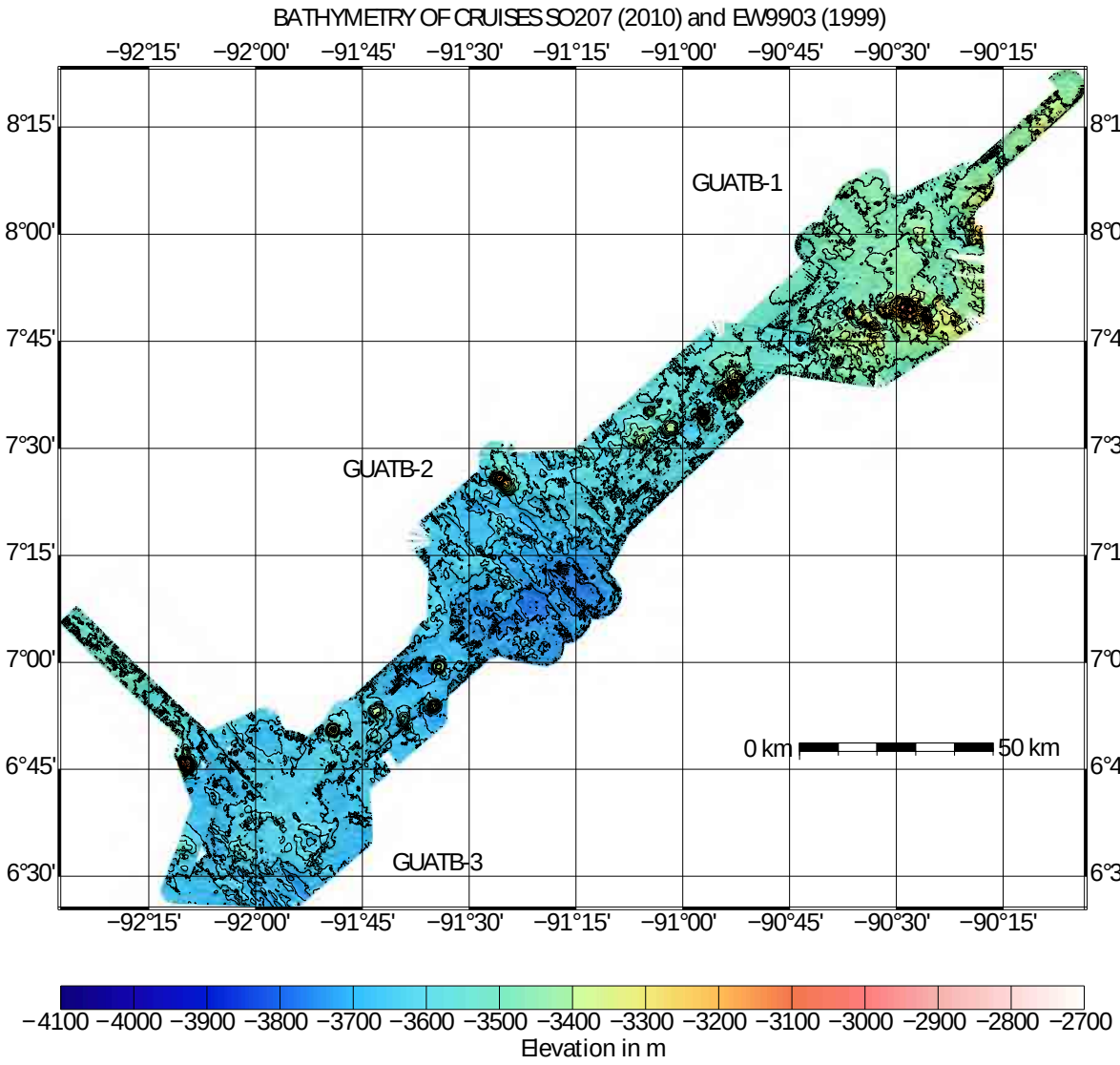

Figure 15: Plot showing the whole area mapped including the old data from cruise EW9903 and our new data from SO207.

5.2 Seismic and Parasound Survey

(H. Villinger)

The goal of the seismic survey was twofold: on the one hand, it is important to map the basement in detail in the investigation area to be able to determine sediment thickness for the interpretation of heat flow measurements, on the other hand, we wanted to map the shape and sediment fill of the pits. Parasound and swath bathymetry (Simrad EM120) were always run in parallel during seismic surveys.

The seismic records are in general all very good and allow to map the mostly smooth sediment-basement interface in great detail. Fig. 17 (GUATB02) shows an example. In addition to our seismic profiles, we can use the published data from the site survey for Site 1256 (Wilson et al.,

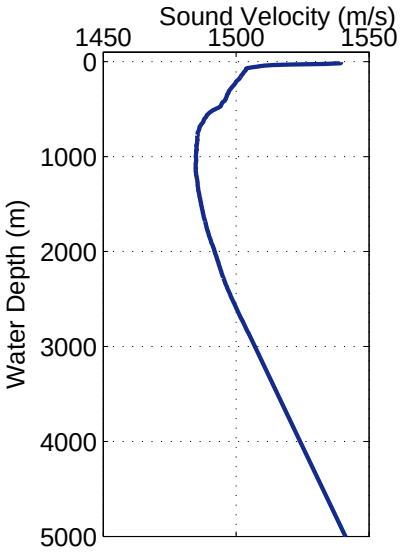

Figure 16: Sound velocity profile obtained with a CTD measurement and used for the bathymetry survey.

2003a) to generate a very detailed picture of basement topography in the three working areas. All seismic and Parasound profiles run during the cruise are listed in Table 14 and 4 respectively. The location of the profiles can be found in Fig. 63 to Fig. 65 (see Appendix, section A.2).

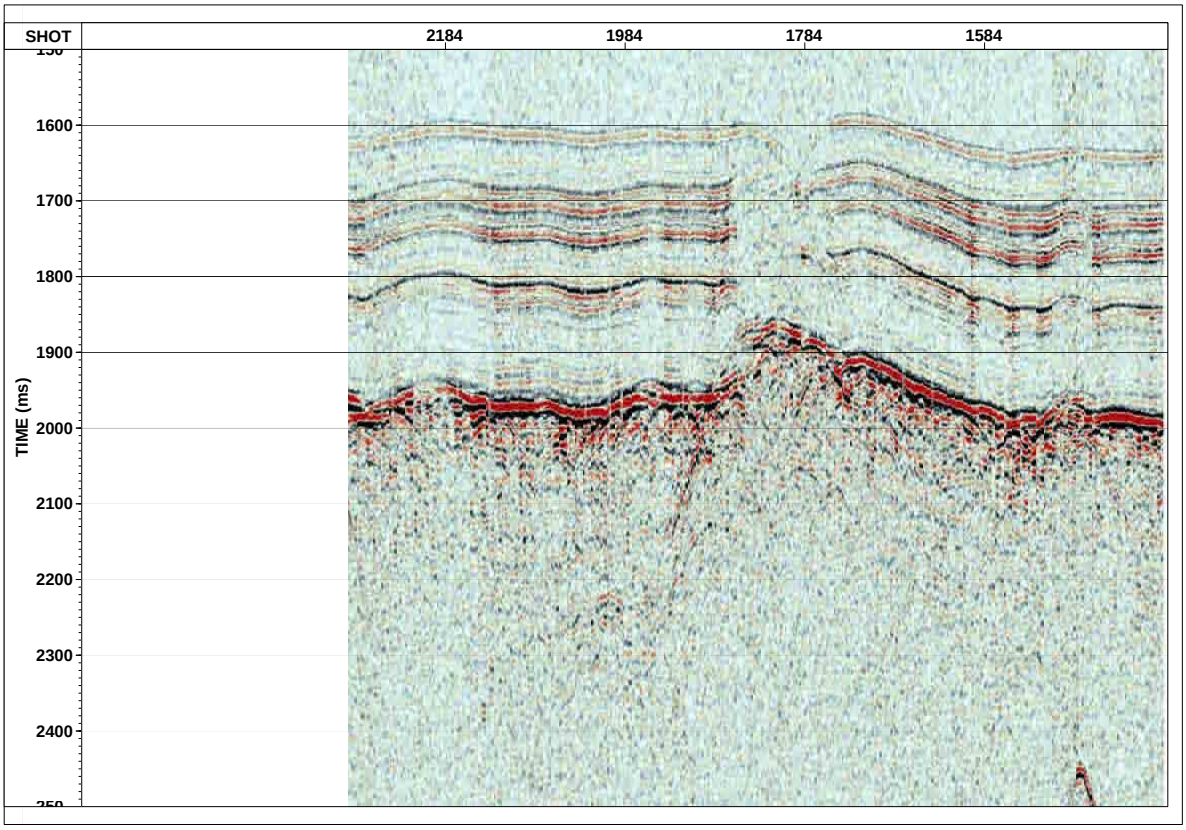

Figure 17: Seismic profile GUATB02 in working area GUATB-1. 200 shots are equivalent to 3.2 km.

To facilitate the interpretation of the seismic records we shot a line (GUATB04) across ODP Site 844 (FFN 4200). In this way we can interpret the reflection pattern we see in terms of lithostratigraphy but also assign ages to the different horizons. This is especially important for the interpretation of the records across the pits. Fig. 18 shows the profile across the location of ODP Site 844. One can clearly identify three sediment packages with the help of the lithostratigraphy of Site 844 (Mayer et al., 1992). The top (0 - 90 ms) layers are composed of silicious and clay-rich Plio-Pleistocene sediments which are underlain by nano-fossil oozes (90 - 350 ms) with carbonate content increasing with depth. Within this unit a band of reflectors from 230 - 280 ms is caused by diatom and clay rich layers. Basement is reached at 350 ms which is according to 844 at a depth of 290 $mbsf$. A detailed velocity profile in (Mayer et al., 1992) allows identifying each of the reflectors seen in our records and converting two-way-travel time to depth. This general reflection pattern was also found in working area GUATB-3, where we could not run a seismic profile across ODP Site 1256 due to time constraints. As seismic profile GUATB24 starts only about 8 km away from Site 1256 and as we can tie in our lines with the EW-profiles (Wilson et al., 2003a) shot in area GUATB-3 the lithostratigraphic interpretation of our profiles is possible.

Seismic line GUATB05 (Fig. 19) shows the image of a pit. The small diameter and the steep boundaries on each side create strong diffractions which may be minimized after migrating the profile. In this way and in combination with Parasound we hope to image the details of the sediment fill and thus determine which part of the sedimentary sequence is missing in a pit.

Parasound records are in general very good and reach a penetration of up to almost 200 m (Fig. 20). It was always run in parallel to seismic surveys and therefore can be used when interpreting the seismic data. In a few cases Parasound even imaged basement. Parasound data were logged during the whole cruise, even when on station, so interesting sections can be reprocessed on shore either using the SEGY-formatted data and VISTA or SeNT.

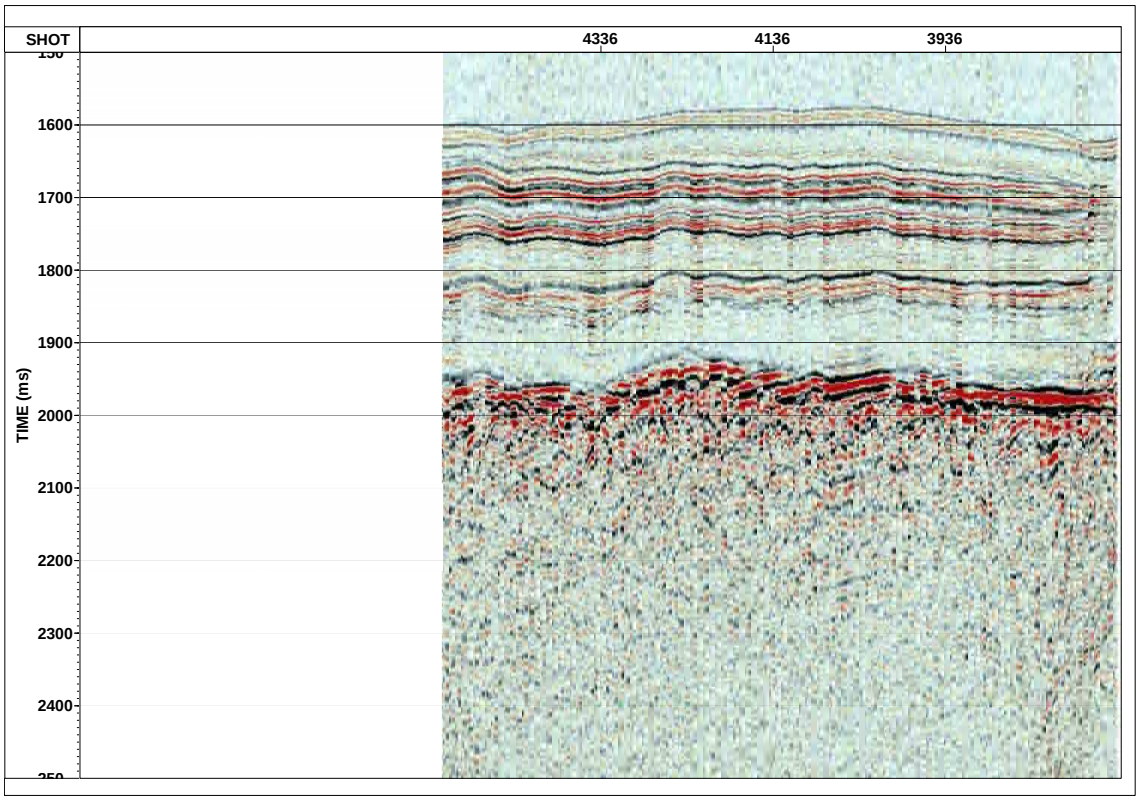

Figure 18: Seismic Profile (GUATB04) across the location of ODP Site 844 (FFN 4200). 200 shots are equivalent to 3.2 km.

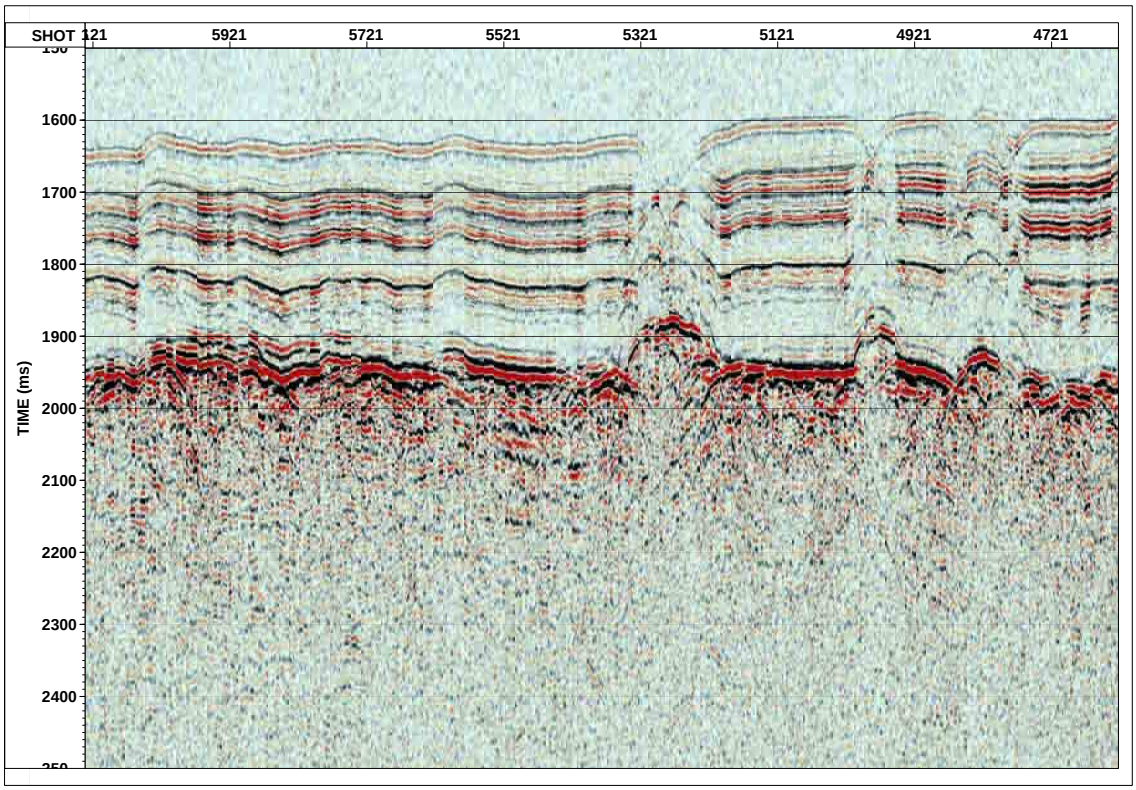

Figure 19: Seismic image of a pit (Profile GUATB05). 200 shots are equivalent to 3.2 km.

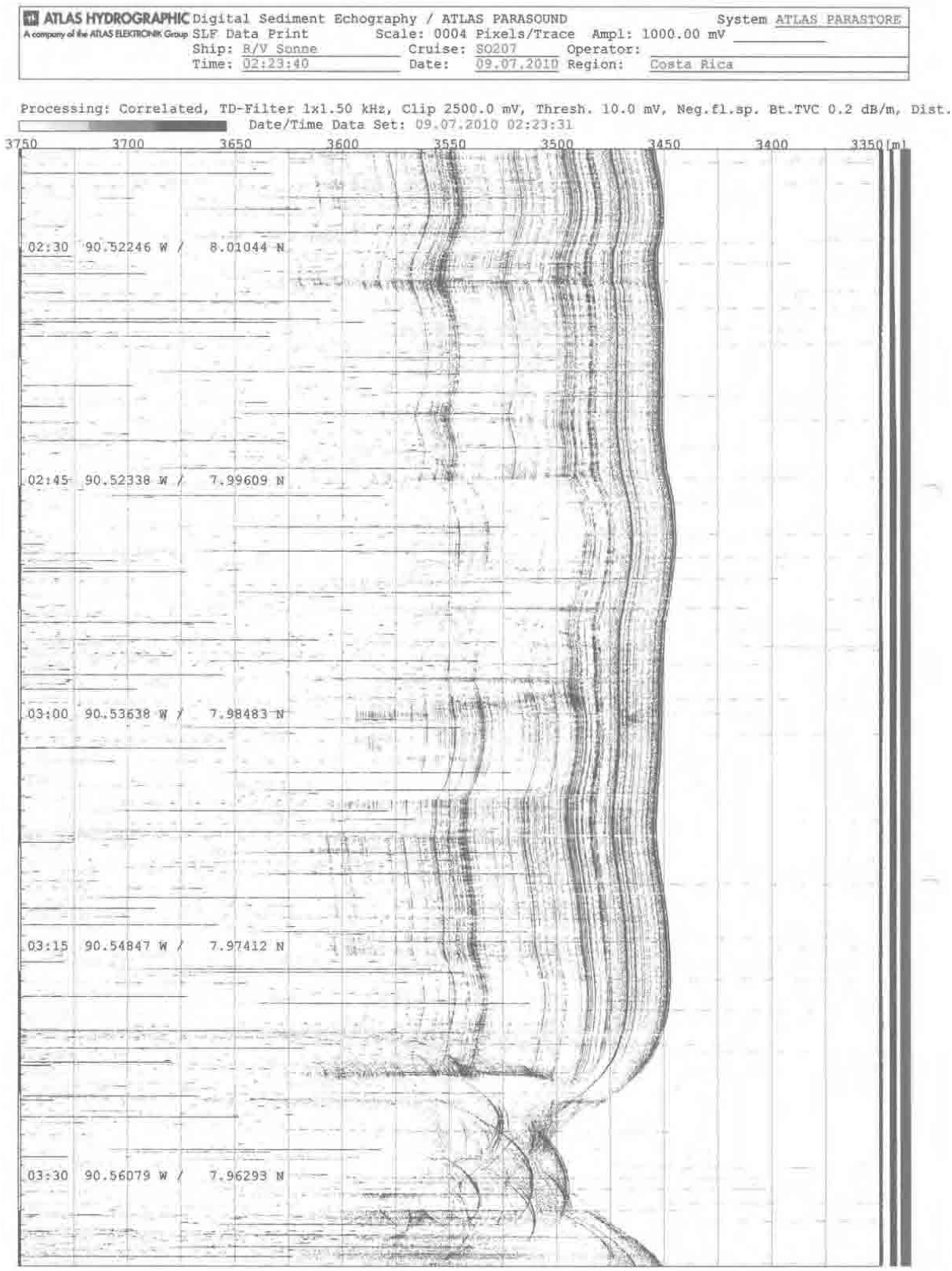

Figure 20: Parasound record in working area GUATB-1 on seismic line GUATB33, perpendicular to GUATB05 and thus showing the same hydrothermal pit. At a speed of 4 *kn*, 15 minutes are equivalent to one nautical mile or 1.852 km.

5.3 Heat Flow

(H. Villinger)

Heat flow measurements around and within pits will be used to characterize the thermal state and identify locations of possible advective fluid transport within the sediment column. Heat flow profiles are located on seismic lines if possible to be able to have basement depth for interpretation of the data. Measurements outside of the pits were meant to establish the background heat flow. If a seamount was located close to pits we tried to measure heat flow close to the base of the seamount in order to see if it is the location of downward flow of seawater into the basement. One profile towards a very nicely circular shaped seamount with no obvious pits associated with it was measured to assess the thermal signature of it. The results of each profile are tabulated and the location of the measurements is shown on one or several maps. In addition the heat flow is plotted vs. distance to show the variation within a profile. All heat flow measurements will be interpreted in conjunction with the seismic results. This includes a correlation of sediment thickness with heat flow.

All heat flow measurements were made with the Bremen 6 m long heat probe. Due to the very soft nature of the sediments we almost always got full penetration (5.46 m) and used the same sensor string for the whole cruise. All results including locations can be found in Tab. 15 to 23 (see Appendix section A.3). In the beginning of the cruise (profiles HF1030 to HF1032 with the exception of HF1031) the heat probe was run on the coax-wire so we had data in real-time during the surveys (Tab. 6). Continuing problems with the termination of the coax-wire forced us to use the 18mm-od-coring wire for the rest of the cruise and therefore the probe was run in autonomous mode. Also precise positioning of the heat probe was possible during stations HF1030 and HF1032 using the ship s Posidonia positioning system by attaching a pinger to the wire 100 m above the probe. For these stations with no precise positioning of the probe a varying offset for each profile (Tab. 6) was applied based on the course and on results from stations where we had Posidonia positions. Due to the prevailing wind and current conditions we run most of the profiles from NW to SE as this course made station keeping easier for the ship. Measurements on one complete profile (HF1031) failed as the pressure case of the heat probe was flooded and all data were lost. The electronics could not be repaired on board and therefore we had to use the spare set of electronics.

We made 140 measurements in total with 44 in situ determinations of thermal conductivity. Fig. 21 shows a histogram of all gradients and measured in situ thermal conductivities. Heat flow varies over a range from 3.2 to 304 mW/m^2 with exceptional small heat flow values close to a seamount in working area GUATB-2. Fig. 22 shows such a measurement. The highest value was measured inside a pit with 304 mW/m^2 in working area GUATB-1. Thermal conductivity is remarkably uniform with 0.78 W/mK as mean and almost identical in all three working areas. Therefore we did not measure in situ thermal conductivity at all penetration in order to save

Table 6: Overview about the heat flow profiles run during cruise SO207.

Profile	Date	Working Area	Short Description	Positioning	Mode
HF1030	24/25/26/27.6.	GUATB 1	Profile over a series of Pits	Posidonia	real-time
HF1031	27.6.	GUATB 1	no data, electronics broken	Posidonia	autonomous
HF1032	29/30.6./1.7.	GUATB 2	Profile over a series of Pits	Posidonia	real-time
HF1033	2.7.	GUATB 2	Profile over Pit	Offset,108m ESE	autonomous
HF1034	4/5.7.	GUATB 3	Profile over Pit and Ridge	Offset,300m ESE	autonomous
HF1035	6.7.	Transit GUATB 3 - 2	Profile to Donut Seamount	Offset,108m ESE	autonomous
HF1036	7.7.	GUATB 2	Profile over Ridges and Troughs	Offset,108m ESE	autonomous
HF1037	7/8.7.	GUATB 2	Profile from Seamount	Offset,106m NW	autonomous
HF1038	9/10.7.	GUATB 1	Profile over Pit	Offset,108m ESE	autonomous
HF1039	10/11.7.	GUATB 1	Profile to Seamount	Offset,108m ESE	autonomous

time. Only within the seamount crater, in situ thermal conductivity was significantly higher with 0.86 W/mK. At some locations, preferably in pits, gravity cores are co-located with heat flow measurements to assess possible advective flow by analyzing pore water geochemistry.

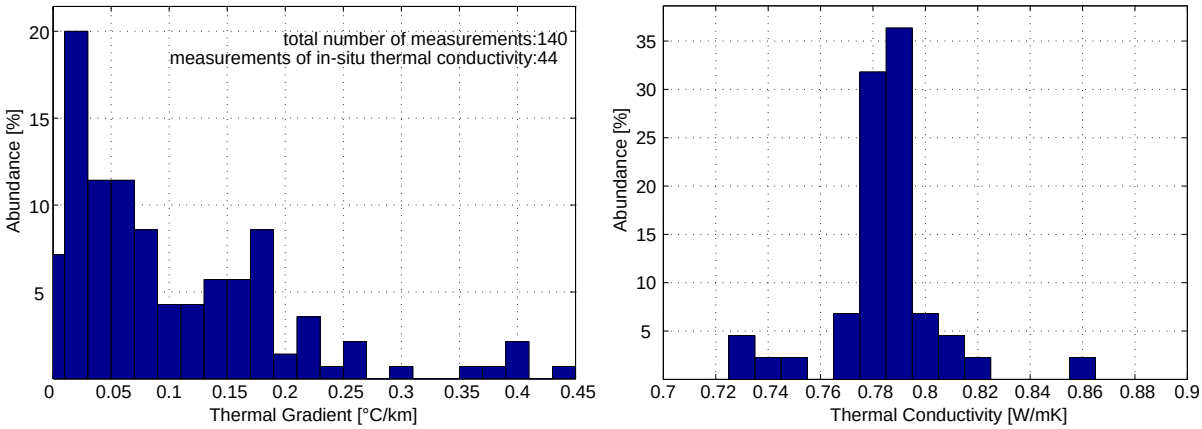

Figure 21: Histograms showing percent of measurements against temperature gradient and thermal conductivity.

5.4 Thermal Conductivity on Cores

(H. Villinger)

The thermal conductivities, measured on split core sections are shown in Fig. 130 to 133 (see Appendix section A.4). A histogram (see Fig. 23) of all measurements shows that the thermal conductivity in all working areas is very uniform with a mean value of 0.68 W/mK (s = 0.04 W/mK) and a median value of 0.67 W/mK. Absolute errors of the measurements are about 5% according to the KD2pro manual which is on the order of ± 0.034 W/mK based on the mean. This is almost exactly the standard deviation of all measurements. The thermal conductivity is remarkable low and points to a very high porosity also reported in the results of physical property measurements from Site 844 (Mayer et al., 1992) and Site 1256 (Wilson et al., 2003b; Teagle et al., 2006b) where porosities in the upper 10 $mbsf$ vary between 85 and 90%. Thermal conductivities on cores from Site 1256 with a value of ~ 0.7 W/mK confirm our measurements on

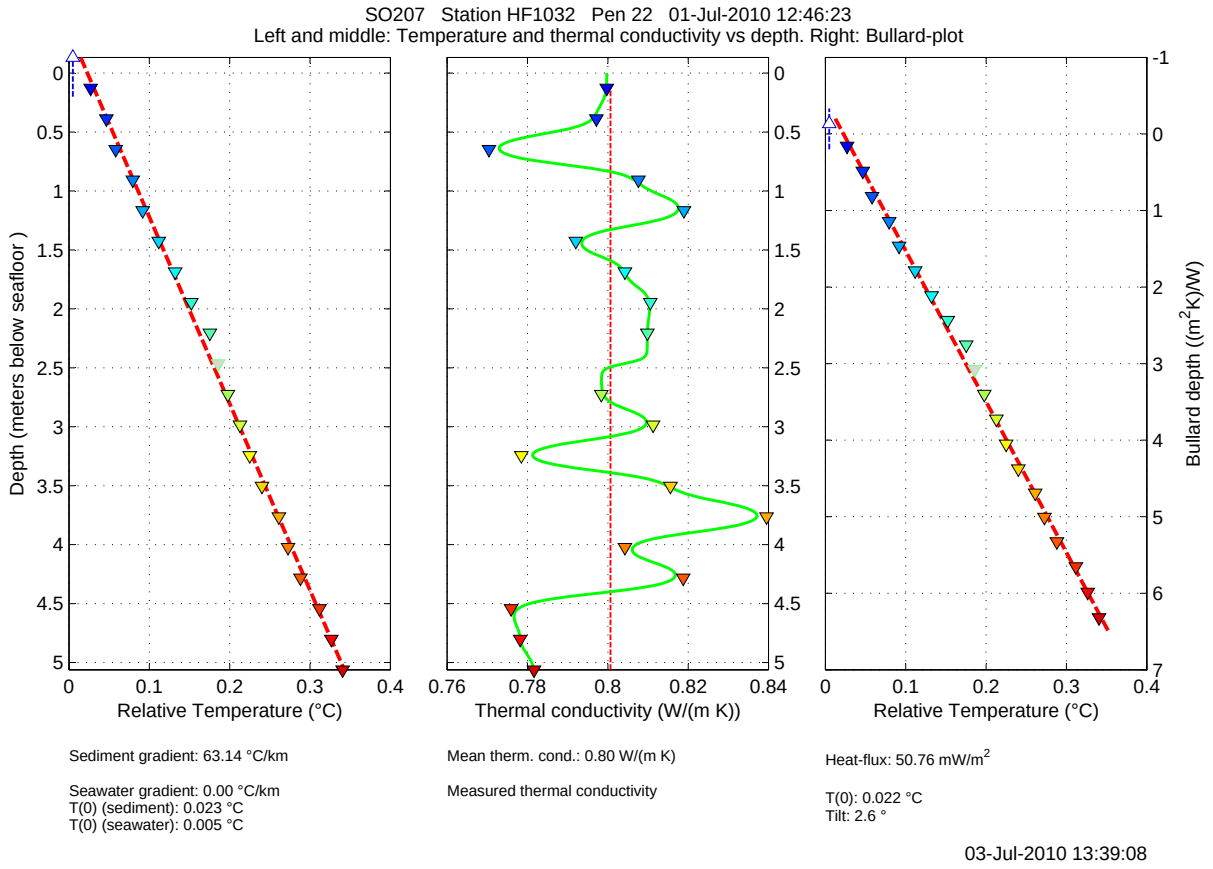

Figure 22: Low values of heat flow were measured near a seamount in working area GUATB-2.

cores. These values will increase by a few percent once they are corrected for in situ conditions. In some of the profiles (e.g. GeoB14603 or GeoB14610) thermal conductivities increase slightly with depth due to a decrease in porosity. High values for example in GeoB14608 are attributed to layers of calcium carbonate.

5.5 LIRmeter

(S. Stephan)

An autonomously operating data logger for acceleration measurements (LIRmeter II, Fig. 13) was mounted in the Bremen Heat Flow Lance on almost all Heat Flow profiles. A second system (LIRmeter I) was mounted on the deep-sea wire to investigate its behavior. A complete list, where acceleration measurements are available, is shown in Tab. 7.

Fig. 24 shows a penetration (HF1038-08) and data from LIRmeter II. The contact of the lance with the seafloor is marked with a sharp rise in acceleration, the end of penetration is characterized by a flat signal around 0 m/s^2. Sensor offsets and the effect of gravitation have already been removed from the data shown here. The timespan between the mentioned events

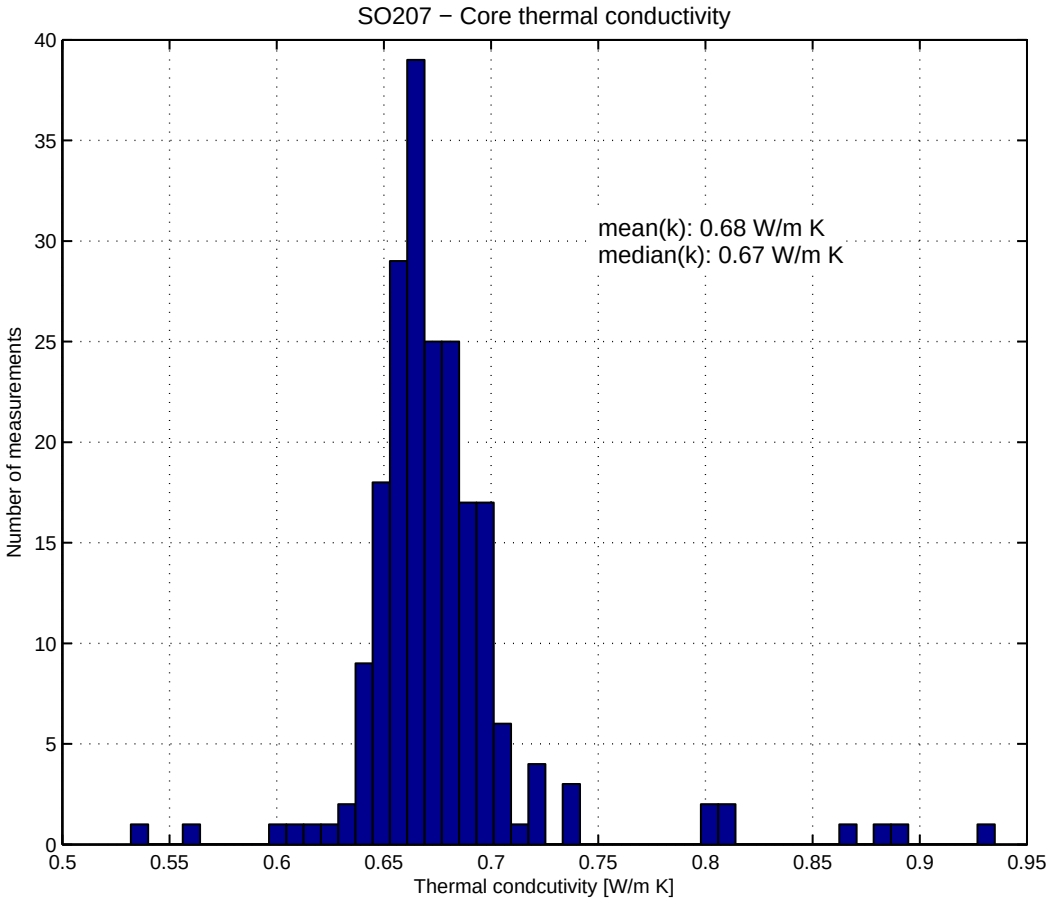

Figure 23: Histogram of measurements showing a uniform picture of thermal conductivity in all working areas.

characterizes the penetration of the lance into the sea floor. The duration is approximately 8 seconds. The high-frequency oscillations at the end of the penetration are caused by the impact of the deep sea wire and its termination on the lance. Further processing of the acceleration data will lead to penetration velocity and penetration distance. Plotting distance versus acceleration is an indication for harder or softer layers in the sea floor.

Table 7: Overview about the profiles measured with LIRmeter I and II.

Profile	Stations	Stations	Start		End	
	LIRmeter I	LIRmeter II	Latitude	Longitude	Latitude	Longitude
HF1030	01 - 11		07 53.6037	-90 29.5214	07 56.4383	-90 32.2718
HF1031	01 - 06	01 - 06	07 55.278	-90 29.562	07 52.489	-90 29.566
HF1032		01 - 09	07 16.0354	-91 15.5233	07 16.3216	-91 19.2613
HF1033	01 - 03	01 - 13	07 14.819	-91 26.532	07 14.4267	-91 26.8433
HF1034	11 - 21	11 - 21	06 37.435	-91 55.469	06 34.843	-91 58.417
HF1035		01 - 12	07 01.610	-91 31.865	06 59.433	-91 34.292
HF1036		01 - 08	07 13.881	-91 19.067	07 11.472	-91 21.774
HF1037		01 - 16	07 23.2719	-91 25.6746	07 19.3657	-91 22.0958
HF1038		01 - 11	07 58.6484	-90 32.5608	07 57.1076	-90 34.2982

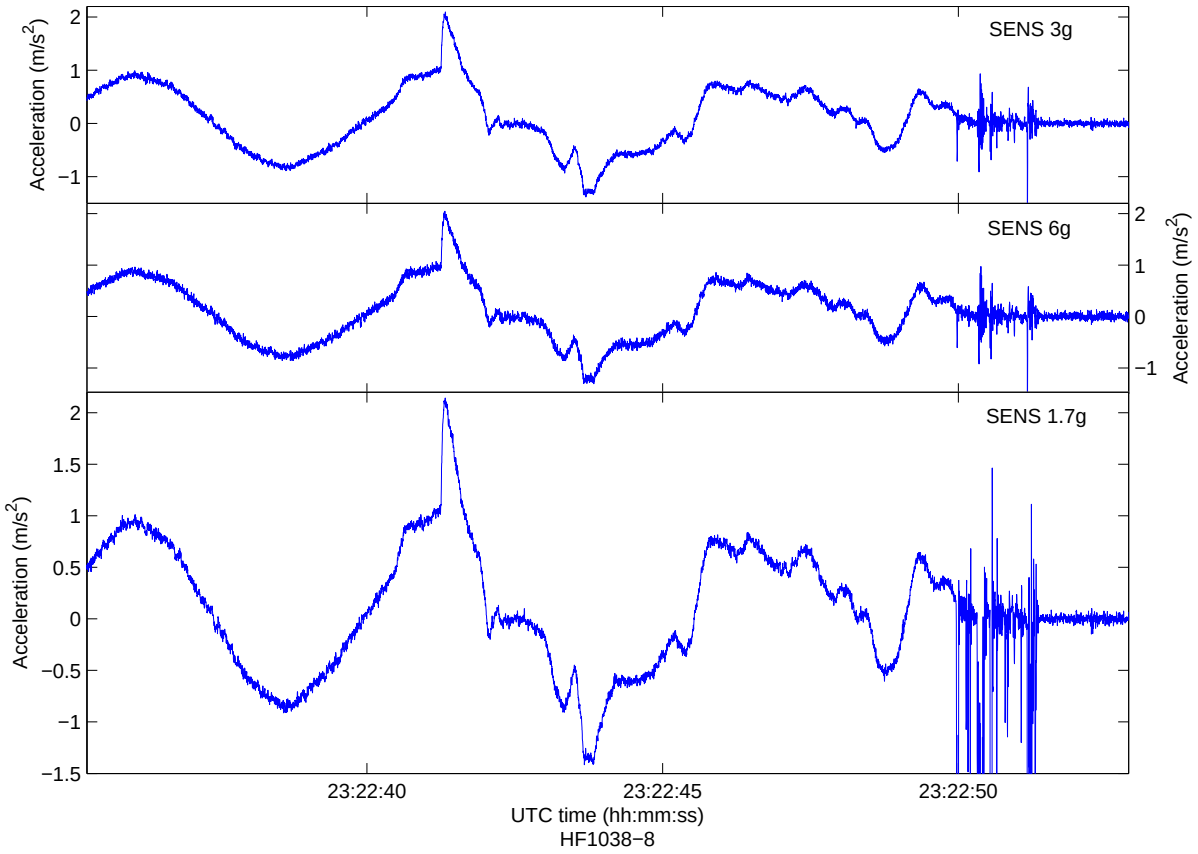

Figure 24: Data Example from LIRmeter II.

5.6 Working Area GUATB-1

5.6.1 Heat Flow

(H. Villinger)

The bathymetry and the existing seismic records of working area GUATB-1 show a number of pits aligned on a profile perpendicular to the flow line. Station HF1030 (co-located with seismic line GUATB05) with 22 measurements was exploratory in nature as we wanted to map the heat flow variations within the numerous pits along this profile. The location of the measurements and the results can be found in Table 15 (see Appendix section A.3) and Fig. 25. The profile started close to a seamount in the southeast with low values around 20 mW/m^2 reflecting the inflow of cold seawater into the upper crust at the seamount. Background values between pits increase continuously towards the western end of station HF1030 and reach a value of over 100 mW/m^2. Superimposed on this trend are higher values measured in the pits with an increasing amplitude reaching a maximum value of 304 mW/m^2 (see Fig. 28).

Station HF1038 (co-located on seismic line GUATB33, Tab. 16 and Fig. 26) is a detailed heat flow map of the westernmost pit where we found the highest values (Fig. 29).

Station HF1039 (co-located on seismic line GUATB37, Tab. 17 and Fig. 27) runs from the ODP Site 844 towards the seamount to the south of the drilling location. With this profile we want to establish the hydrogeological signal of the seamount. Measurements on HF1030 near the seamount show low heat flow values already (see Fig. 30).

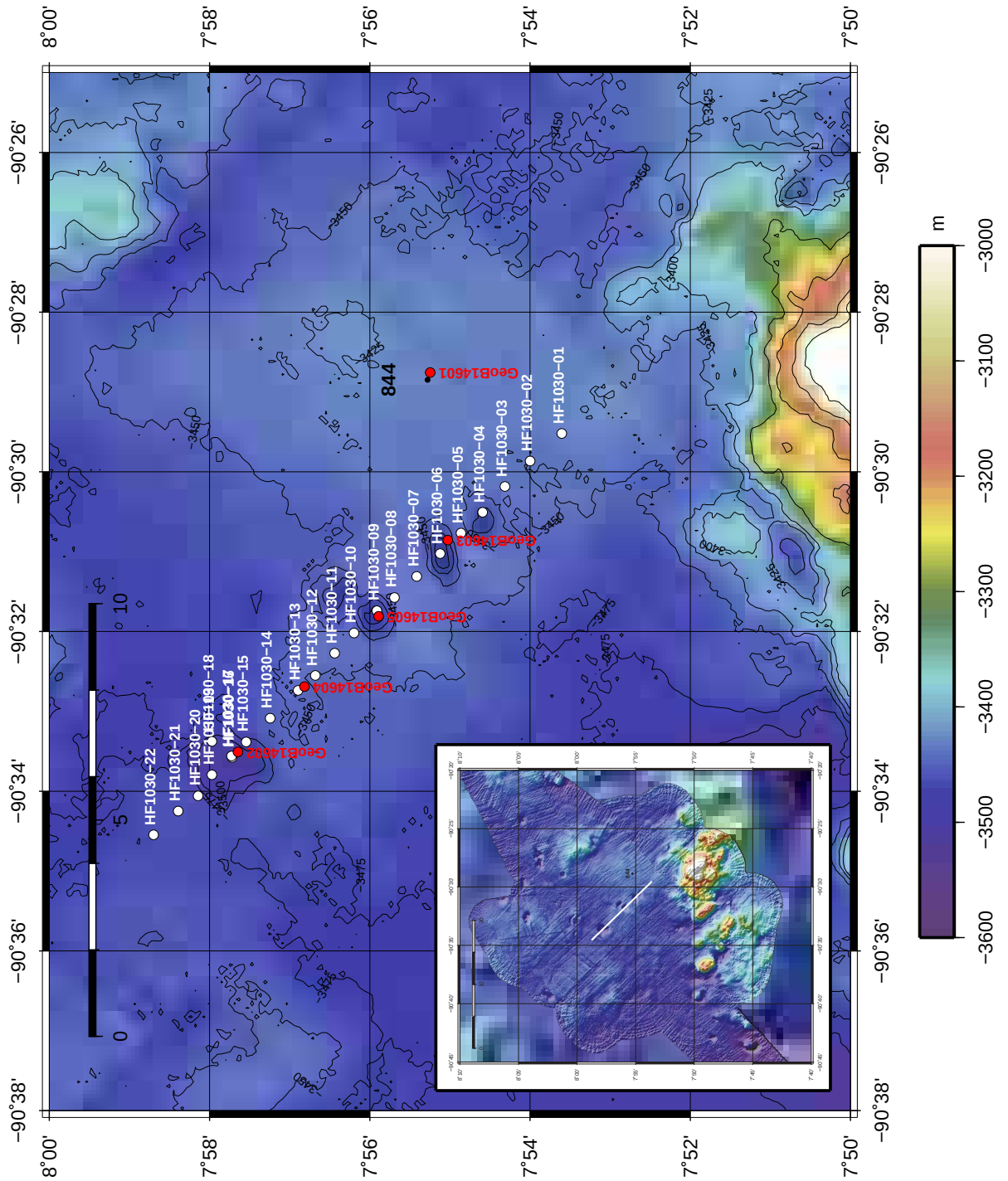

Figure 25: Location of penetrations with the heat flow probe on profile HF1030 (white filled circles) and core positions as red filled circles. The inset shows an overview about working area GUATB-1 with the heat flow profile in white.

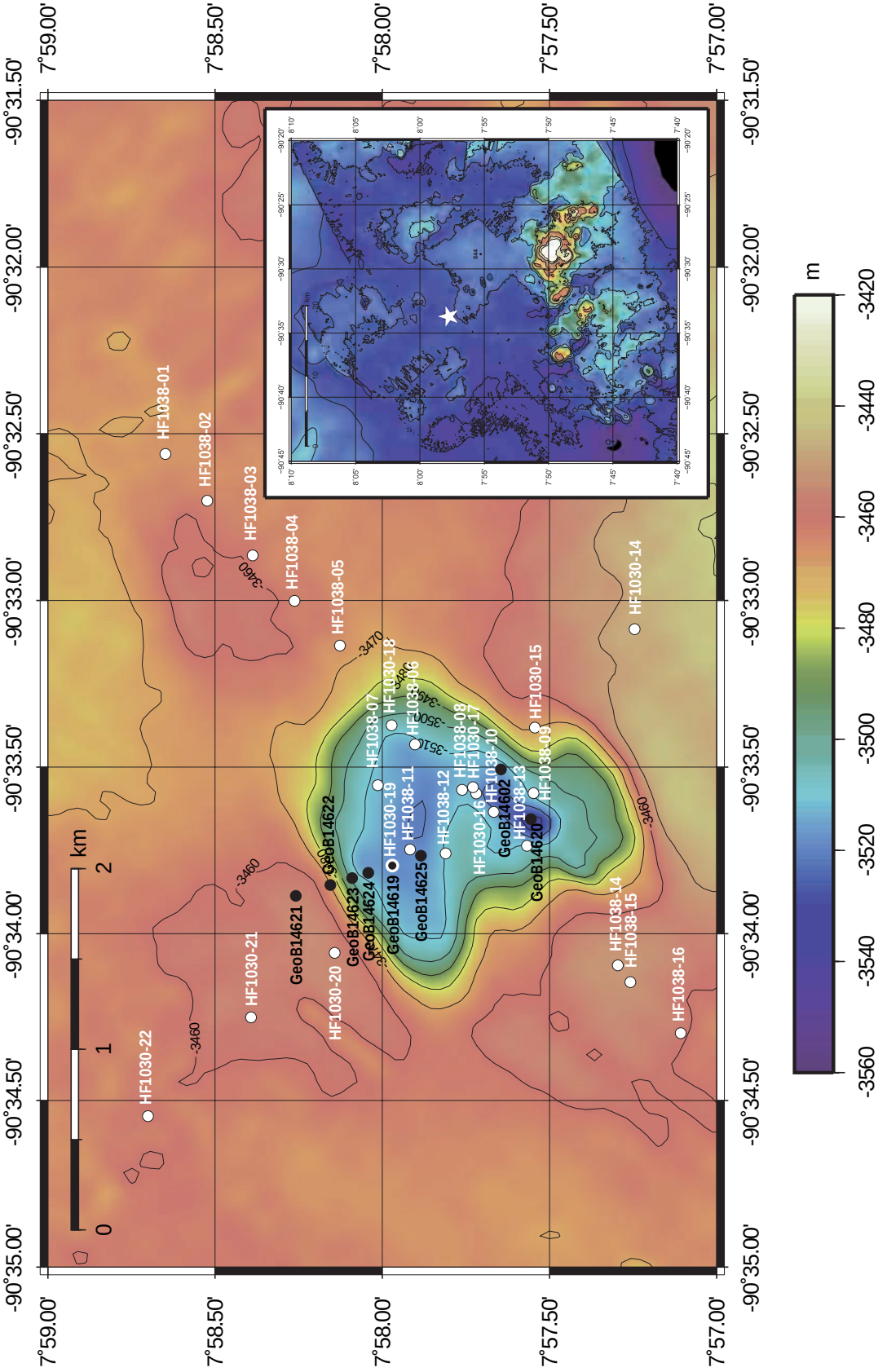

Figure 26: Location of penetrations with the heat flow probe on profile HF1038 (white filled circles) and core positions as black filled circles. The location of the pit is marked as a white star in the overview map.

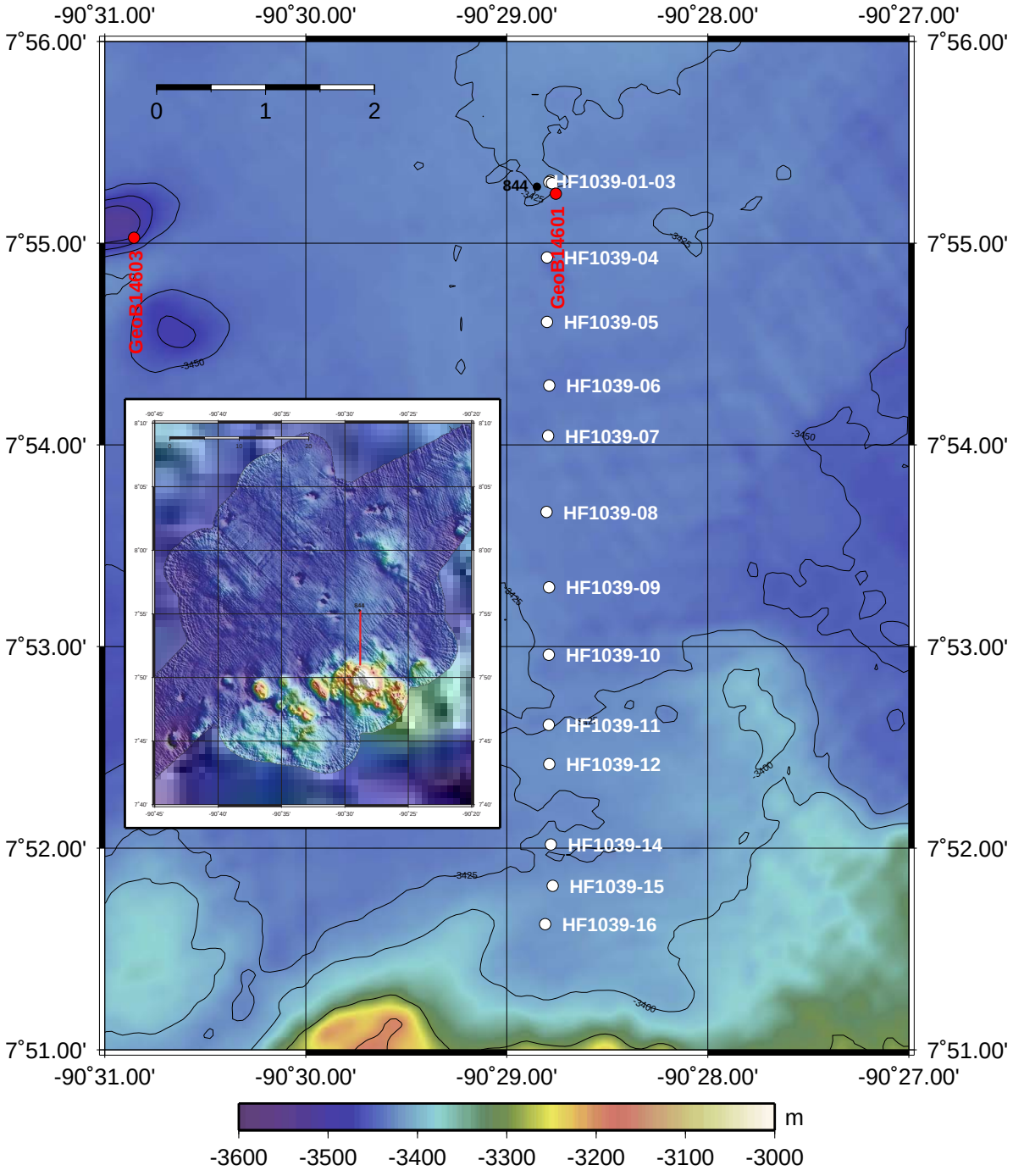

Figure 27: Location of penetrations with the heat flow probe on profile HF1039 (white filled circles) and core positions as red filled circles. The inset shows an overview about working area GUATB-1 with the heat flow profile in red.

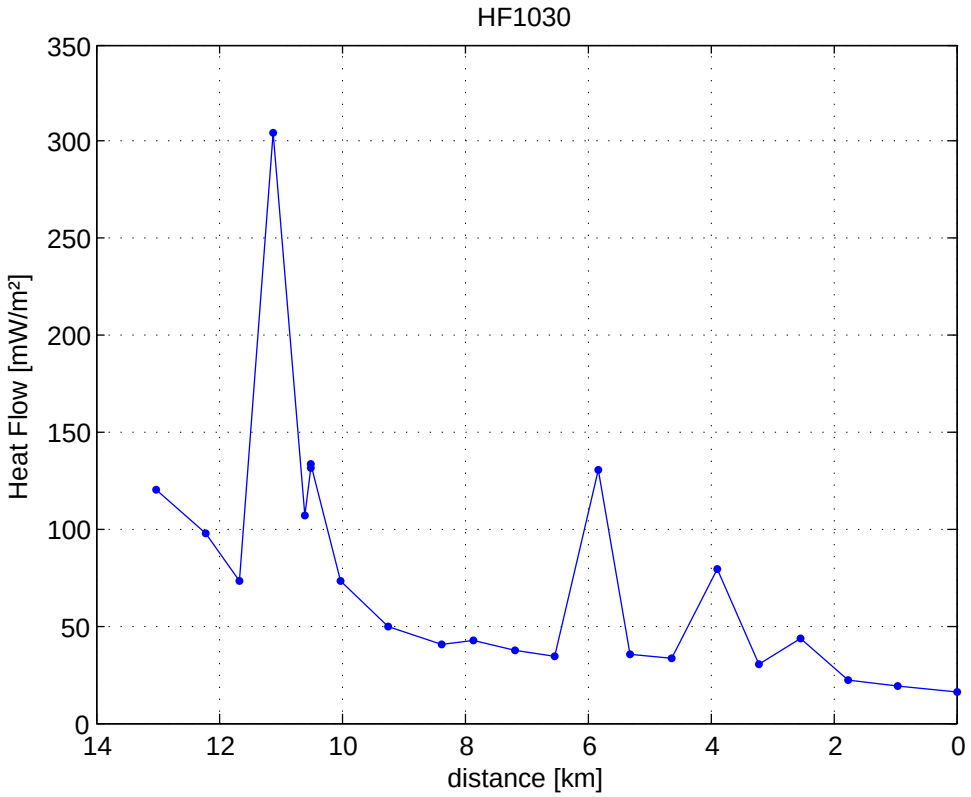

Figure 28: Heat flow values of profile HF1030 vs distance from the first penetration of the profile.

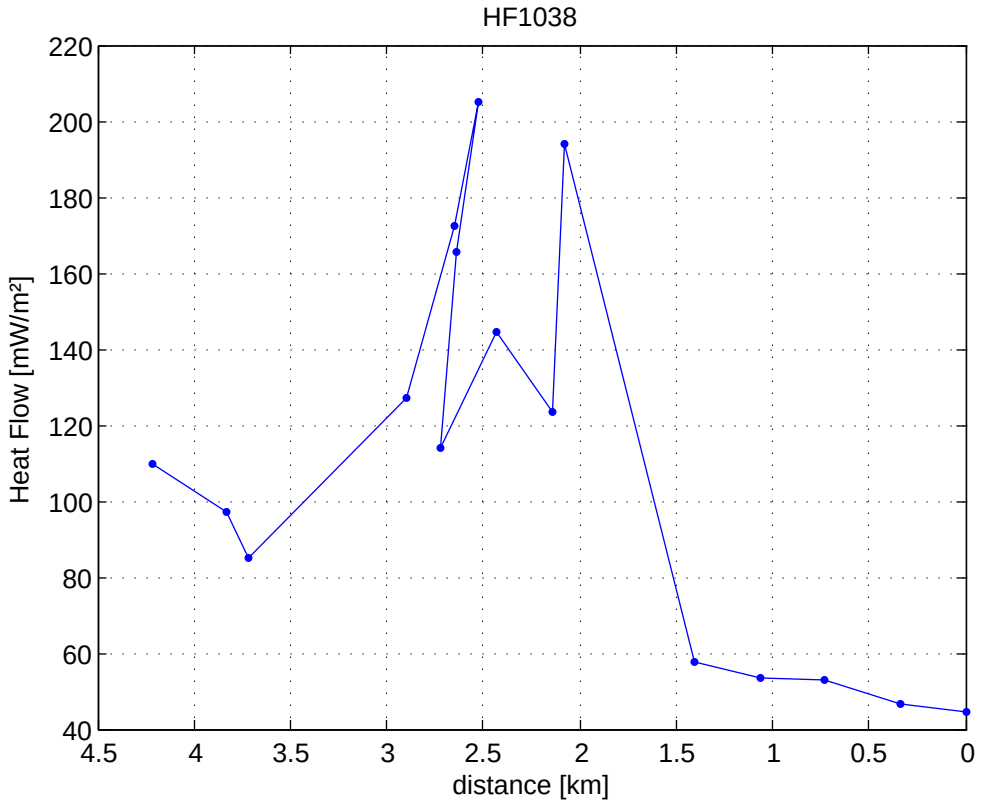

Figure 29: Heat flow values of profile HF1038 vs distance from the first penetration of the profile.

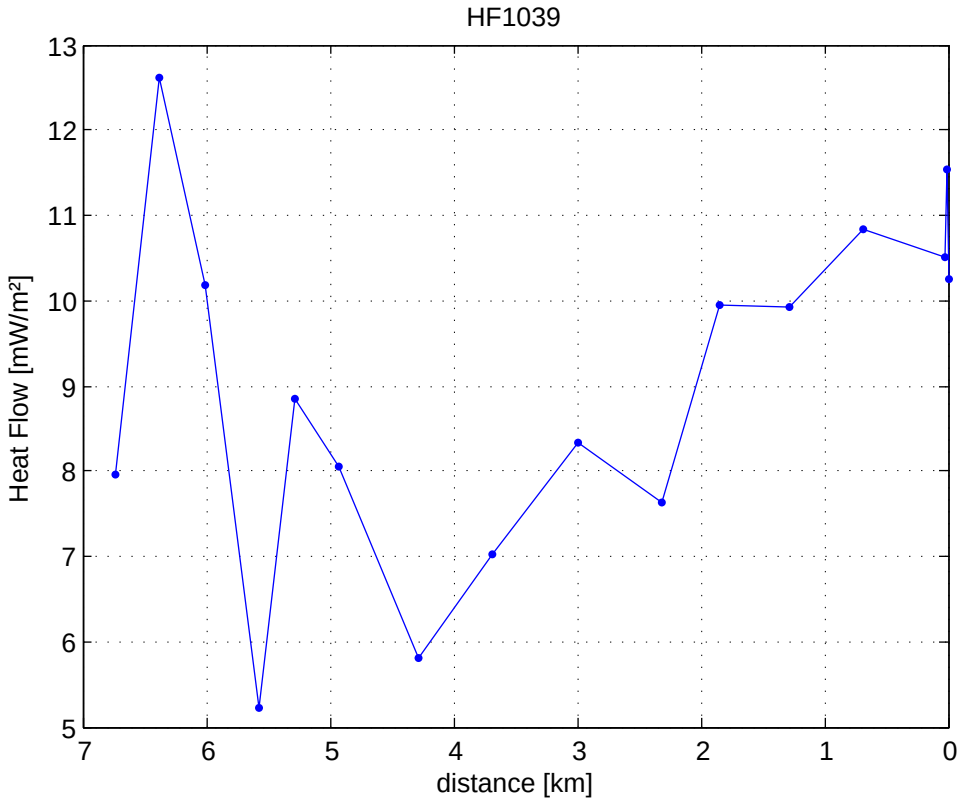

Figure 30: Heat flow values of profile HF1039 vs distance from the first penetration of the profile.

5.6.2 Sediment sampling and core description

(P. Alt-Epping, R. Becke, K. Enneking, T. Fleischmann, K. Gaida, C. Janssen, T. Pichler, M. Ruiz and M. Zwick)

In this working area, 12 cores were taken (Table 8). The strategy was to obtain a general overview by taking cores GeoB14601, 14602, 14603, 14604, 14605 and 14619 from inside and outside the pits (Fig. 25). These cores underwent the complete geochemical program. In addition cores GeoB14620, 14621, 14622, 14623, 14624 and 14625 were taken closely spaced across the transition from pit to normal seafloor (Fig. 31). An exact listing of each core location is given in Table 8.

To obtain further information about the surface sediments in the pit where core GeoB14605 was taken the micro coring device (MIC) was deployed and successfully retrieved with two of the four possible coring tubes filled with approximately 40 *cm* sediment and 20 *cm* seawater.

In summary the lithology of cores in GUATB-1 was chiefly comprised of slightly to extensively bioturbated clayey nannofossil ooze and nannofossil silty clay. Sandy ash was found in several cores. The sediment color varied from dark olive at the top to light olive and grayish at the base. The strong bioturbated sections are much darker. The color of the white clayey sandy ash layers, varied from 10YR8/1 to 10YR8/2.

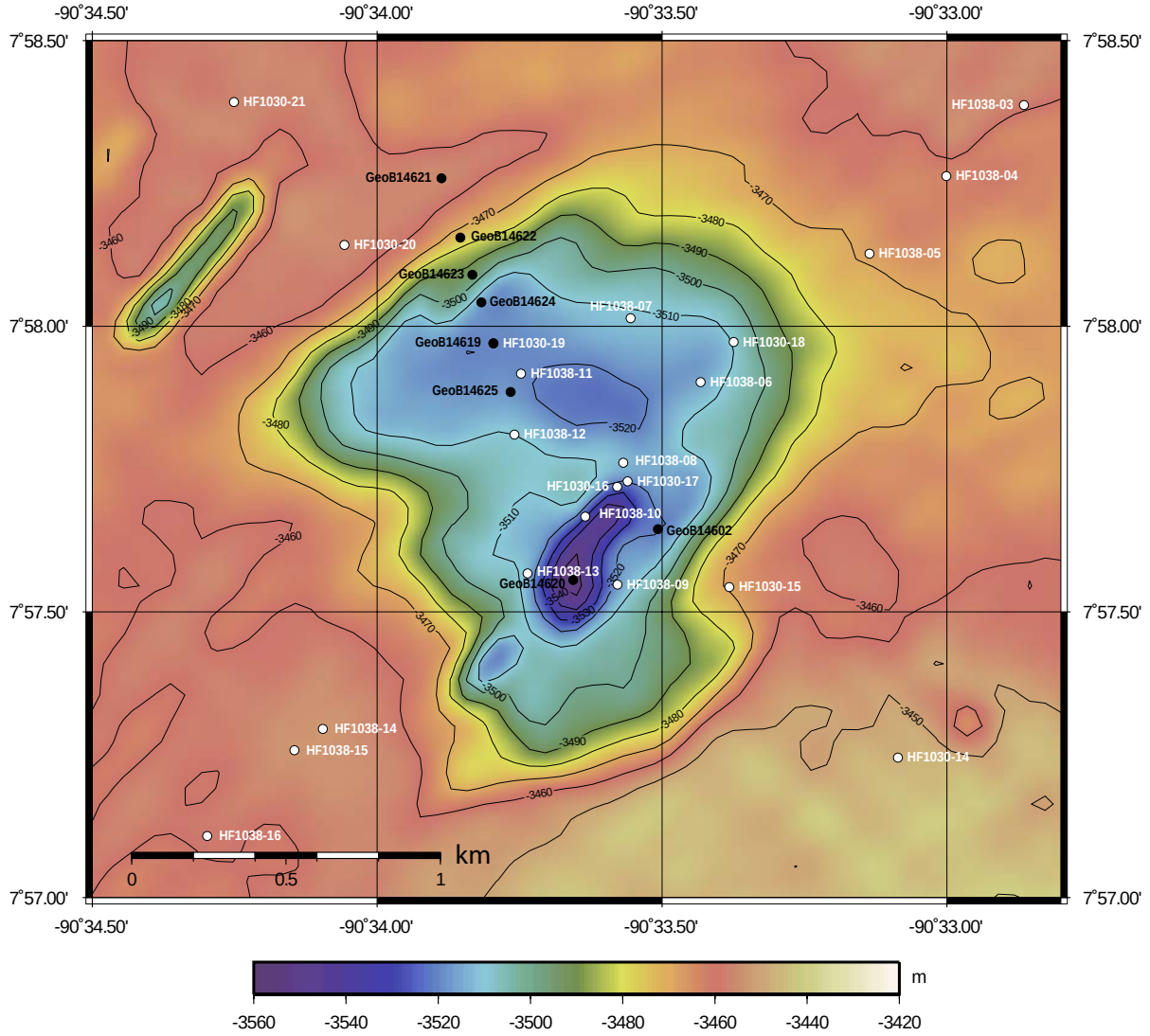

Figure 31: Detailed overview of the sampling positions of cores taken across the transition from pit to normal seafloor in working area GUATB-1. The apparent deep area in the southern part of the pit is a data artifact. The surface sediments collected with the MIC correlated well to the uppermost sediments in core GeoB14605-1 and were not further described.

Detailed core descriptions of individual cores are presented in Appendix (Core Logs) and an overview of all sediment cores which were collected in GUATB-1 and how they compare to cores from other working areas is given in Figure 32.

5.6.3 Geochemistry of pore water

The first core, GeoB14601 was taken outside the pits to be considered as a background or normal seafloor reference for pore water and sedimentological analyses. Eh in the pore waters of this core was immediately below 0 mV and continued to vary with depth between -54.6 and -219 mV. The low Eh was associated with a relatively high concentration of Fe^{2+} and at depths

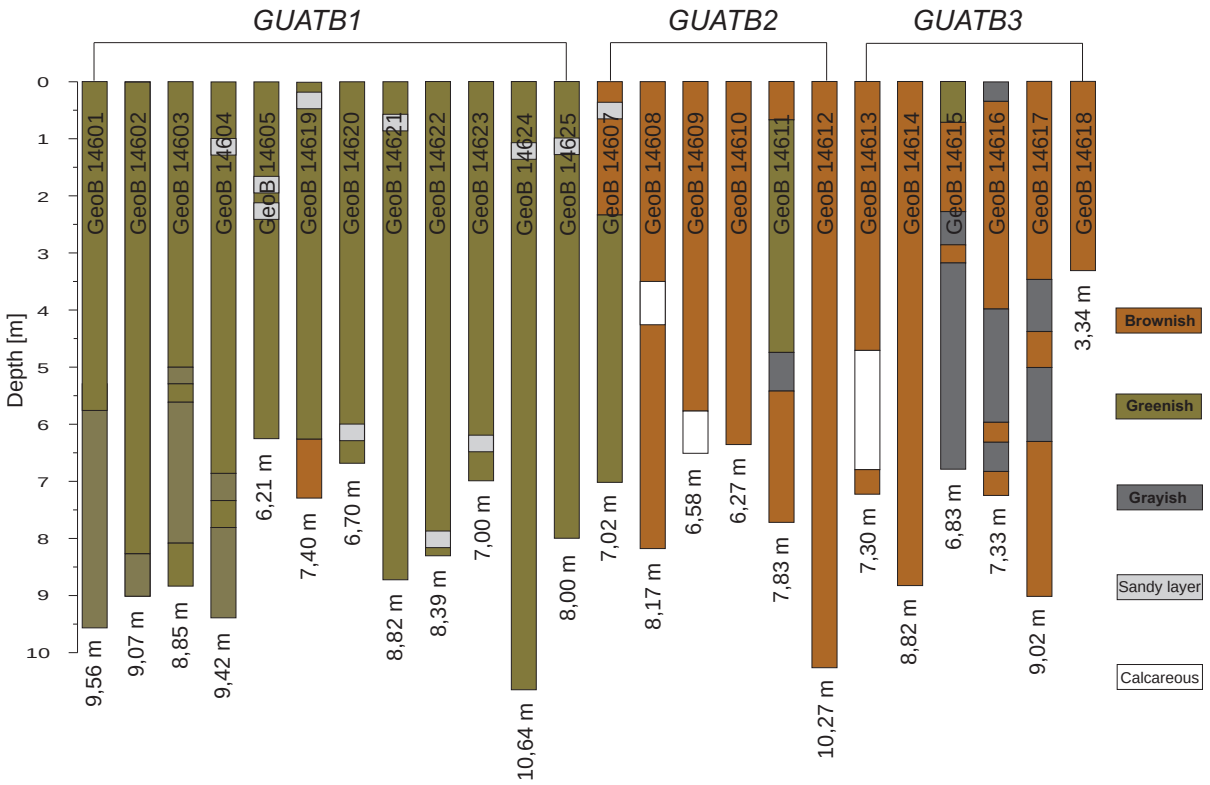

Figure 32: Generalized overview showing mainly color features of all cores taken during the Seamountflux cruise (SO207).

below 2.68 m of NH_4^+. Both elevated Fe^{2+} and NH_4^+ were consistent with reducing conditions. The pH changed from 7.7 to 7.4 with depth and alkalinity remained between 3 to 4 $mmolL^{-1}$, while the PO_4^{3-} concentration was without a clear correlation with depth.

In core GeoB14602, which was taken from the center of a pit the main characteristics remained similar to GeoB14601: the environment was reducing and the fluid was enriched in NH_4^+ (Figure 33). Unfortunately, Fe^{2+} could not be measured. The most distinct feature of the profile was a thin sandy layer, potentially a volcanic ash layer, at shallow depth ($\sim 1.30\ m$). Here the chemical conditions changed from reducing to oxidizing and the pH showed a marked increase to 8.1. It was also observed that within the layer the withdrawal rate of pore water was substantially higher than in the more clayey parts of the core, suggesting a much higher permeability. This may indicate that this sandy layer acts as a conduit for fluids, which have chemical characteristics different from the porewater in the surrounding clay. The high pH and Eh could be interpreted as caused by infiltrating seawater. The alkalinity values fall into the same range as in the previous core, whereas the PO_4^{3-} concentration showed somewhat higher values than in GeoB14601 and a trend of decreasing concentrations with depth.

The porewater profiles in core GeoB14603 were reducing except in the upper 30 cm, which also showed some bioturbation (Figure 33). There was a strong Eh increase in a discrete layer

at 4.9 m. The pH was relatively high throughout the profile ranging from 7.57 to 8.01. The fluid was rich in Fe^{2+} and the NH_4^+ concentration increased to about 0.4 mgL^{-1} below 3.9 m. The alkalinity varied throughout the profile without any clear correlation with depth. In contrast, the PO_4^{3-} content in the fluid generally decreased with depth although displaying some variability.

At location GeoB14604 the sandy layer was found at a depth of 0.96 m, perturbing the otherwise reducing conditions (Figure 33). The Eh within the sandy layer was +145 mV changing sharply to strongly negative values in the over and underlying clayey units. The pH was 8.07 and virtually identical to site GeoB14602. The similar depth and the similarity of the pore water characteristics suggest that the sandy layer is the same stratigraphic unit. In the lower section of the core (6.3 - 7.8 m) the Eh increased again to positive values while the pH remained constant at about 7.6. It appears that this interval constituted another more permeable layer with fluid buffering properties, which were different from those of the sandy layer. In terms of the other chemical constituents measured on board, the pore fluid was consistent with those from the previous cores.

The core GeoB14605 showed multiple occurrences of a sandy layer within the depth interval of 1.81 - 2.37 m (Figure 34). In terms of the porewater chemistry, these sandy units were consistent with those from the previous cores: each layer constituted a discrete horizon with oxidizing conditions, surrounded by clayey units with reducing pore water. Because the distance between individual sand layers was only on the order of tens of centimeters, there is evidence of fluid mixing throughout the interval of 1.81 - 2.37 m. As a consequence, the pH did not show the marked peak as in the previous profiles. One interesting observation was that Fe^{2+} concentrations were lower, in some samples even below detection limit, but NH_4^+ and PO_4^{3-} were higher (up to 1.46 and 1.17 mgL^{-1}) than in the previous cores. In contrast the alkalinity profile was consistent with that in the previous cores.

The first working area was revisited at the end of the journey to take a transect of seven cores (GeoB14619-25) across one pit in which heat flow values in excess of 300 mW/m^2 were measured. The goal was to track the changes in pore water and sediment composition from the outside of the pit across its interior. Because of limited resources for chemical analysis on board at this time of the journey, only the Eh, pH and the alkalinity were measured in cores GeoB14621-25. The samples were stowed away for further analyses in Bremen.
All 7 cores were consistent in that the redox conditions were reducing. Only in the bottom meter of GeoB14619 and in discrete sand layers were conditions more oxidizing (Figure 34). The Eh profile GeoB14619 in Figure 34 is remarkable in that it shows the inverse Eh-depth relationship, which is commonly found in upper marine sediments, which is oxidizing conditions near the seafloor and more reducing conditions with increasing depth. The appearance of the sediments, a grayish color with black streaks, is consistent with that of sediments exhibiting reducing conditions in cores from other working areas, suggesting a common redox buffering process.

Redox gradients near the seafloor are normally extremely steep and there is no indication of vertical seawater infiltration at all. In the bottom meter of GeoB14619 where conditions became oxidizing, the appearance of the sediments changed to a brownish color, similar to the oxidized sediments in working areas two and three. There is no macroscopic difference in appearance of the sediments or the chemical parameters Eh, pH and the alkalinity between samples taken from outside and inside the pit.
The sand layer was found in all but two of the seven cores. Some cores contained multiple sand layers (e.g. GeoB14619 at 38 cm and 151 cm (Figure 34)) others only fragments. Fluids sampled from the sand layer were oxidizing and had a somewhat higher pH than the fluids in the surrounding clays which, could be a consequence of seawater recharge and focused flow along this layer. Where the sand layer was preserved, extreme redox gradients occurred above and below this layer often exceeding 400 mV over a distance of a few cm (e.g. GeoB14619 in Figure 34).
The alkalinity was essentially uniform in all profiles with values of around 3 $mmolL^{-1}$. Only at sites GeoB14619 and GeoB14624 was the alkalinity lower, around 2.7 $mmolL^{-1}$. The Fe^{2+}, NH_4^+ and PO_4^{3-} concentrations were measured only in pore waters from cores GeoB14619 and GeoB14620. All species Fe^{2+}, NH_4^+ and PO_4^{3-} were higher in GeoB14620 than in GeoB14619. The PO_4^{3-} profile exhibited a strong decrease with depth from about 0.9 mgL^{-1} at the seafloor to 0.16 mgL^{-1} at 7.49 m. One interesting observation was that the highest Fe^{2+} and the highest PO_4^{3-} concentrations in GeoB14619 occurred in the shallowest sample at 0.08 m.

5.6.4 Visual Survey of Seafloor

The RV Sonne s Oceanfloor Oberservation System (OFOS) was deployed in GUATB-1 to carry out a video survey across pit bottom, pit slope, pit to normal seafloor transition and the seafloor between two pits. To achieve this, a transect was established starting at 7°55.8820 N, 90°31.7560 W and finishing at 7°57.0810 N, 90°33.9910 W (Fig. 35).

Besides some crustaceans, holothurians, jellyfish, sea anemones and fishlike animals also white patches some with a hole in its center were observed (Fig. 36). It seems as if those were slightly more abundant in pits especially at their inner flanks. No distinct differences between the pit bottom, slope and transition zone to normal seafloor were observed. The only noticeable difference observed was that whenever the bottom weight of the OFOS touched the sediment there was less sediment suspended inside the pits than outside. This observation, although completely of a qualitative nature, could be interpreted in such a way that the sediments inside the pits were more compacted or harder than those of the normal seafloor adjacent to the pits.

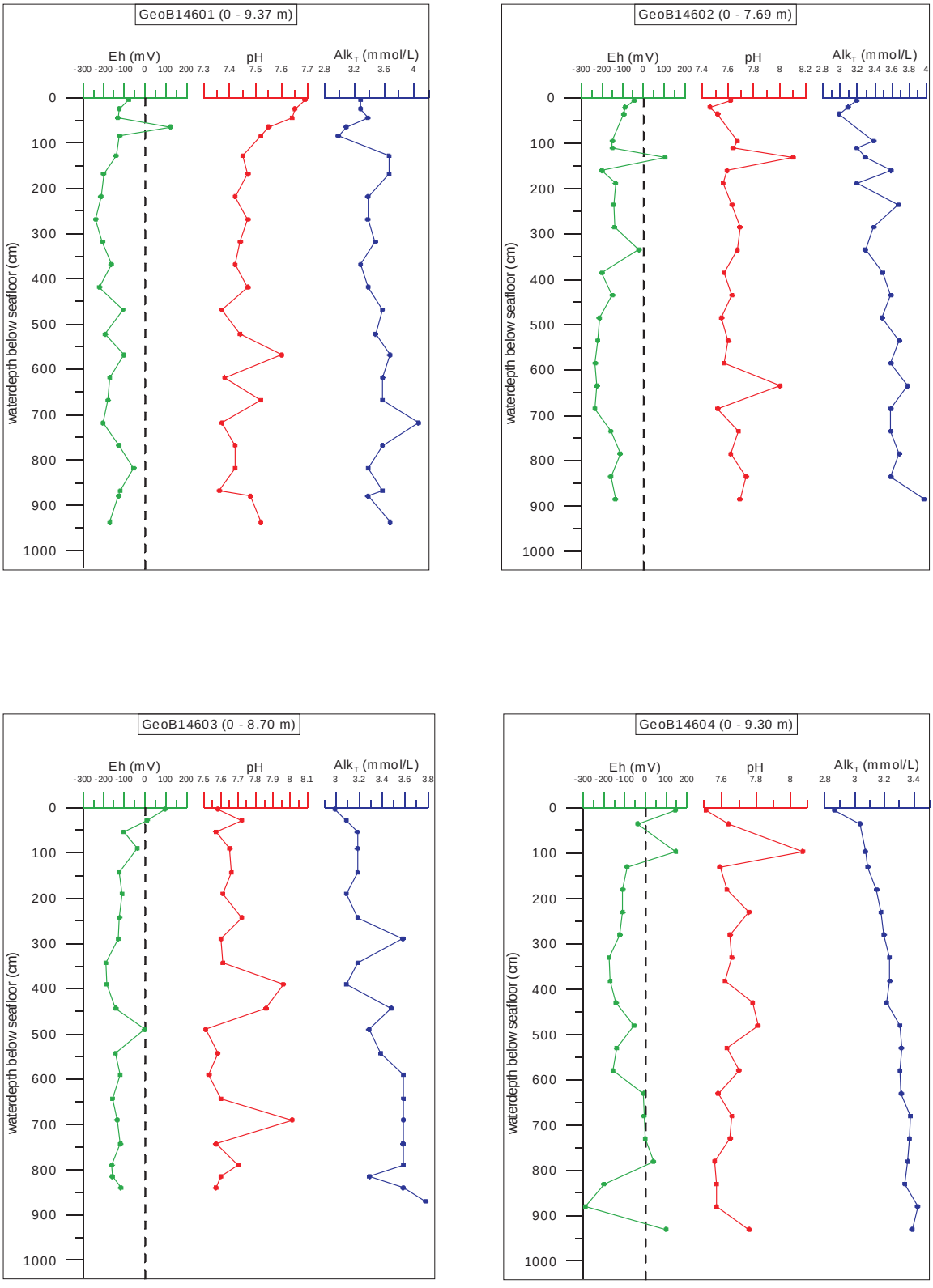

Figure 33: Eh, pH and alkalinity (AlkT) values obtained in cores GeoB14601 (outside a pit), GeoB14602 (inside a pit) GeoB 14603 (inside a pit) and GeoB14604 (outside a pit).

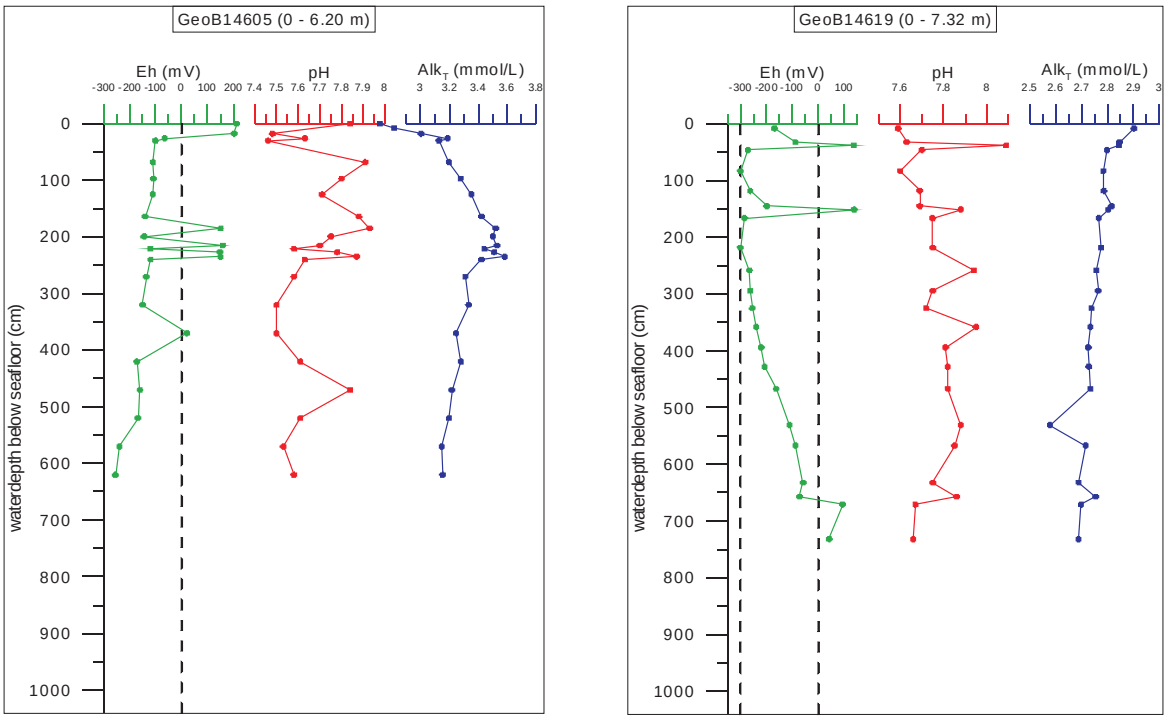

Figure 34: Eh, pH and alkalinity (AlkT) values obtained for two cores from the inside of a pit, GeoB14605 and GeoB14619.

Table 8: Stations overview for the GUATB-1 working area.
Note: SL = Gravity Corer, MIC = Multi Corer, RL = length of rope

Station	Gear	Station coordinates		Gear coordinates		Water Depth	Core recovery	Date
		latitude	longitude	latitude	longitude	(m)	(m)	
GeoB14601-1	SL	7° 55,300' N	90° 28,800' W	7° 55,246' N	90° 28,756' W	3431	9,7	23.06.2010
GeoB14602-1	SL	7° 57,670' N	90° 33,500' W	7° 57,645' N	90° 33,507' W	3500	9,3	24.06.2010
GeoB14603-1	SL	7° 55,049' N	90° 30,929' W	7° 55,027' N	90° 30,855' W	3497	8,9	24.06.2010
GeoB14604-1	SL	7° 56,841' N	90° 32,685' W	7° 56,817' N	90° 32,692' W	3425	9,4	25.06.2010
GeoB14605-1	SL	7° 55,891' N	90° 31,809' W	7° 55,883' N	90° 31,806' W	3489	6,2	26.06.2010
GeoB14605-2	MIC	7° 55,891' N	90° 31,809' W	7° 55,892' N	90° 31,810' W	3482	2 x 0.4	26.06.2010
GeoB14619-1	SL	7° 57,970' N	90° 33,796' W	7° 57,970' N	90° 33,796' W	3512 (RL), 3507 (EM)	7,4	08.07.2010
GeoB14620-1	SL	7° 57,572' N	90° 33,656' W	7° 57,572' N	90° 33,656' W	3505 (RL)	7,67	08.07.2010
GeoB14621-1	SL	7° 58,259' N	90° 33,887' W	7° 58,259' N	90° 33,887' W	3448 (RL), 3440 (EM)	9,82	09.07.2010
GeoB14622-1	SL	7° 58,155' N	90° 33,854' W	7° 58,155' N	90° 33,854' W	3448 (EM), 3473 (RL)	8,39	09.07.2010
GeoB14623-1	SL	7° 58,090' N	90° 33,833' W	7° 58,090' N	90° 33,833' W	3484 (RL)	7	09.07.2010
GeoB14624-1	SL	7° 57,885' N	90° 33,766' W	7° 57,885' N	90° 33,766' W	3508 (RL), 3502 (EM)	10,64	10.07.2010
GeoB14625-1	SL	7° 57,885' N	90° 33,766' W	7° 57,885' N	90° 33,766' W	3506 (RL), 3505 (EM)	8	10.07.2010

Table 9: Summary of pore water analyses performed on-board the RV Sonne during the Seamountflux Cruise (SO207) in working area GUATB-2. Note: n.d. = not determined.

Core	Samples (n)	pH	Eh (mV)	Alk_T (mmol/L)	NH_4^+ (mg/L)	Fe^{2+} (mg/L)	PO_4^{3-} (mg/L)
GeoB14601	23	7.4 - 7.7	-238 - 123	3.0 - 4.1	0.2 - 0.3	0.1 - 0.4	0.3 - 0.7
GeoB14602	22	7.5 - 8.1	-235 - 104	3.0 - 4.0	0.4 - 0.6	n.d.	0.3 - 0.7
GeoB14603	21	7.5 - 8.0	-189 - 97	3.0 - 3.8	0.4 - 0.5	<0.05 - 0.5	0.3 - 0.6
GeoB14604	20	7.5 - 8.1	-290 - 146	2.9 - 3.4	0.4 - 0.6	<0.05 - 0.4	0.3 - 0.7
GeoB14605	20	7.5 - 7.9	-255 - 159	3.1 - 3.6	0.5 - 1.5	<0.05 - 0.3	0.3 - 1.2
GeoB14619	23	7.6 - 8.1	-300 - 43	2.6 - 2.9	<0.5	<0.05 - 0.2	0.1 - 0.2
GeoB14620	24	7.6 - 7.9	-271 - 98	3.0 - 3.6	<0.5 - 1.4	0.1 - 0.2	0.2 - 0.9
GeoB14621	18	7.6 - 8.0	-272 - 168	3.1 - 3.4	n.d.	n.d.	n.d.
GeoB14622	19	7.5 - 8.0	-221 - 233	2.7 - 3.3	n.d.	n.d.	n.d.
GeoB14623	15	7.6 - 7.9	-215 - (-86)	3.0 - 3.2	n.d.	n.d.	n.d.
GeoB14624	22	7.7 - 8.0	-339 - (-105)	2.7 - 2.9	n.d.	n.d.	n.d.
GeoB14625	17	7.6 - 7.8	-324- 152	3.0 - 3.2	n.d.	n.d.	n.d.

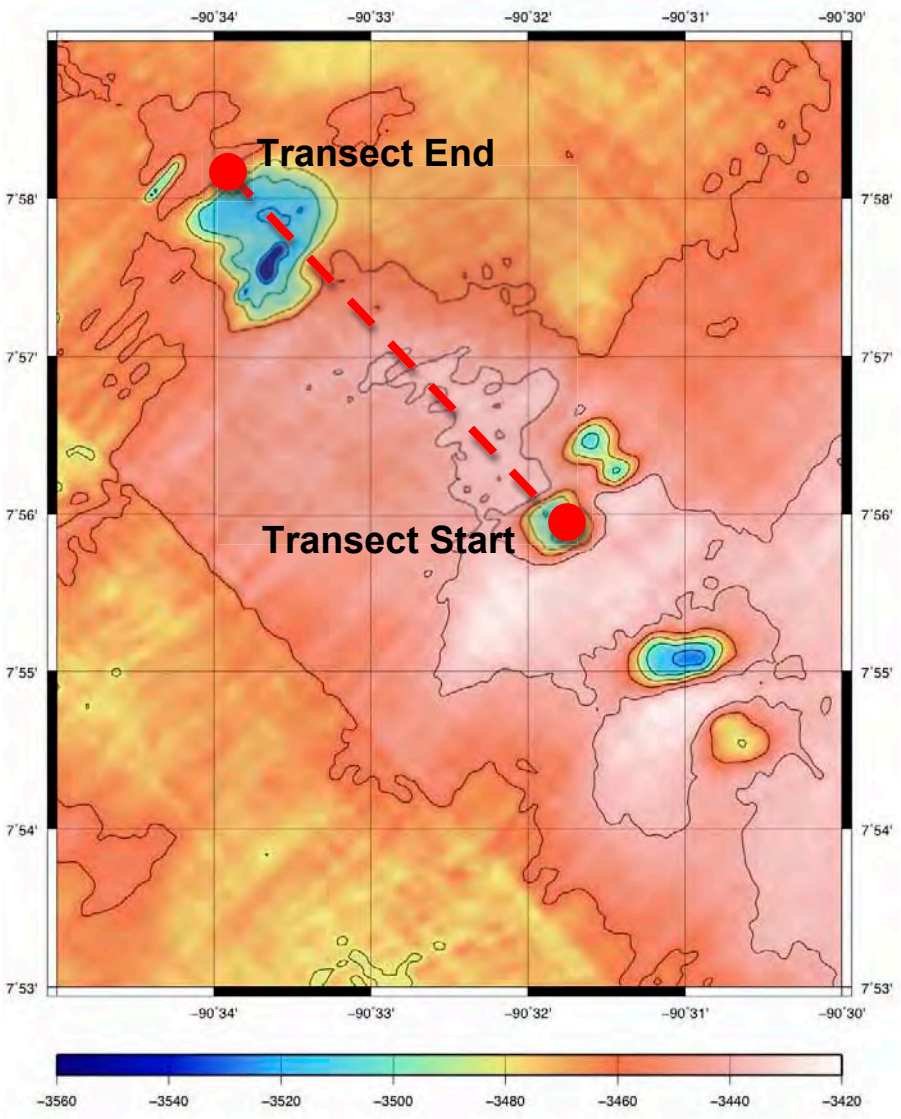

Figure 35: OFOS profile for the visual survey through two pits and adjacent "normal" seafloor.

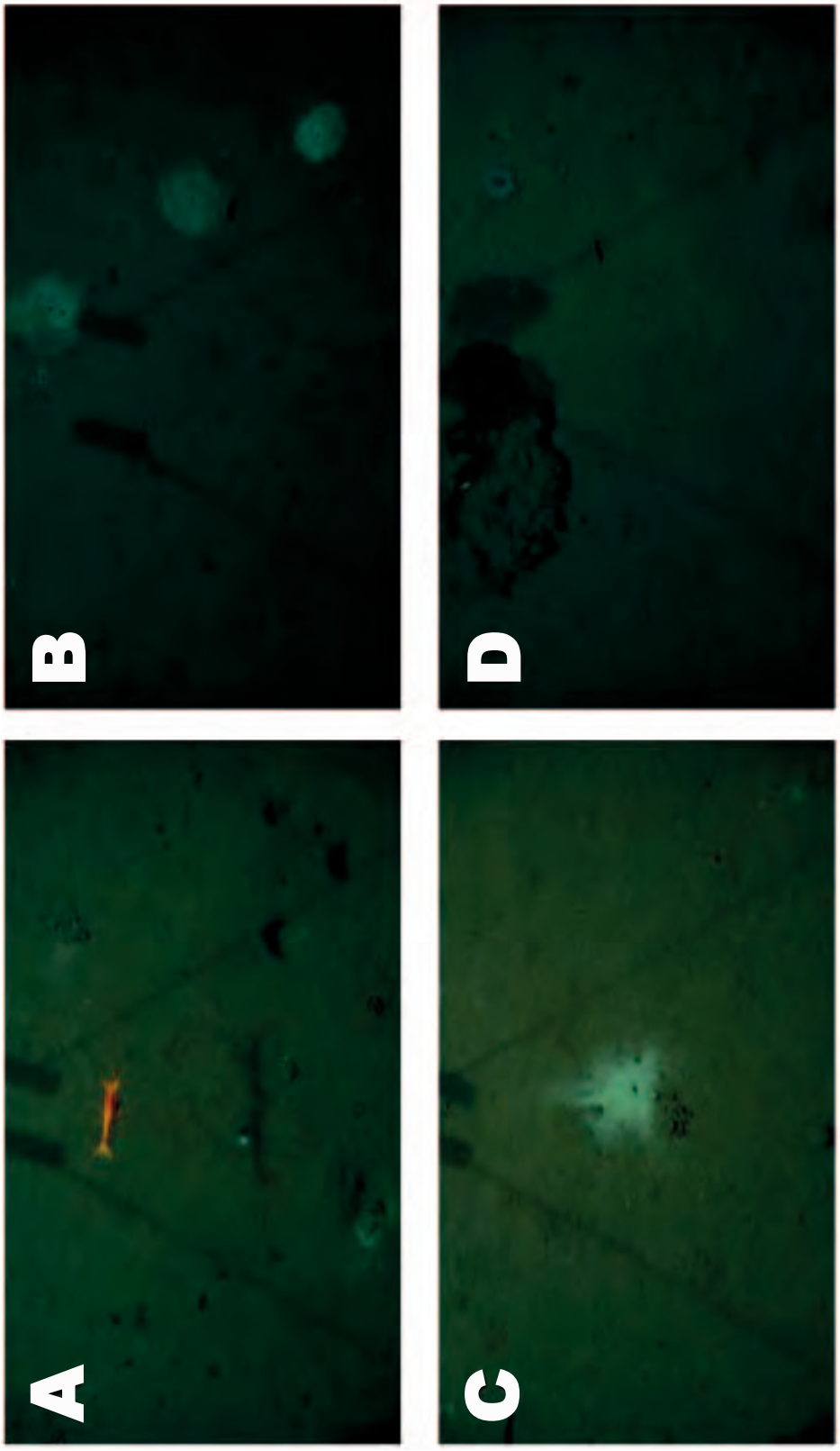

Figure 36: Under water photographs taken during the OFOS survey. Field of view is approximately 3 m. Photograph A shows a crustacean, photographs B and D show the white patches and photograph D shows the sediment suspension during touchdown of the OFOS bottom weight.

5.7 Working Area GUATB-2

5.7.1 Heat Flow

(H. Villinger)

In working area GUATB-2 we surveyed a number of pits on the western side of GUATB-2 which are also aligned on a profile perpendicular to the flow line. Values on station HF1032 (see Tab. 18 in Appendix section A.3 and Fig. 37) in the pits show again high heat flow of almost up to 300 mW/m^2 with low background values increasing from about 20 mW/m^2 in the southeastern part of the profile to $\sim$ 50 mW/m^2 in the northwest (Fig. 41). Station HF1037 (Tab. 19 in Appendix section A.3), roughly parallel to HF1032 and only about 3 km further north was intended to characterize the influence of the large seamount in relation to the pits of HF1032 (Fig. 38). Values close to the seamount are extremely small and some valid measurement show very strange temperature-depth profiles which are not interpretable at the moment. Along the profile heat flow increases very slowly to values around 20 mW/m^2.

A detailed survey (station HF1033, see Tab. 20 in Appendix section A.3 and Fig. 39) of one isolated pit in the southwestern part of GUATB-2 shows a very consistent pattern of background values at the boundary of 60 to mW/m^2 and very high values of up to $\sim$ 350 mW/m^2 in the center of the pit (Fig. 43).

A profile (station HF1036, see Tab. 21 in Appendix section A.3 and Fig. 40) located on multi-channel line 11 from site survey cruise EW9903 across a basement ridge is very puzzling as heat flow is consistently high ($\sim$ 140 mW/m^2) and shows almost no correlation with decreasing sediment thickness over the basement high (Fig. 43). This high value is also surprising in a sense that it is 2 to 3 times higher than the values around the pits.

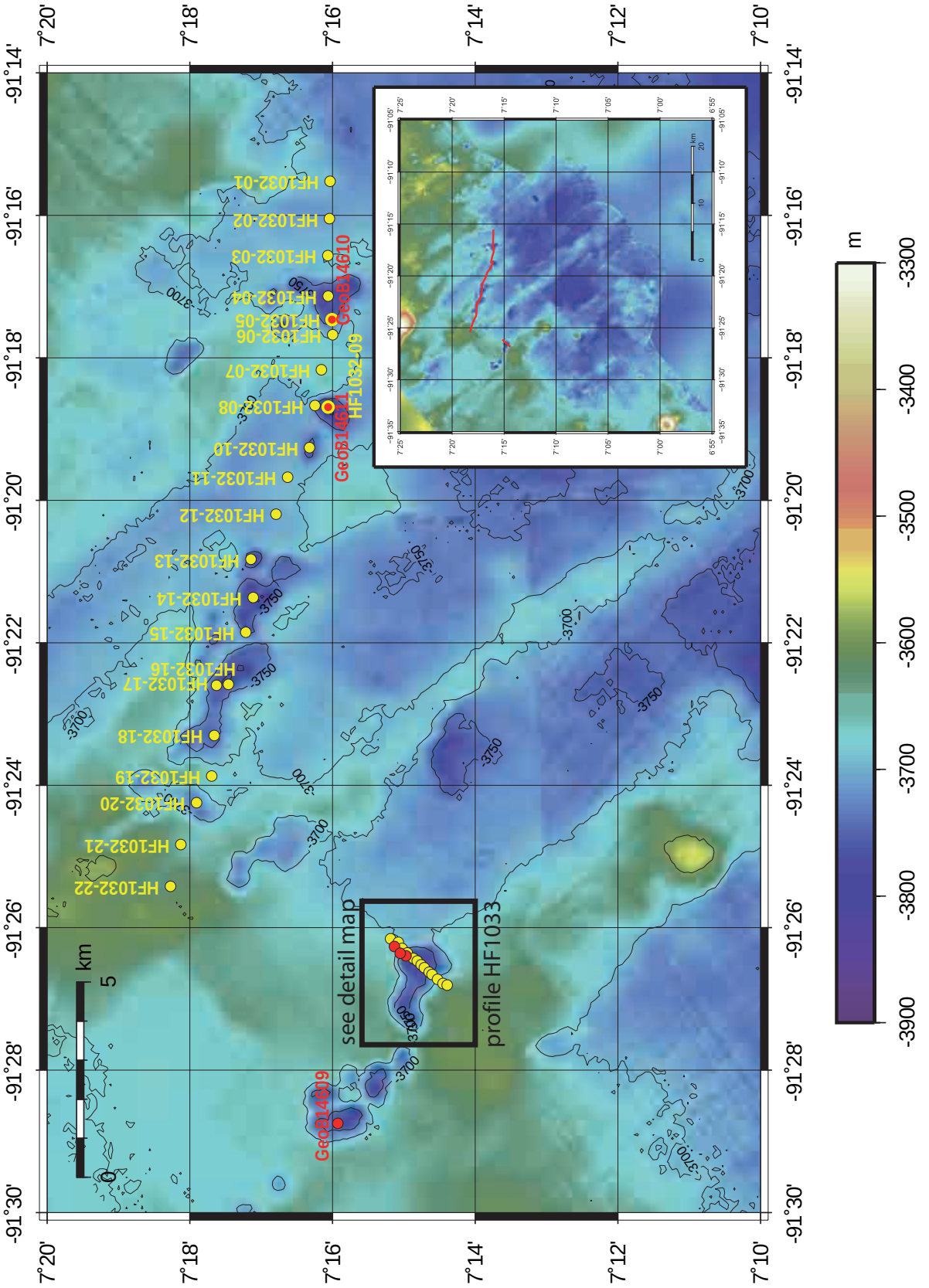

Figure 37: Location of penetrations with the heat flow probe on profile HF1032 (yellow filled circles) and core positions as red filled circles. The inset shows an overview about working area GUATB-2 with the heat flow profile in red. Profile HF1033 was run over a pit in the western part of the area (enlarged view in Fig. 39.)

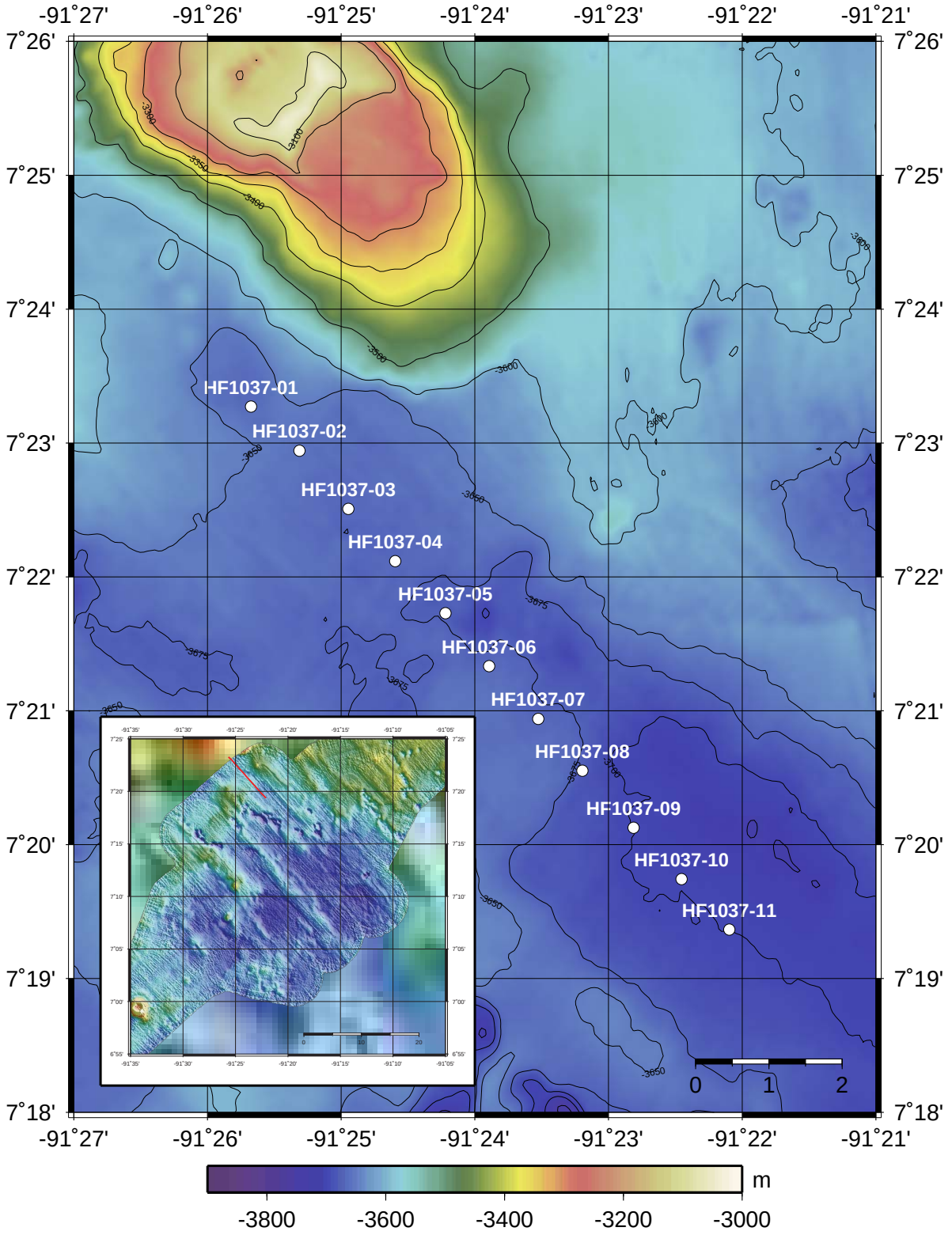

Figure 38: Location of penetrations on profile HF1037. Location of penetrations with the heat flow probe on profile HF1030 (white filled circles). The inset shows an overview about working area GUATB-2 with the heat flow profile in red.

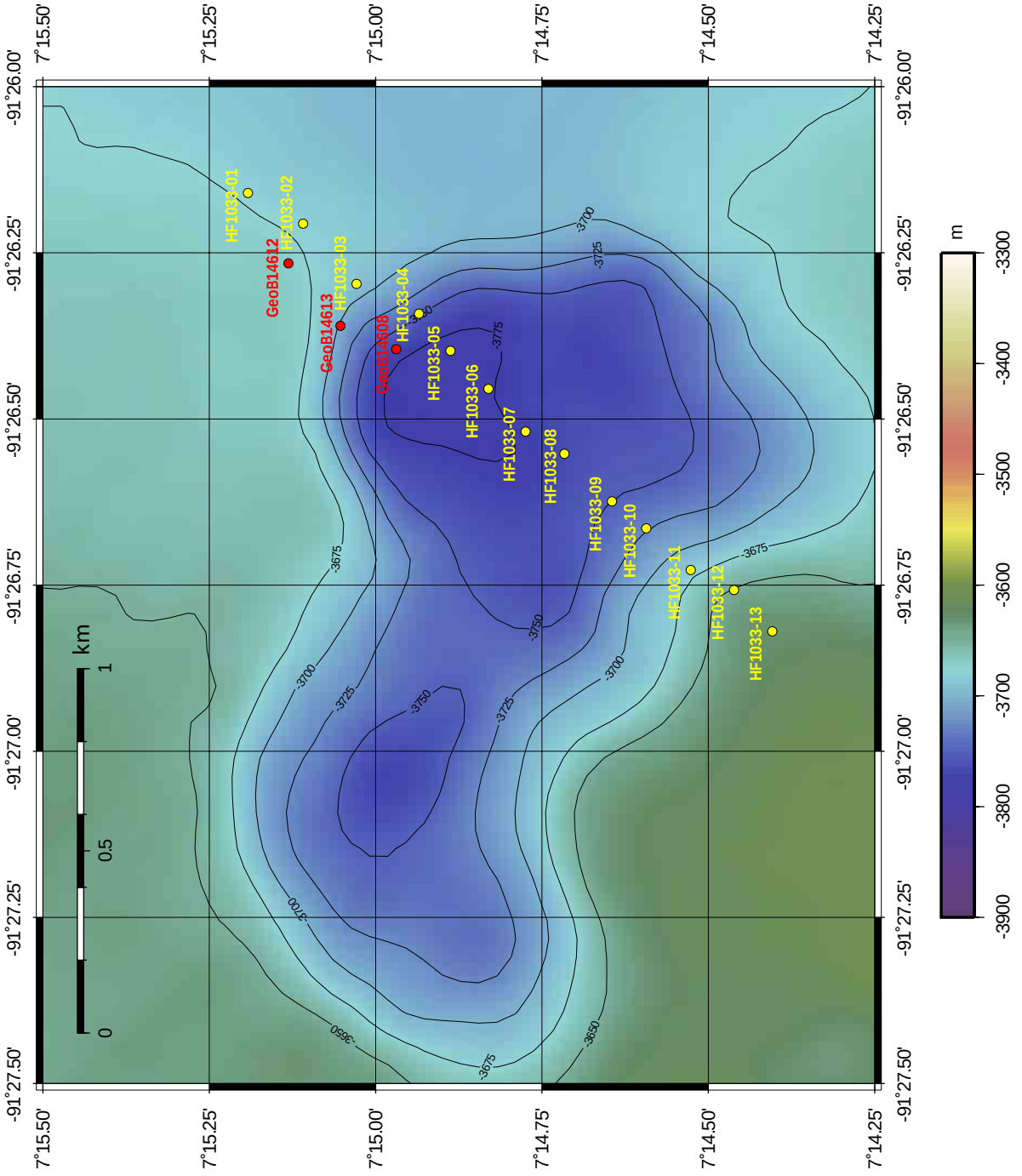

Figure 39: Location of penetrations with the heat flow probe on profile HF1033 (yellow filled circles) and core positions as red filled circles.

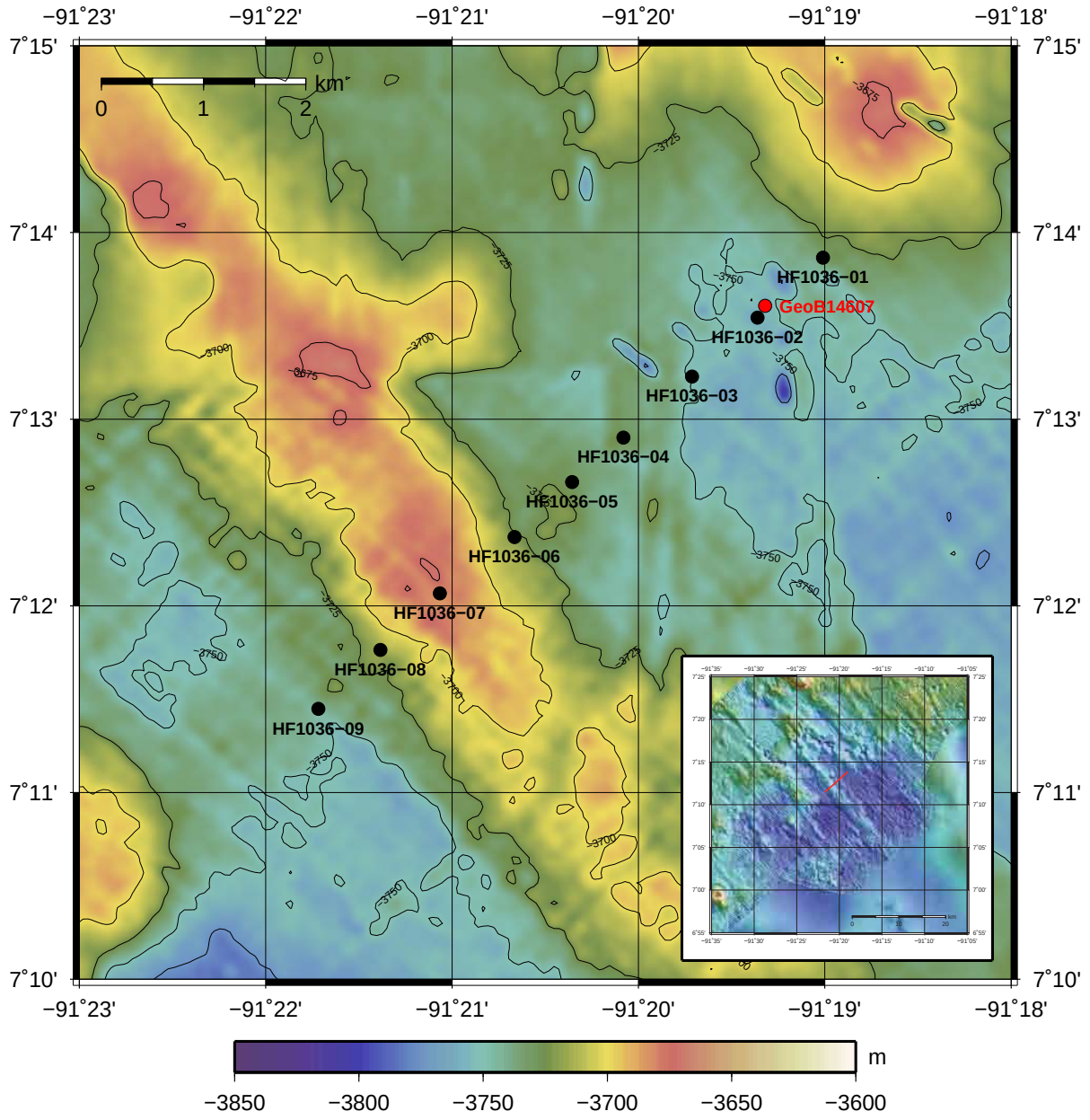

Figure 40: Location of penetrations with the heat flow probe on profile HF1036 (black filled circles) and core positions as red filled circles. The inset shows an overview about working area GUATB-2 with the heat flow profile in red.

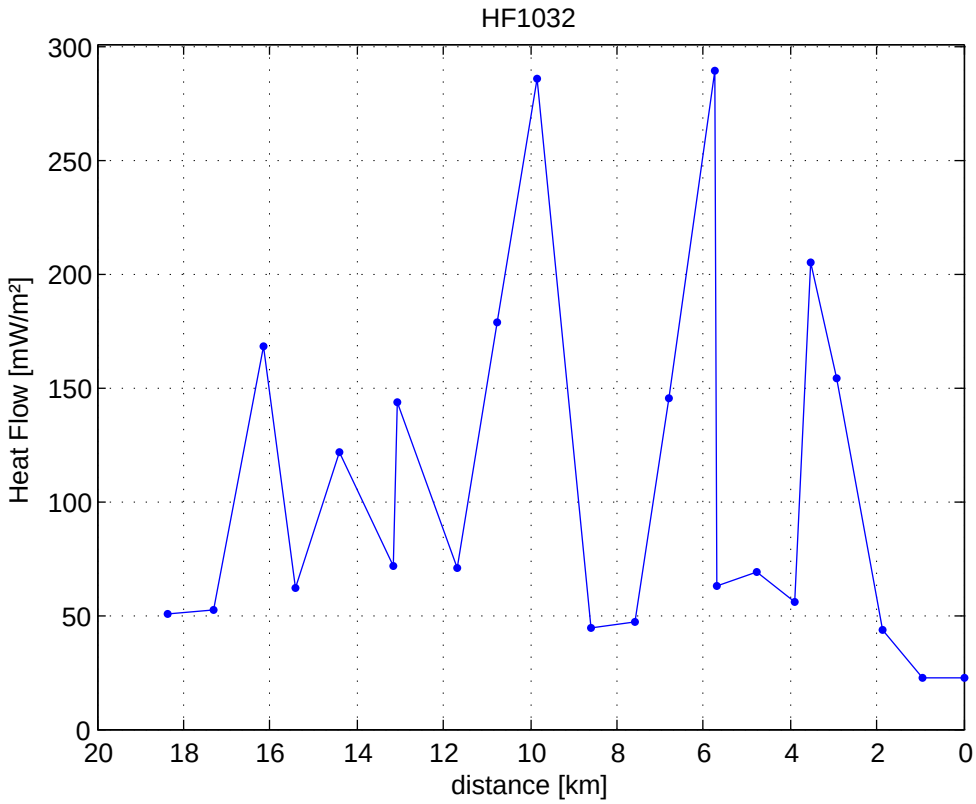

Figure 41: Heat flow values of profile HF1032 vs distance from the first penetration of the profile.

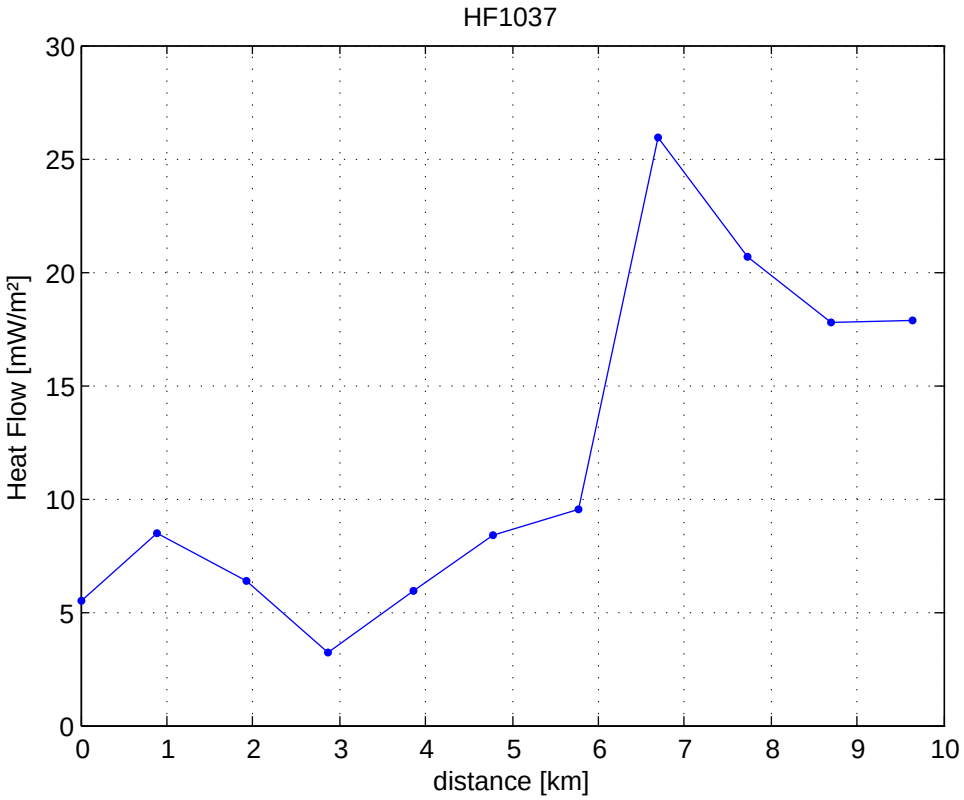

Figure 42: Heat flow values of profile HF1037 vs distance from the first penetration of the profile.

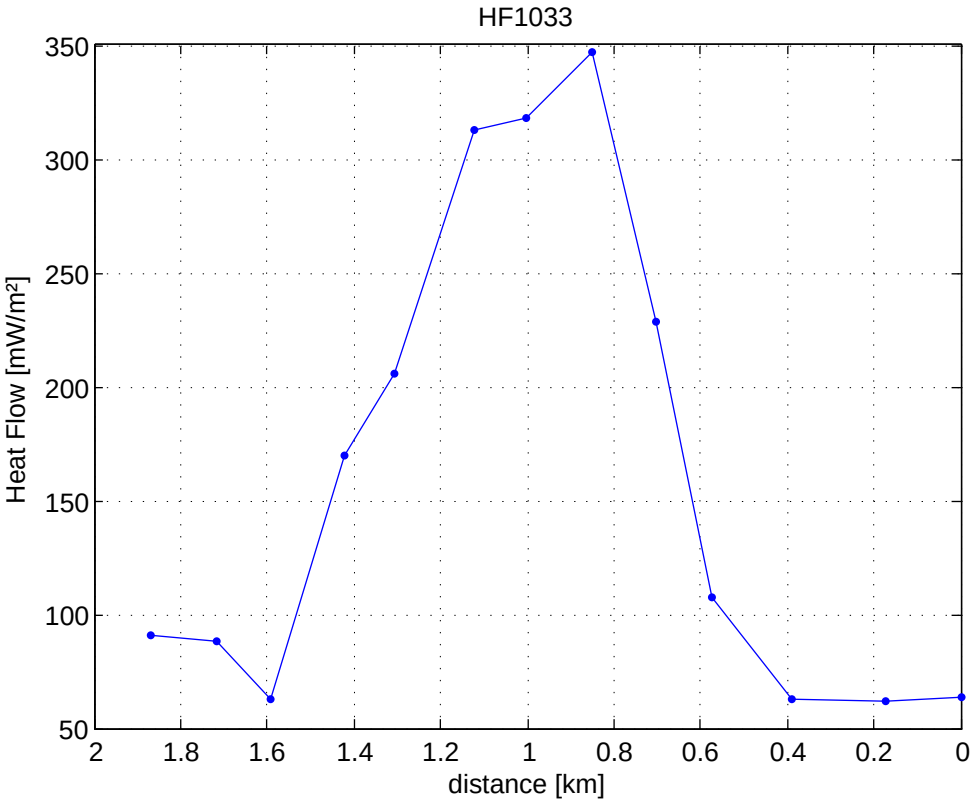

Figure 43: Heat flow values of profile HF1033 vs distance from the first penetration of the profile.

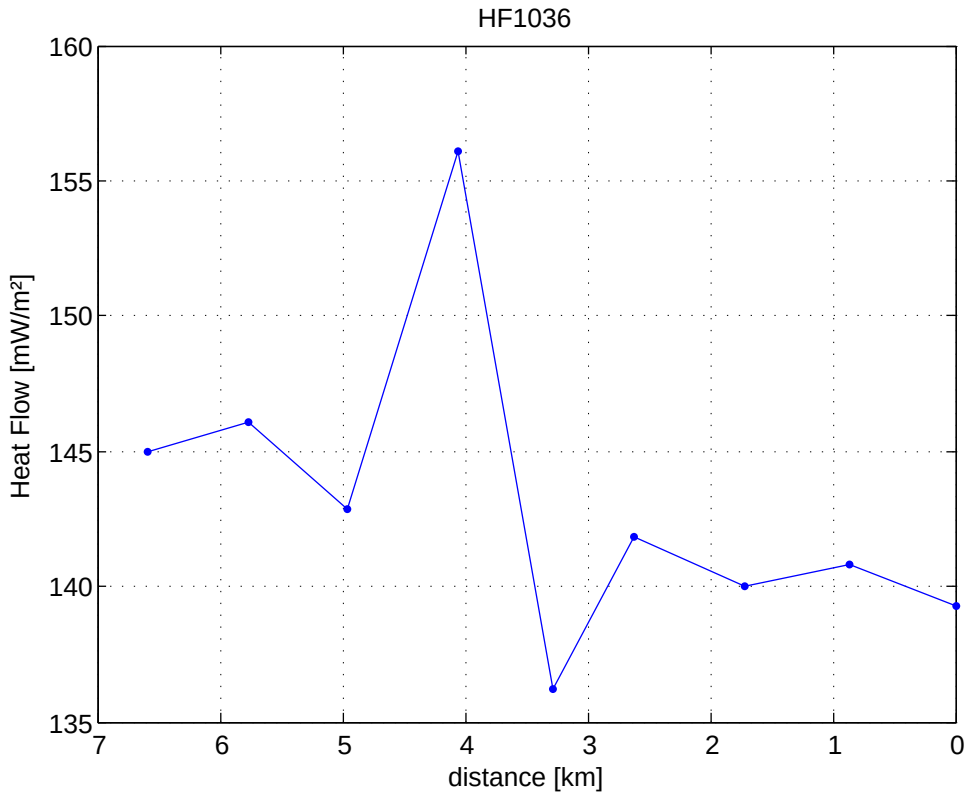

Figure 44: Heat flow values of profile HF1036 vs distance from the first penetration of the profile.

5.7.2 Sediment sampling and core description

(P. Alt-Epping, R. Becke, K. Enneking, T. Fleischmann, K. Gaida, C. Janssen, T. Pichler, M. Ruiz and M. Zwick)

In this working area, six cores were taken (GeoB14607, 14608, 14609, 14610, 14611, 14612 and 14613). The strategy was to obtain cores from outside of the pits, inside the pits and to carry out a transect across pit bottom, pit slope and the adjacent seafloor out side of the pit. An exact listing of each core location is given in Table 10. Cores from the base of the pits were 14608, 14609 and 14611. GeoB 14613 was taken in the slope and GeoB 14607 was taken outside the pit as reference. The transect across the pit to normal seafloor boundary is show in Figure 43.

To obtain further information about the surface sediments in the pit shown in Figure 5.2.1 the micro coring device (MIC) was deployed and successfully retrieved with three of the four possible coring tubes filled with approximately 40 *cm* sediment and 20 *cm* seawater.

Table 10: Stations overview for the GUATB-2 working area.
Note: SL = Gravity Corer, MIC = Multi Corer, RL = length of rope

Station	Gear	Station coordinates		Gear coordinates		Water Depth	Core recovery	Date
		latitude	longitude	latitude	longitude	(m)	(m)	
GeoB14607-1	SL	7° 13,606' N	91° 19,344' W	7° 13,608' N	91° 19,320' W	3733	7,0	28.06.2010
GeoB14608-1	SL	7° 14,982' N	91° 26,396' W	7° 14,969' N	91° 26,395' W	3760	8,1	29.06.2010
GeoB14608-2	MIC	7° 14,520' N	91° 26,350' W	7° 14,969' N	91° 26,395' W	3748(RL)	3 x ca. 0.4	07.07.2010
GeoB14609-1	SL	7° 15,990' N	91° 28,652' W	7° 15,927' N	91° 28,747' W	3717	6,6	29.06.2010
GeoB14610-1	SL	7° 16,014' N	91° 17,460' W	7° 16,009' N	91° 17,462' W	3763	6,1	30.06.2010
GeoB14611-1	SL	7° 16,068' N	91° 18,696' W	7° 16,064' N	91° 18,692' W	3788	7,8	30.06.2010
GeoB14612-1	SL	7° 15,130' N	91° 26,260' W	7° 15,131' N	91° 26,266' W	3656	10,4	01.07.2010
GeoB14613-1	SL	7° 15,049' N	91° 26,370' W	7° 15,053' N	91° 26,360' W	3657	7,3	02.07.2010

In summary the lithology of cores in GUATB-2 was slightly to extensively bioturbated clayey nannofossil ooze and nannofossil silty clay, respectively. Sandy ash and calcareous layers were found in several cores as well as black concretions (Manganese?). The sediment color varied from dark brown (5YR2,5/2 or 10YR4/3) at the top to light olive and grayish brown at the base. The strong bioturbated sections were much darker. The color of the white clayey calcareous layers, varied from 10YR8/1 to 10YR8/2. The surface sediments collected with the MIC correlated well to the uppermost sediments in core GeoB14608-1 and were not further described.

Detailed core descriptions of individual cores are presented in Appendix (Core Logs) and an overview of all sediment cores which were collected in GUATB-2 and how they compare to cores from other working areas is given in Figure 32.

5.7.3 Geochemistry of pore water

In the second working area (GUATB-2) a total of 7 gravity cores (GeoB14607-GeoB14613) and one MIC (GeoB14608-2) were sampled for pore water. Eh and pH were measured at the same locations where pore waters were sampled. A summary of the measurements is presented in Table 11. A complete listing of the results for all parameters is shown in Appendix (Pore Water Chemistry). Description of the onboard used methods and preservation of samples were described above (see section 4.2.3).

Table 11: Summary of pore water analyses performed on-board the RV Sonne during the Seamountflux Cruise (SO 207) in working area GUATB-2.

Core	Samples (n)	pH	Eh (mV)	Alk_T (mmol/L)	NH_4^+ (mg/L)	Fe^{2+} (mg/L)	PO_4^{3-} (mg/L)
GeoB14607	24	7.3 - 7.8	-150 - 260	2.9 - 3.2	<0.1 - 0.4	<0.05 - 0.5	0.3 - 0.5
GeoB14608	22	7.2 - 8.0	123 - 354	2.7 - 3.2	<0.5	<0.05	0.2 - 0.4
GeoB14609	13	7.5 - 7.7	148 - 242	2.8 - 3.0	<0.5	<0.05	0.1 - 0.4
GeoB14610	19	7.5 - 7.7	119 - 237	2.9 - 3.0	<0.5	<0.05	0.2 - 0.4
GeoB14611	23	7.5 - 7.8	-82 - 302	2.9 - 3.1	<0.5	<0.05	0.2 - 0.6
GeoB14612	21	7.5 - 7.7	150 - 264	2.9 - 3.0	<0.5	<0.05	0.1 - 0.3
GeoB14613	11	7.3 - 7.6	200 - 256	2.8 - 3.0	<0.5	<0.05	0.2 - 0.3

The first core, GeoB 14607 with a total length of 7.04 m showed a similar trend in pore water composition versus depth as the cores in the first working area in that the Eh decreased with depth. It exhibited a marked drop at about 2.32 $mbsf$ with a minimum value of -150 mV at 6.50 m (Fig. 45). This drop in Eh corresponded to the bottom end of the bioturbated zone. The decrease in Eh was accompanied by a slight increase in pH (up to 7.84) and in the NH_4^+ and Fe^{2+} concentrations, which showed a maximum of 0.39 and 0.45 mgL^{-1}, respectively (Table 11). In contrast, at shallower depths (0 - 2.32 $mbsf$) the core showed extensive bioturbation and the pore water was near uniform in composition, which was characterized by strongly oxidizing conditions (max. Eh = 260 mV) and a pH of around 7.5. The oxidizing conditions and near uniform pore water chemistry suggested that the depth of bioturbation corresponded to the depth to which the pore water composition was affected by seawater. Somewhat surprising was that the alkalinity profile did not reflect the transition from a seawater-dominated, oxidizing regime to a reducing, (more) sediment buffered regime at 2.32 $mbsf$. Instead, the alkalinity remained essentially uniform at about 3 $mmolL^{-1}$ throughout the entire profile. The PO_4^{3-} measurements were homogeneous throughout the profile.

The profile at location GeoB14608 was well within the oxidized zone with Eh values exceeding 120 mV throughout (Figure 45). As a result, measured Fe^{2+} and NH_4^+ values fell below the detection limit. The most distinct characteristic of the pore water profile was the interval between 176 - 453 m in which pH values were as high as 8.02. The alkalinity measurements did not reflect this pH increase but were uniformly distributed and slightly lower than at site

GeoB14607. The phosphate concentration decreased with depth, from $\sim 0.35\ mgL^{-1}$ near the seafloor to 0.17 mgL^{-1} at a depth of 8 m. The seawater-sediment interface was sampled in detail for the first 0.3 $mbsf$ at this site through use of the multi corer (MIC). The sampling interval was every 6 cm starting at a depth of 6 cm. Alkalinity, pH and PO_4^{3-} increased from 2.7 to 2.8 $mmolL^{-1}$, 7.2 to 7.5 and 0.3 to 0.4 mgL^{-1}, respectively. Eh decreased from 354 to 189 mV continuously. These values tie in nicely with those obtained in pore waters collected from the top of core GeoB14608-1.

The profiles from locations GeoB14609 and GeoB14610 were similar to those at location GeoB14608 except that pH values remained uniform ($\sim$ 7.6) (Figure 45).

The pore water profile obtained at location GeoB14611 exhibited greater variations in the Eh than the previous 3 profiles (Fig. 46). Eh minima with values on the order of -50 - -80 mV occurred in discrete layers and correlated with a distinct change in the color of the sediments from brownish to gray. These layers of reducing conditions were also characterized by a slightly elevated pH. None of other chemical parameters measured on board indicated a noticeable correlation with the variations in Eh in pH. The Fe^{2+} and NH_4^+ concentration were below the detection limit and the alkalinity remained uniform throughout the profile at values of about 3 $mmolL^{-1}$. The PO_4^{3-} concentration near the seafloor was the highest of all profiles in this working area (up to 0.55 $mgL - 1$), implying a somewhat steeper PO_4^{3-} versus depth profile.

Profiles GeoB14612 and GeoB14613 were similar to profiles GeoB14609 and GeoB14610 (Figure 46) in that they do not exhibited any noticeable features in the chemical parameters measured on board. The Eh and pH values were essentially uniform, suggesting oxidizing, seawater influenced conditions. Similarly, the alkalinity remained uniform. Solely the PO_4^{3-} decreased slightly with depth, consistent with profiles from the previous locations.

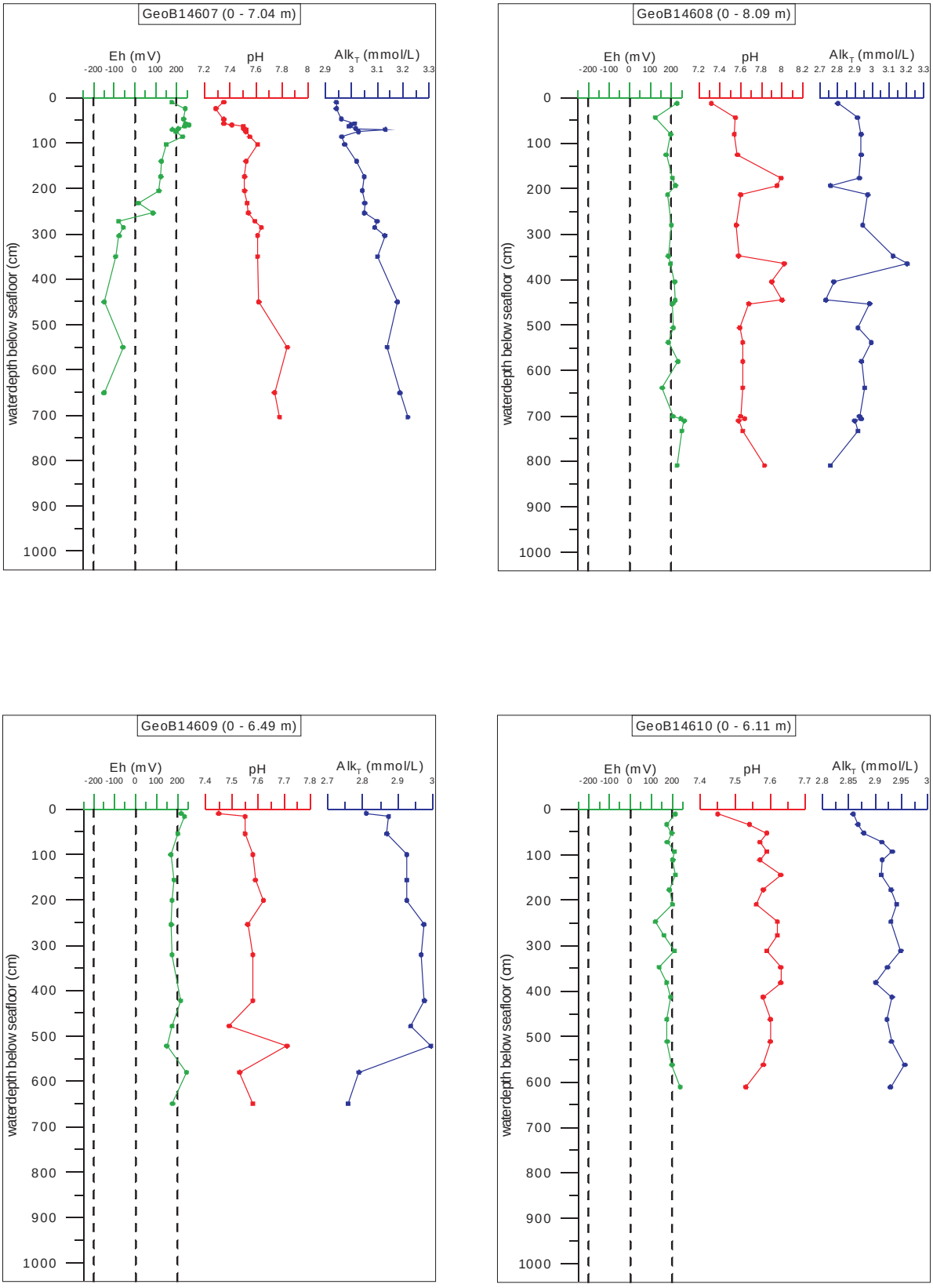

Figure 45: Eh, pH and alkalinity (AlkT) values obtained in cores GeoB 14607 (outside the pit), GeoB 14608-10 (within a pit).

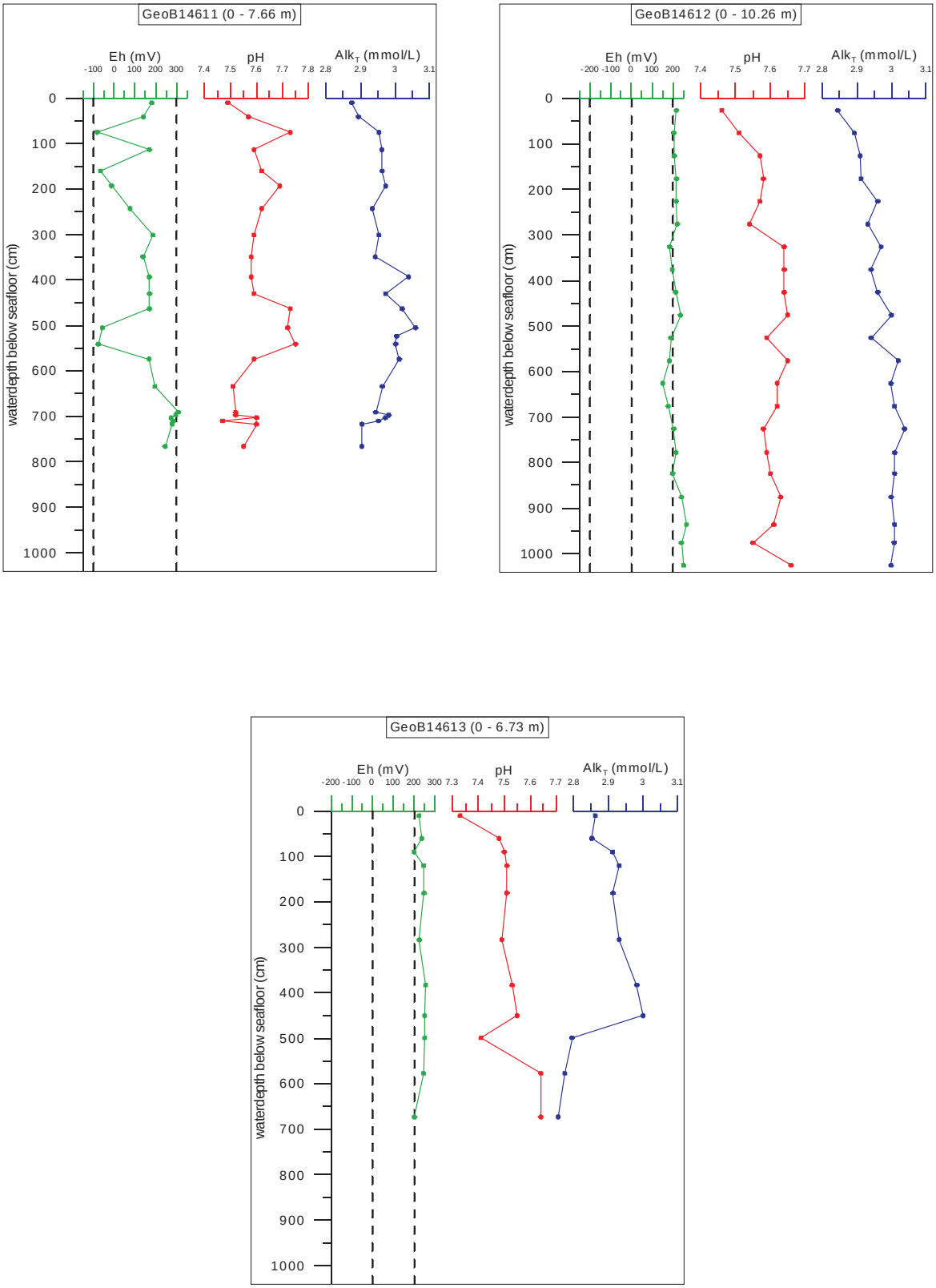

Figure 46: Eh, pH and alkalinity (AlkT) values obtained for cores GeoB 14611 (within the pit), GeoB 14612 (outside the pit) and GeoB 14613 (in the transition zone).

5.8 Working Area GUATB-3

5.8.1 Heat Flow

(H. Villinger)

In working area GUATB-3 we investigated in detail a small isolated pit in the southeastern corner. Station HF1034 (see Tab. 22 in Appendix section A.3 and Fig. 47) shows a very consistent cooling influence with values decreasing from about 130 mW/m^2 to minimum values of almost no temperature gradient in the middle of the profile. Superimposed on this big variation is the thermal and positive anomaly of the pit (Fig. 48). It is however unclear just from looking at the bathymetry and seismic records which feature causes this big cooling effect.

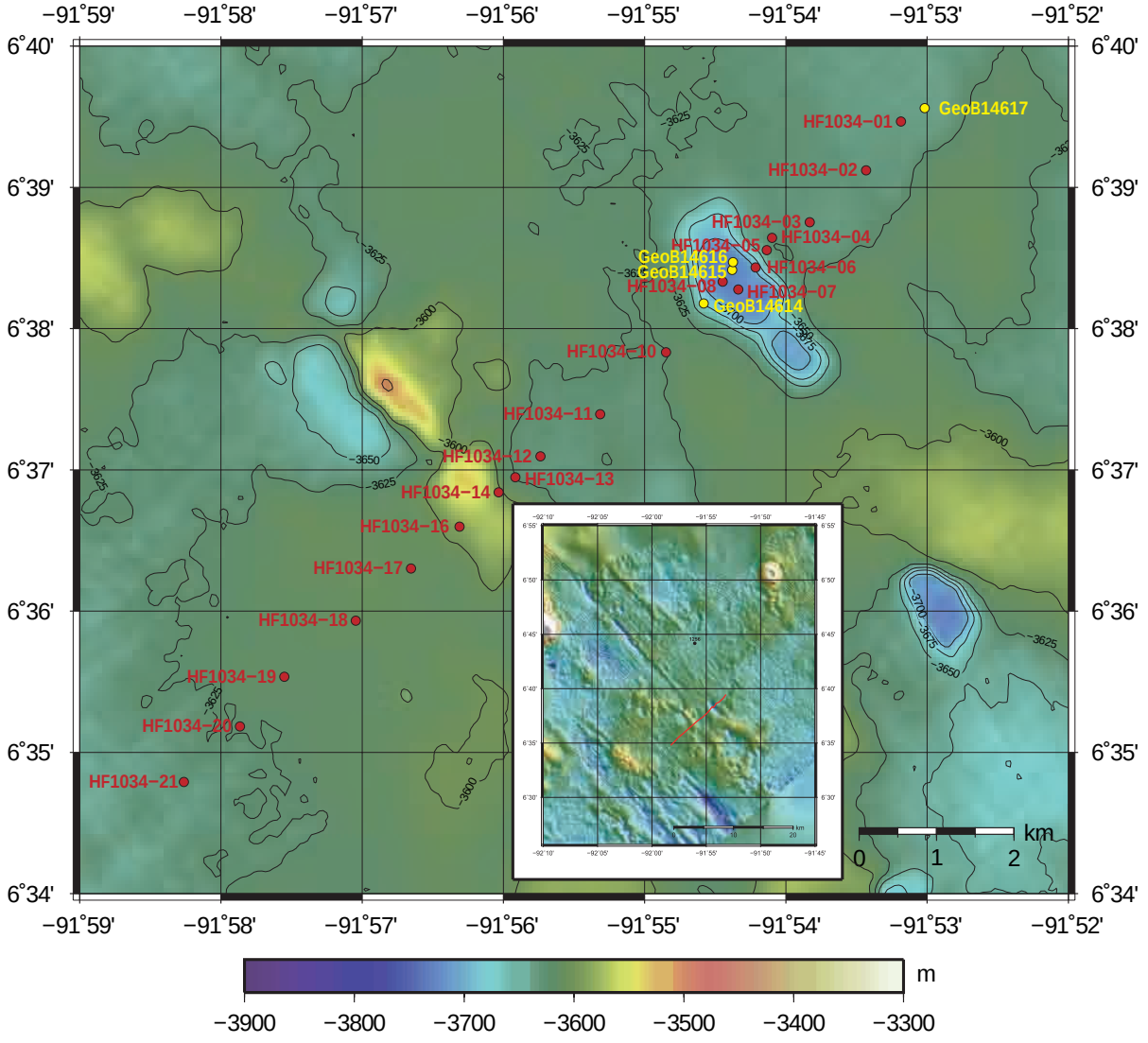

Figure 47: Location of penetrations with the heat flow probe on profile HF1034 (red filled circles) and core positions as yellow filled circles. The inset shows an overview about working area GUATB-3 with the heat flow profile in red.

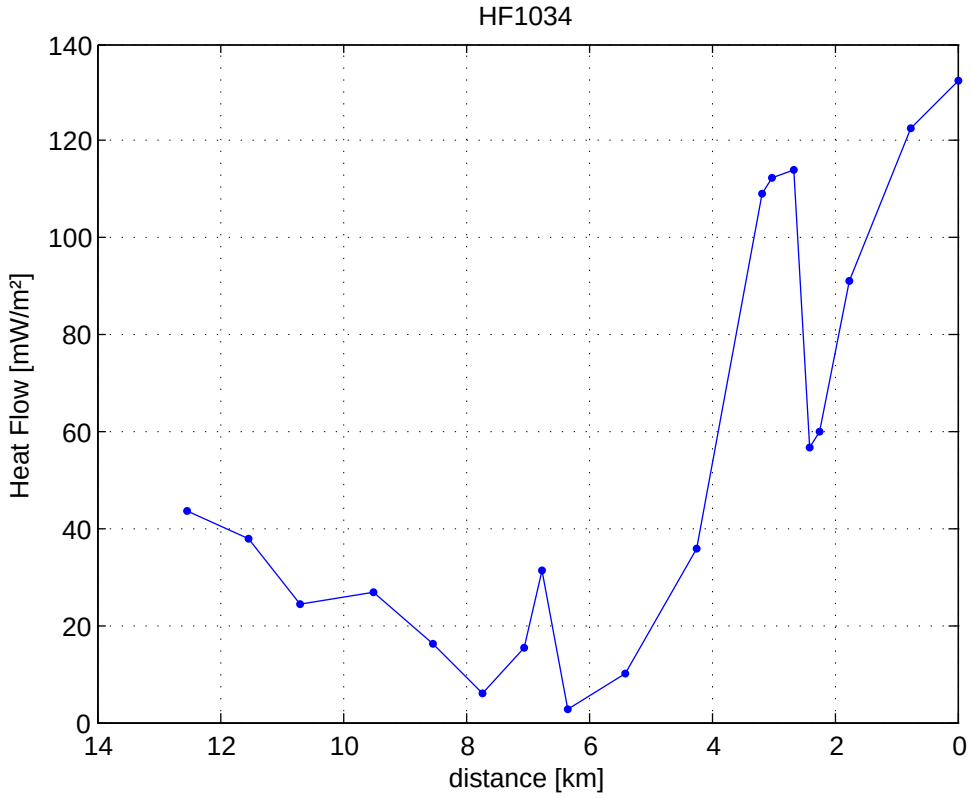

Figure 48: Heat flow values of profile HF1034 vs distance from the first penetration of the profile.

5.8.2 Sediment sampling and core description

(P. Alt-Epping, R. Becke, K. Enneking, T. Fleischmann, K. Gaida, C. Janssen, T. Pichler, M. Ruiz and M. Zwick)

In this working area, four cores were taken (GeoB14614, 14615, 14616, 14617). The strategy was to obtain cores from outside of the pits, the transition zone and inside the pits. An exact listing of each core location is given in Table 12. Cores from the base of the pits were 14615 and 14616. GeoB14614 was taken in the transition zone (i.e., the beginning of the slope into the pit) and 14617 was taken outside the pit as a reference core. The map with the detailed core sampling positions is show in Figure 49.

Table 12: Stations overview for the GUATB-3 working area.
Note: SL = Gravity Corer, MIC = Multi Corer, RL = length of rope

Station	Gear	Station coordinates		Gear coordinates		Water Depth	Core Recovery	Date
		latitude	longitude	latitude	longitude	(m)	(m)	
GeoB14614-1	SL	6° 38,137' N	91° 54,775' W	6° 38,178' N	91° 54,582' W	3637	9,0	04.07.2010
GeoB14615-1	SL	6° 38,399' N	91° 54,455' W	6° 38.454' N	91° 54.451' W	3715-3720 (RL)	7,0	04.07.2010
GeoB14616-1	SL	6° 38,472' N	91° 54,374' W	6° 38.472' N	91° 54.374' W	3715	7,3	05.07.2010
GeoB14617-1	SL	6° 39,565' N	91° 53,104' W	6° 39,565' N	91° 53,104' W	3628 (RL), 3625 (EM120)	9,0	05.07.2010

In summary the lithology of cores in GUATB-3 was slightly to extensively bioturbated clayey nannofossil ooze and nannofossil silty clay, respectively. Very dark layers with sharp boundaries

were found in several cores as well as white hard concretions in one of the cores from the pit. Water rich layers with small clay pellets were common in the core 14616. The sediment color varied from dark brown (10YR2/2) at the top to light yellowish and grayish brown (2,5Y5/2) at the base. The strong bioturbated sections were much darker. The color of the two cores at the pit was more grayish and varied from light brownish gray (10YR6/2) to grayish brown (2,5Y5/2).

Detailed core descriptions of individual cores are presented in Appendix (Core Logs) and an overview of all sediment cores which were collected in GUATB-3 and how they compare to cores from other working areas is given in Figure 32.

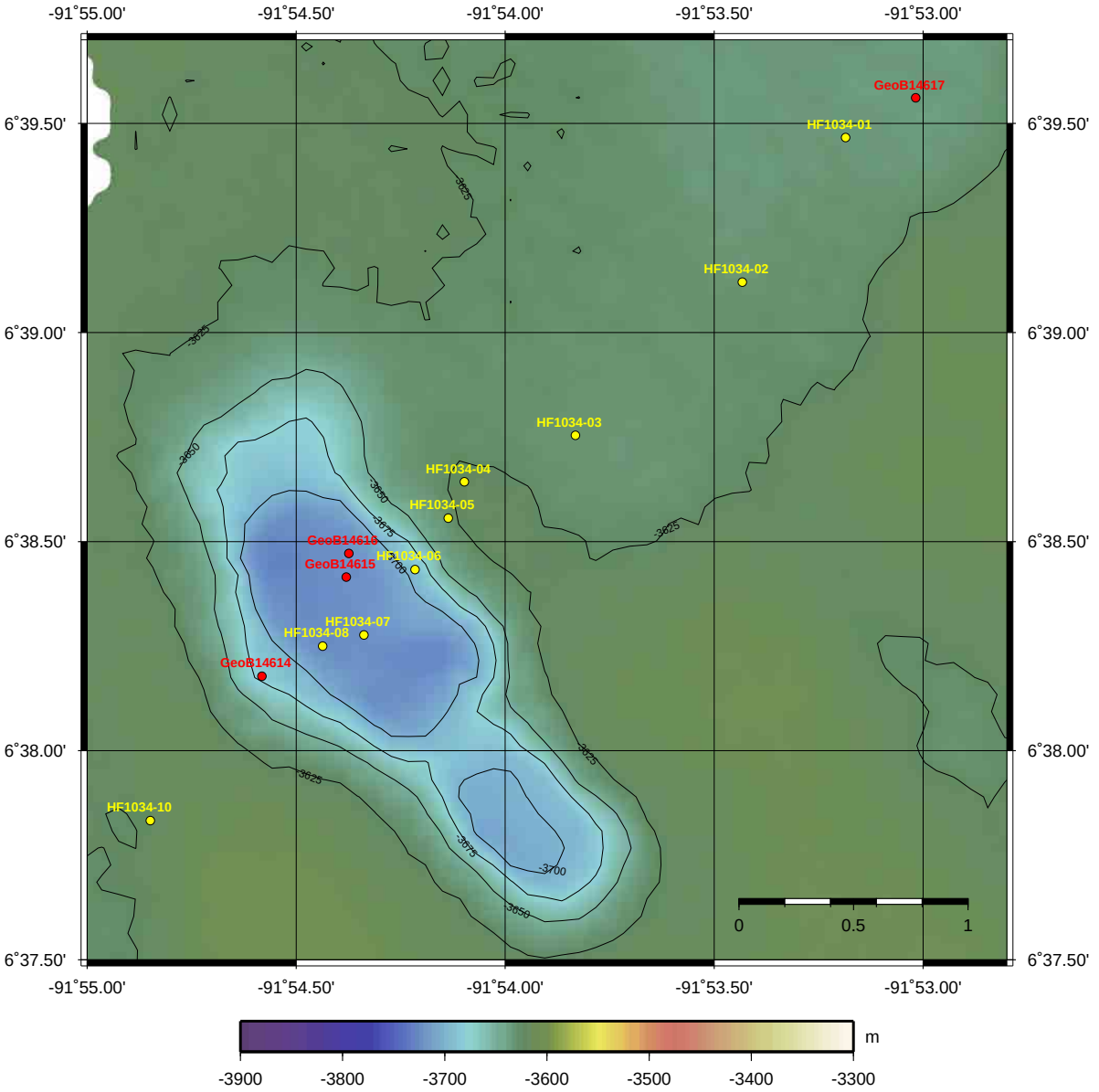

Figure 49: Detailed overview of the sampling positions of cores GeoB14614, GeoB14615 and GeoB14616 and GeoB14617

5.8.3 Geochemistry of pore water

In the third working area (GUATB-3) a total of 4 cores were taken. Eh and pH were measured at the same locations where pore waters were sampled. A summary of the measurements is presented in Table 13. A complete listing of the results for all parameters is shown in Appendix (Pore Water Chemistry). Description of the on-board used methods and preservation of samples were described above (see section 4.2.3).

Table 13: Summary of pore water analyses performed on-board the RV Sonne during the Seamountflux Cruise (SO 207) in working area GUATB-3.

Core	Samples (n)	pH	Eh (mV)	Alk_T (mmol/L)	NH_4^+ (mg/L)	Fe^{2+} (mg/L)	PO_4^{3-} (mg/L)
GeoB14614	10	7.6 - 7.7	145 - 250	3.0 - 3.1	<0.5	<0.05	0.2 - 0.4
GeoB14615	17	7.6 - 7.8	-74 - 197	2.9 - 3.1	<0.5	<0.05	0.3 - 0.6
GeoB14616	13	7.6 - 7.9	-12 - 201	2.8 - 3.1	<0.5	<0.05	0.3 - 0.6
GeoB14617	14	7.6 - 7.8	41 - 191	3.0 - 3.1	<0.5	<0.05	0.2 - 0.5

This working area had comparatively less pits and thus collection and analyses of gravity cores were limited to one location situated approximately in the center of the working area. The first core GeoB14614 was taken from outside the pit and thus was considered a reference core. The sediments in GeoB14614 did show a high degree of bioturbation and, consequently, the number of samples was limited to a total of 10. The pore water profiles illustrated the homogenizing effect of bioturbation and infiltration of seawater as it can be observed in Figure 50.: the profiles of Eh, pH, alkalinity and PO_4^{3-} were uniform and there were no detectable amounts of Fe^{2+} and NH_4^+.

Core GeoB14615 showed a sequence of different sediment coloration (rather than distinct layers), which could be correlated with the redox conditions in the pore water. A grayish color generally had a more reducing pore water than fluid from brownish sediments. The lowest Eh measured in the core was -74 mV, which occurred 53 cm below the seafloor. Another discrete layer of more reducing conditions was found at a depth of 5.5 m. There was no correlation between the Eh and other chemical properties of the pore fluid. The pH and alkalinity showed little variability, whereas the PO_4^{3-} concentration decreased with depth as in most other profiles. Fe^{2+} and NH_4^+ were below detection.

The following two cores, GeoB14616 and GeoB14617, showed essentially the same characteristics as GeoB14615 and were not discussed in greater detail.

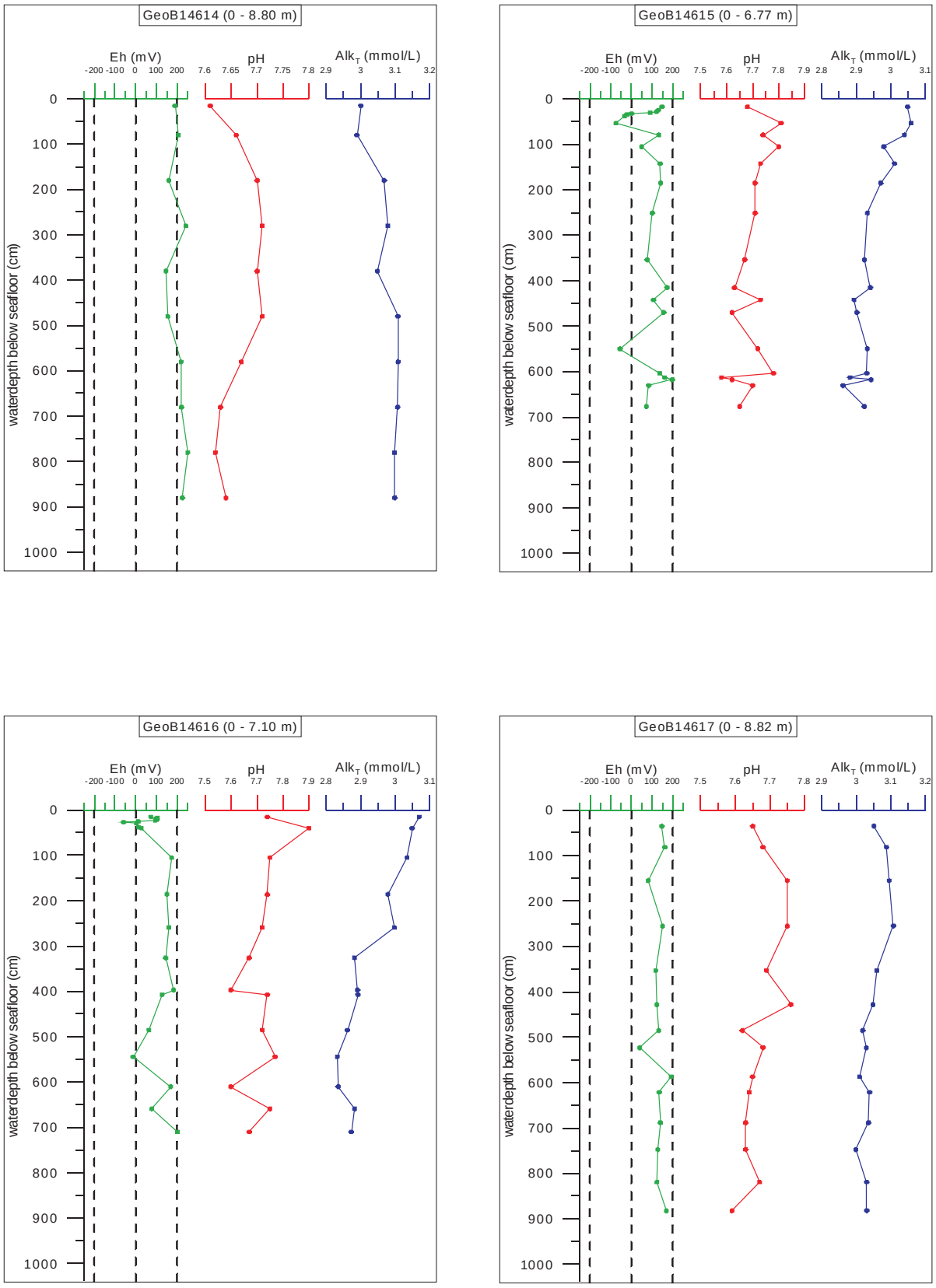

Figure 50: Eh, pH and alkalinity (AlkT) values obtained in cores GeoB14614, 14615, 14616 and 14617.

5.9 Transit from GUATB-3 to GUATB-2

5.9.1 Heat Flow

(H. Villinger)

On the way back from working area GUATB-3 to GUATB-2 we run a short heat flow profile from north-east towards a very regular shaped seamount which we surveyed on the way south (see Tab. 23 in Appendix section A.3 and Fig. 52). From this survey we knew that the seamount has a large caldera where we might be able to make some heat flow measurements and take a gravity core. The measurements of HF1035 are not located on a seismic line due to time constraints but a line shot during the site survey (Wilson et al., 2003a) almost crosses the seamount at its western flank. The data of this line are not available on the Internet but we will try to get them from the PIs of this site survey project. The result of the survey is somewhat puzzling but may be better explainable once we have the seismic data. Heat flow steadily increases toward the seamount from values around 30 mW/m^2 to almost 100 mW/m^2 (Fig. 51). It then suddenly drops within 2 km to 20 mW/m^2 but rises again to 35 mW/m^2 close to the seamount. Two measurements within the caldera where the probe did not fully penetrate are almost identical and give very low values of 12 mW/m^2.

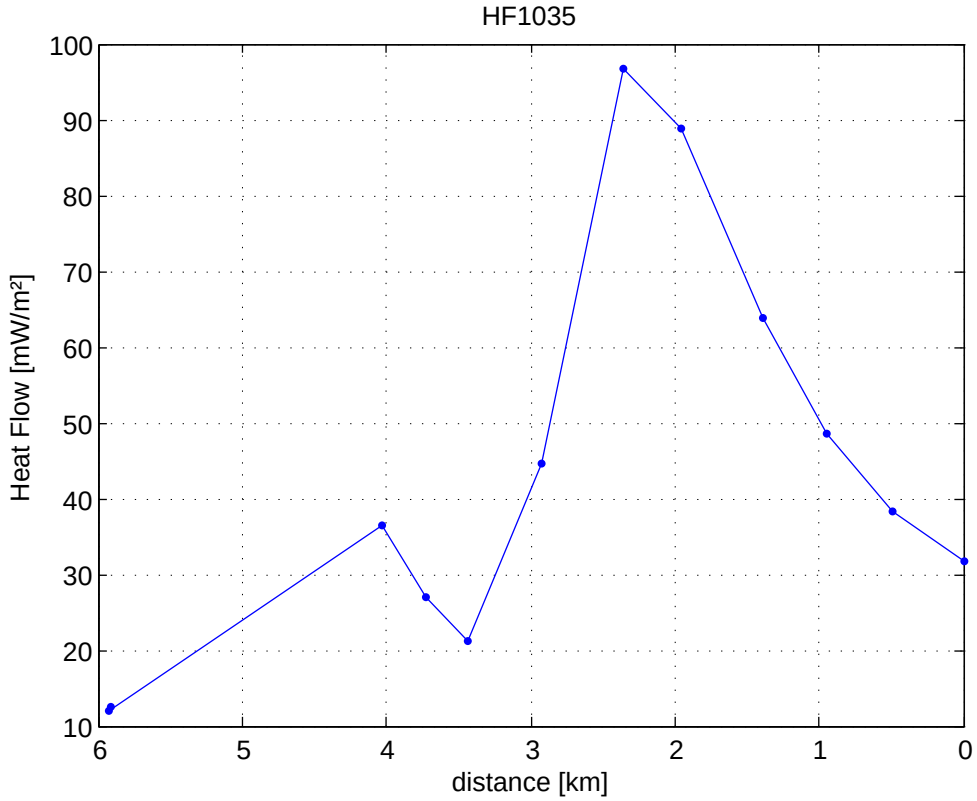

Figure 51: Heat flow values of profile HF1035 vs distance from the first penetration of the profile.

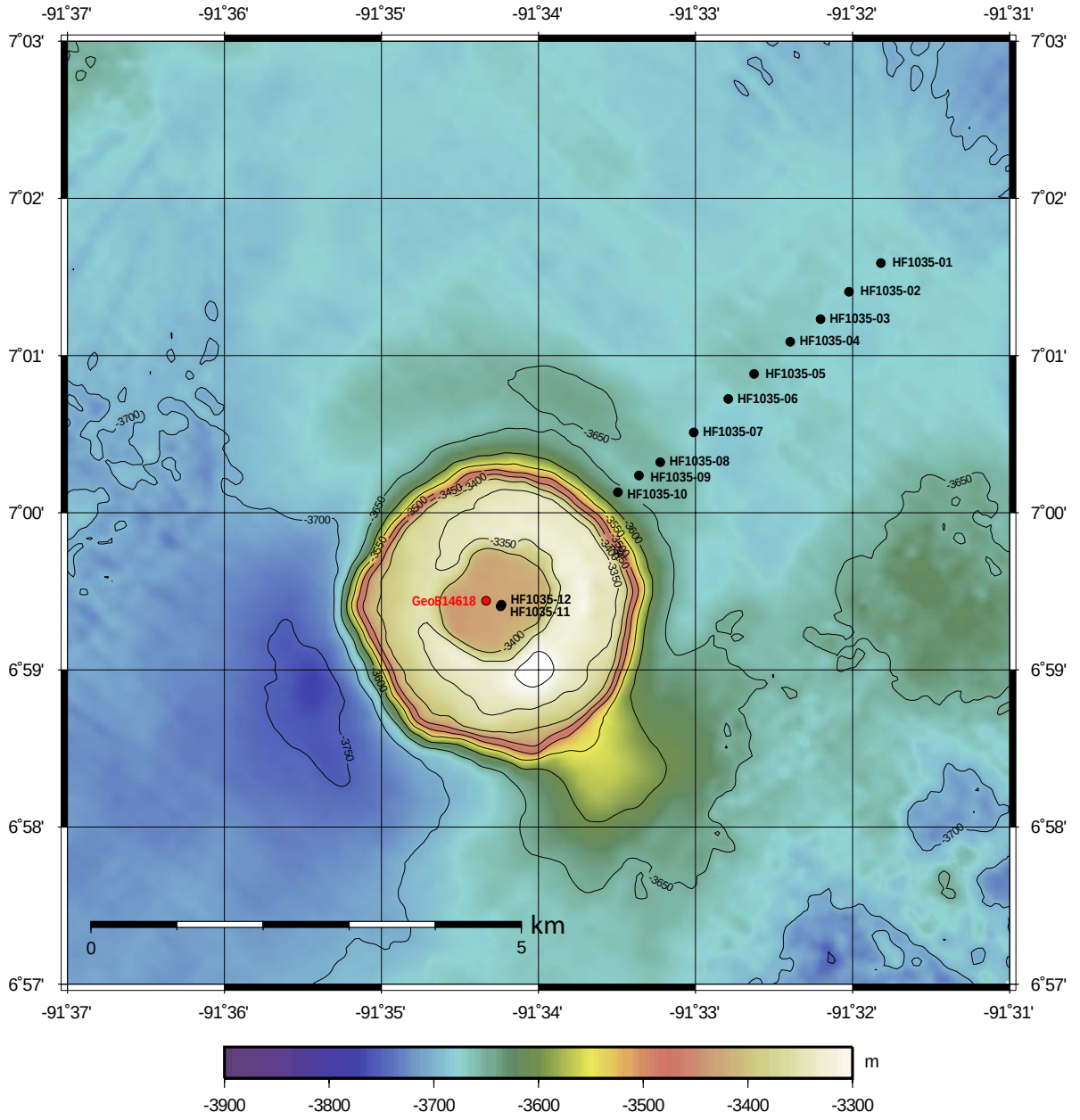

Figure 52: Location of penetrations with the heat flow probe on profile HF1035 (black filled circles) and core positions as red filled circles.

5.9.2 Sediment sampling and core description

(P. Alt-Epping, R. Becke, K. Enneking, T. Fleischmann, K. Gaida, C. Janssen, T. Pichler, M. Ruiz and M. Zwick)

In this working area, which was located between GUATB-2 and GUATB-3, one gravity core (GeoB14618) was taken in sediments, which accumulated in the summit caldera of a seamount (Fig. 52). The exact location was 6°59.441 N and 91°34.335 W and the water depth was 3414 *m*.

The recovery at this site was only 334 *cm*, the shortest core of the whole cruise. The sediments recovered were more or less uniform and showed no primary sediment features. In summary, the sediments were slightly to extensively bioturbated and consisted of clayey nannofossil ooze and nannofossil silty clay. Foraminifers as well as a few black concretions (manganese nodules?) were found. The sediment color varied from very dark brown (10YR2/2) at the top to pale brown (10YR7/4) and deeper light yellowish brown (10YR6/4) at the base. The strong bioturbated sections were generally darker.

A detailed core description is presented in Appendix (Core Logs).

5.9.3 Geochemistry of pore water

Due to the uniformity of the core only 5 pore water samples were collected. The spacing was approximately 50 *cm*, starting at a depth of 4 *cm* below seafloor. The pH was uniform at 7.6. The Eh varied between 128 - 158 mV without showing a trend., Alkalinity varied from 2.9 - 3 $mmolL^{-1}$ and PO_4^{3-} from 0.2 - 0.3 mgL^{-1}, while Fe^{2+} and NH_4^+ stayed below their respective detection limits of 0.05 and 0.5 mgL^{-1}. A complete listing of the results for all parameters is shown in Appendix (Pore Water Chemistry). Description of the on-board used methods and preservation of samples were described above (see section 4.2.3).

5.10 Data and sample storage and availability

Data will be stored in the database Pangaea about one year after the cruise. The moratorium period will expire after two years.

5.11 Acknowledgements

We thank the crew of R/V Sonne with Captain Meyer for their efforts, their enthusiasm and the warm welcome on board. This project is gratefully financed by the BMBF (Federal Ministry of Education and Research), Forderkennzeichen 03G0207A.

References

Alt, J., 2004. Hydrogeology of the oceanic lithosphere. Cambridge, Ch. 15, pp. 495 533.

Bekins, B. A., Spivack, A. J., Davis, E. E., Mayer, L. A., 2007. Dissolution of biogenic ooze over basement edifi ces in the equatorial Pacific with implications for hydrothermal ventilation of the oceanic crust. Geology 35 (8), 679 682.

Bredehoeft, J., Papadopolous, I., 1965. Rates of vertical groundwater movement estimated from the Earths thermal profile. Water Resources Research 1, 325 328.

Bullard, E., Mar. 1954. The Flow of Heat through the Floor of the Atlantic Ocean. Proceedings of the Royal Society A: Mathematical, Physical and Engineering Sciences 222 (1150), 408 429.

Caress, D. W., Chayes, D. N., 2009. MB-System: Mapping the Seafloor.
URL `http://www.mbari.org/data/mbsystem`

Fabian, M., Gmeinder, T., Kaul, N., 2008. The Bremen Lance Insertion Retardation Meter for Assessing Seafloor Stability. Sea Technology, 10 13.

Fisher, A. T., Feb. 2005. Marine hydrogeology: recent accomplishments and future opportunities. Hydrogeology Journal 13 (1), 69 97.
URL `http://www.springerlink.com/index/10.1007/s10040-004-0400-y`

Fisher, A. T., Becker, K., Davis, E. E., 1997. The permeability of young oceanic crust east of Juan de Fuca Ridge determined using borehole thermal measurements. Geophysical Research Letters 24 (11), 1311 1314.

Fisher, A. T., Davis, E., Becker, K., 2008. Borehole-to-borehole hydrologic response across 2.4 km in the upper oceanic crust: Implications for crustal-scale properties, J. J. Geophys. Res. 113 (B07106).

Harris, R. N., Fisher, A. T., Chapman, D. S., 2004. Fluid flow through seamounts and implications for global mass fluxes. Geology 32 (8), 725 728.

Hartmann, A., Villinger, H., 2002. Inversion of marine heat flow measurements by expansion of the temperature decay function. Geophysical Journal International 148 (3), 628 636.

Hutnak, M., Fisher, A. T., 2007. Influence of sedimentation, local and regional hydrothermal circulation, and thermal rebound on measurements of seafloor heat flux. Journal of Geophysical Research 112 (B12101), 1 19.

Hutnak, M., Fisher, A. T., Harris, R., Stein, C., Wang, K., Spinelli, G., Schindler, M., Villinger, H., Silver, E., 2008. Large heat and fluid fluxes driven through mid-plate outcrops on ocean crust. Nature Geoscience 1 (9), 611 614.

Hyndman, R., Davis, E., Wright, J., 1979. The measurements of marine geothermal heat flow by a multipenetration probe with digital acoustic telemetry and insitu thermal conductivity. Marine Geophysical Researches 4 (2), 181 205.

Landrø, M., Oct. 1992. Modelling of Gi Gun Signatures. Geophysical Prospecting 40, 721 747. URL http://doi.wiley.com/10.1111/j.1365-2478.1992.tb00549.x

Lister, C. R. B., 1970. Measurement of in situ sediment conductivity by means of a Bullard-type probe. Geophys. J. R. astr. Soc. 19, 521 532.

Lister, C. R. B., 1979. The pulse-probe method of conductivity measurement. Geophys. J. R. astr. Soc. 57, 451 461.

Mayer, L., Isias, N., Janecek, T., 1992. 9. Site 844. Proceedings of the Ocean Drilling Program 138, 119 188.

Mayer, L. A., 1981. Erosional troughs in deep-sea carbonates and their relationship to basement structure. Marine Geology 39, 59 80.

Michaud, F., Chabert, A., Collot, J.-Y., 2005. Fields of multi-kilometer scale sub-circular depressions in the Carnegie Ridge sedimentary blanket: Effect of underwater carbonate dissolution? Marine Geology 216, 205 219.

Moore, T. C., Mitchell, N. C., Lyle, M., Backman, J., Palike, H., 2007. Hydrothermal pits in the biogenic sediments of the equatorial Pacific Ocean. Geochemistry Geophysics Geosystems 8 (3).

Ratcliffe, E. H., 1960. The Thermal Conductivities of Ocean Sediments. Journal of Geophysical Research 65 (5), 1535.

Stein, C. A., Stein, S., 1992. A model for the global variation in oceanic depth and heat flow with lithospheric age. Nature 359, 123 129.

Teagle, D. A. H., Alt, J. C., Umino, S., Miyashita, S., Banerjee, N. R., Wilson, D. S., 2006a. Expedition 309 / 312 summary. Proceedings of the Integrated Ocean Drilling Program 309/312, 1 127.

Teagle, D. A. H., Umino, S., Miyashita, S., Banerjee, N. R., Wilson, D. S., 2006b. Site 1256. Proceedings of the Integrated Ocean Drilling Program 309/312.

Villinger, H., Davis, E. E., 1987. A New Reduction Algorithm for Marine Heat Flow Measurements. Journal of Geophysical Research 92 (B12), 12846 12856.

Wessel, P., Smith, W., 2010. The Generic Mapping Tools (GMT), Version 4.5.2, Technical Reference and Cookbook.
URL http://gmt.soest.hawaii.edu/

Wilson, D. S., Hallenborg, E., Harding, A. J., Kent, G. M., 2003a. 4. Data Report: Site survey results from cruise EW9903. Proceedings of the Ocean Drilling Program 206.

Wilson, D. S., Teagle, D. A. H., Acton, G. D., 2003b. 3. Site 1256. Proceedings of the Ocean Drilling Program 206.

A Appendix Geophysics

A.1 Bathymetry

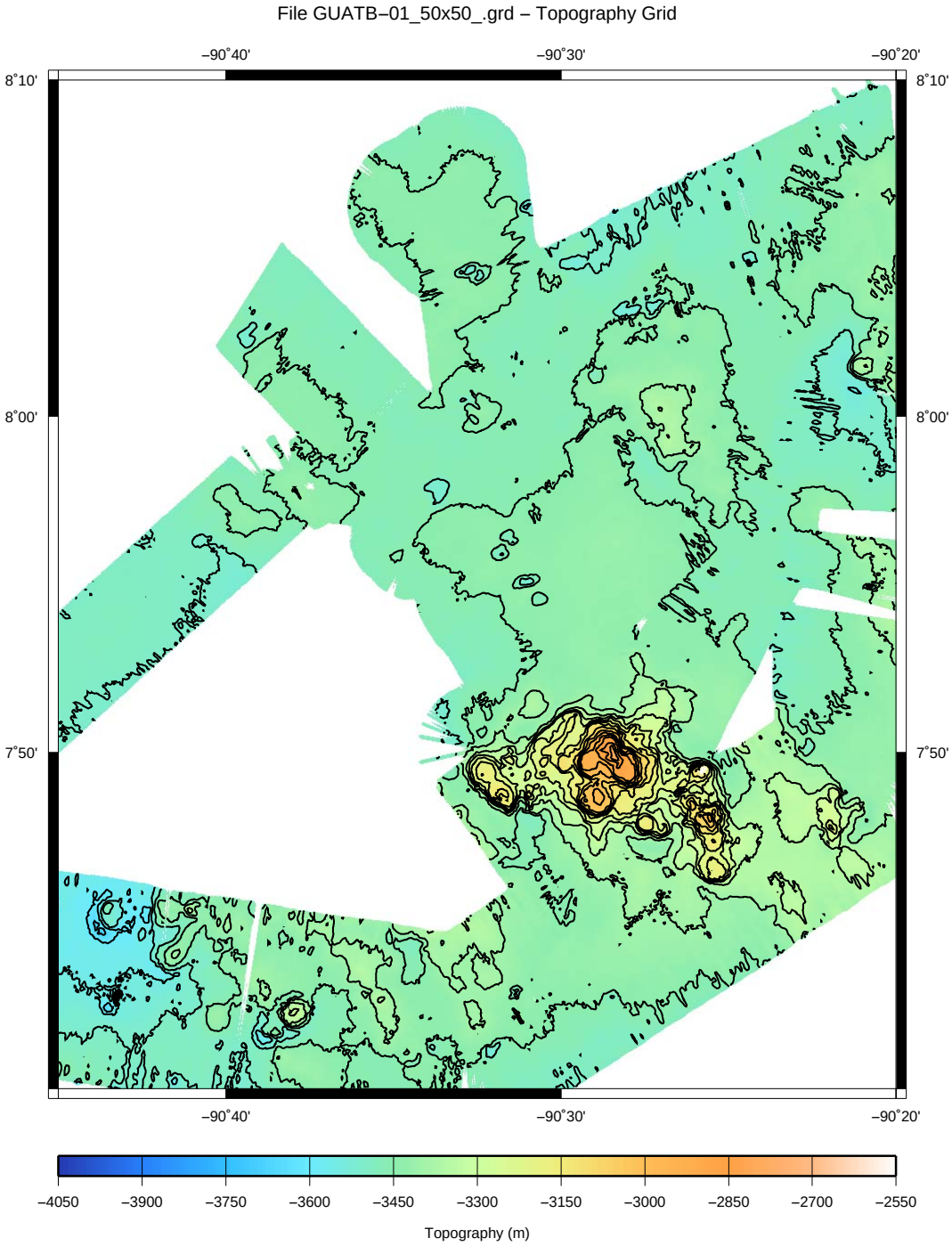

Figure 53: Map showing data from SO207, working area GUATB-01.

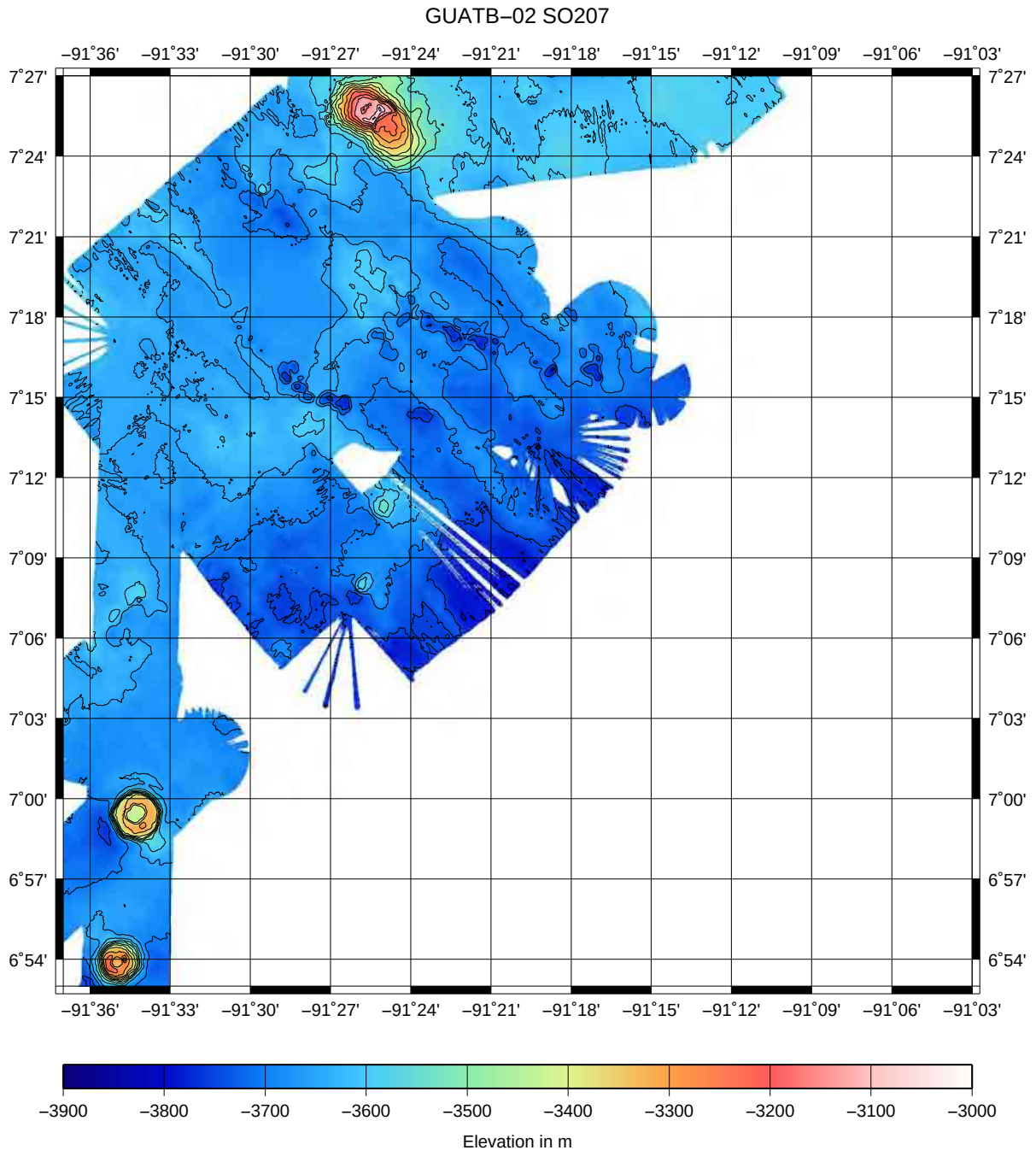

Figure 54: Map showing data from SO207, working area GUATB-02.

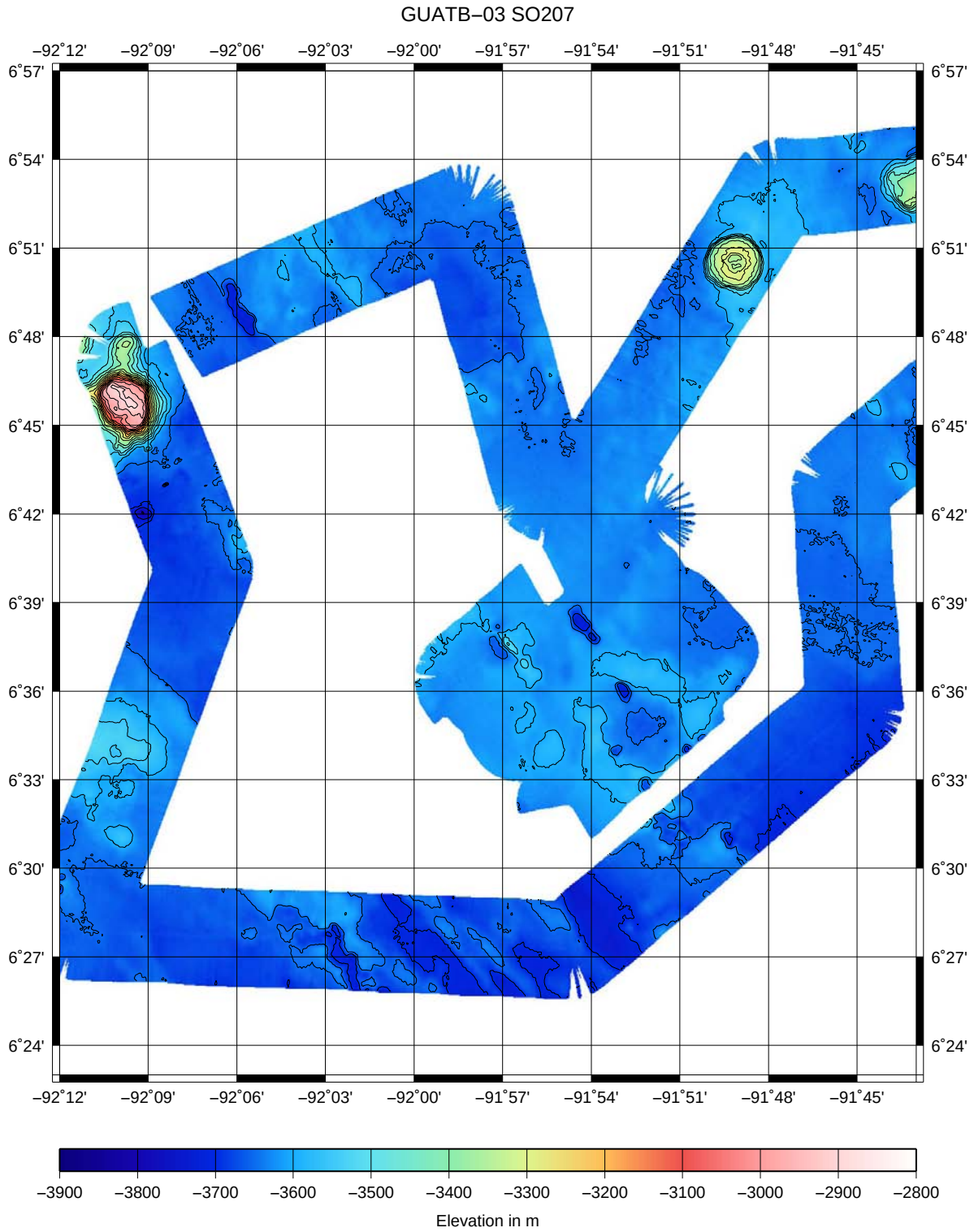

Figure 55: Map showing data from SO207, working area GUATB-03.

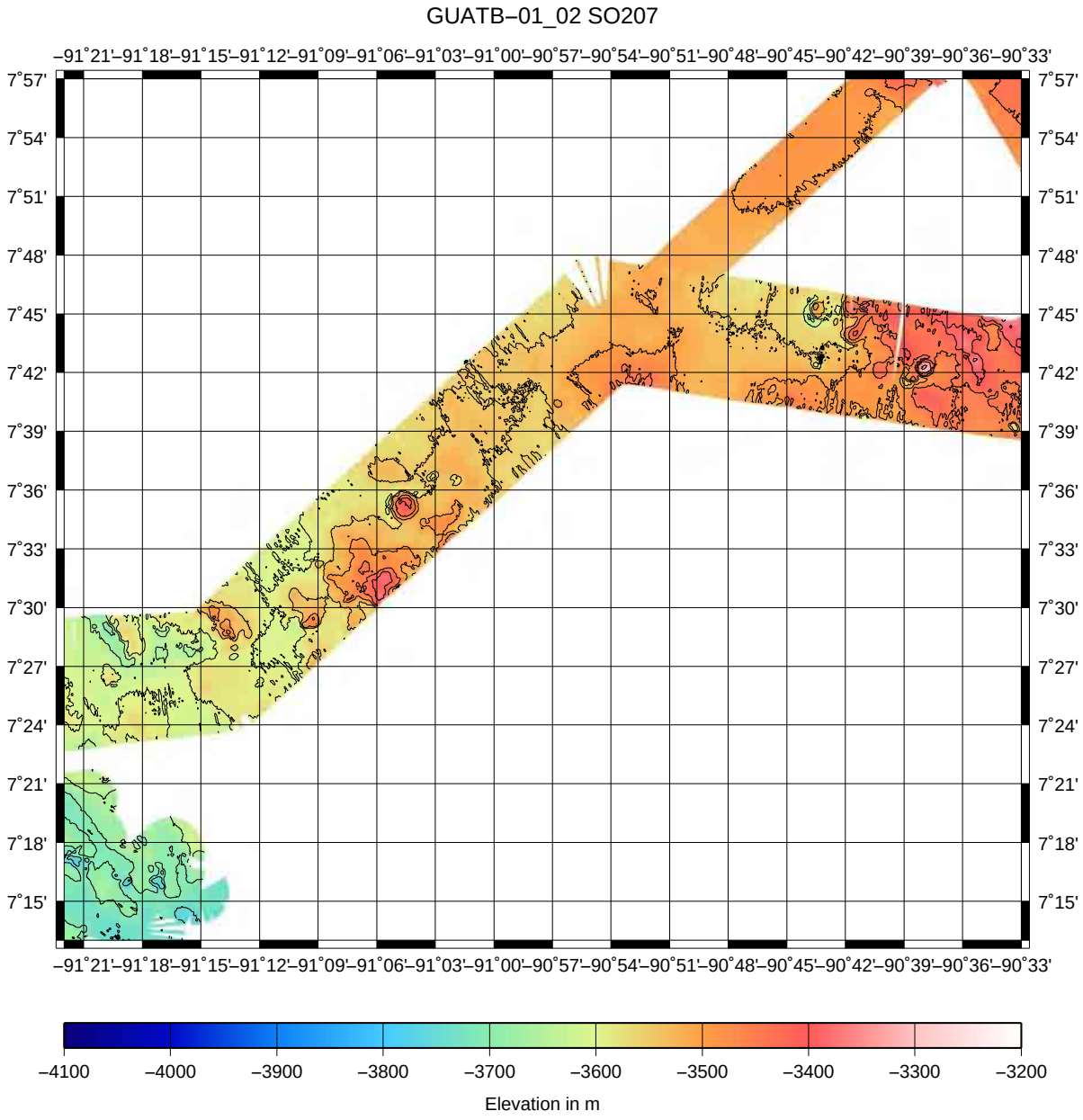

Figure 56: Map showing data from SO207, transition from working area GUATB-01 to GUATB-02.

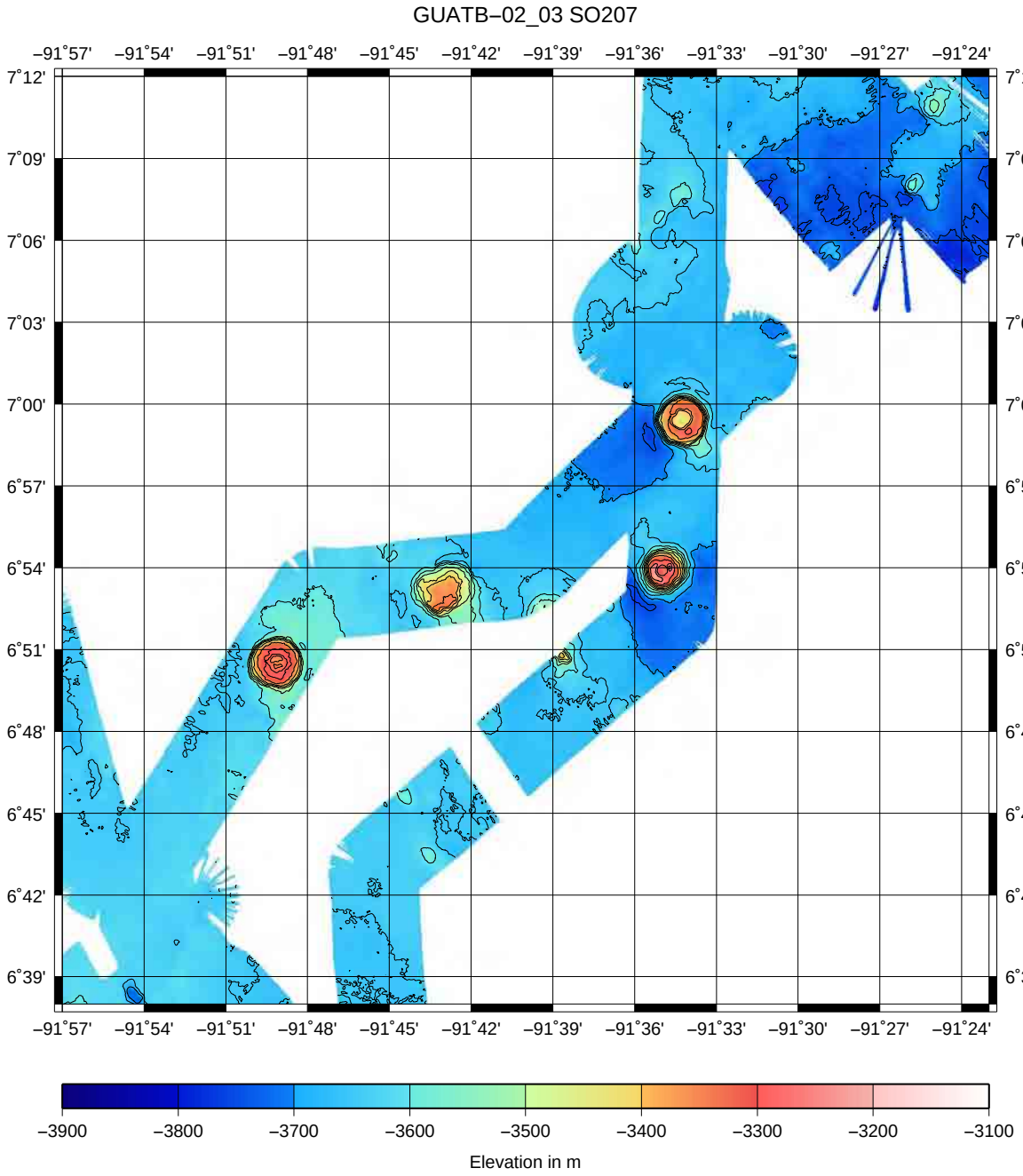

Figure 57: Map showing data from SO207, transition from working area GUATB-02 to GUATB-03.

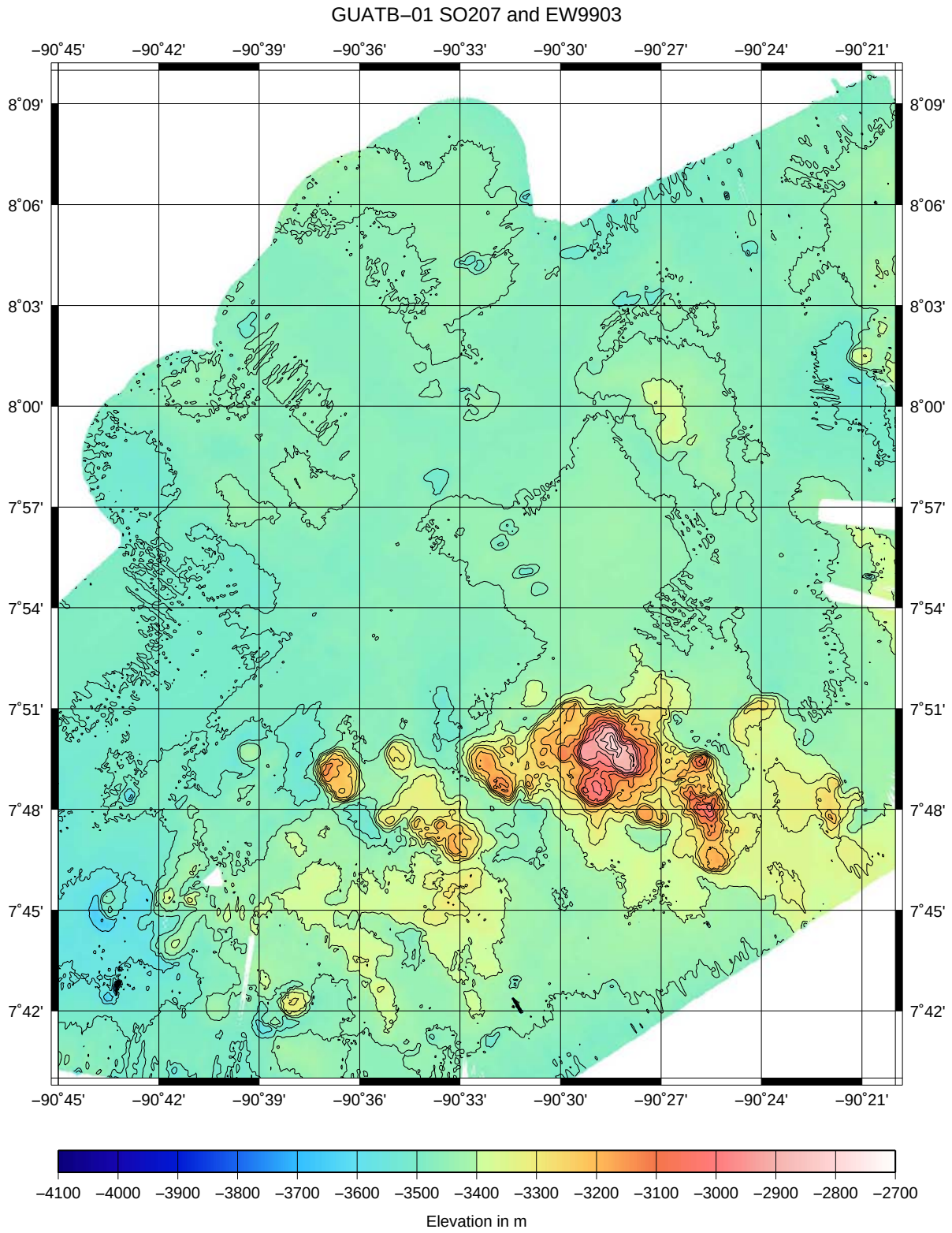

Figure 58: Map of working area GUATB-01 with joint data from SO207 and cruise EW9903.

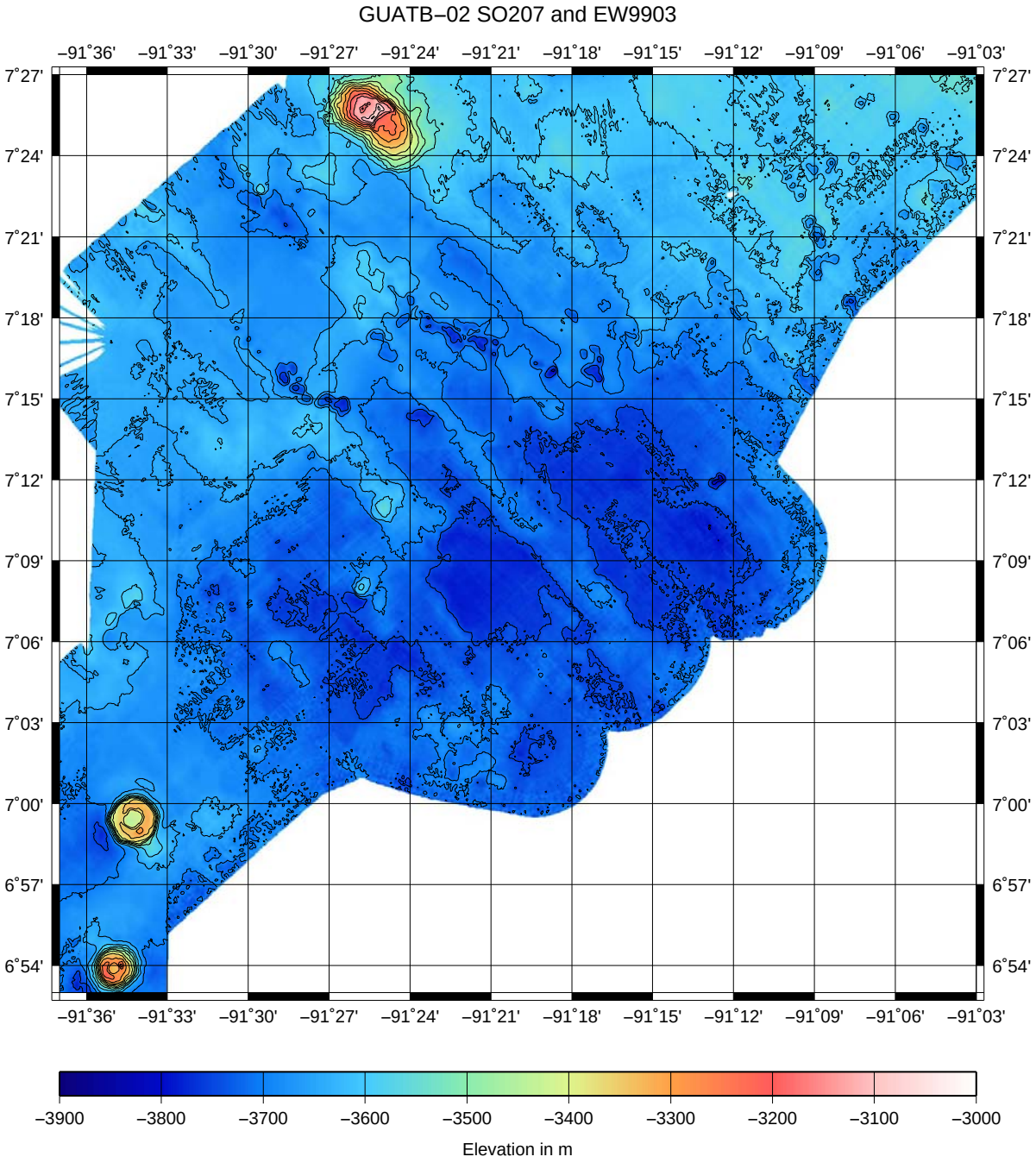

Figure 59: Map of working area GUATB-02 with joint data from SO207 and cruise EW9903.

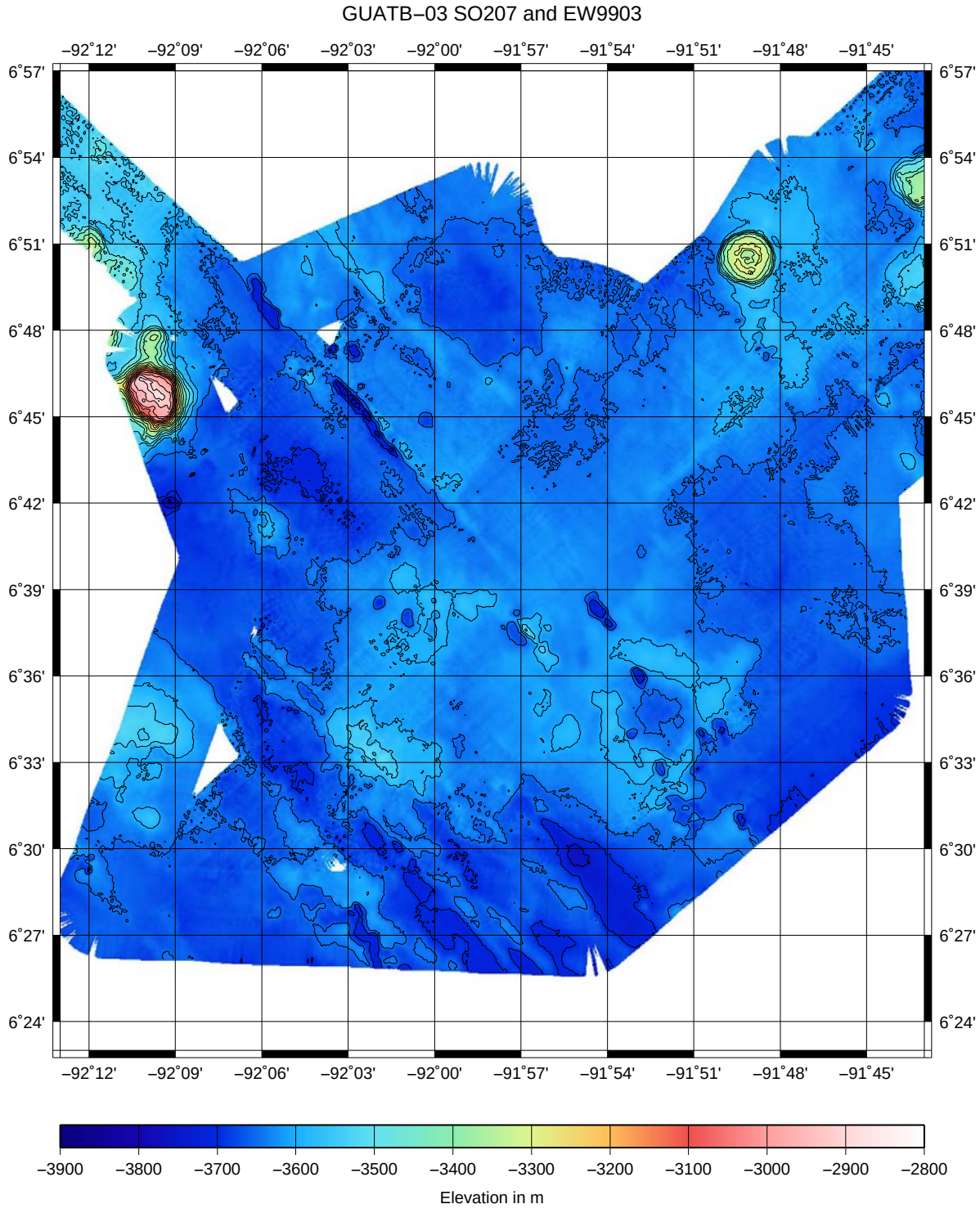

Figure 60: Map of working area GUATB-03 with joint data from SO207 and cruise EW9903.

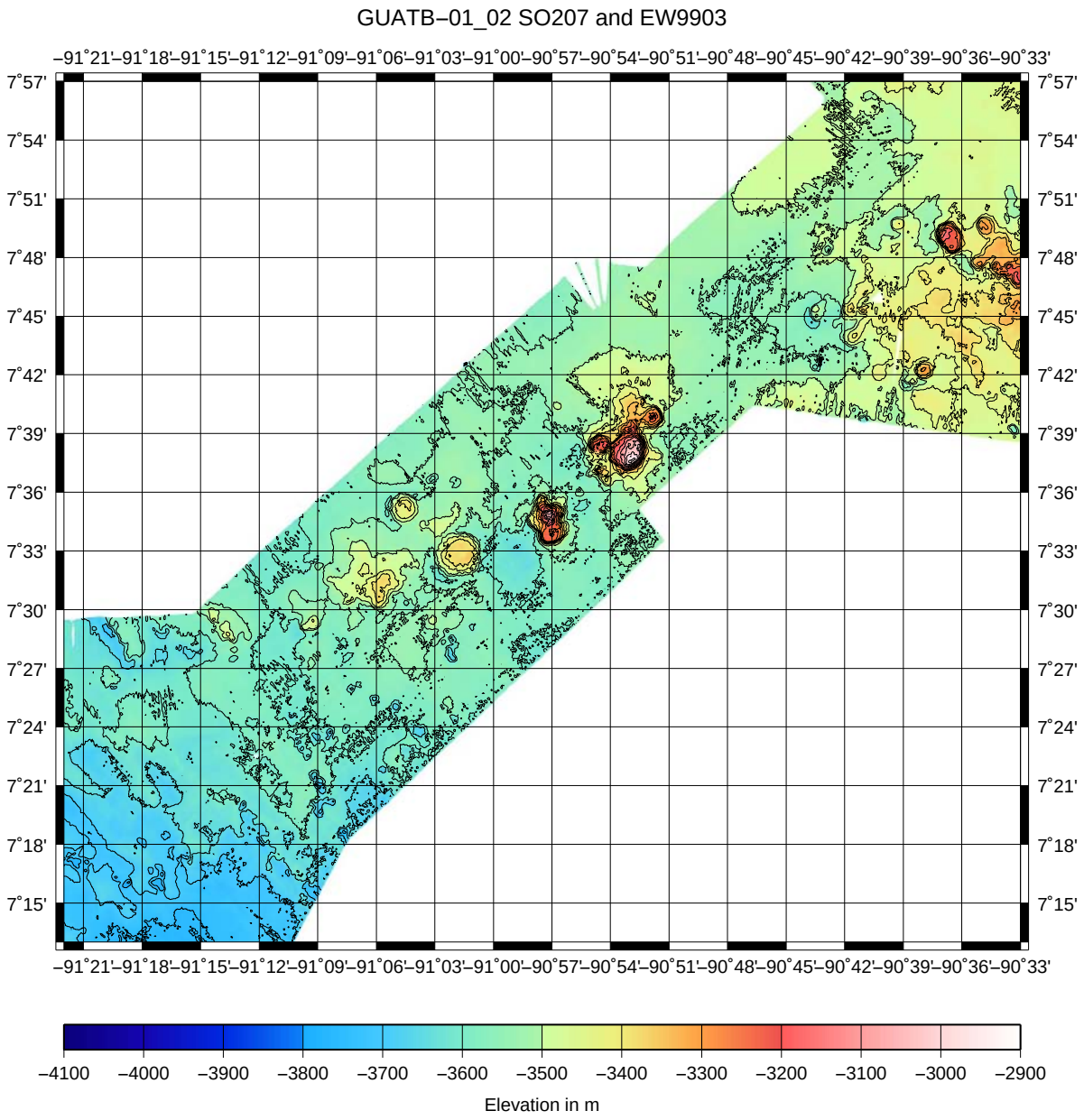

Figure 61: Map of the transition from working area GUATB-01 to GUATB-02 with joint data from SO207 and cruise EW9903.

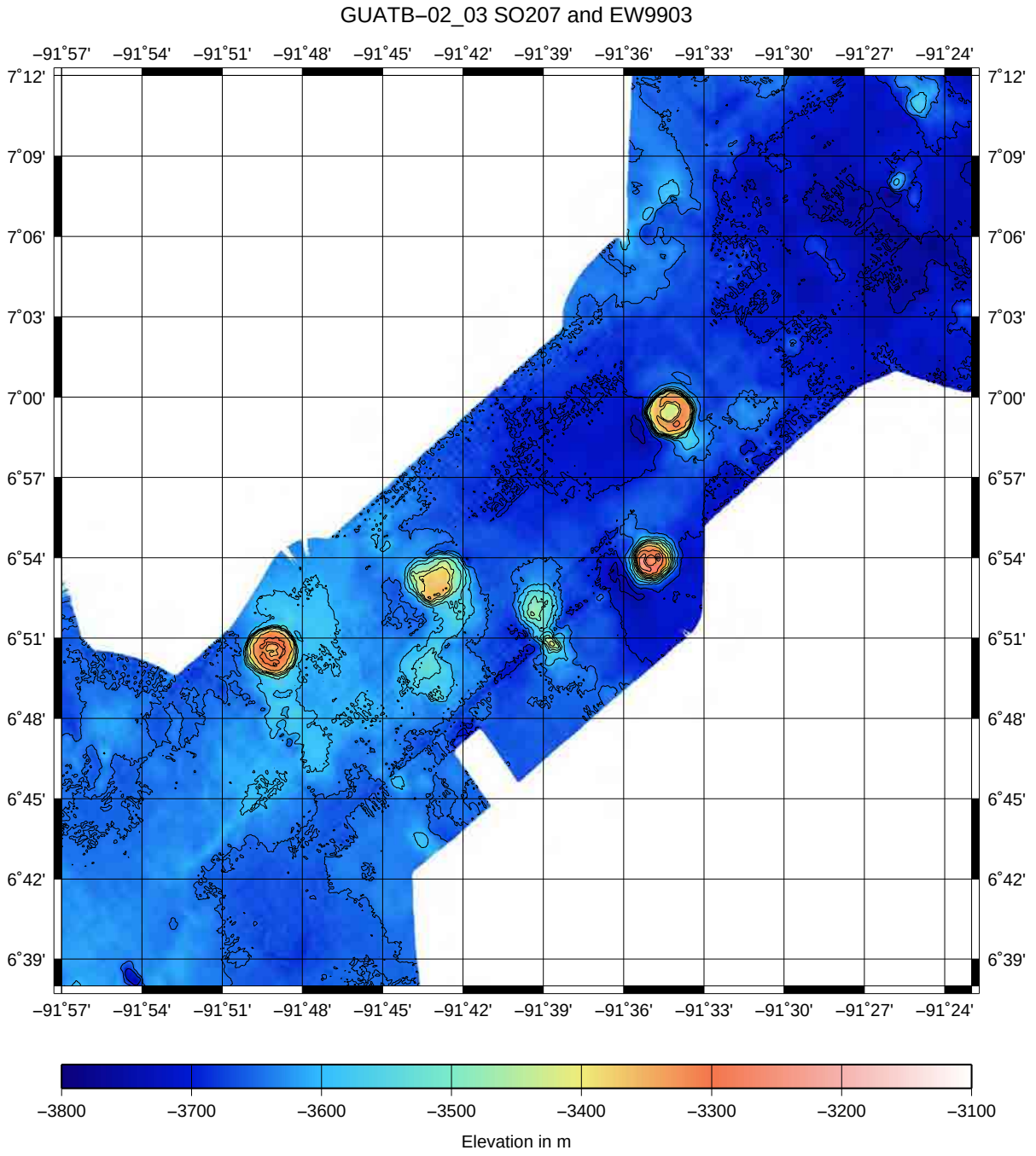

Figure 62: Map of the transition from working area GUATB-02 to GUATB-03 with joint data from SO207 and cruise EW9903.

A.2 Seismic and Parasound Survey

A.2.1 Profile Maps

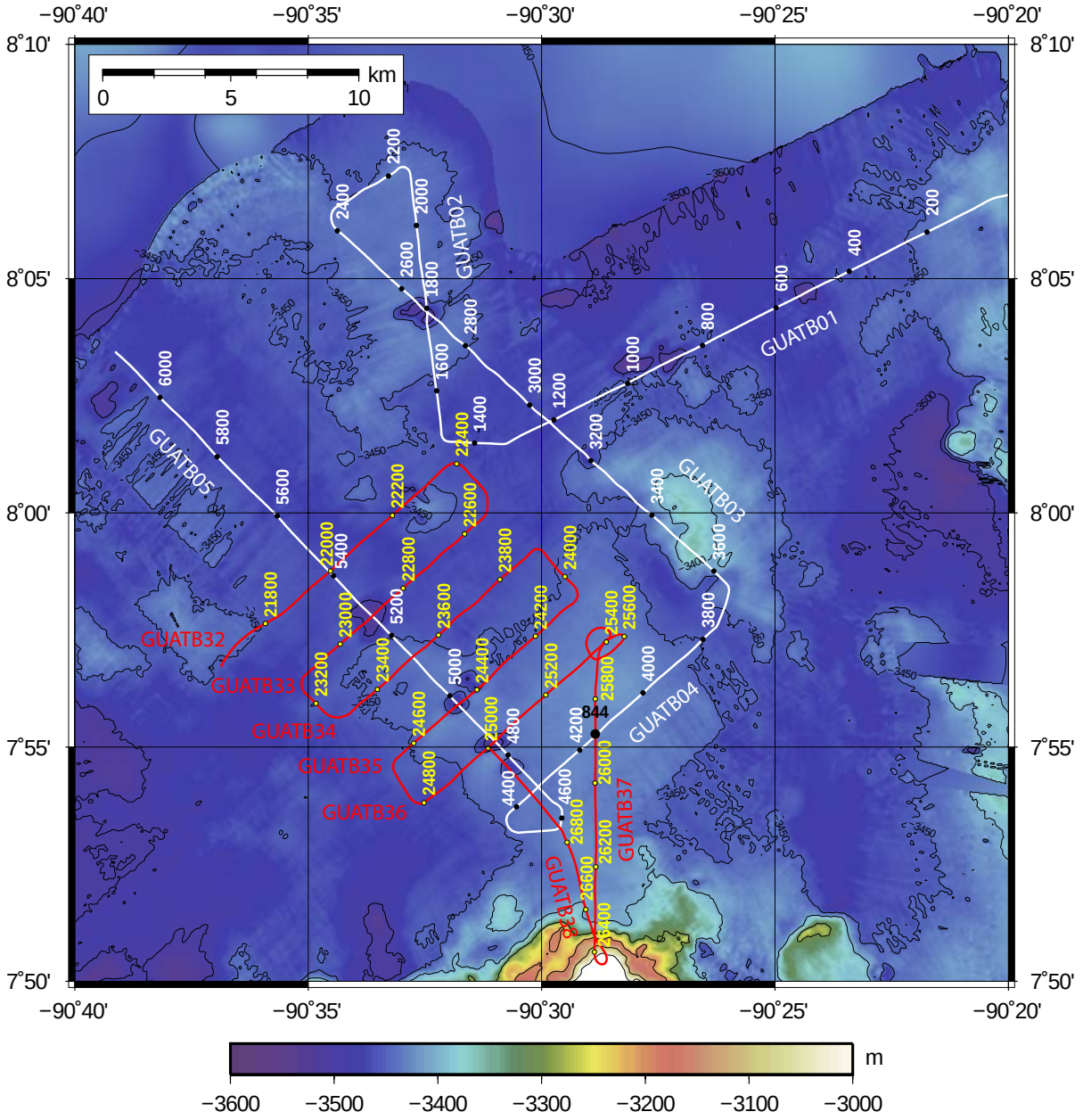

Figure 63: Seismic and Parasound survey with shotpoint navigation in working area GUATB-01. Lines GUATB01 to GUATB05 (white) and GUATB32 to GUATB38 (red lines with yellow numbers).

Table 14: Overview about all seismic profiles shot during cruise SO207.

Profile	StartFFN	EndFFN	StartTime	EndTime	StartPosition[Lat/Lon]				EndPosition[Lat/Lon]				Dist[nm]	#Shots
GUATB01	26	1318	23.06.2010 22:25:34	24.06.2010 01:17:53	8	6.7510	-90	20.1660	8	1.4900	-90	30.7350	181.61	1292
GUATB02	1467	2126	24.06.2010 01:37:44	24.06.2010 03:05:36	8	1.5230	-90	32.0050	8	7.2770	-90	32.8250	5.88	659
GUATB03	2399	3662	24.06.2010 03:42:00	24.06.2010 06:30:58	8	6.0340	-90	34.3800	7	58.3440	-90	25.9830	11.4	1263
GUATB04	3781	4428	24.06.2010 06:46:50	24.06.2010 08:13:07	7	57.4330	-90	26.4080	7	53.5440	-90	30.7320	5.79	647
GUATB05	4623	6129	24.06.2010 08:39:07	24.06.2010 11:59:56	7	53.7130	-90	29.5930	8	3.3030	-90	38.9800	13.39	1506
GUATB08	6325	6860	28.06.2010 21:43:58	28.06.2010 22:55:40	7	14.4400	-91	20.3870	7	14.1830	-91	25.1400	5.4	535
GUATB09	6863	7639	28.06.2010 22:55:40	29.06.2010 00:39:08	7	14.1670	-91	25.0790	7	16.8690	-91	31.4310	164.98	776
GUATB10	7683	8056	29.06.2010 00:45:00	29.06.2010 01:34:45	7	17.2220	-91	31.4410	7	19.2580	-91	28.7530	3.38	373
GUATB11	8074	9605	29.06.2010 01:37:09	29.06.2010 05:01:18	7	19.2960	-91	28.6060	7	15.3840	-91	15.4630	13.69	1531
GUATB12	9818	10551	29.06.2010 05:29:42	29.06.2010 07:07:27	7	16.0580	-91	15.5040	7	16.1370	-91	22.1200	6.59	733
GUATB13	10552	11205	29.06.2010 07:07:35	29.06.2010 08:34:40	7	16.1420	-91	22.1260	7	20.5940	-91	25.7880	5.79	653
GUATB14	11269	11756	29.06.2010 08:43:12	29.06.2010 09:48:08	7	21.0370	-91	25.4310	7	20.3450	-91	21.1520	4.44	487
GUATB15	11845	12918	29.06.2010 10:00:00	29.06.2010 12:23:06	7	20.0980	-91	20.6850	7	13.7140	-91	27.9180	9.64	1073
GUATB16	12975	13365	01.07.2010 20:14:42	01.07.2010 21:06:42	7	14.6280	-91	30.0810	7	16.8970	-91	27.5600	3.38	390
GUATB17	13569	14089	01.07.2010 21:34:00	01.07.2010 22:43:15	7	16.5410	-91	25.8670	7	19.5510	-91	22.4540	3.11	520
GUATB18	14405	14756	01.07.2010 23:25:23	02.07.2010 00:12:11	7	18.3290	-91	21.2160	7	16.3760	-91	23.5270	3.02	351
GUATB19	14903	15287	02.07.2010 00:31:47	02.07.2010 01:23:00	7	15.6720	-91	22.9280	7	18.0190	-91	20.3690	3.45	384
GUATB20	15399	15765	02.07.2010 01:37:56	02.07.2010 02:26:44	7	18.1570	-91	20.4640	7	14.9960	-91	20.0300	3.19	366
GUATB21	15909	16383	02.07.2010 02:45:56	02.07.2010 03:49:09	7	15.0400	-91	20.0460	7	17.8240	-91	16.7670	4.29	474
GUATB22	16557	16982	02.07.2010 04:12:21	02.07.2010 05:09:01	7	17.1310	-91	16.3070	7	14.6320	-91	19.0130	3.67	425
GUATB24	17068	17829	03.07.2010 17:15:52	03.07.2010 18:57:21	6	41.0010	-91	53.2150	6	36.5020	-91	58.3260	6.84	761
GUATB25	17992	18742	03.07.2010 19:19:05	03.07.2010 20:59:06	6	35.7300	-91	57.3780	6	40.1790	-91	52.4240	6.64	750
GUATB26	18838	19613	03.07.2010 21:11:54	03.07.2010 22:55:22	6	39.6050	-91	51.9490	6	35.1100	-91	57.0890	6.86	775
GUATB27	19793	20554	03.07.2010 23:19:23	04.07.2010 01:00:51	6	34.4060	-91	56.2530	6	39.0370	-91	51.2370	6.81	761
GUATB28	20602	20816	04.07.2010 01:07:15	04.07.2010 01:35:48	6	38.9270	-91	50.8160	6	37.5130	-91	49.5110	1.94	214
GUATB29	20865	21639	04.07.2010 01:42:20	04.07.2010 03:25:32	6	37.1290	-91	49.6220	6	32.5230	-91	54.7190	6.9	774
GUATB32	21800	22364	09.07.2010 01:03:04	09.07.2010 02:18:16	7	57.6400	-90	35.9170	8	0.9300	-90	32.1150	5.01	564
GUATB33	22545	23105	09.07.2010 02:42:28	09.07.2010 03:57:05	7	59.8620	-90	31.2930	7	56.6040	-90	34.9890	4.51	560
GUATB34	23325	23886	09.07.2010 04:26:25	09.07.2010 05:41:13	7	55.7860	-90	34.0370	7	59.0790	-90	30.3050	4.96	561
GUATB35	24081	24669	09.07.2010 06:07:14	09.07.2010 07:25:39	7	58.0720	-90	29.3230	7	54.6360	-90	33.1790	5.15	588
GUATB36	24818	25398	09.07.2010 07:45:31	09.07.2010 09:02:51	7	53.9170	-90	32.3860	7	57.2380	-90	28.6290	5	580
GUATB37	25672	26383	09.07.2010 09:39:24	09.07.2010 11:14:12	7	57.1300	-90	28.7250	7	50.7830	-90	28.8650	6.36	711
GUATB38	26500	26734	09.07.2010 11:29:48	09.07.2010 12:01:00	7	50.7480	-90	28.7370	7	52.6900	-90	29.3400	2.04	234

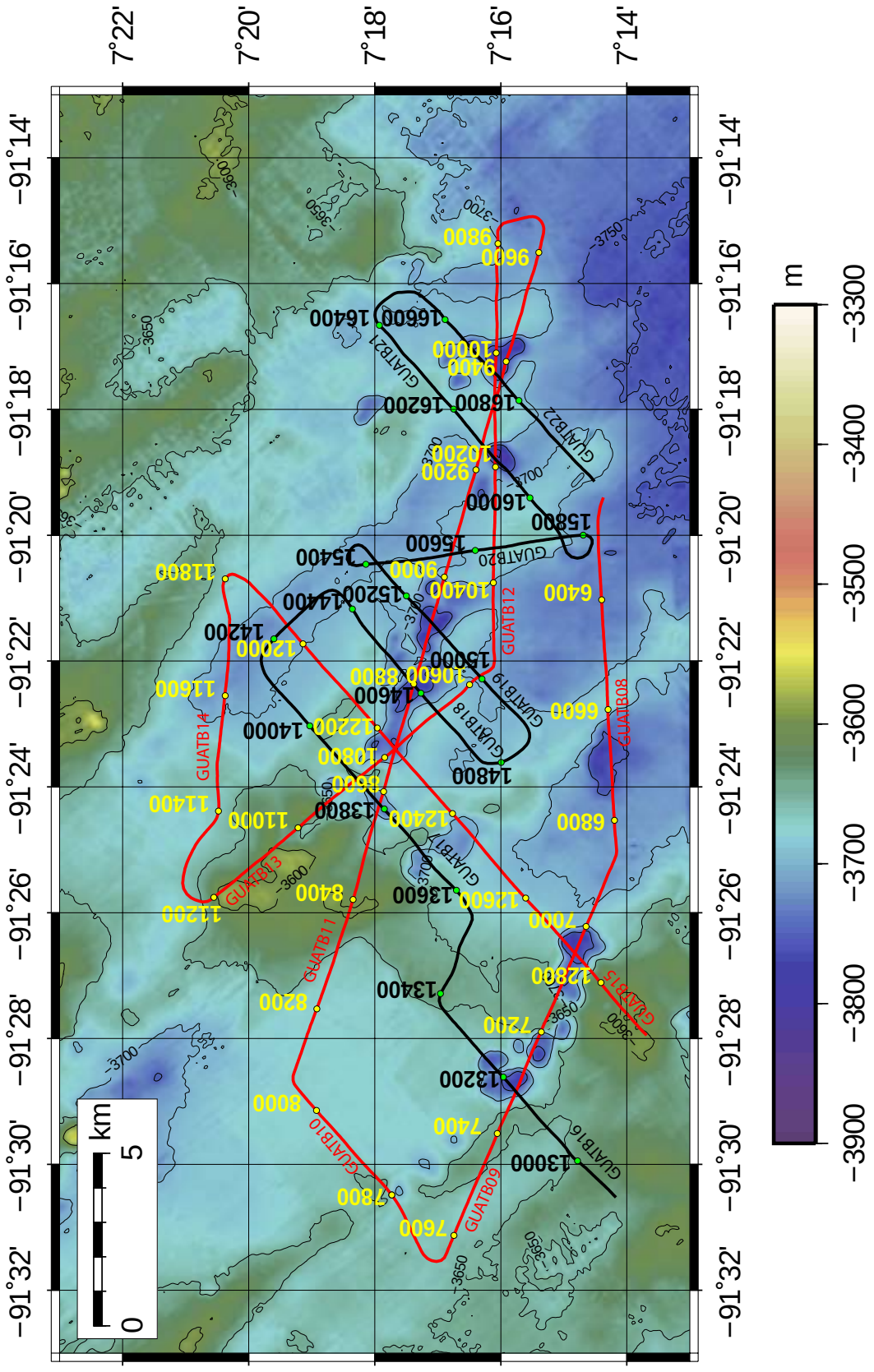

Figure 64: Seismic and Parasound survey with shotpoint navigation in working area GUATB-02. Lines GUATB08 to GUATB15 (red lines with yellow numbers) and GUATB16 to GUATB22 (black).

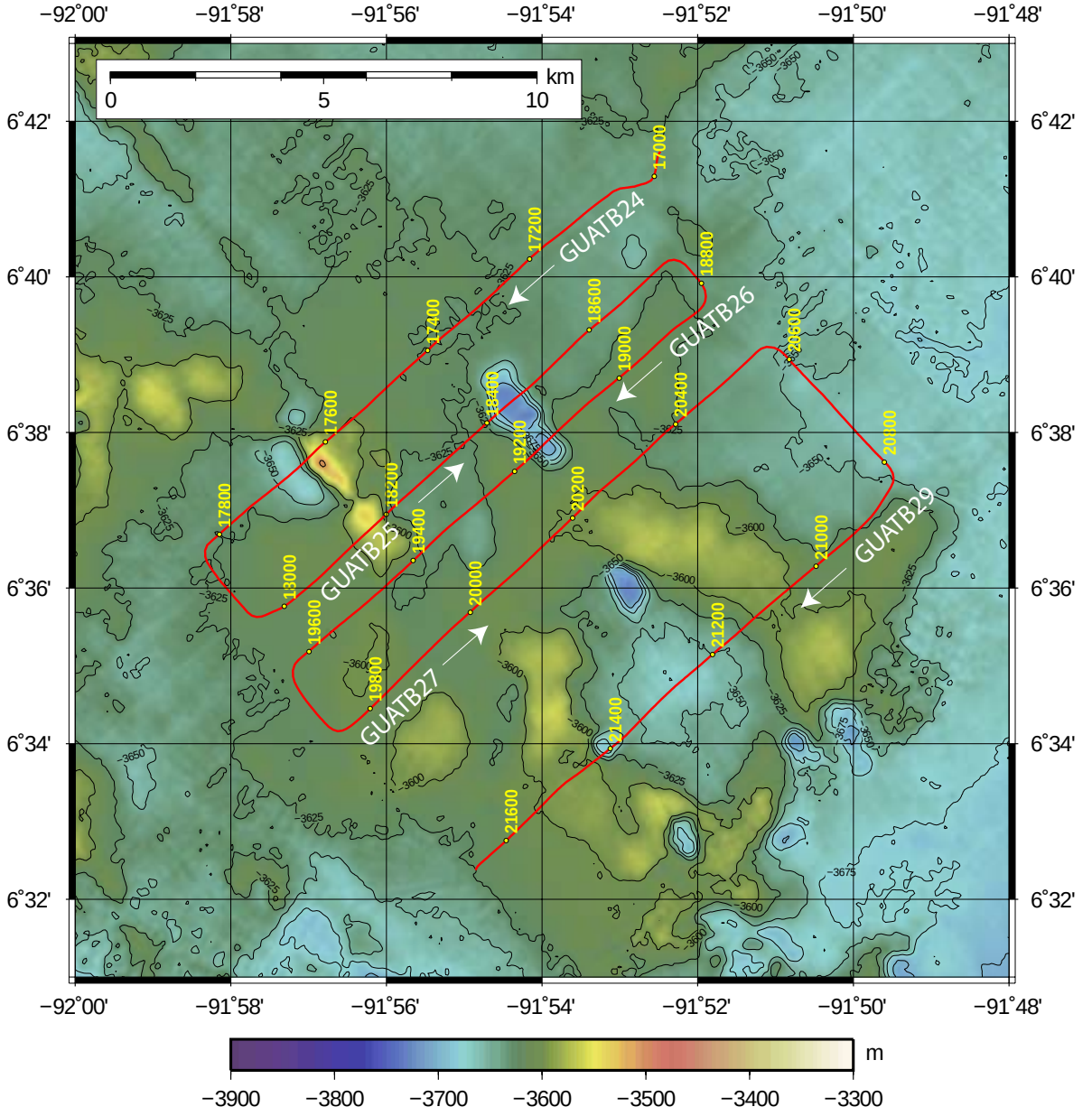

Figure 65: Seismic and Parasound survey with shotpoint navigation in working area GUATB-03. Lines GUATB024 to GUATB29.

A.2.2 Seismic Profiles

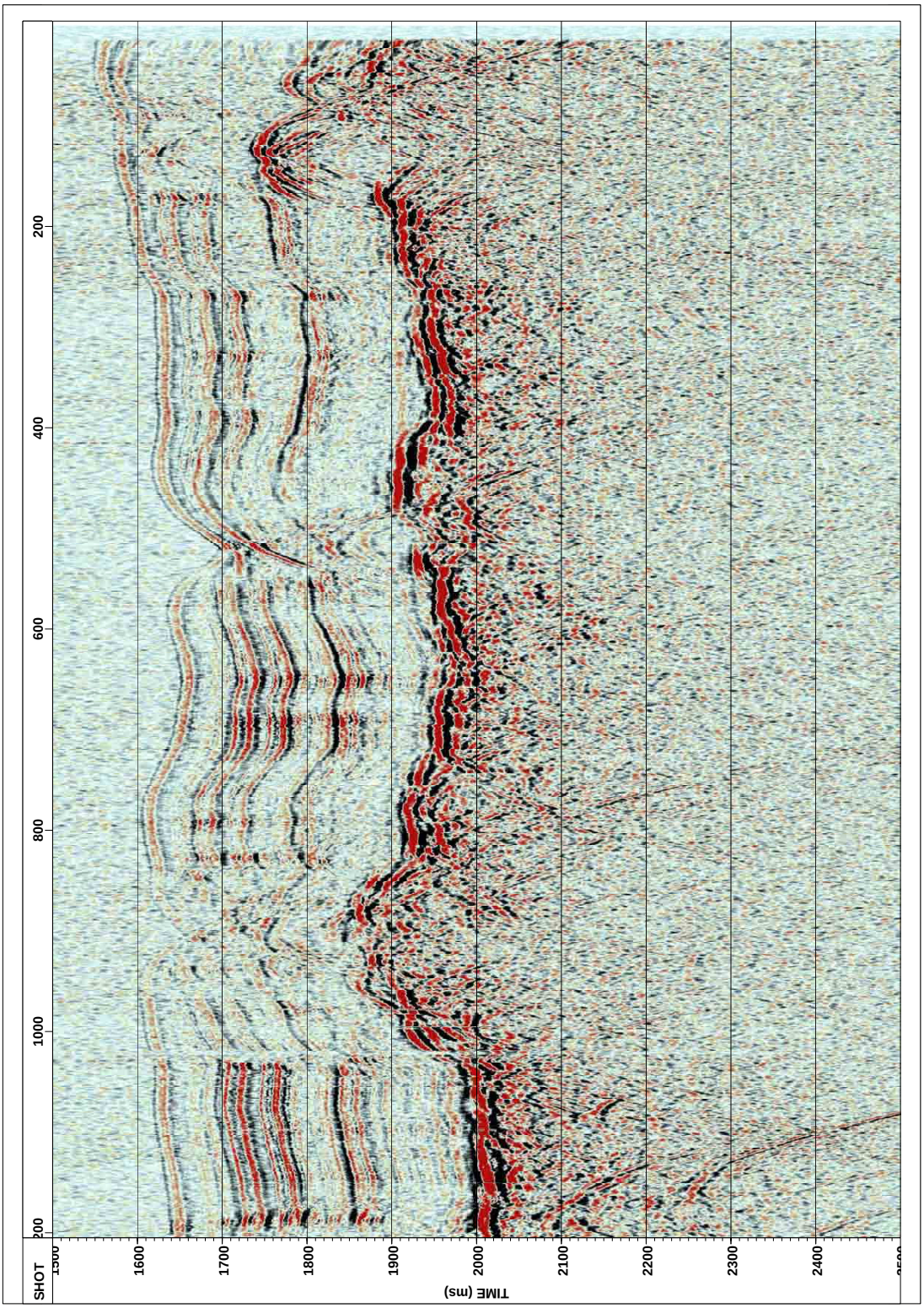

Figure 66: Seismic Profile GUATB01 in working area GUATB-01.

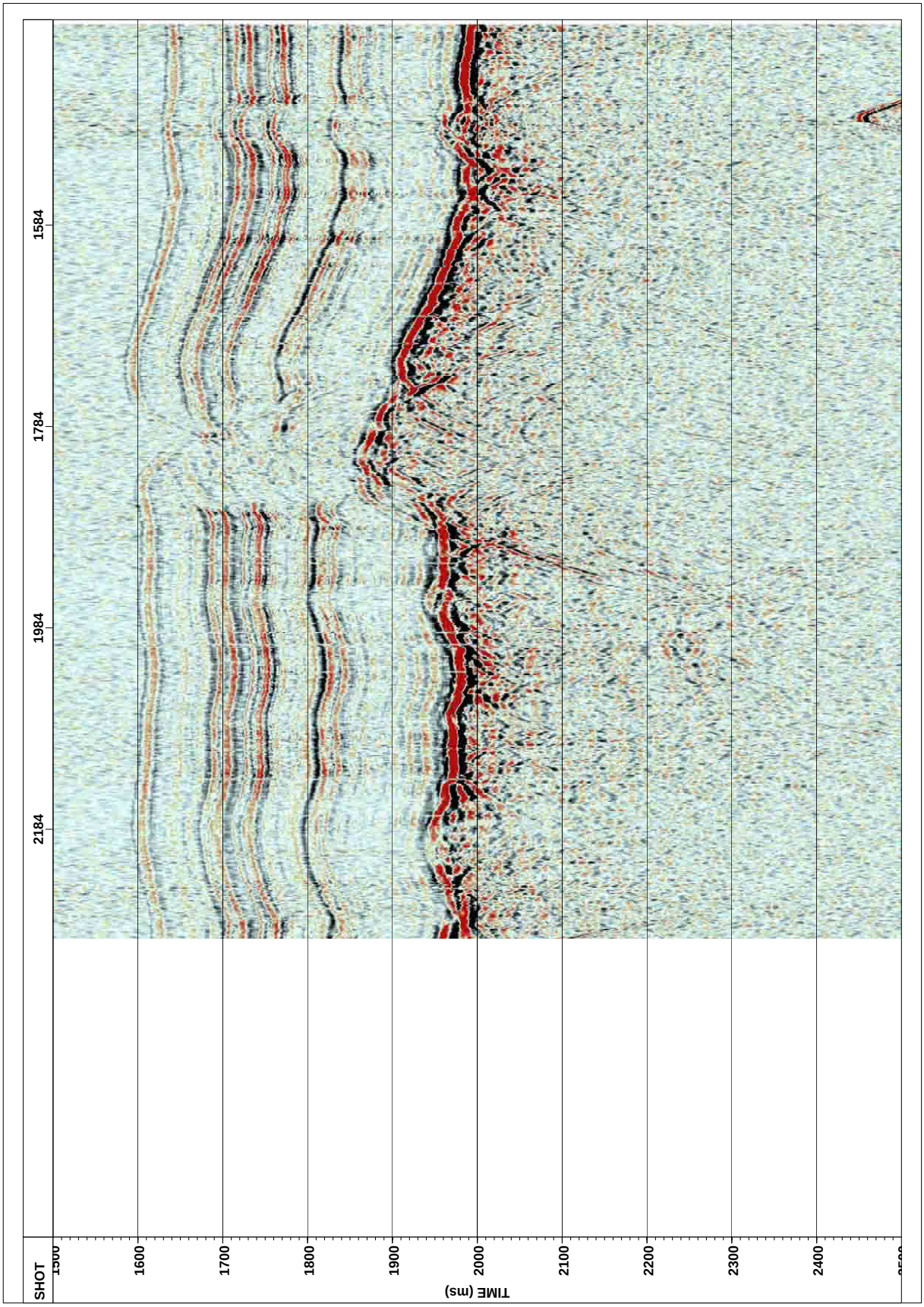

Figure 67: Seismic Profile GUATB02 in working area GUATB-01.

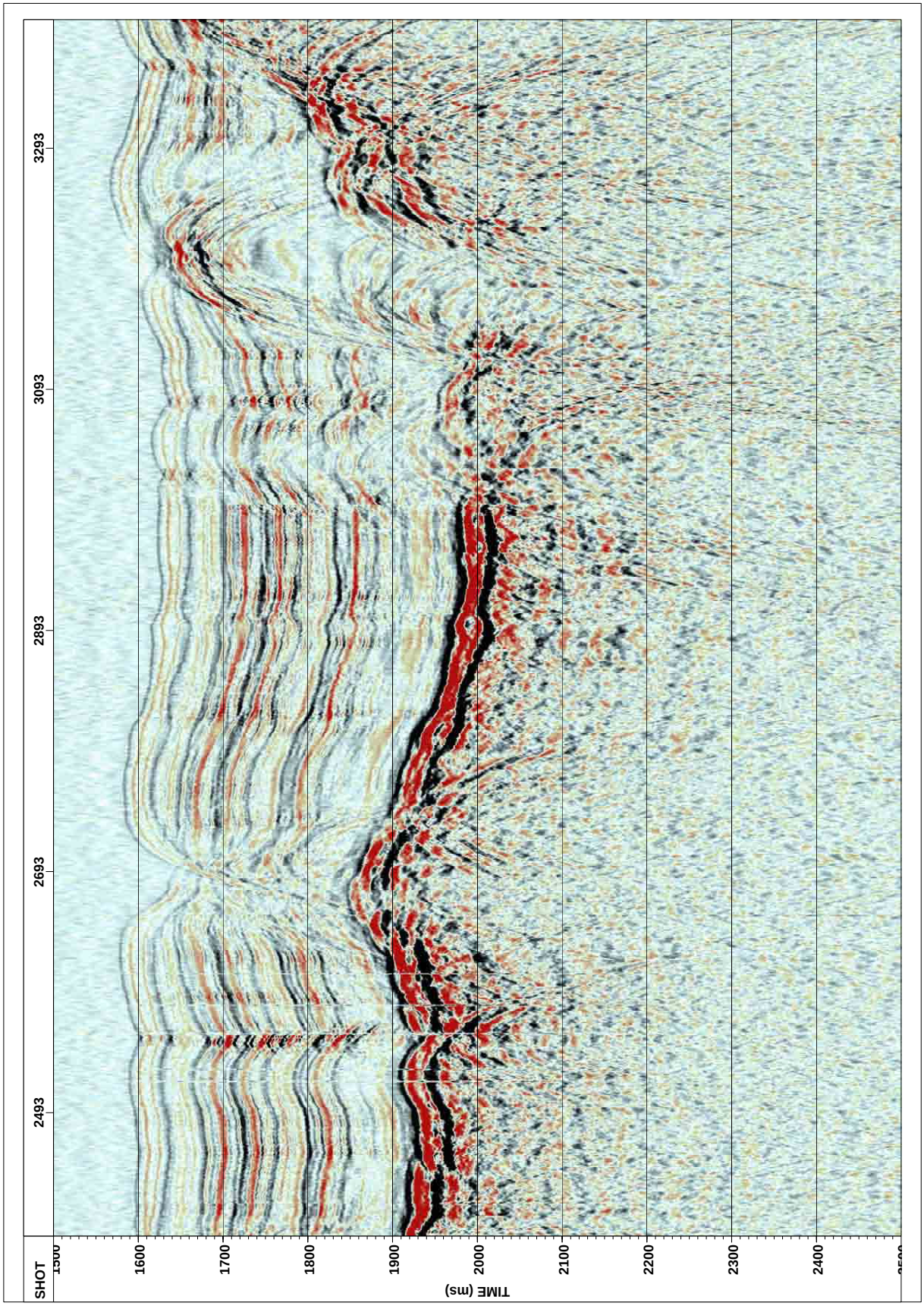

Figure 68: Seismic Profile GUATB03 in working area GUATB-01.

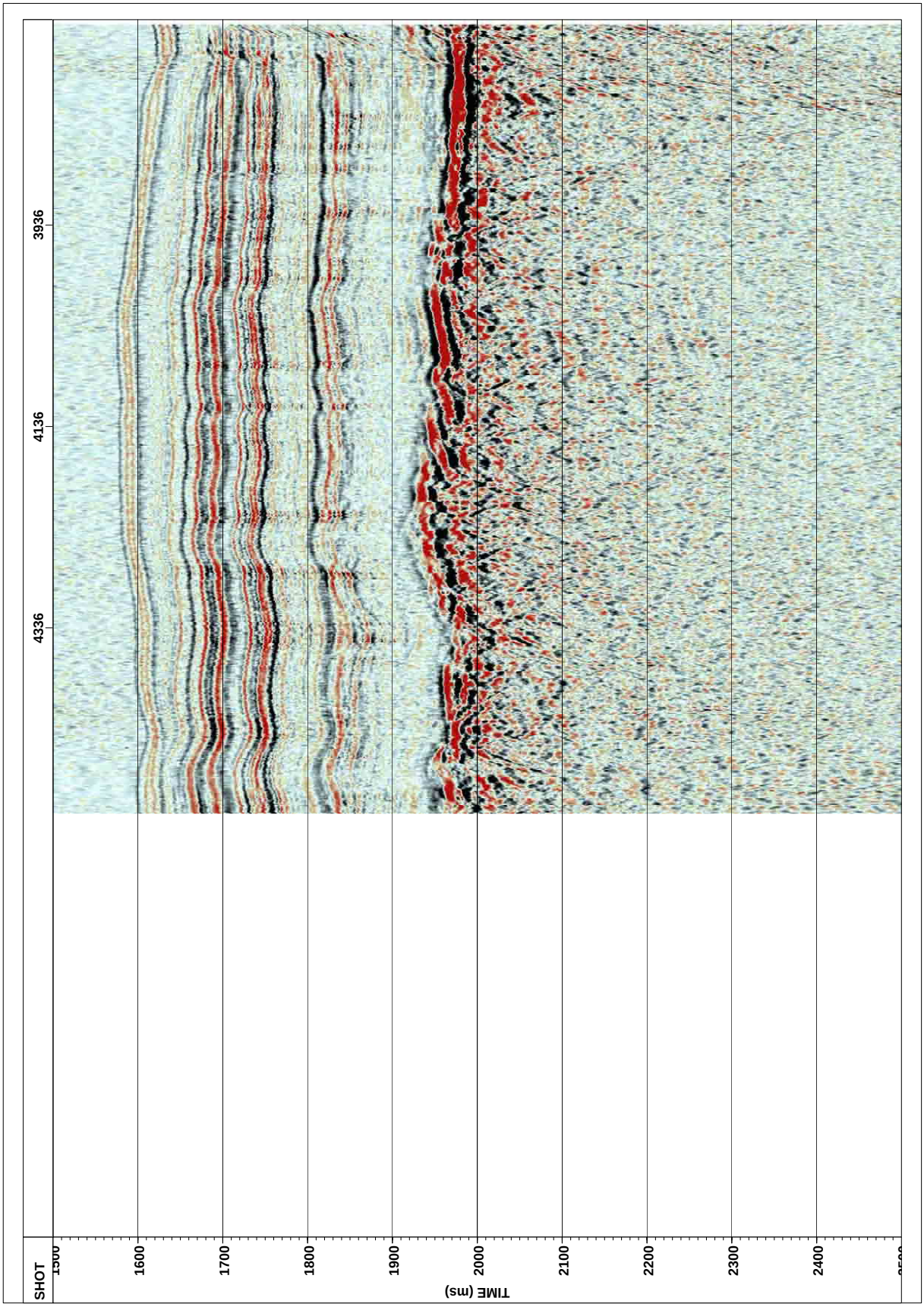

Figure 69: Seismic Profile GUATB04 in working area GUATB-01.

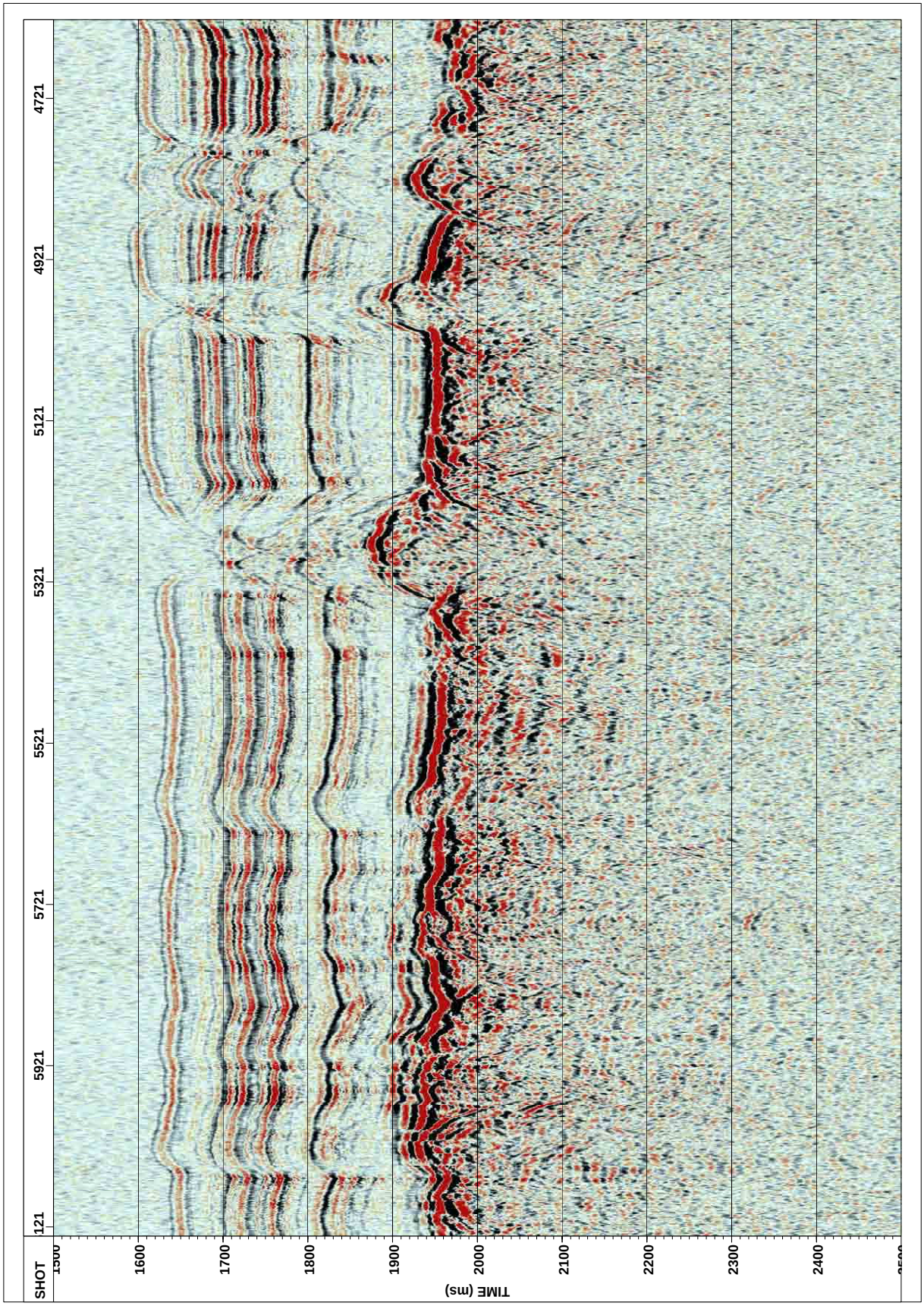

Figure 70: Seismic Profile GUATB05 in working area GUATB-01.

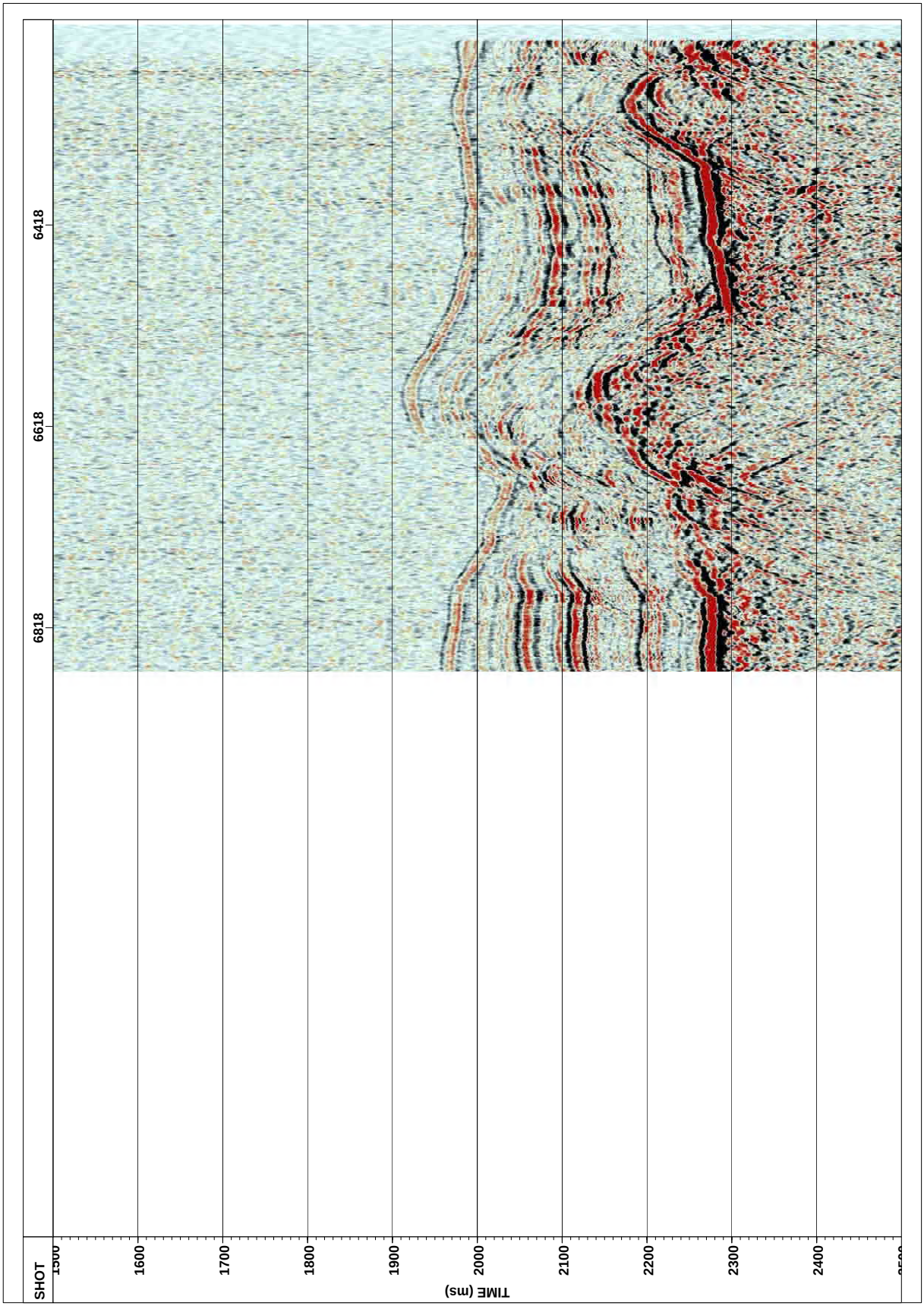

Figure 71: Seismic Profile GUATB08 in working area GUATB-02.

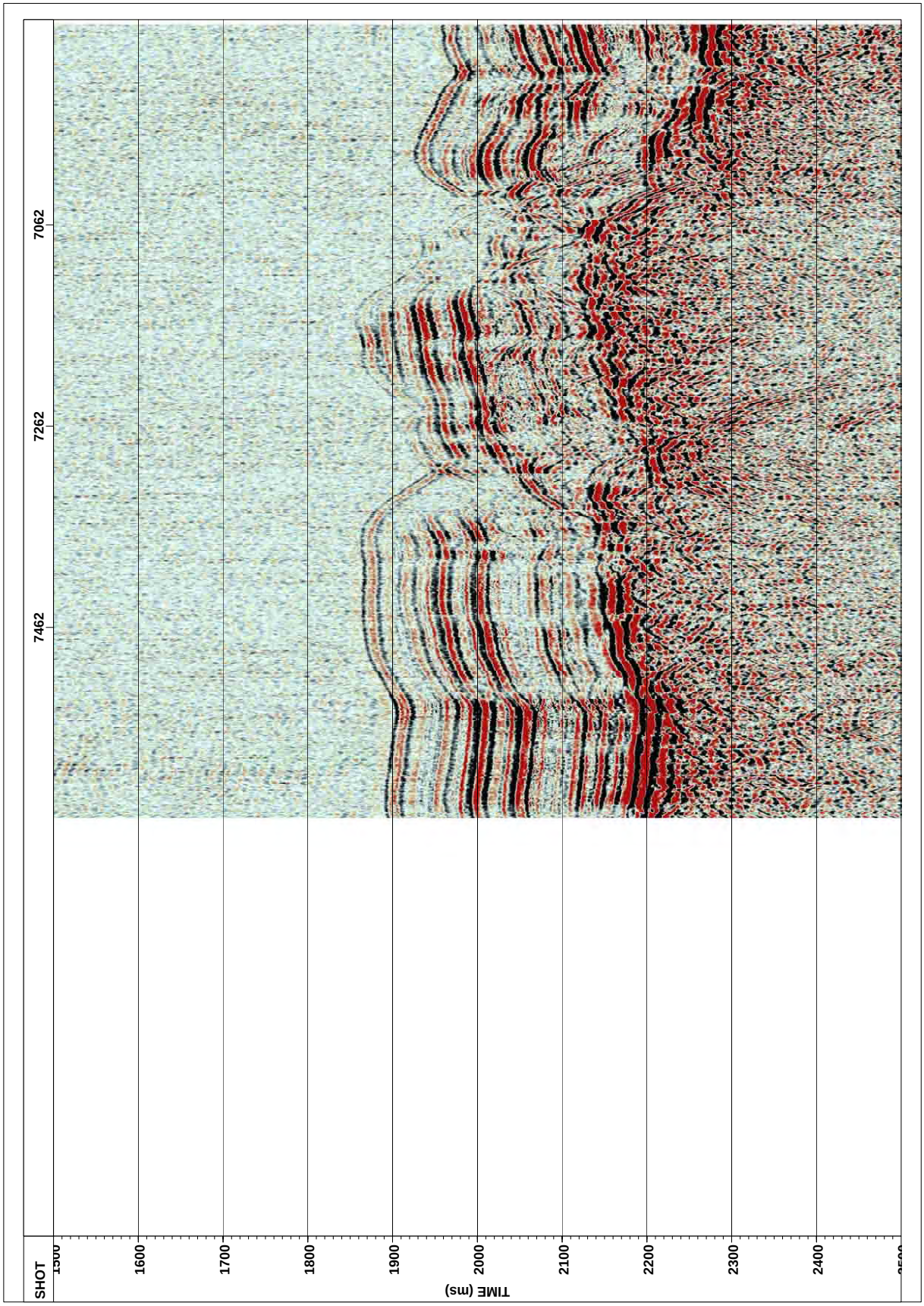

Figure 72: Seismic Profile GUATB09 in working area GUATB-02.

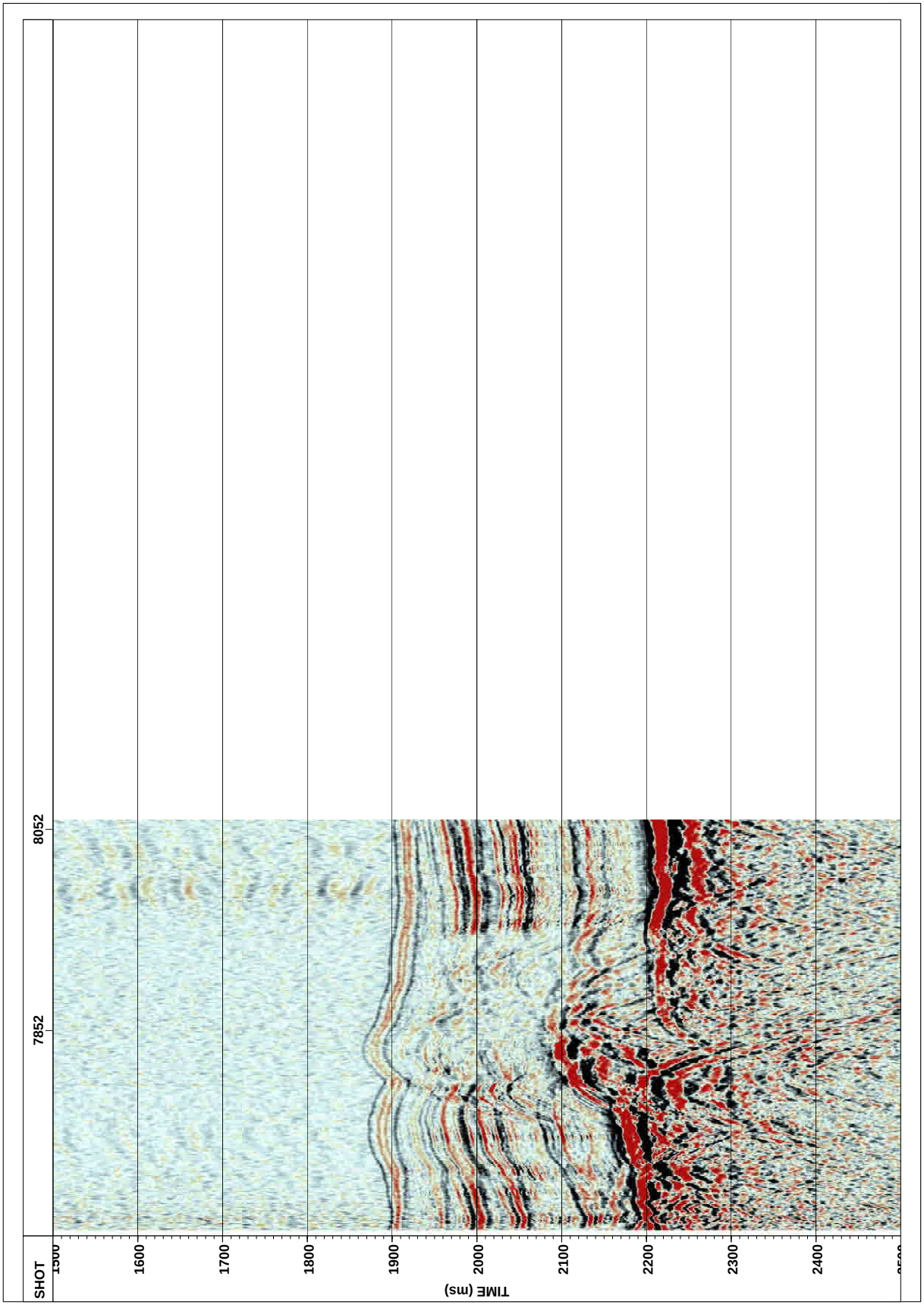

Figure 73: Seismic Profile GUATB10 in working area GUATB-02.

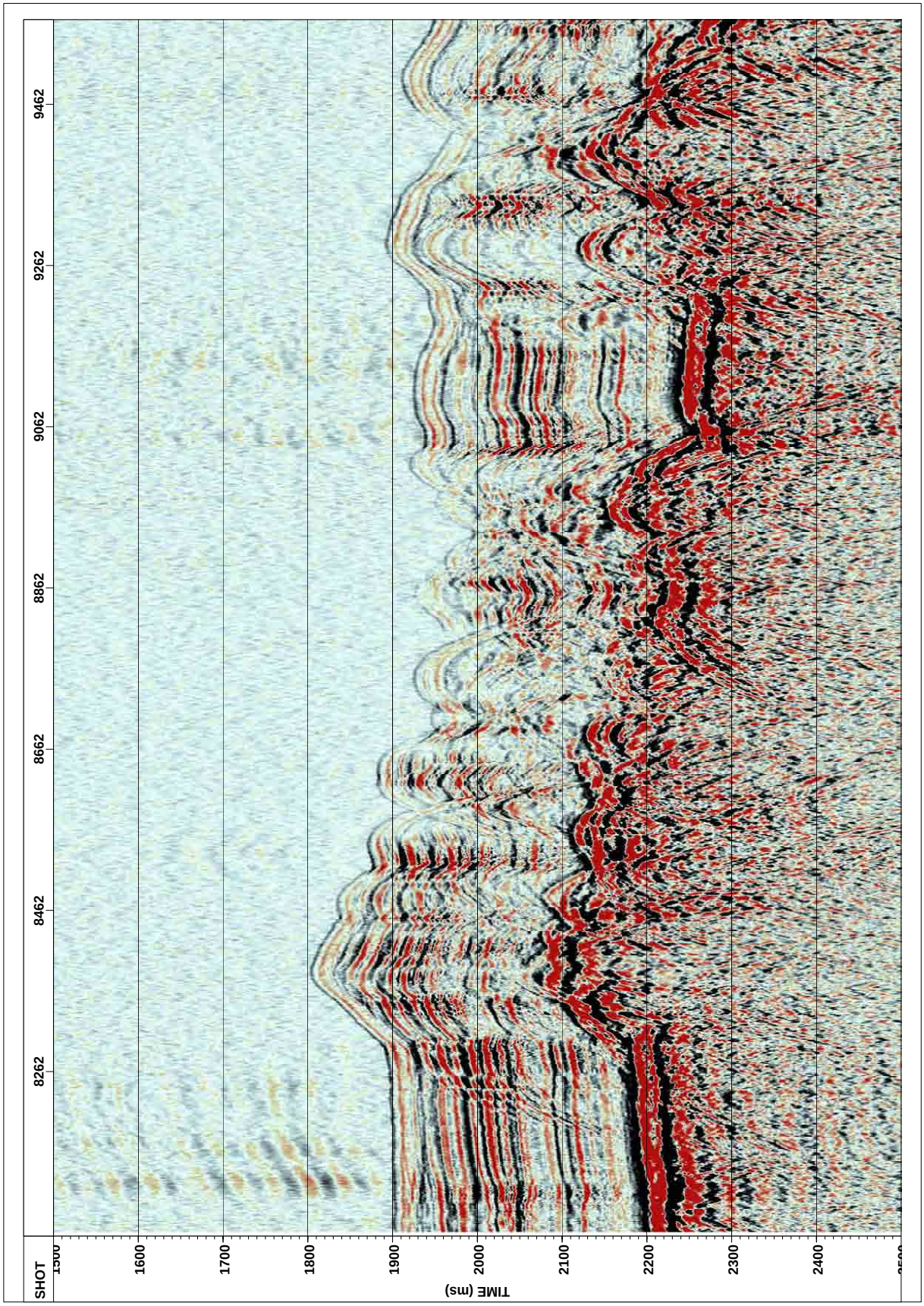

Figure 74: Seismic Profile GUATB11 in working area GUATB-02.

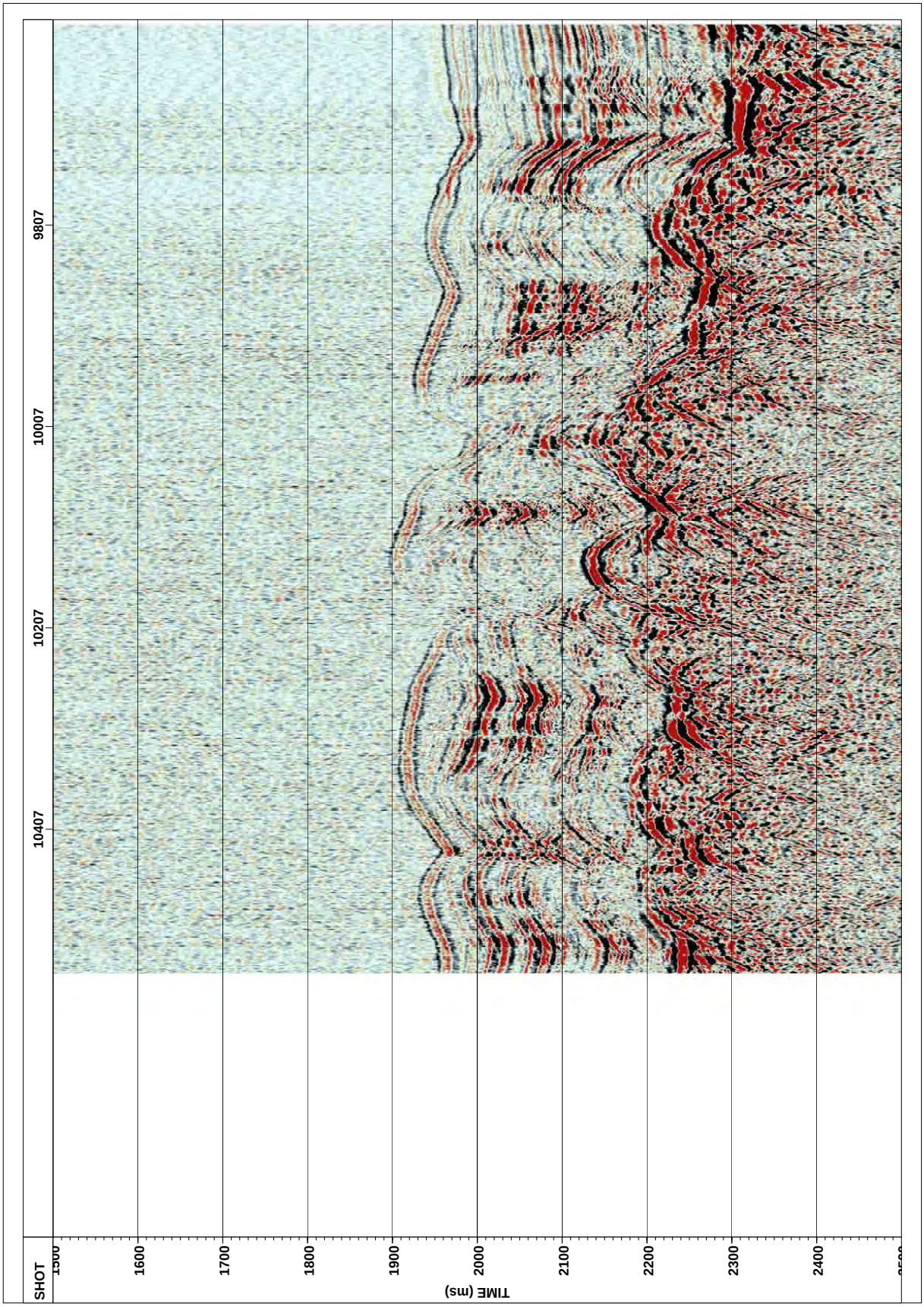

Figure 75: Seismic Profile GUATB12 in working area GUATB-02.

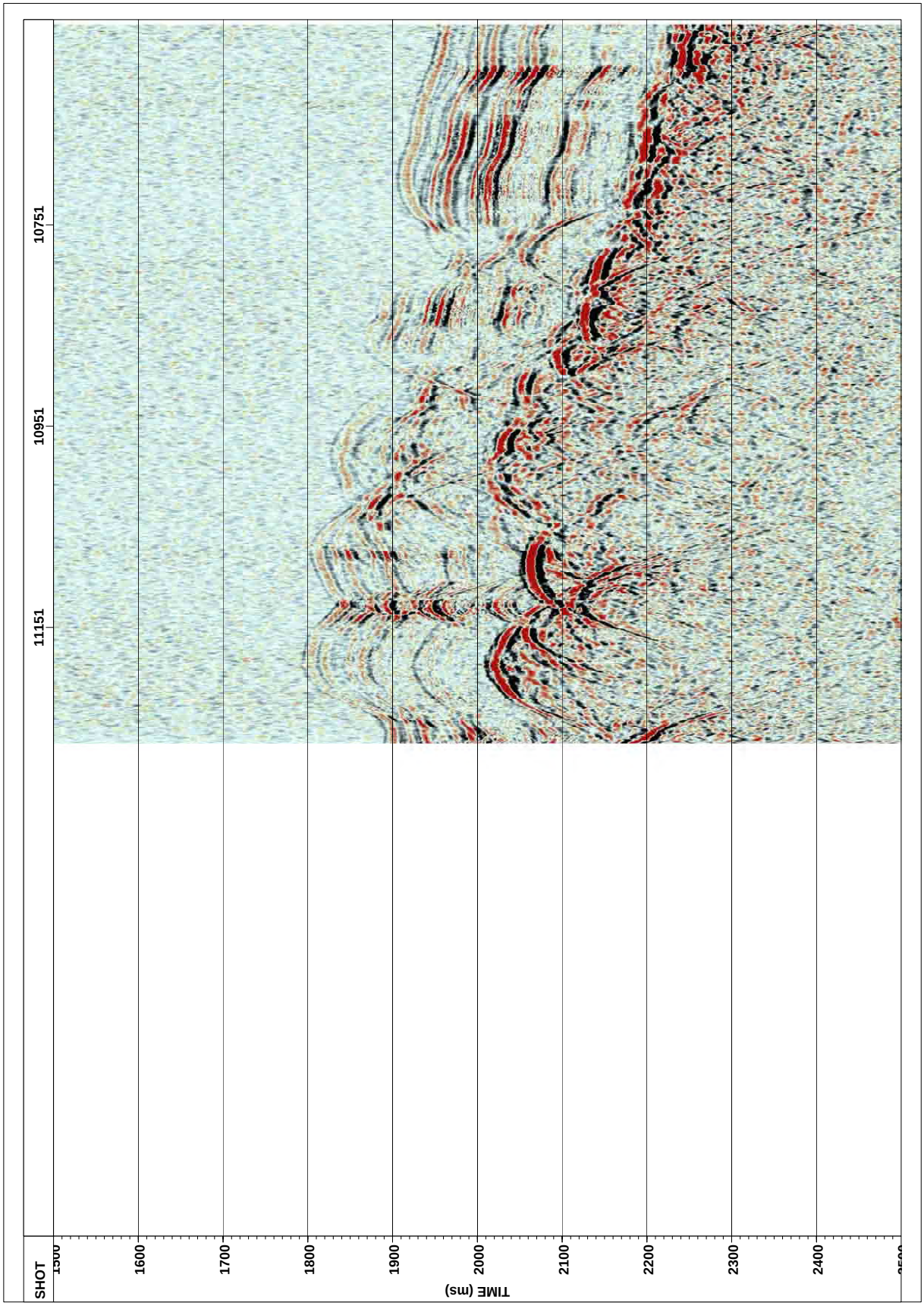

Figure 76: Seismic Profile GUATB13 in working area GUATB-02.

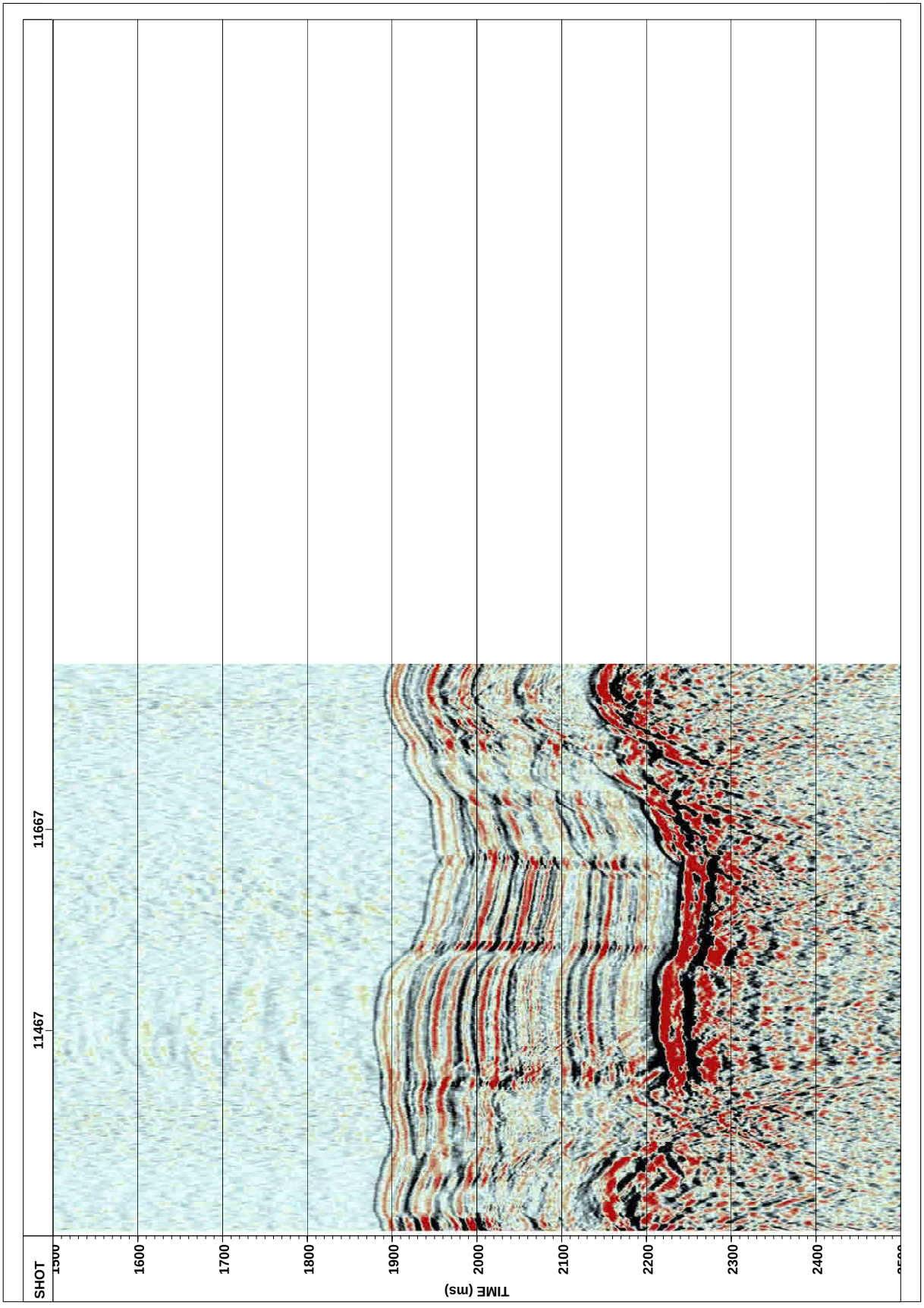

Figure 77: Seismic Profile GUATB14 in working area GUATB-02.

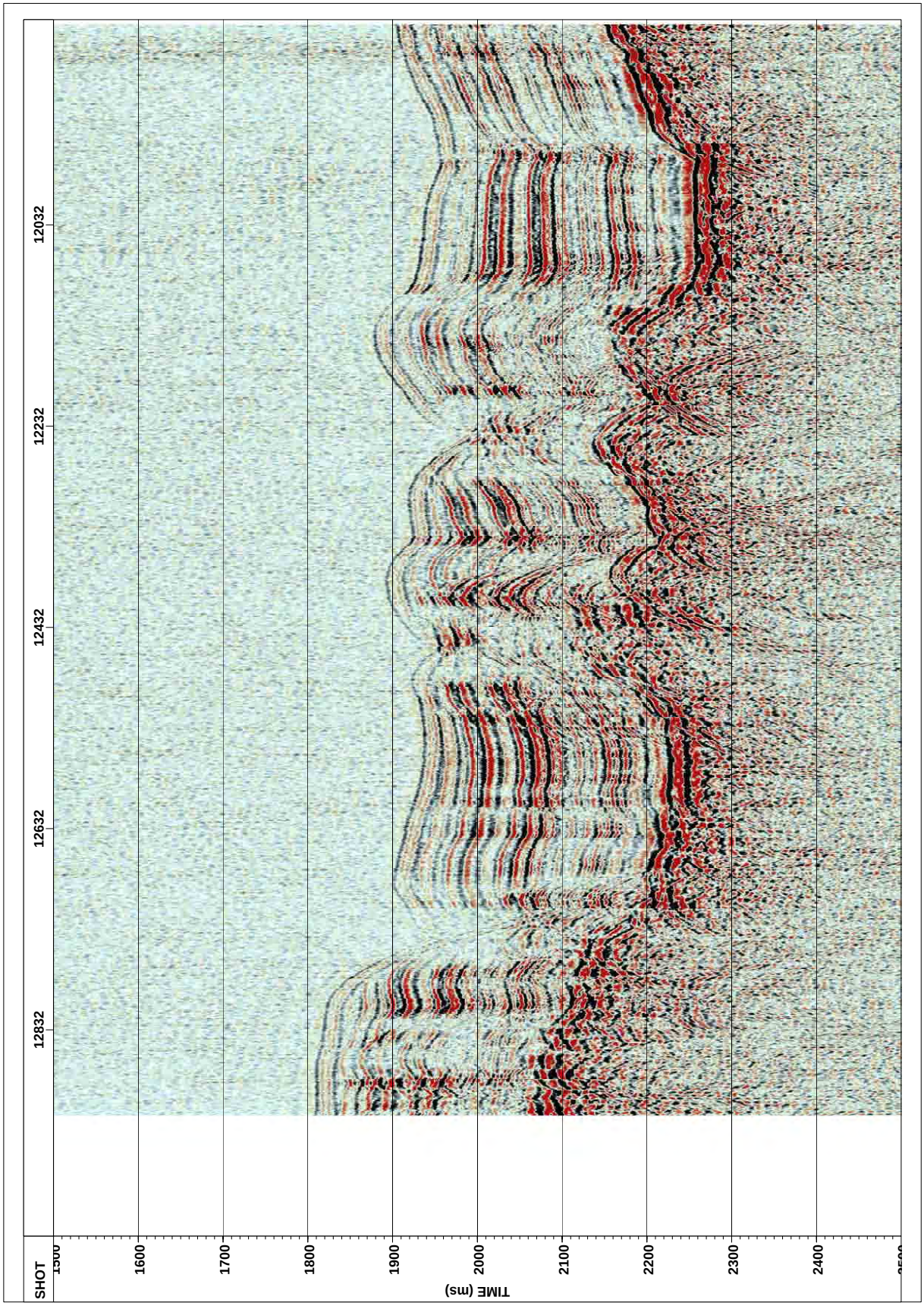

Figure 78: Seismic Profile GUATB15 in working area GUATB-02.

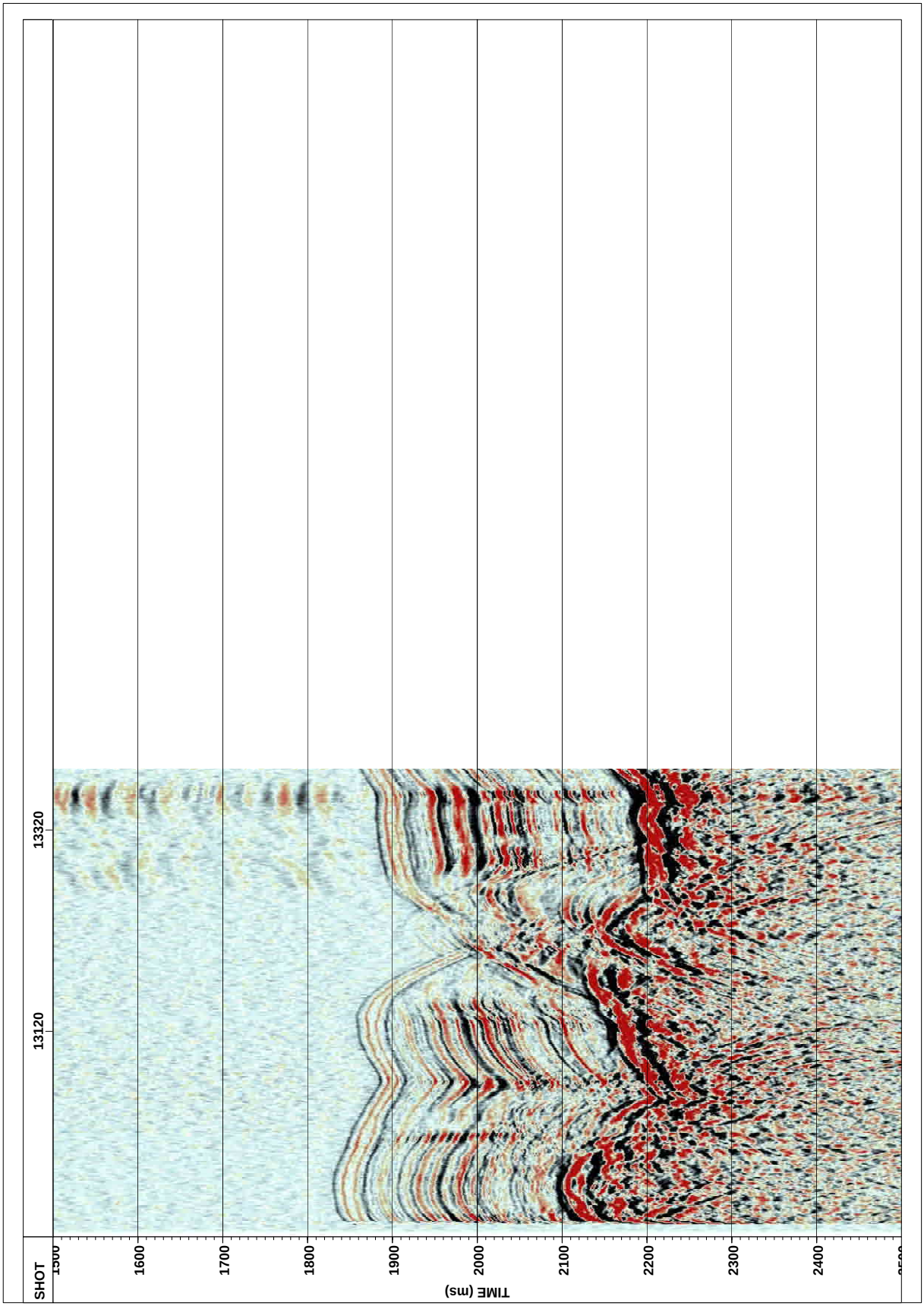

Figure 79: Seismic Profile GUATB16 in working area GUATB-02.

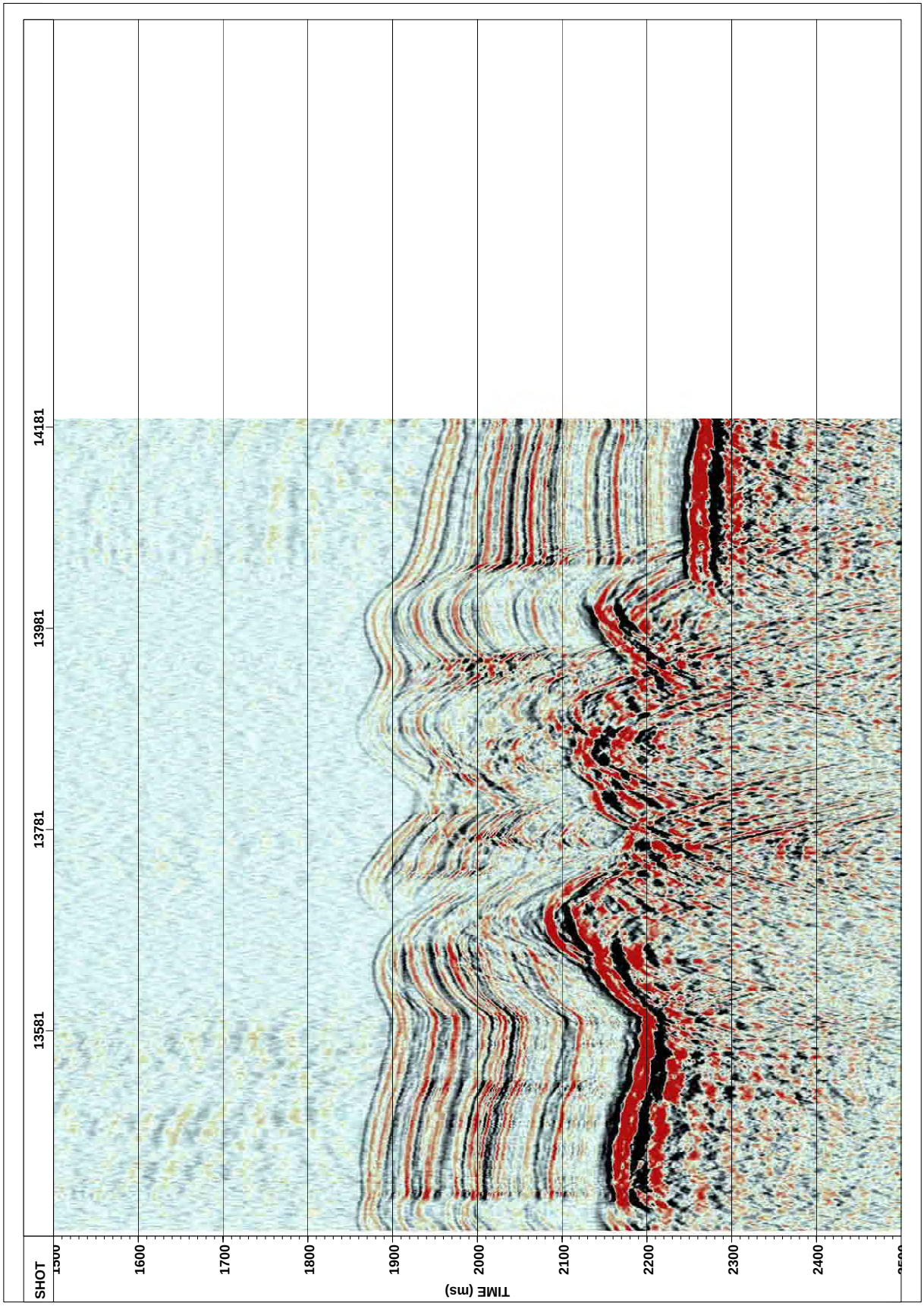

Figure 80: Seismic Profile GUATB17 in working area GUATB-02.

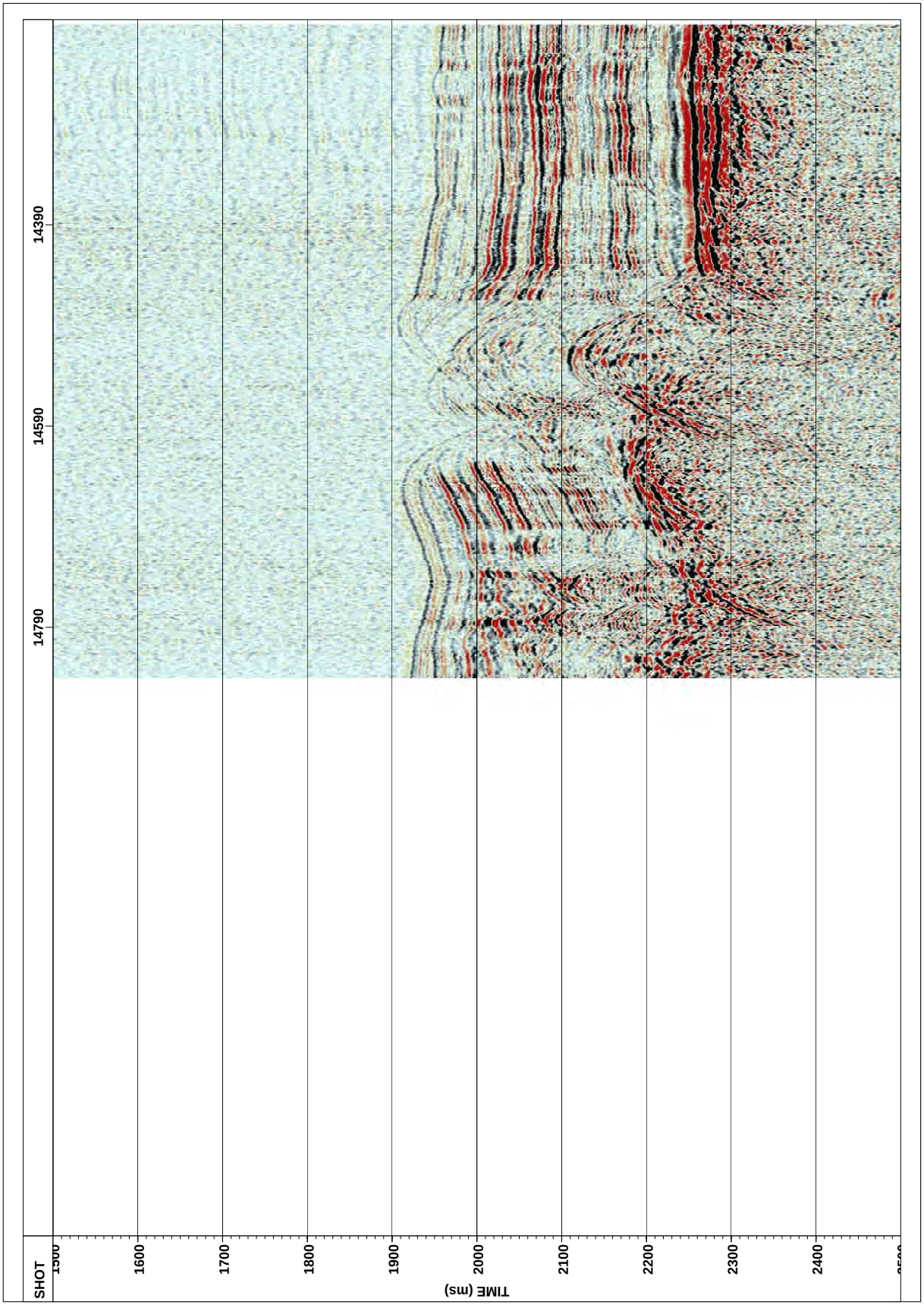

Figure 81: Seismic Profile GUATB18 in working area GUATB-02.

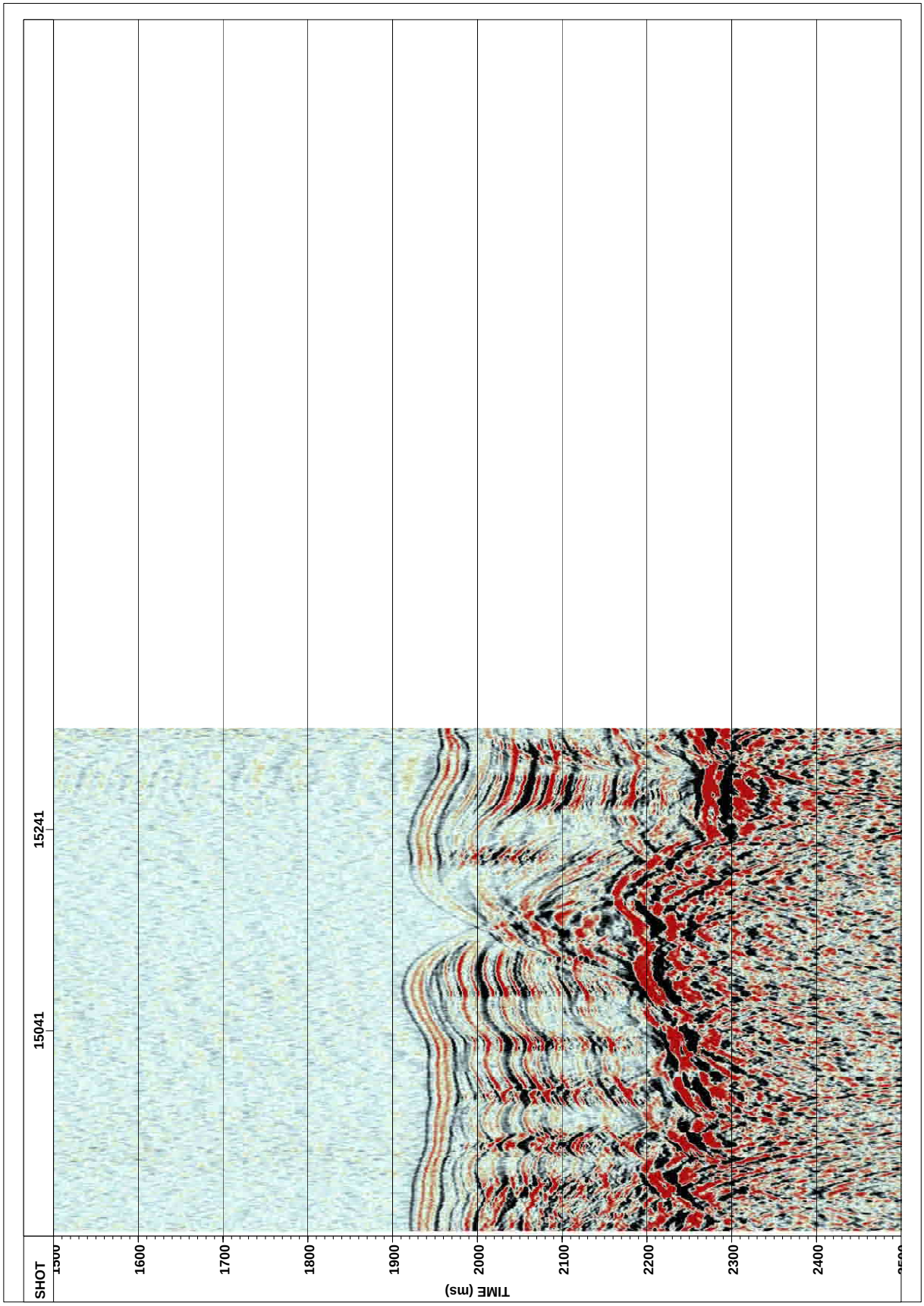

Figure 82: Seismic Profile GUATB19 in working area GUATB-02.

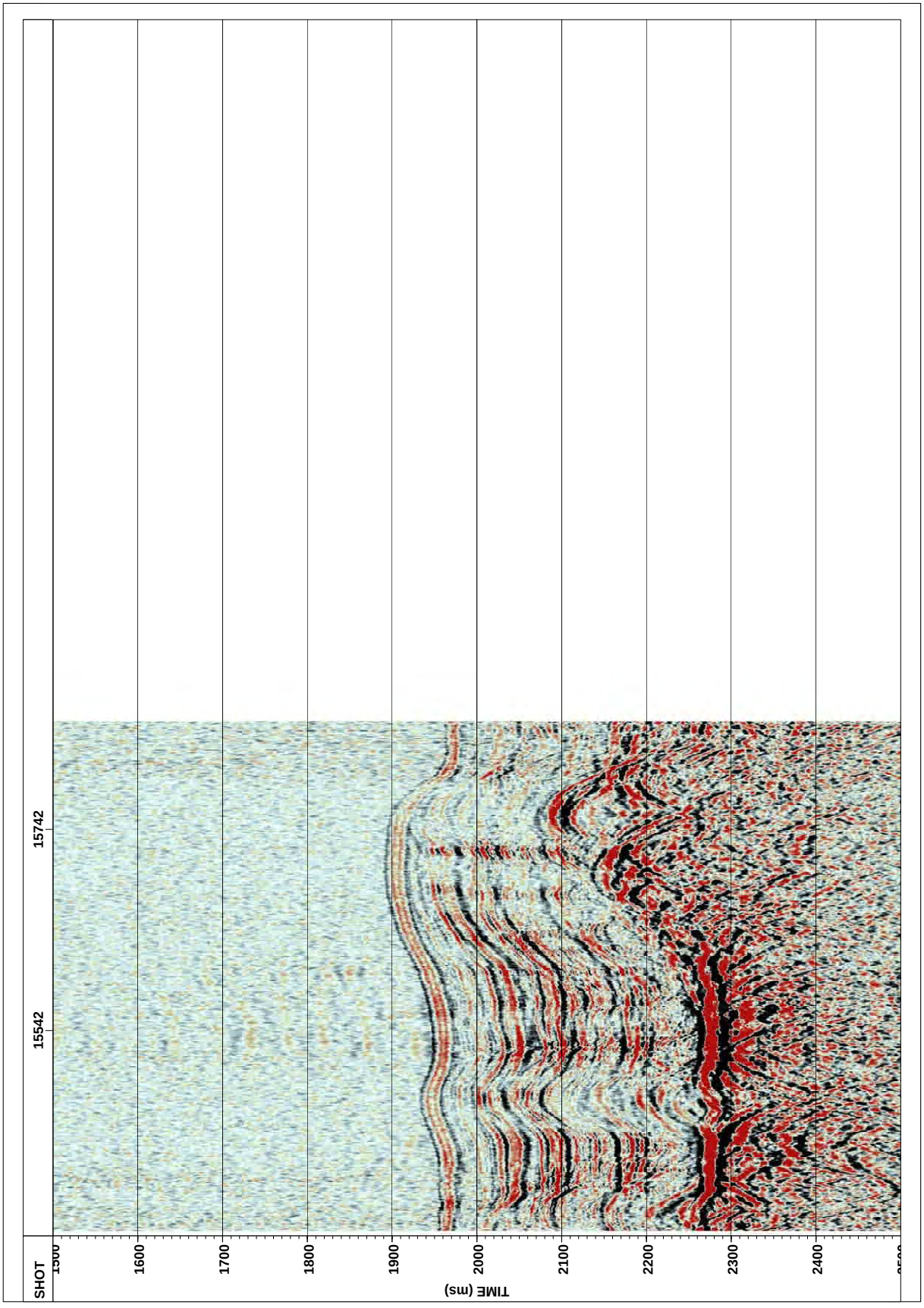

Figure 83: Seismic Profile GUATB20 in working area GUATB-02.

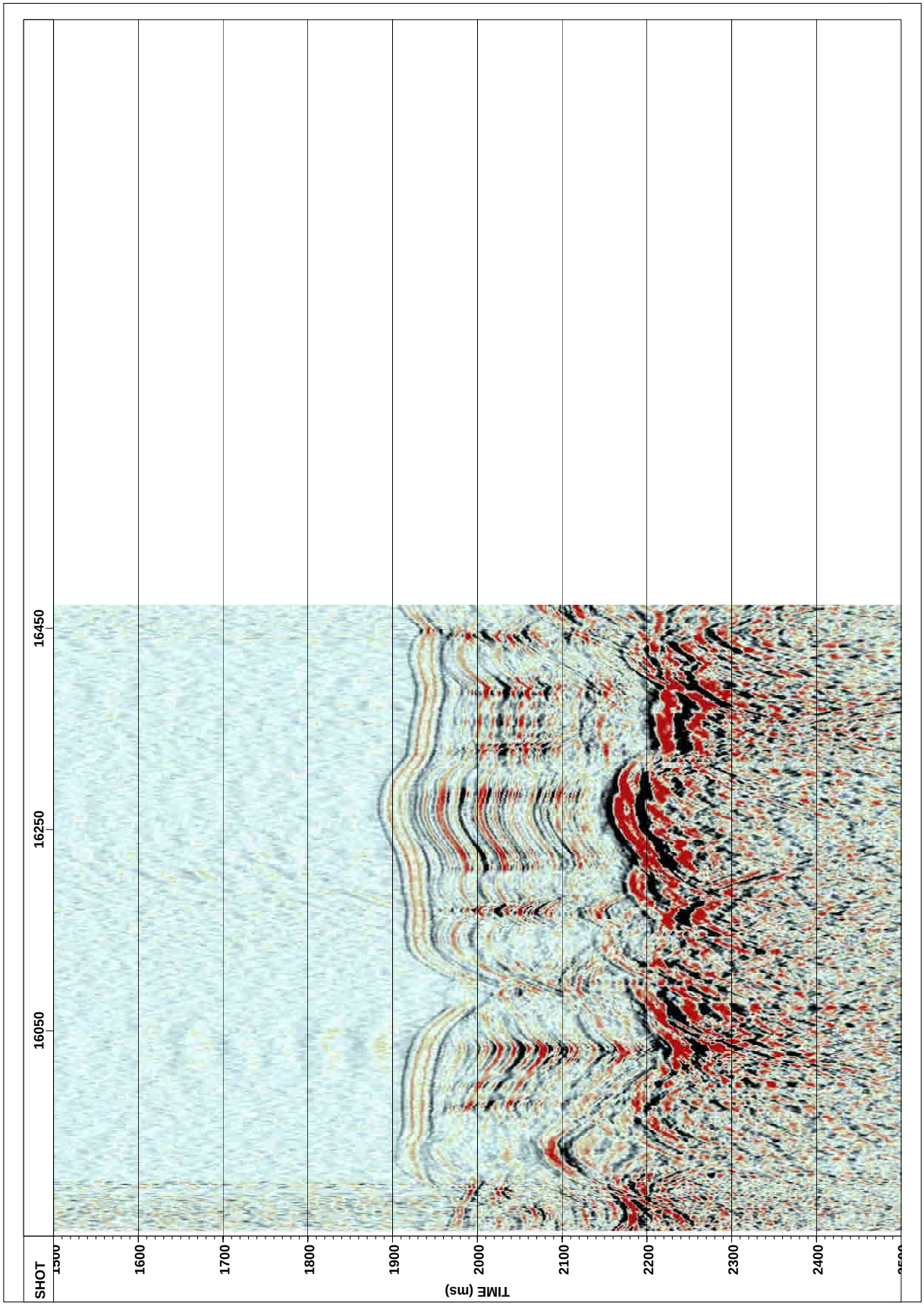

Figure 84: Seismic Profile GUATB21 in working area GUATB-02.

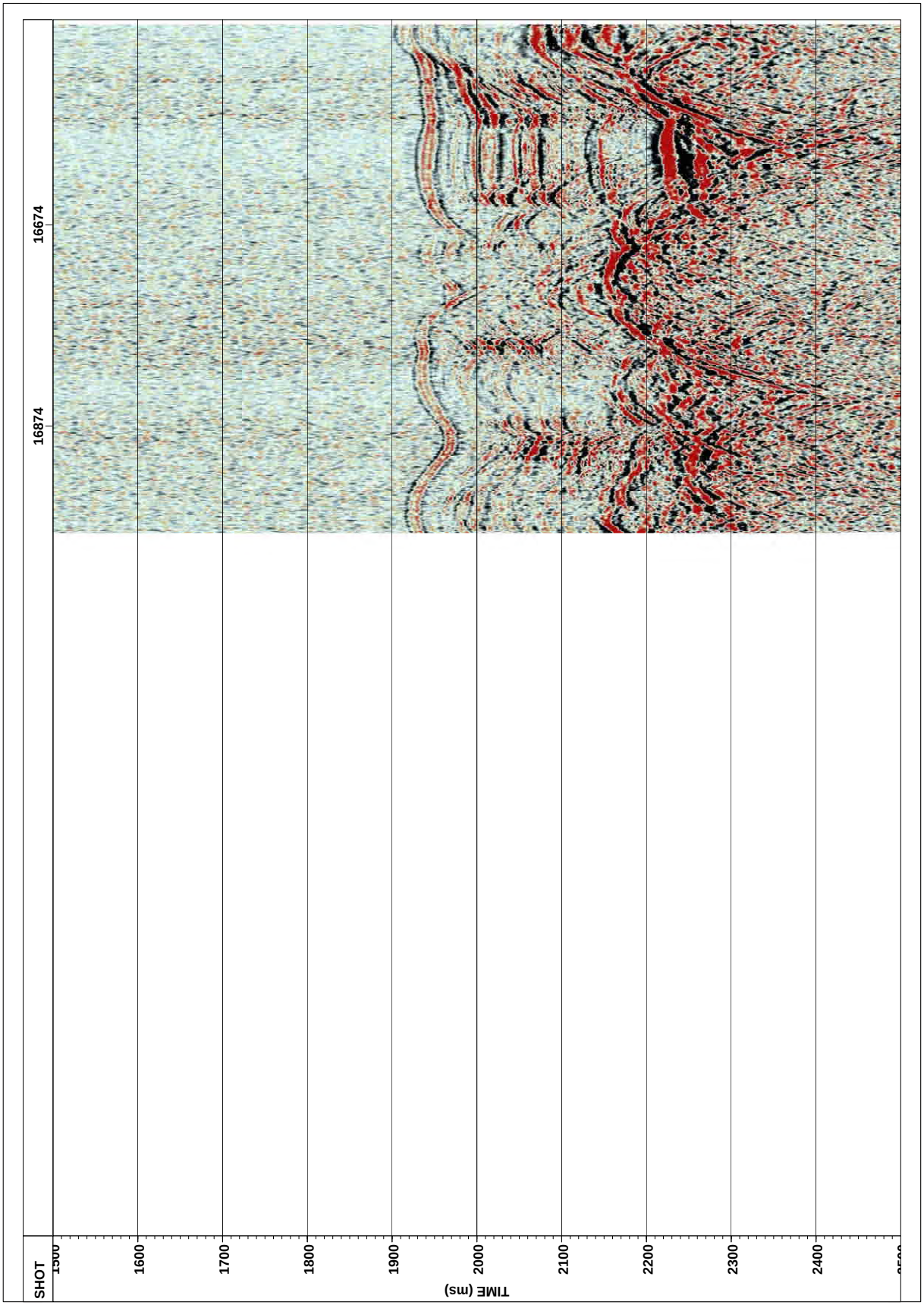

Figure 85: Seismic Profile GUATB22 in working area GUATB-02.

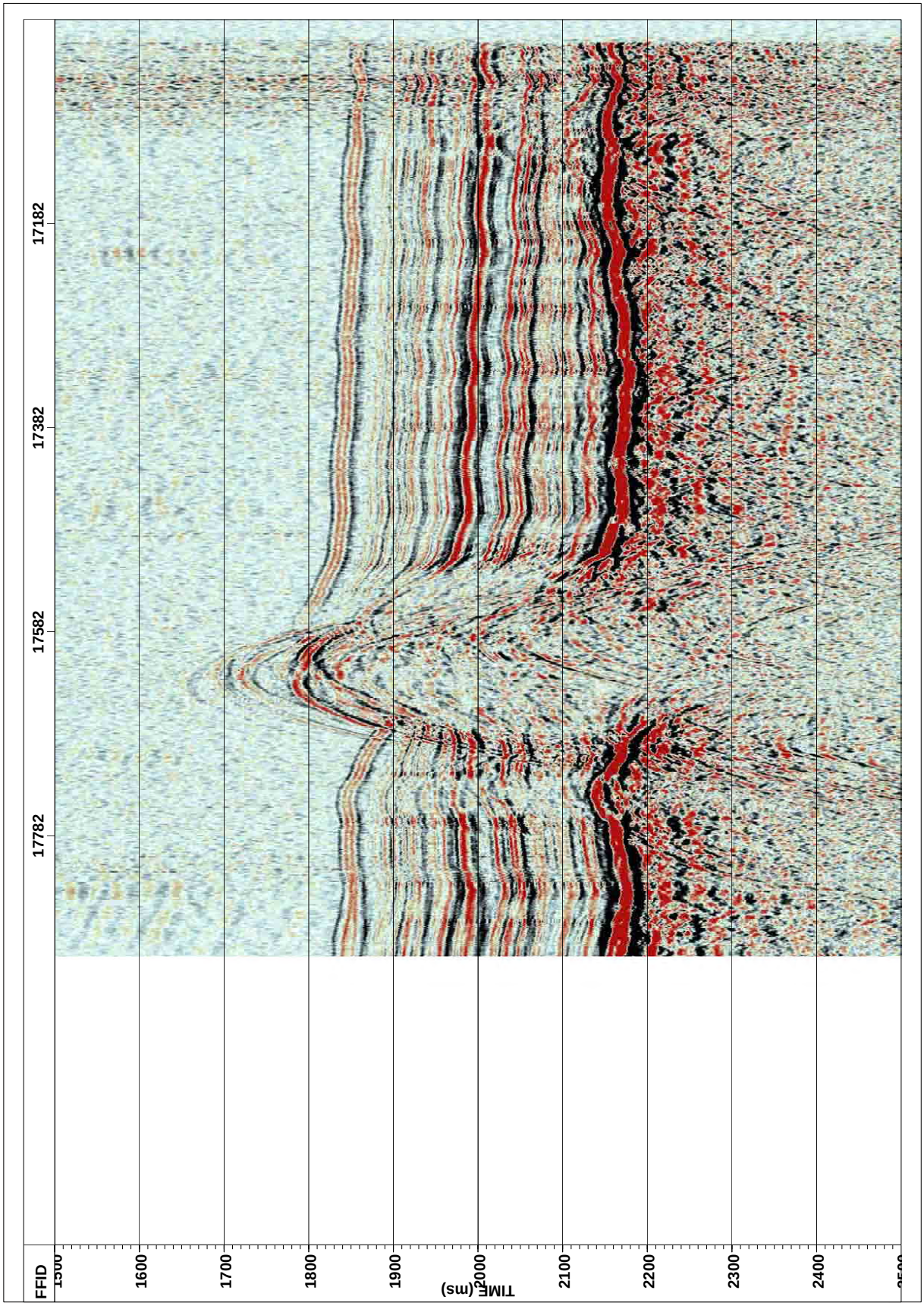

Figure 86: Seismic Profile GUATB24 in working area GUATB-03.

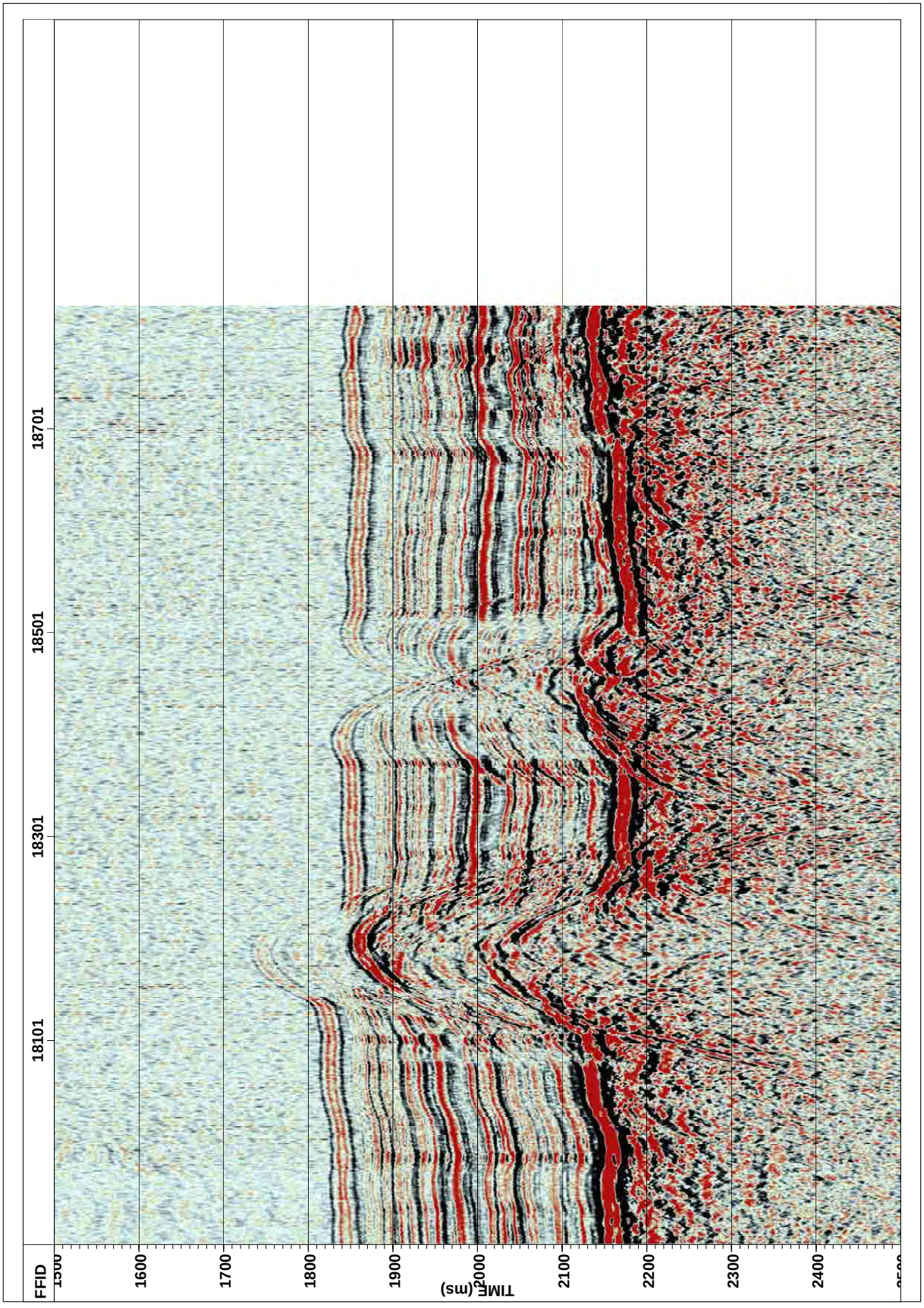

Figure 87: Seismic Profile GUATB25 in working area GUATB-03.

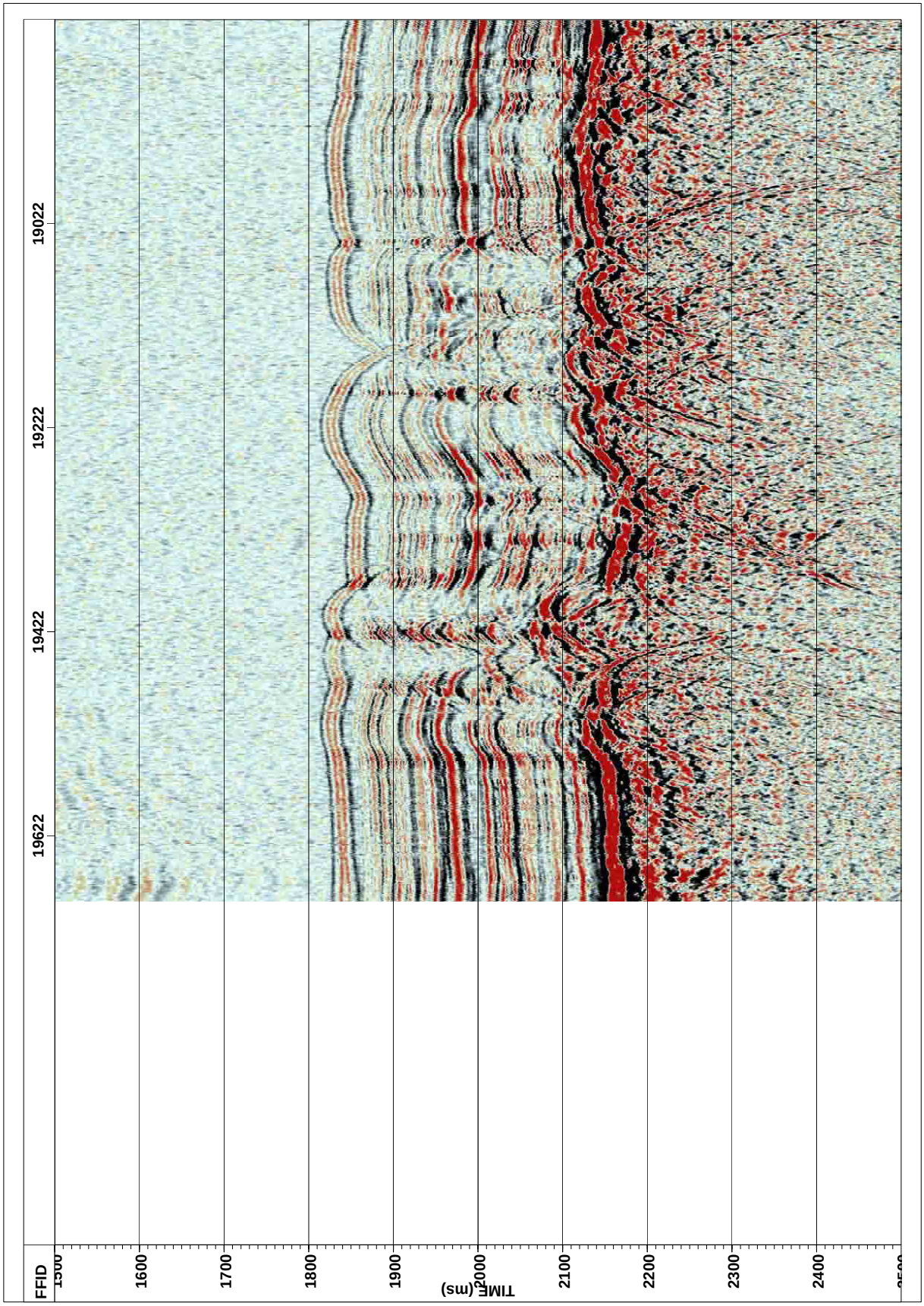

Figure 88: Seismic Profile GUATB26 in working area GUATB-03.

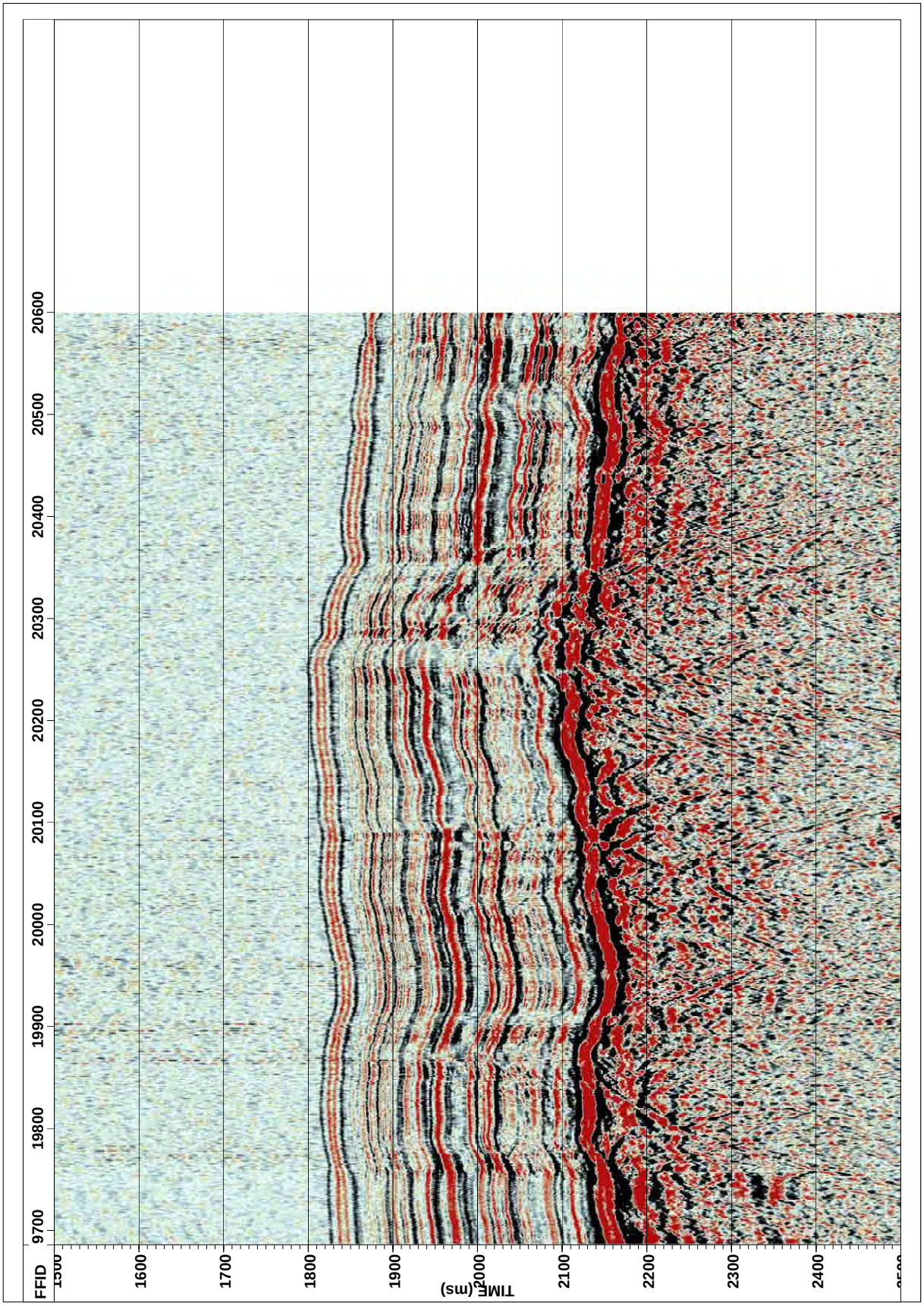

Figure 89: Seismic Profile GUATB27 in working area GUATB-03.

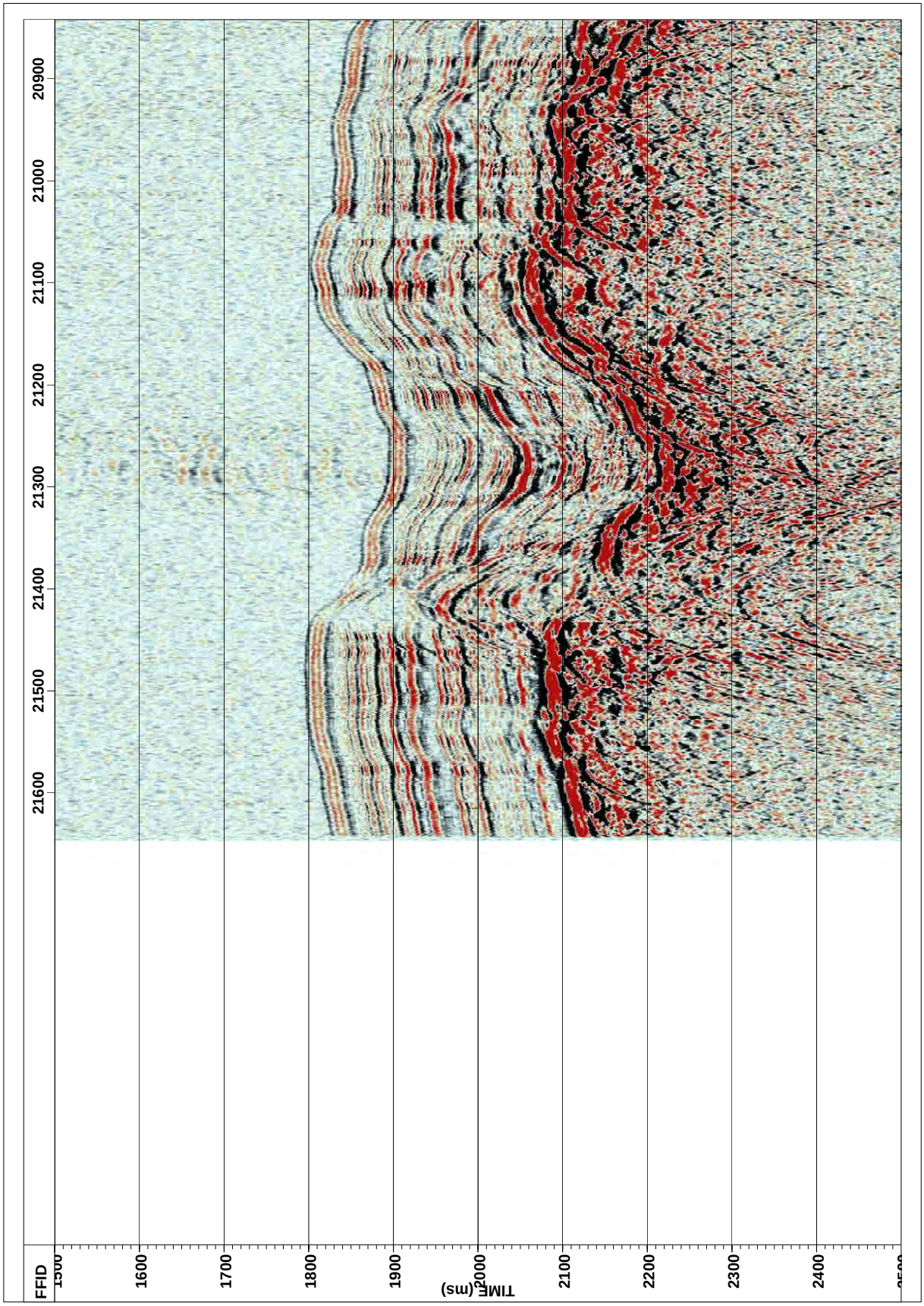

Figure 90: Seismic Profile GUATB29 in working area GUATB-03.

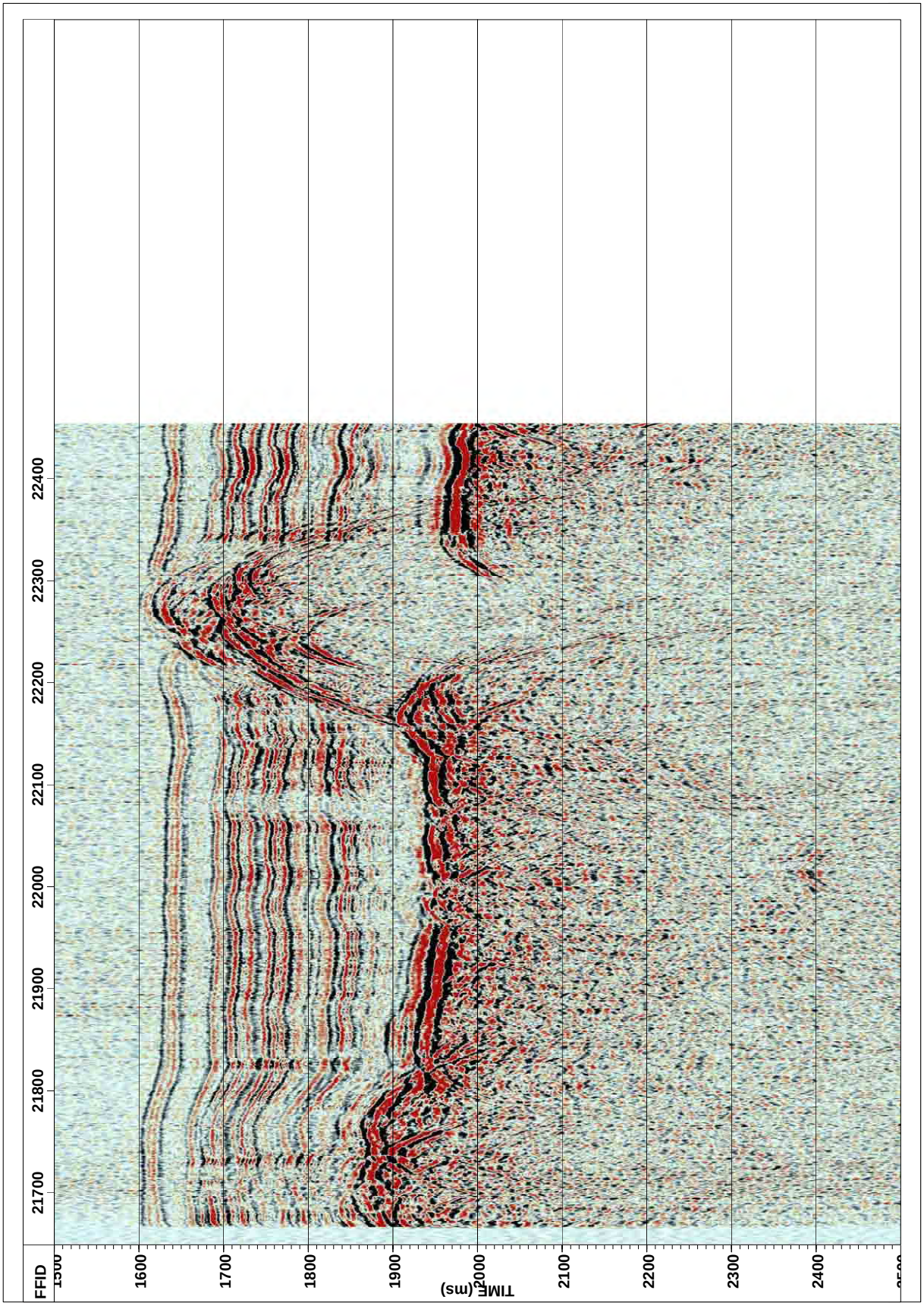

Figure 91: Seismic Profile GUATB32 in working area GUATB-01.

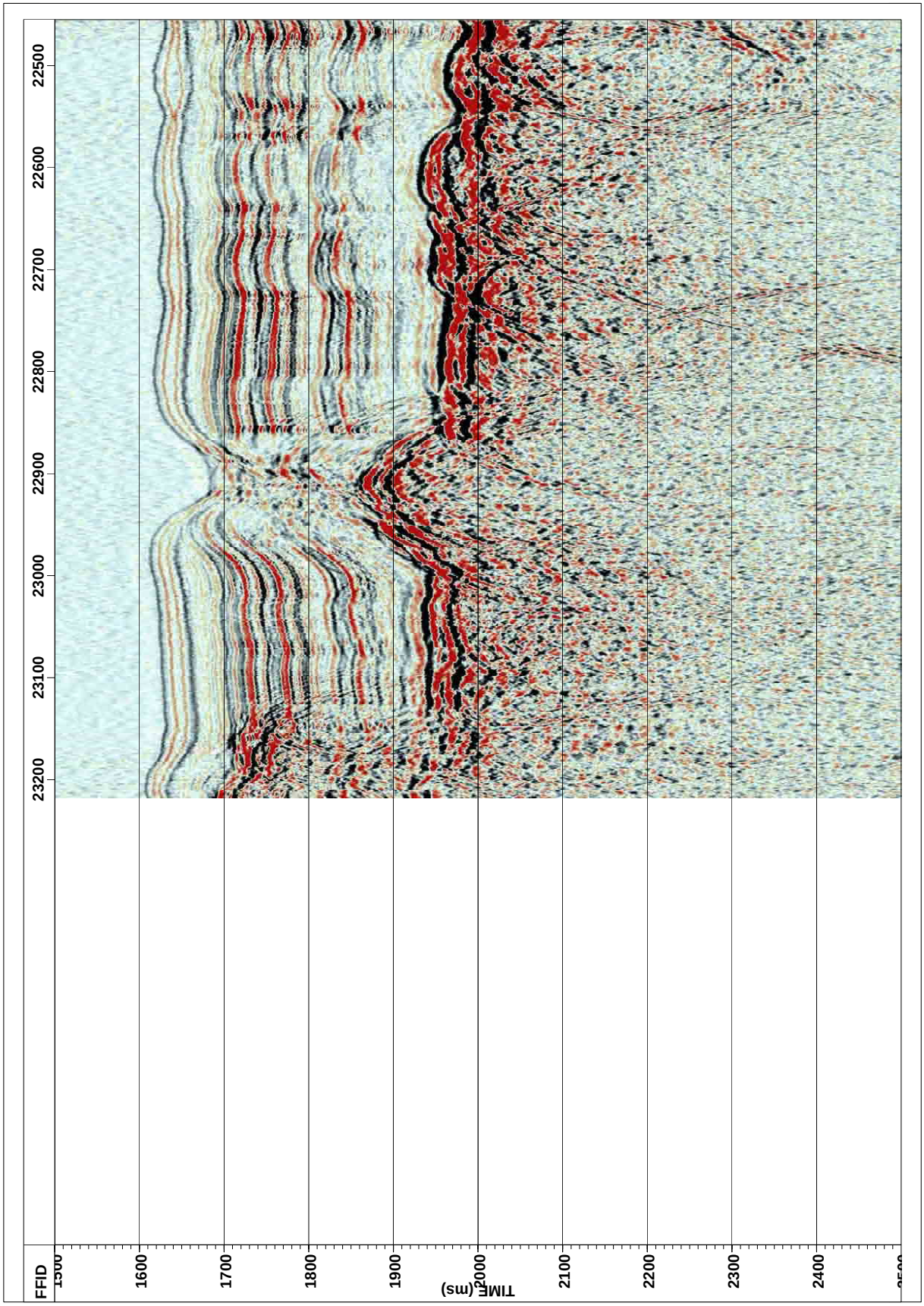

Figure 92: Seismic Profile GUATB33 in working area GUATB-01.

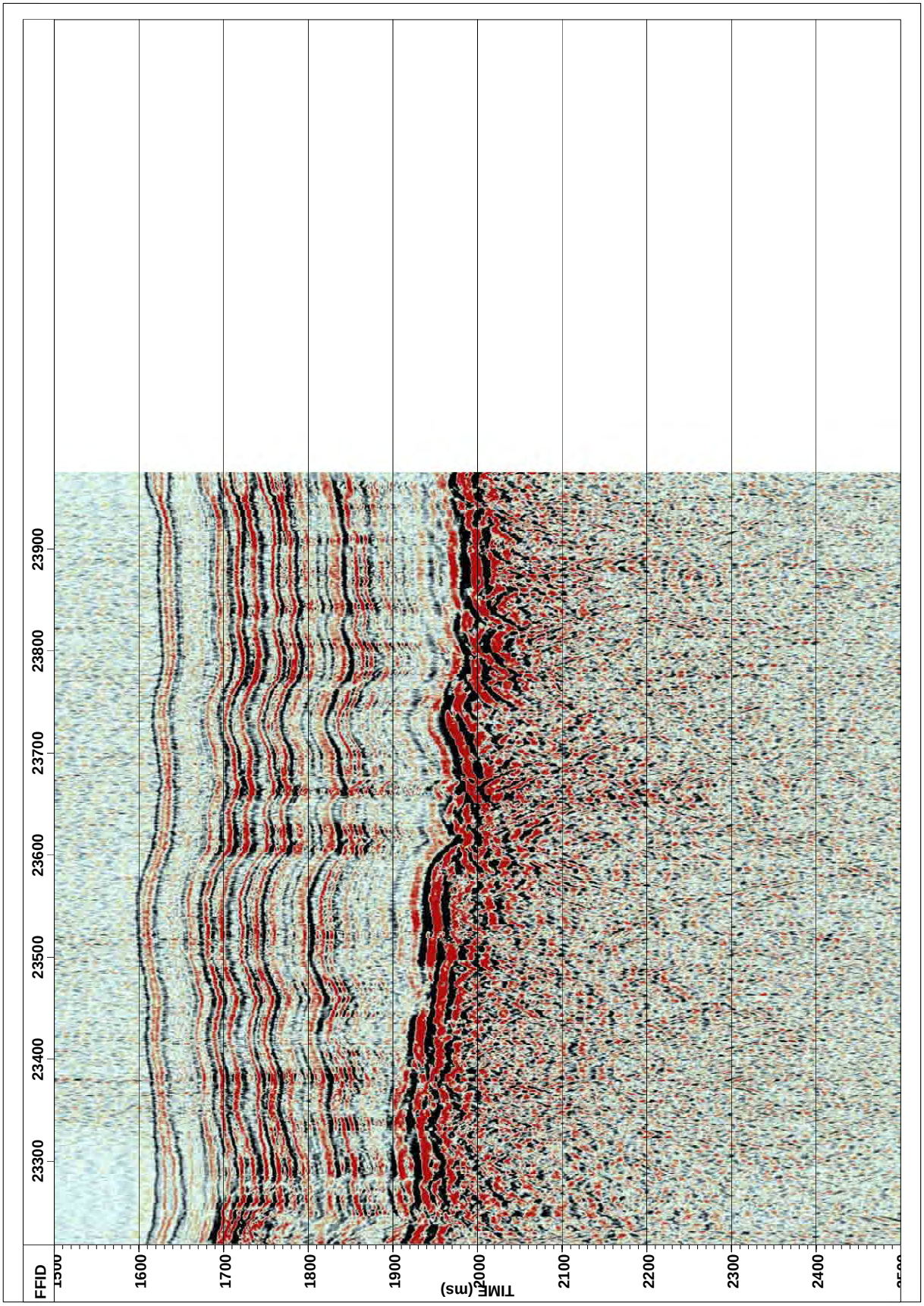

Figure 93: Seismic Profile GUATB34 in working area GUATB-01.

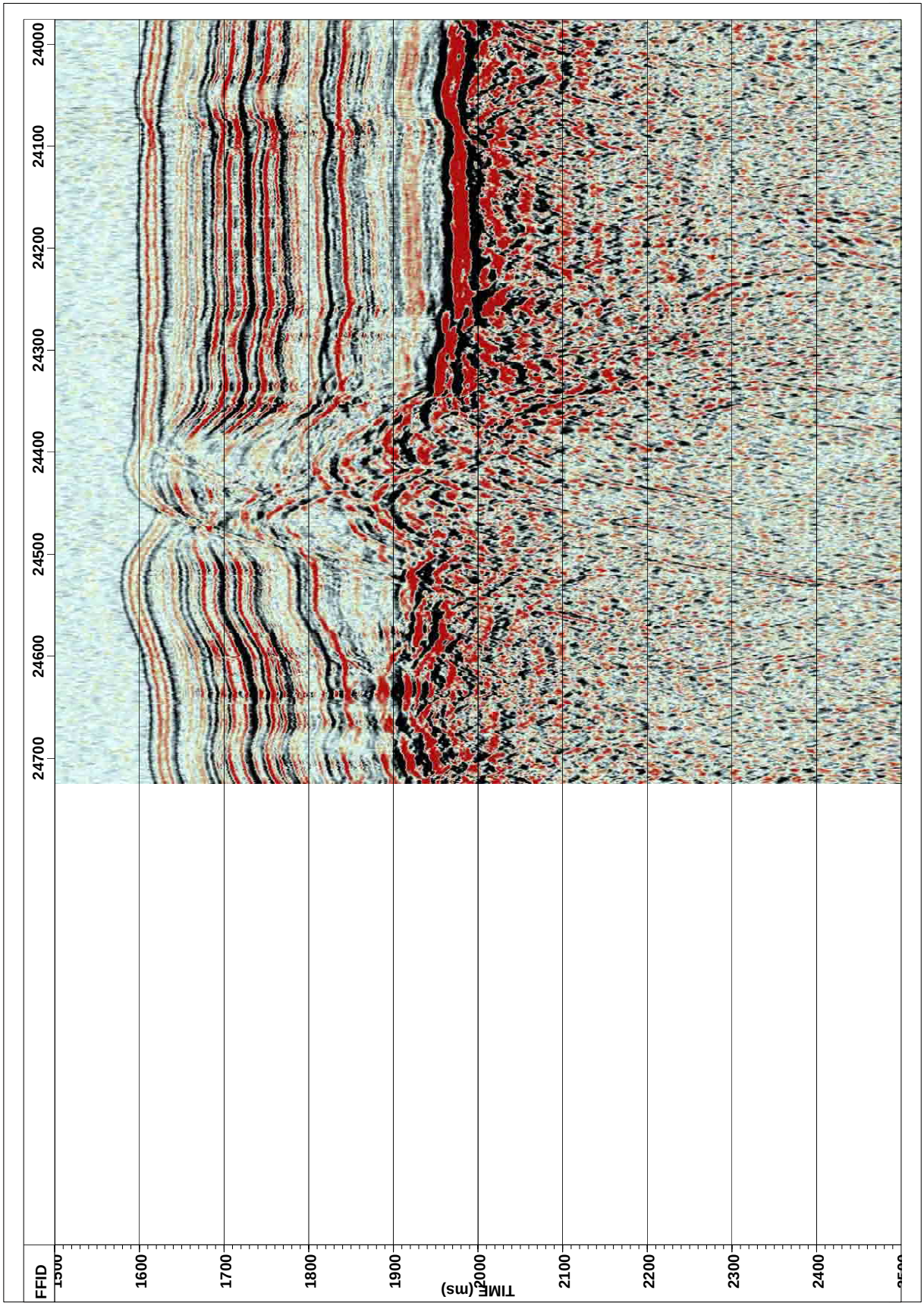

Figure 94: Seismic Profile GUATB35 in working area GUATB-01.

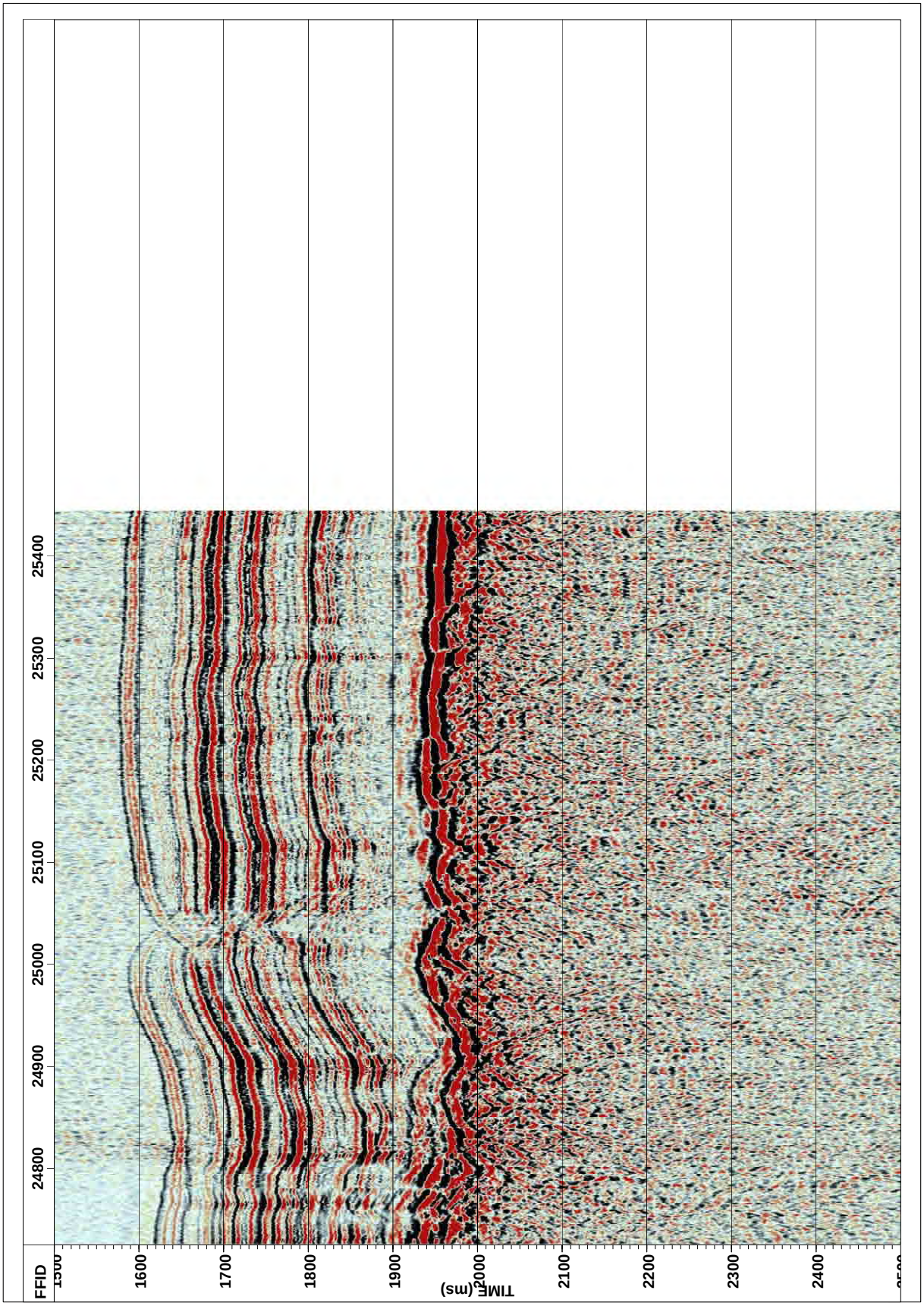

Figure 95: Seismic Profile GUATB36 in working area GUATB-01.

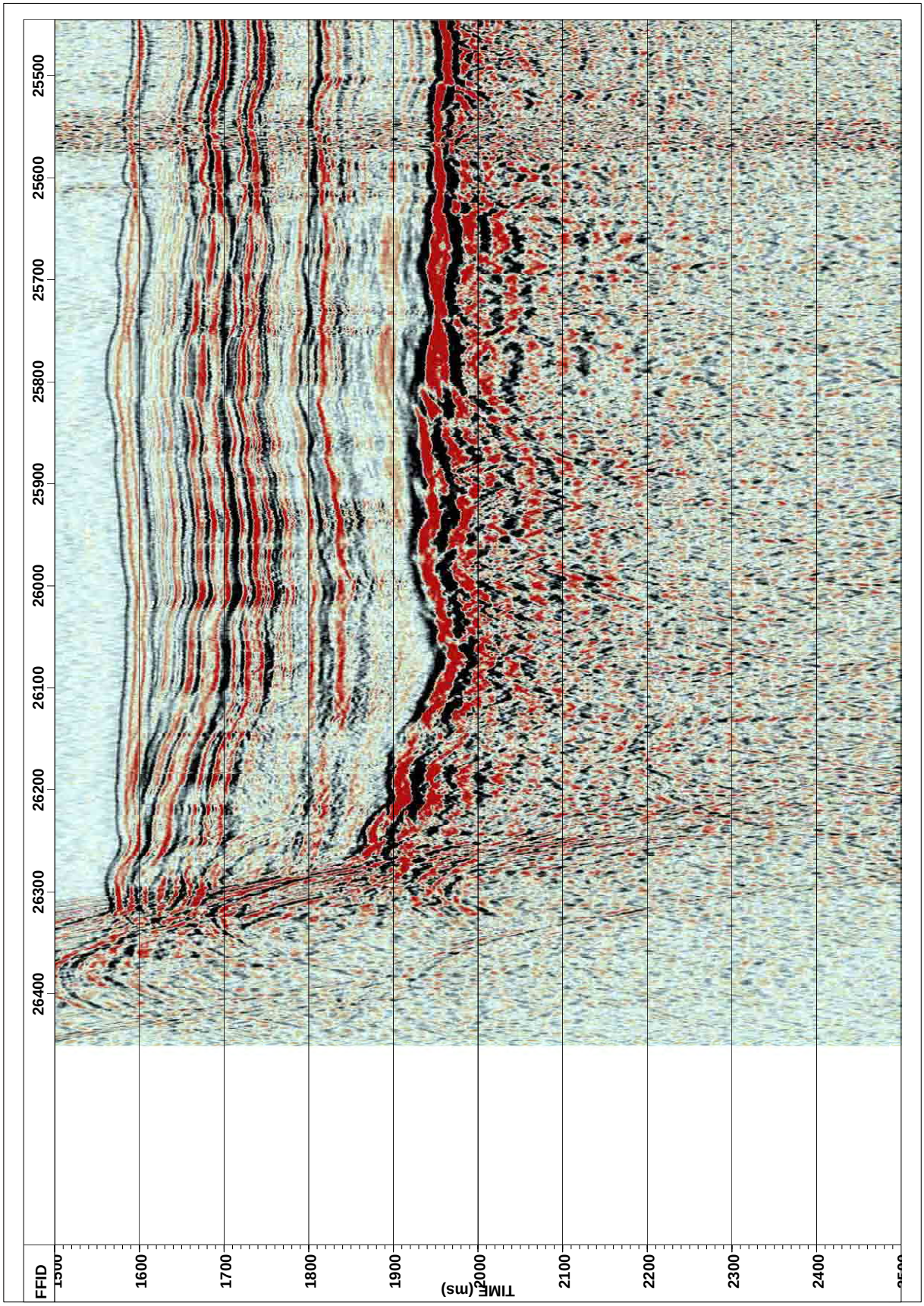

Figure 96: Seismic Profile GUATB37 in working area GUATB-01.

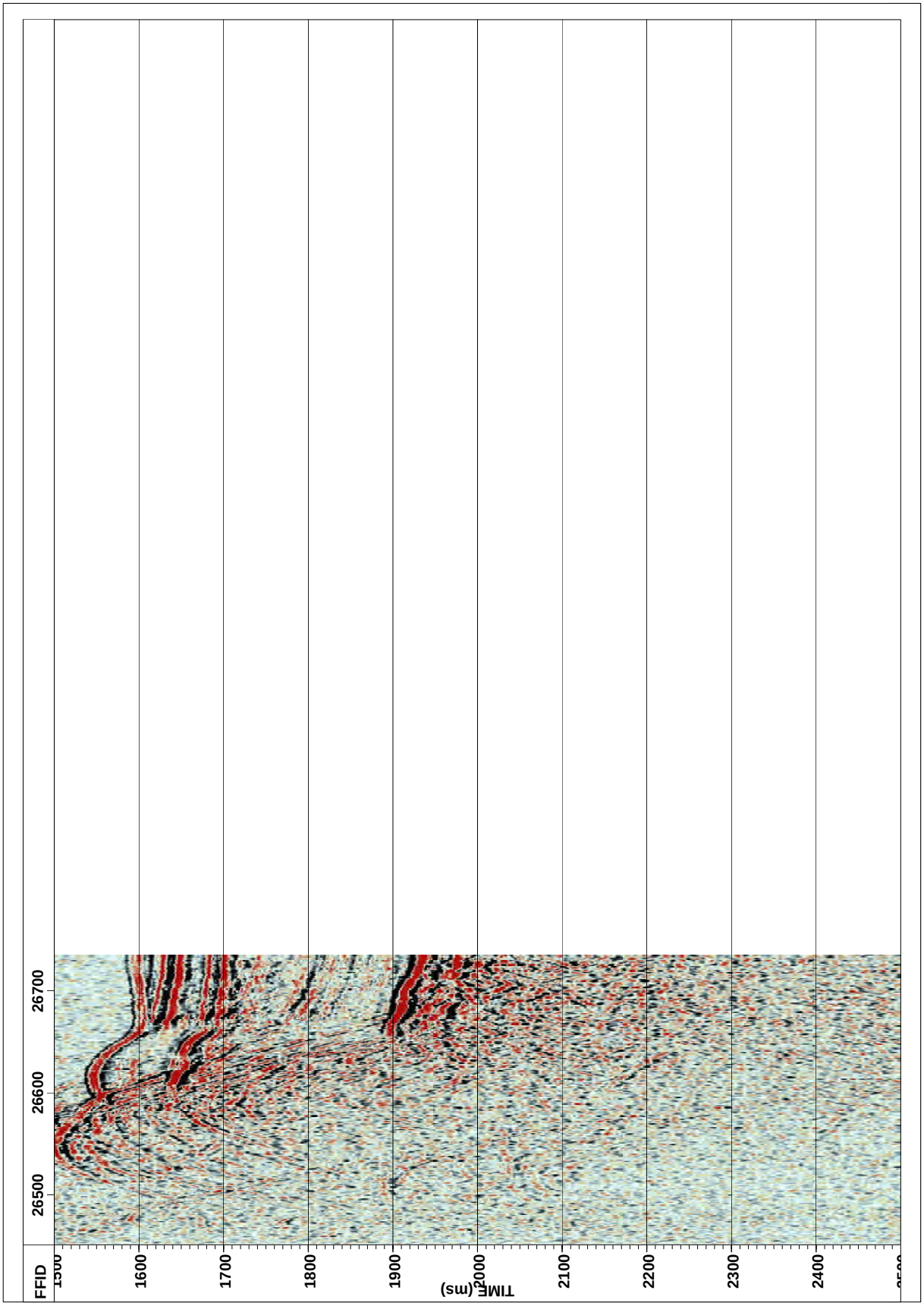

Figure 97: Seismic Profile GUATB38 in working area GUATB-01.

A.2.3 Parasound Profiles

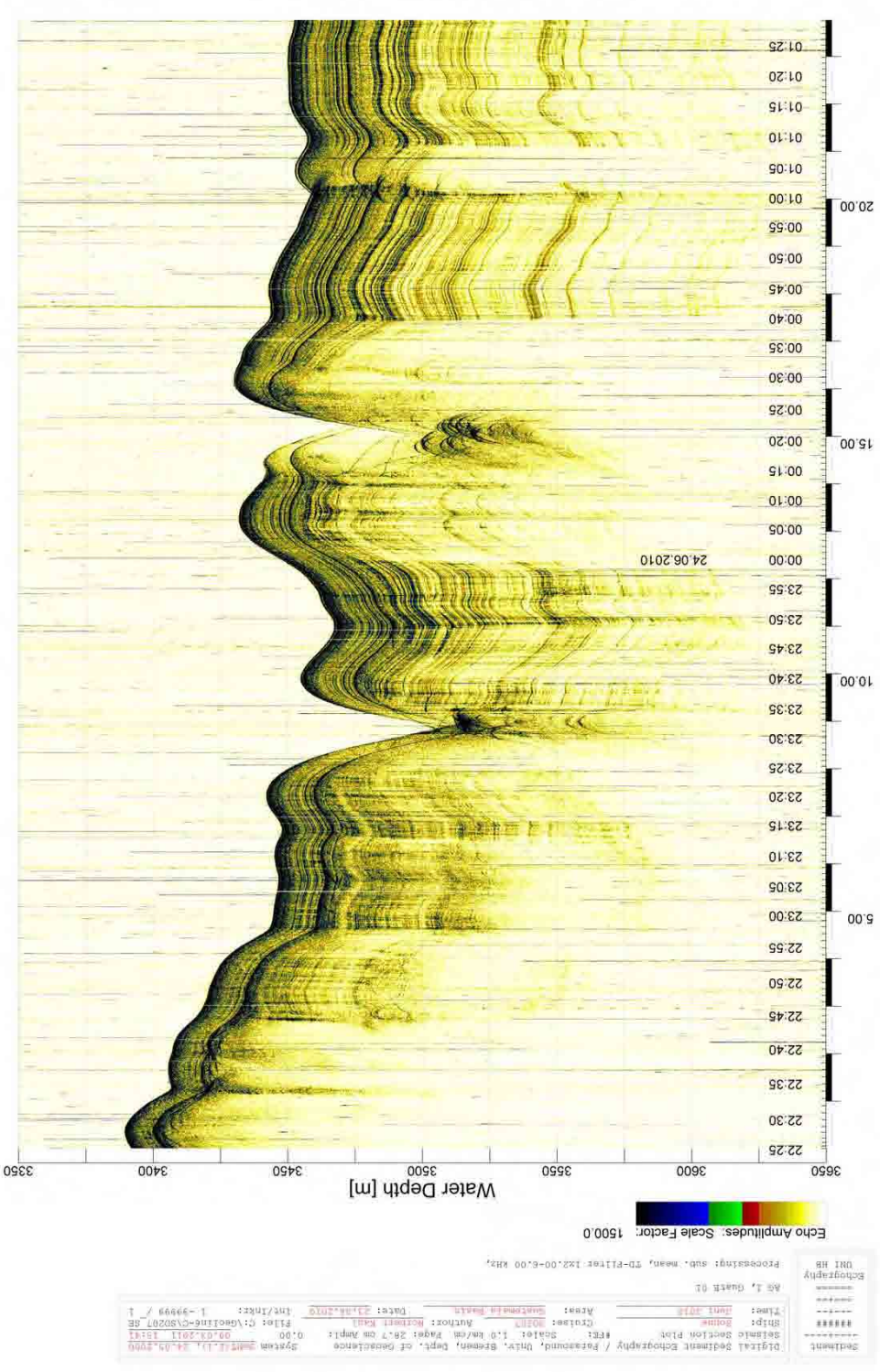

Figure 98: Parasound Profile GUATB01 in working area GUATB-01.

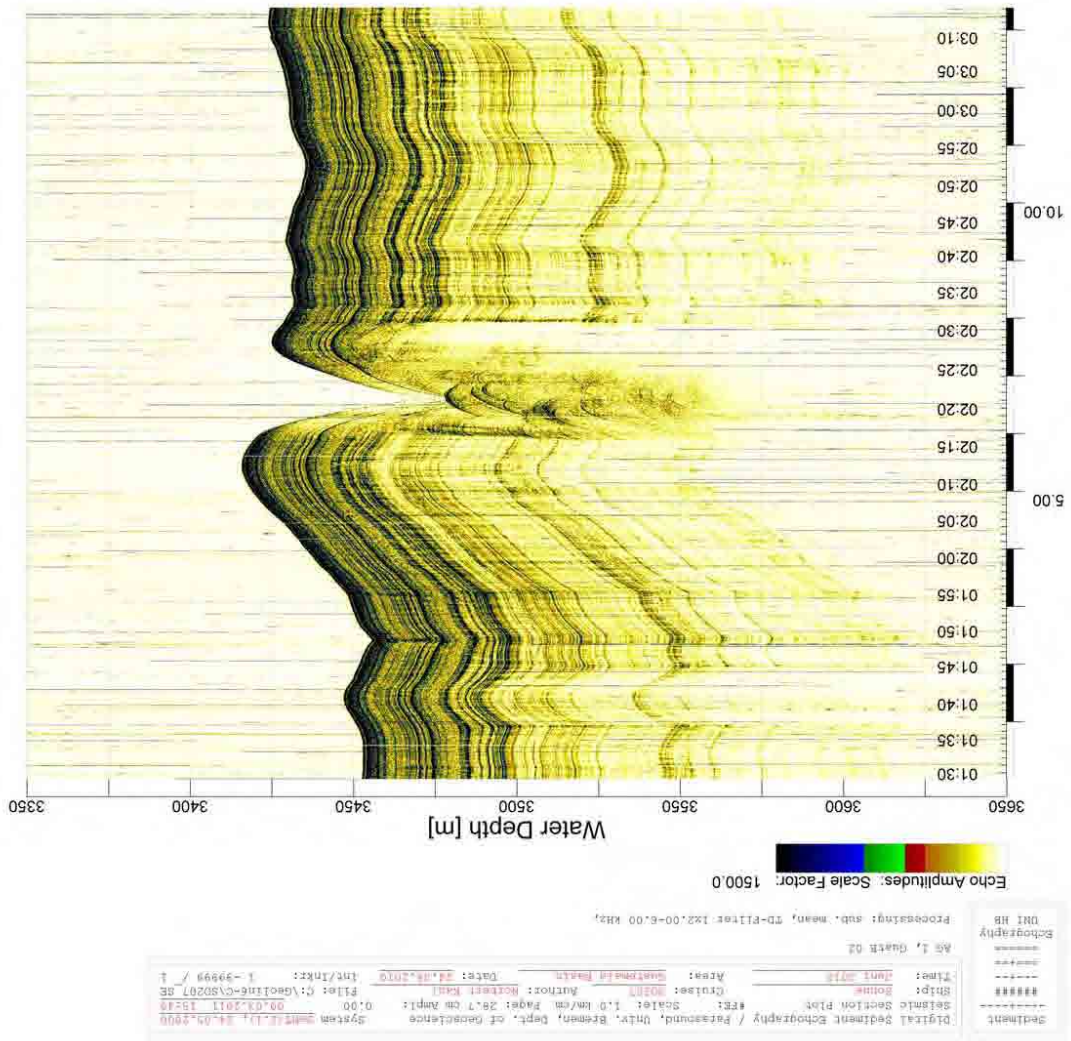

Figure 99: Parasound Profile GUATB02 in working area GUATB-01.

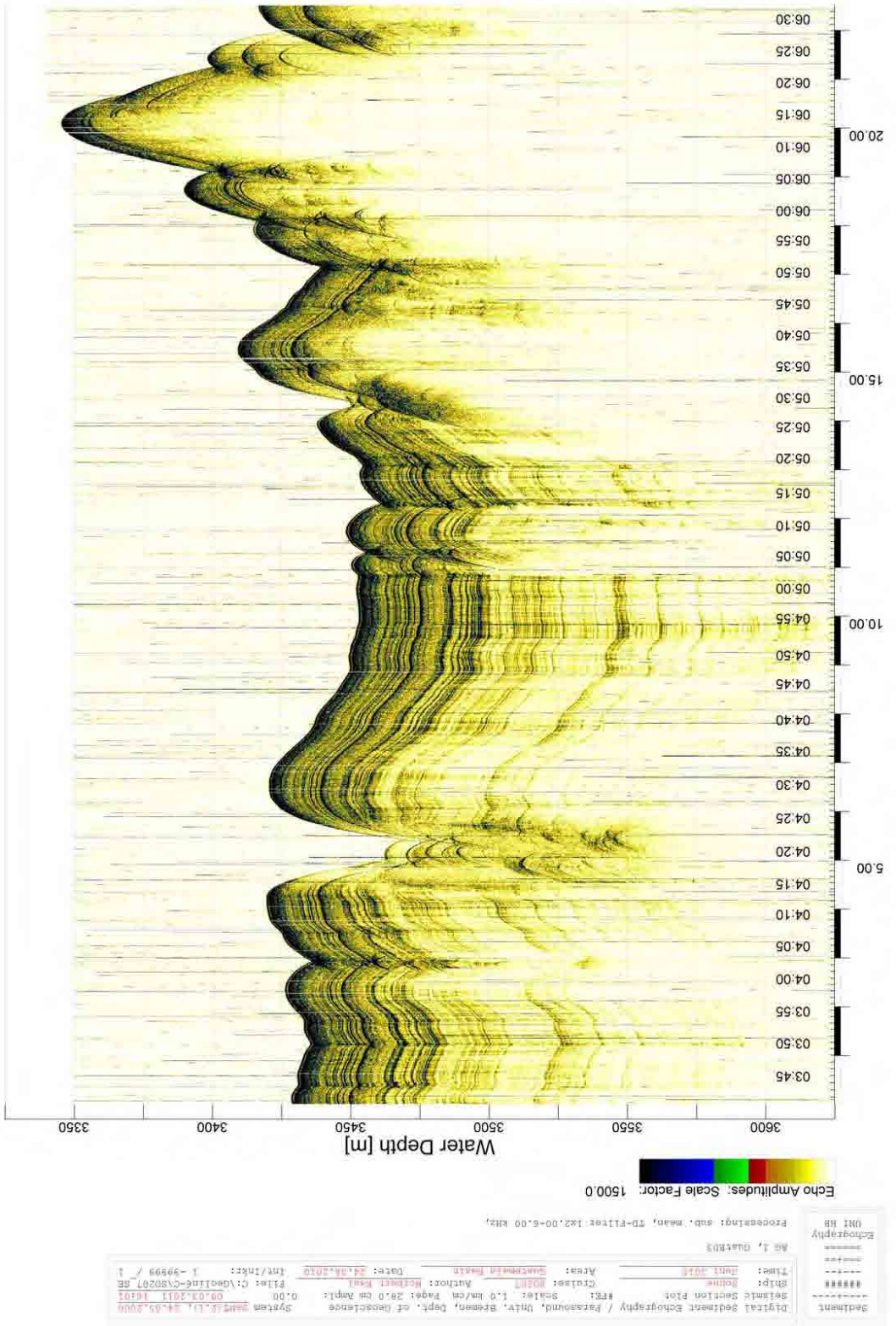

Figure 100: Parasound Profile GUATB03 in working area GUATB-01.

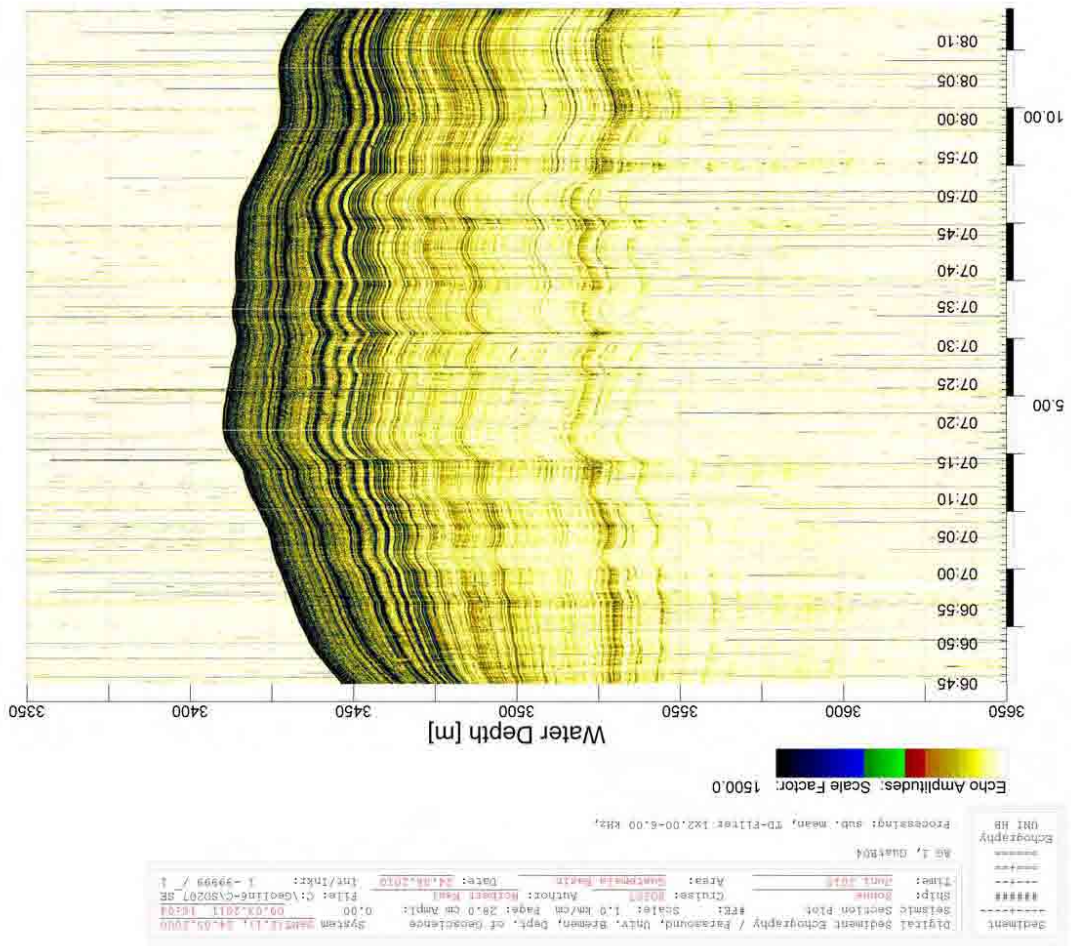

Figure 101: Parasound Profile GUATB04 in working area GUATB-01.

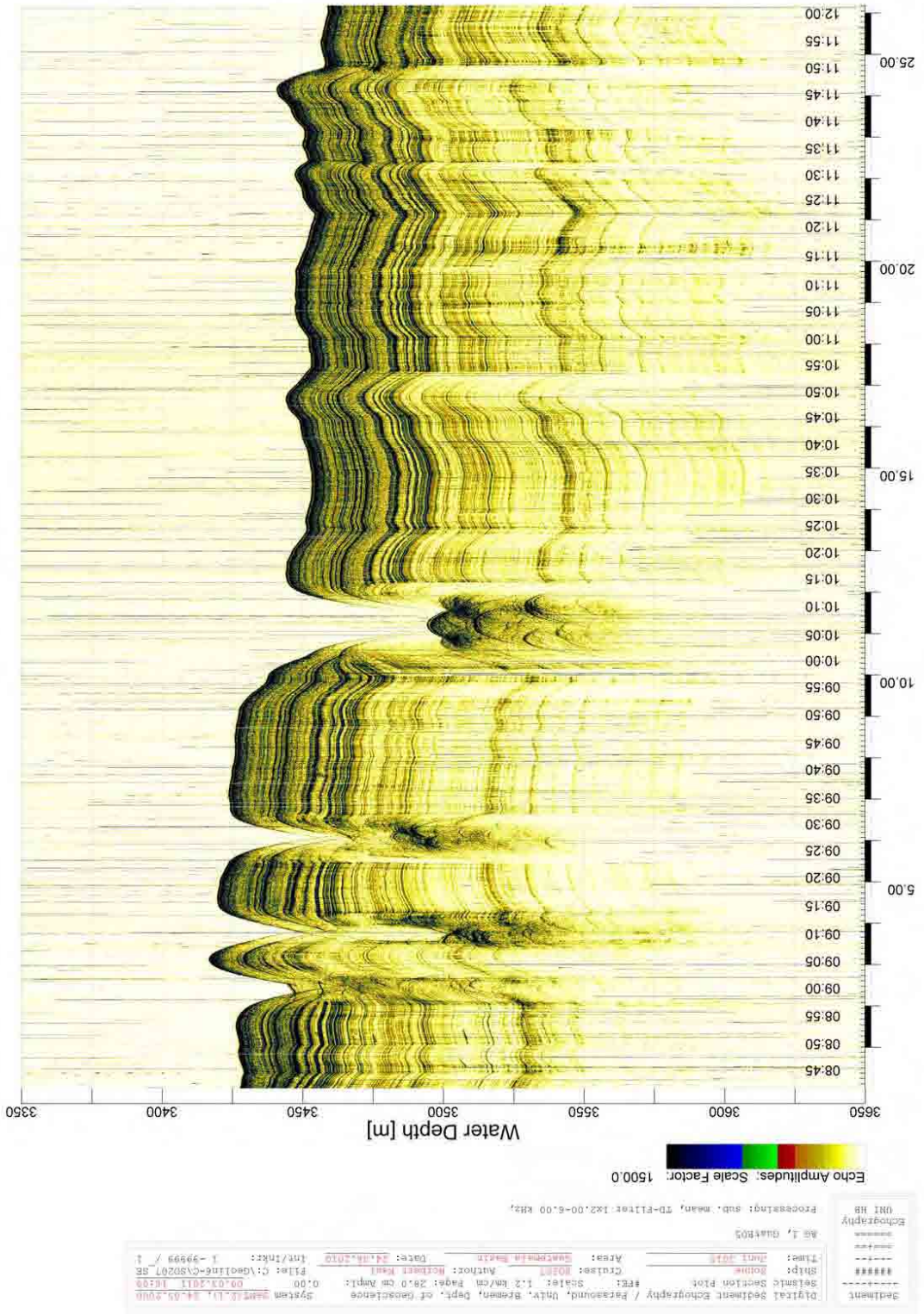

Figure 102: Parasound Profile GUATB05 in working area GUATB-01.

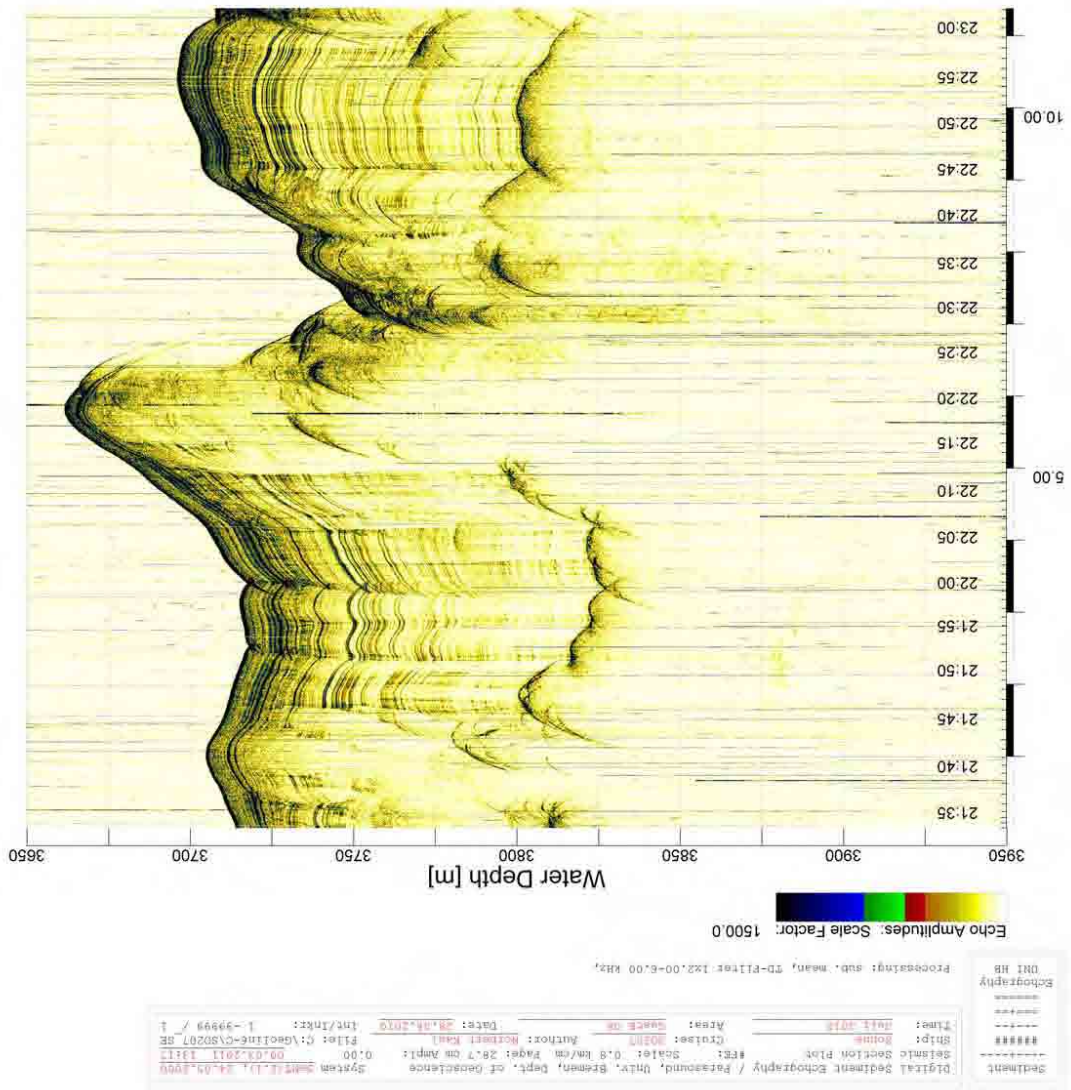

Figure 103: Parasound Profile GUATB08 in working area GUATB-02.

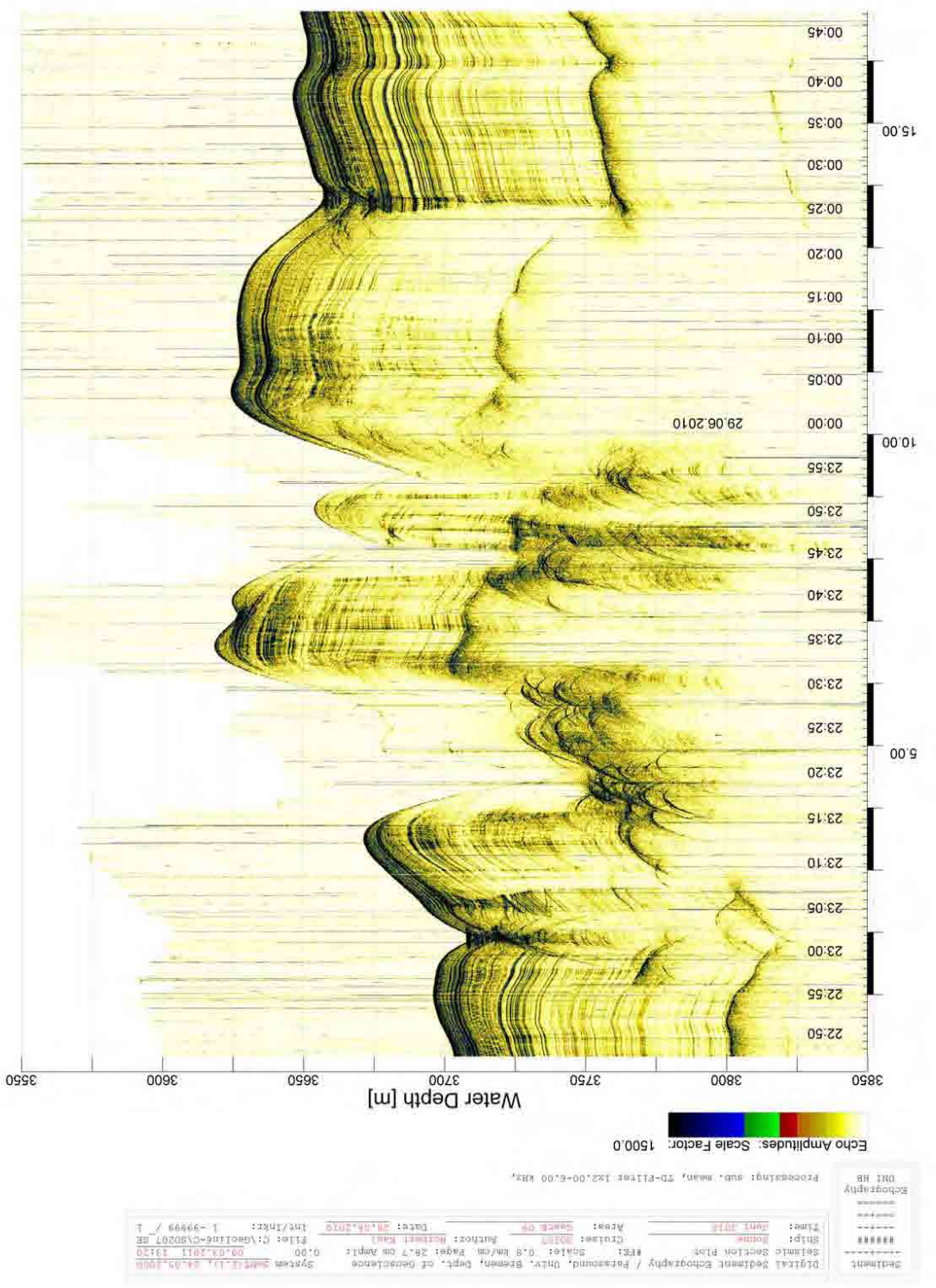

Figure 104: Parasound Profile GUATB09 in working area GUATB-02.

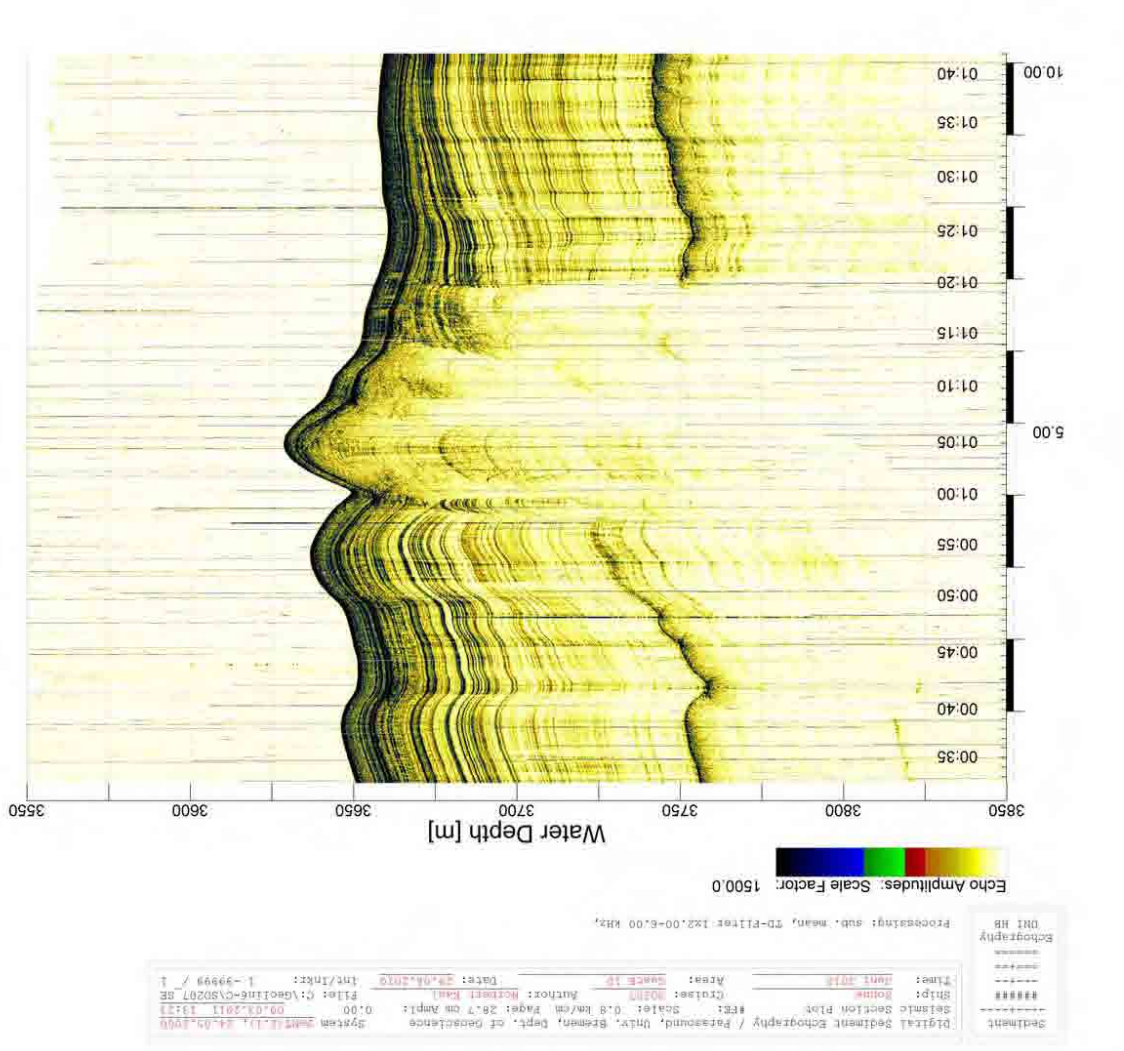

Figure 105: Parasound Profile GUATB10 in working area GUATB-02.

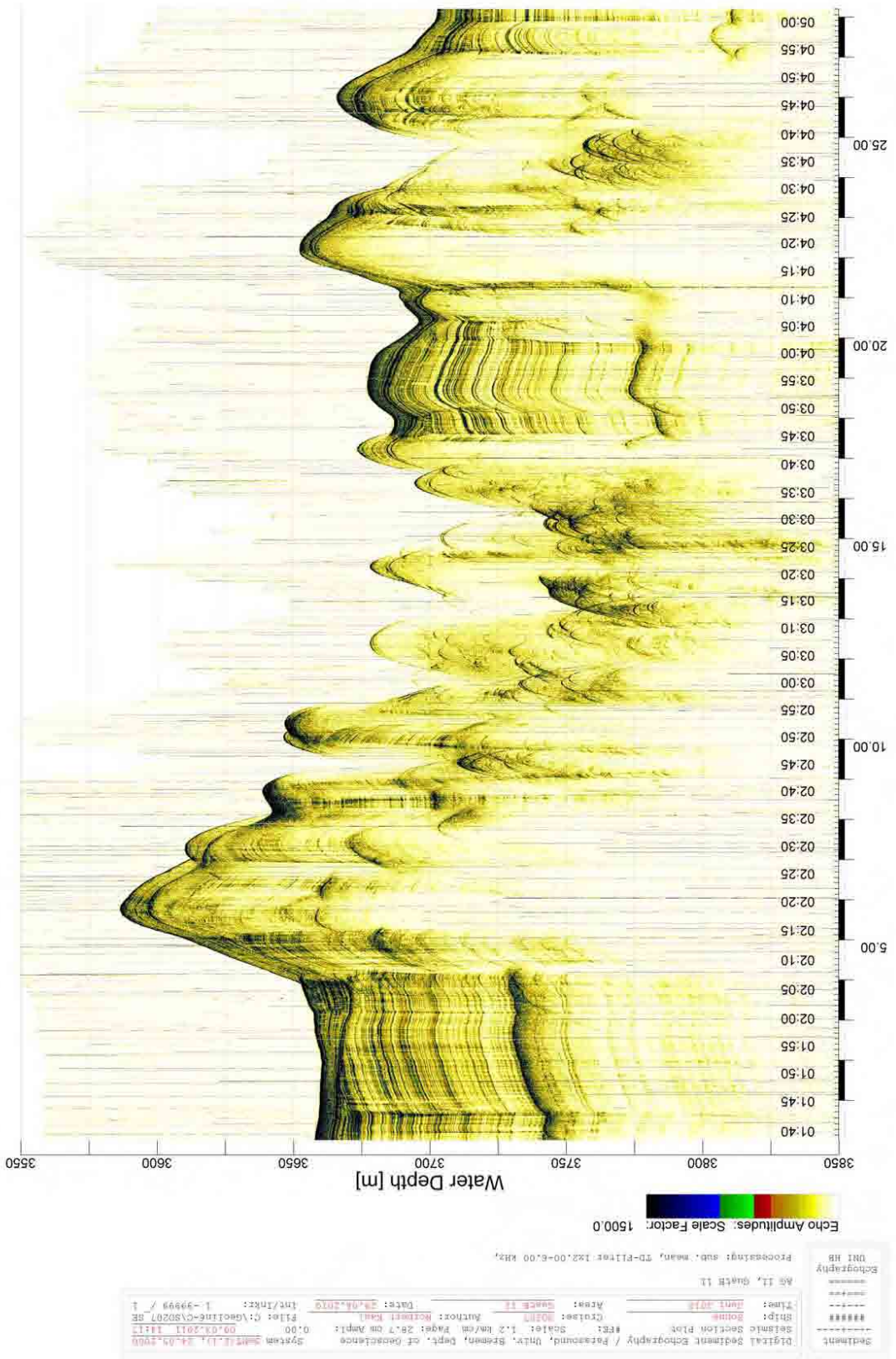

Figure 106: Parasound Profile GUATB11 in working area GUATB-02.

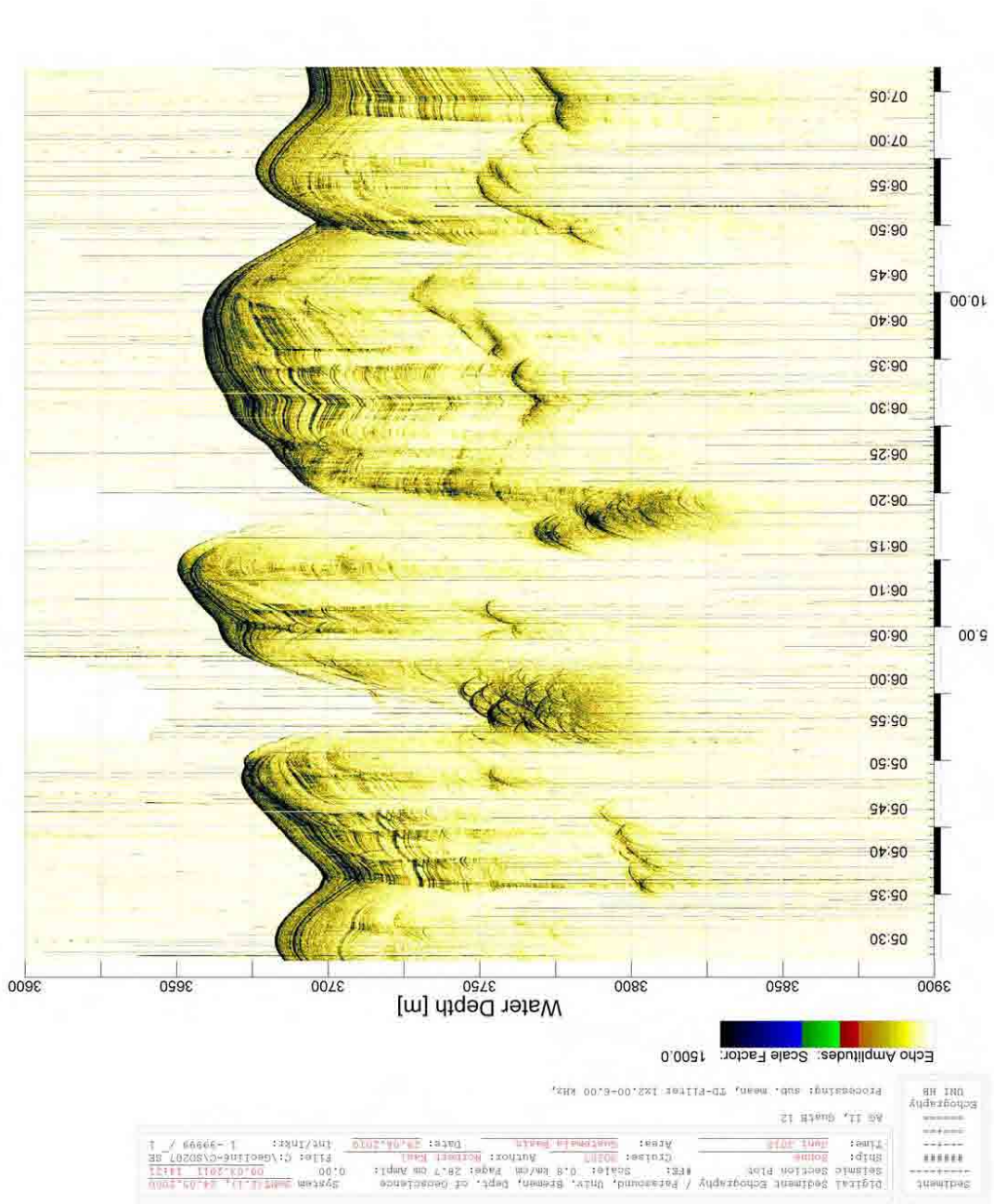

Figure 107: Parasound Profile GUATB12 in working area GUATB-02.

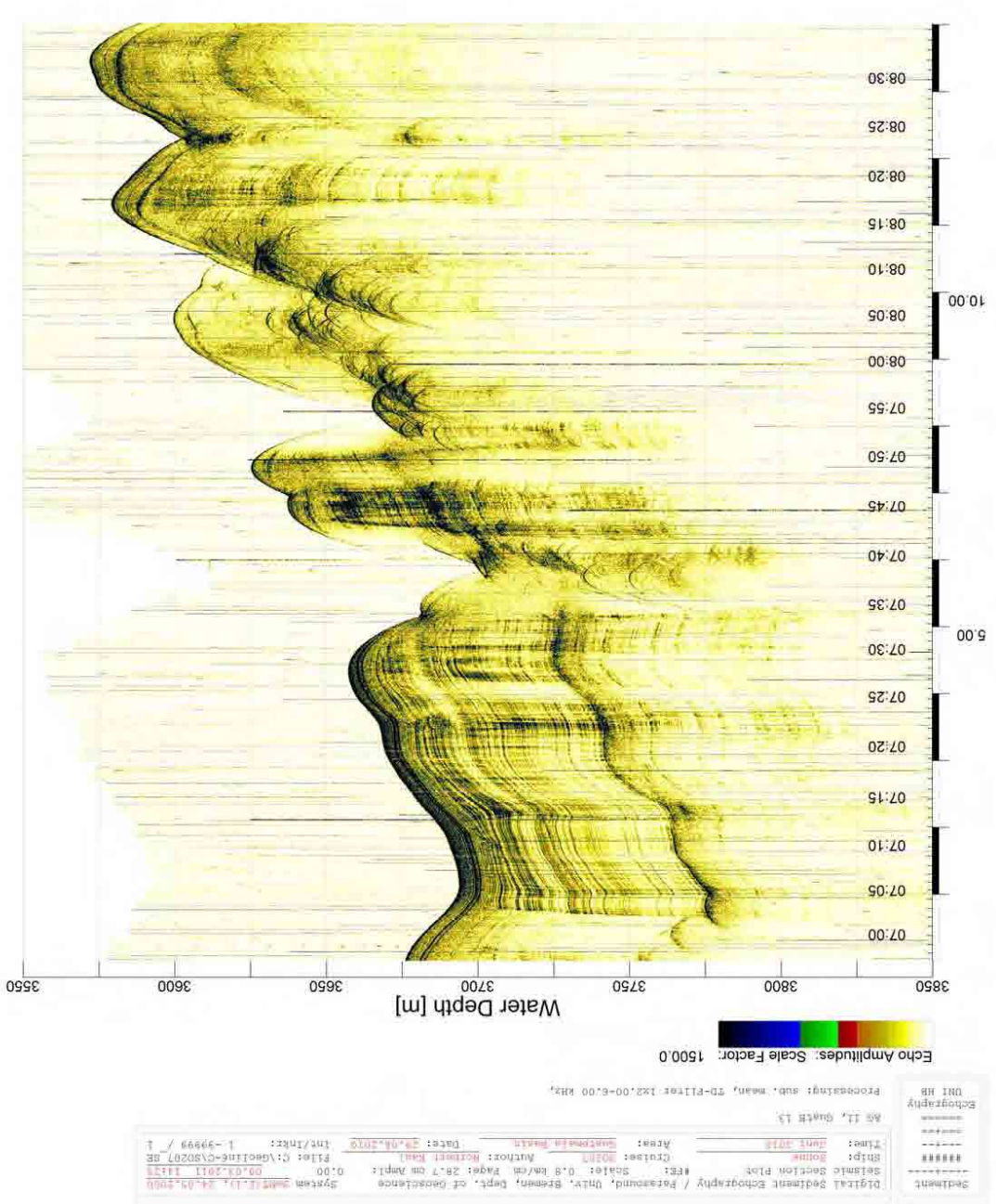

Figure 108: Parasound Profile GUATB13 in working area GUATB-02.

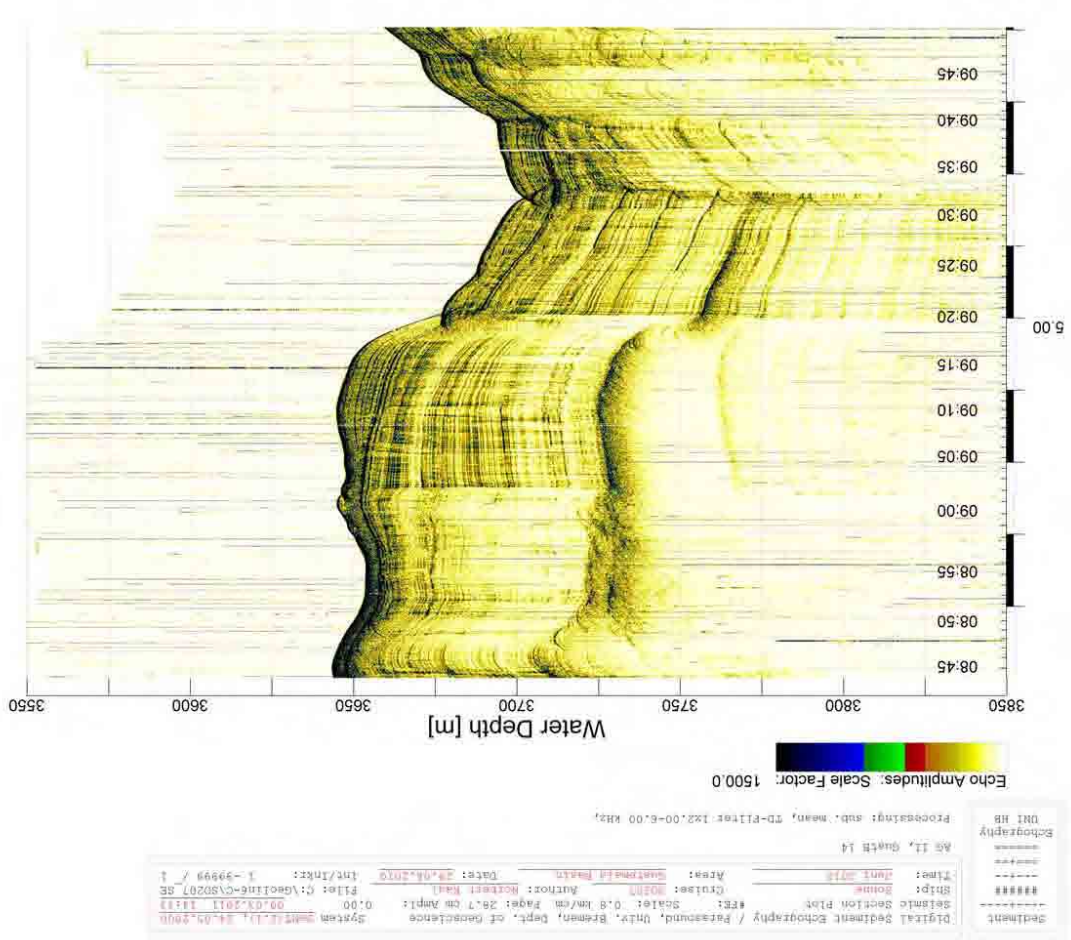

Figure 109: Parasound Profile GUATB14 in working area GUATB-02.

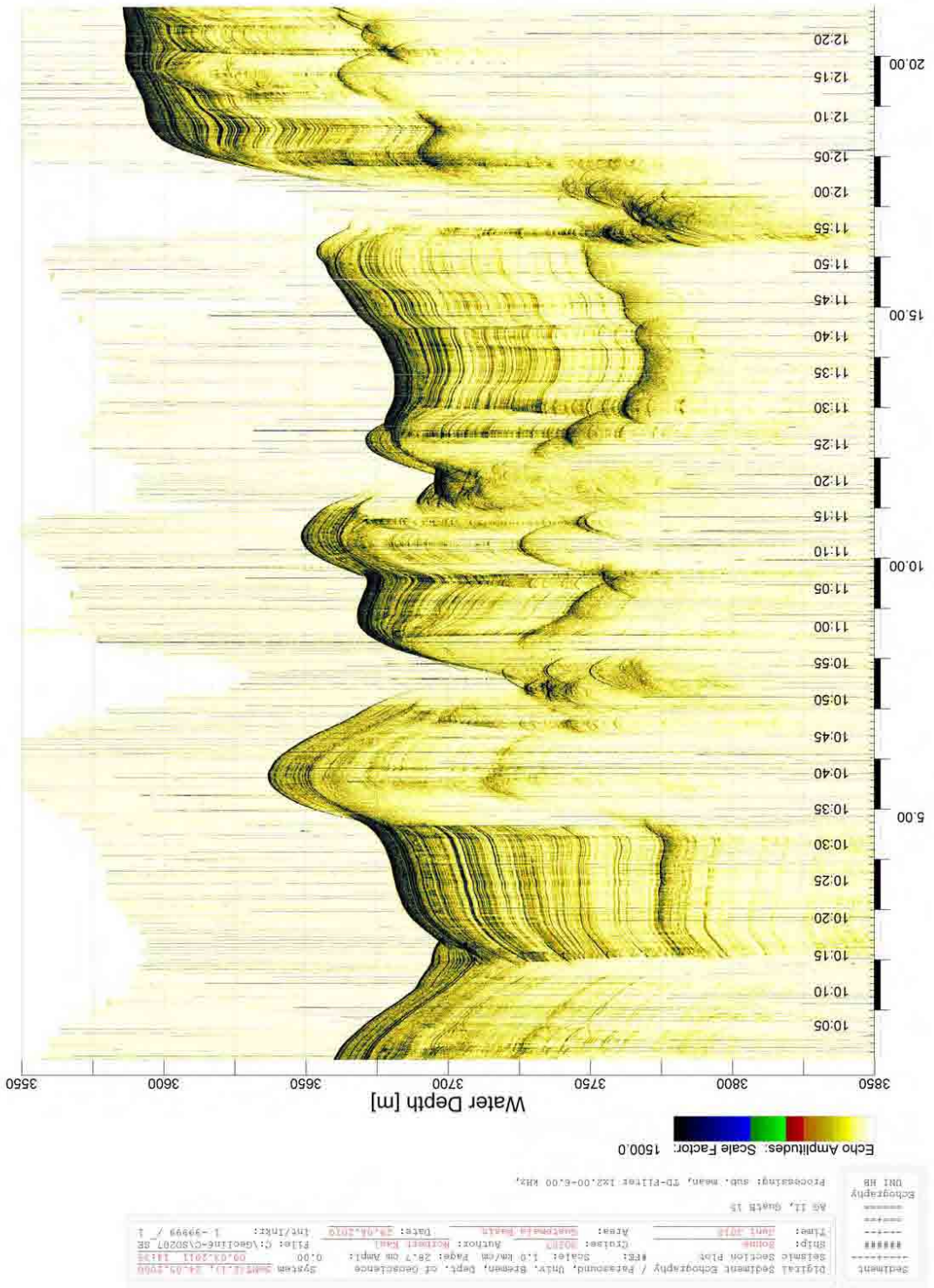

Figure 110: Parasound Profile GUATB15 in working area GUATB-02.

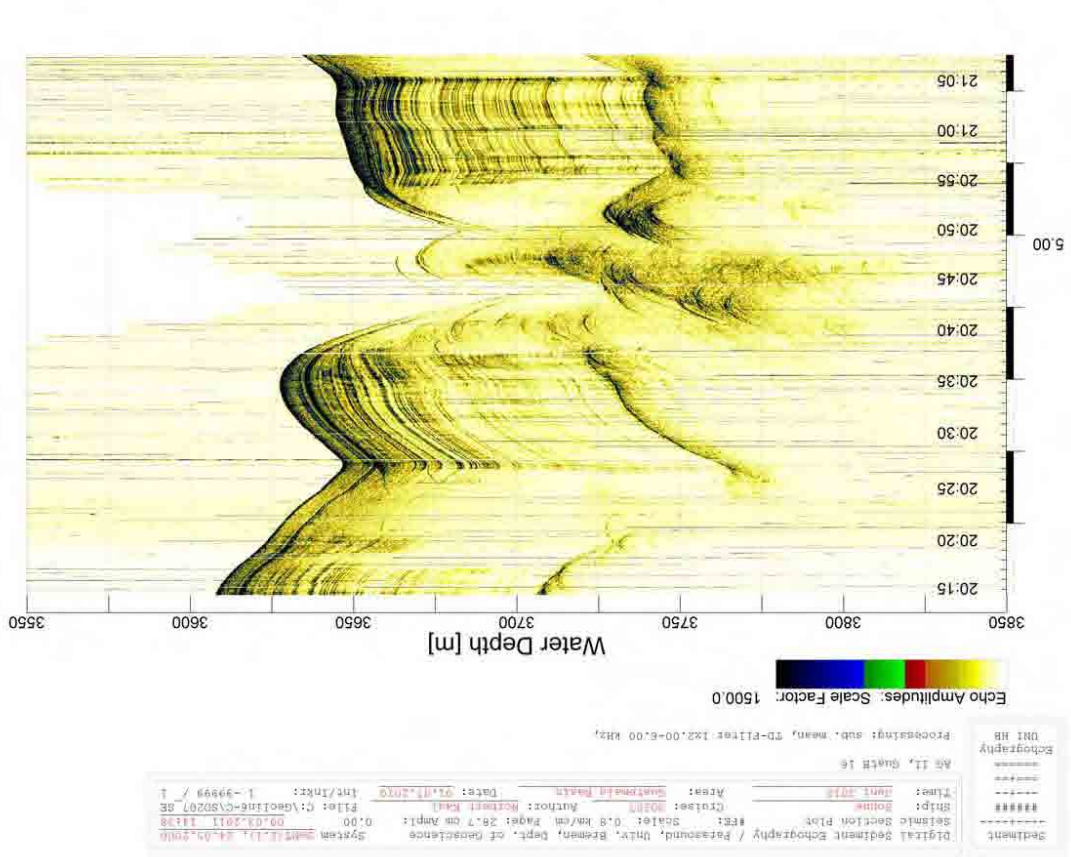

Figure 111: Parasound Profile GUATB16 in working area GUATB-02.

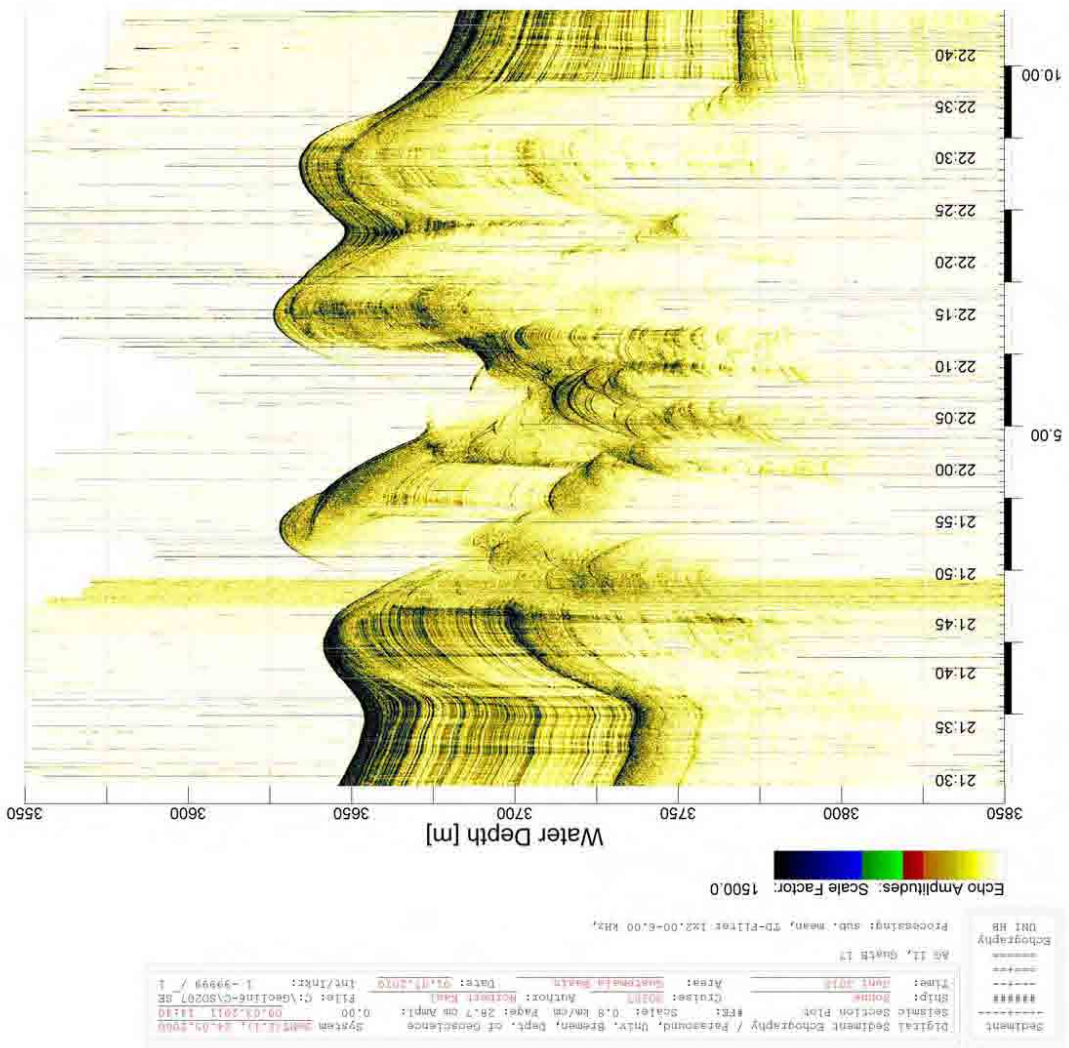

Figure 112: Parasound Profile GUATB17 in working area GUATB-02.

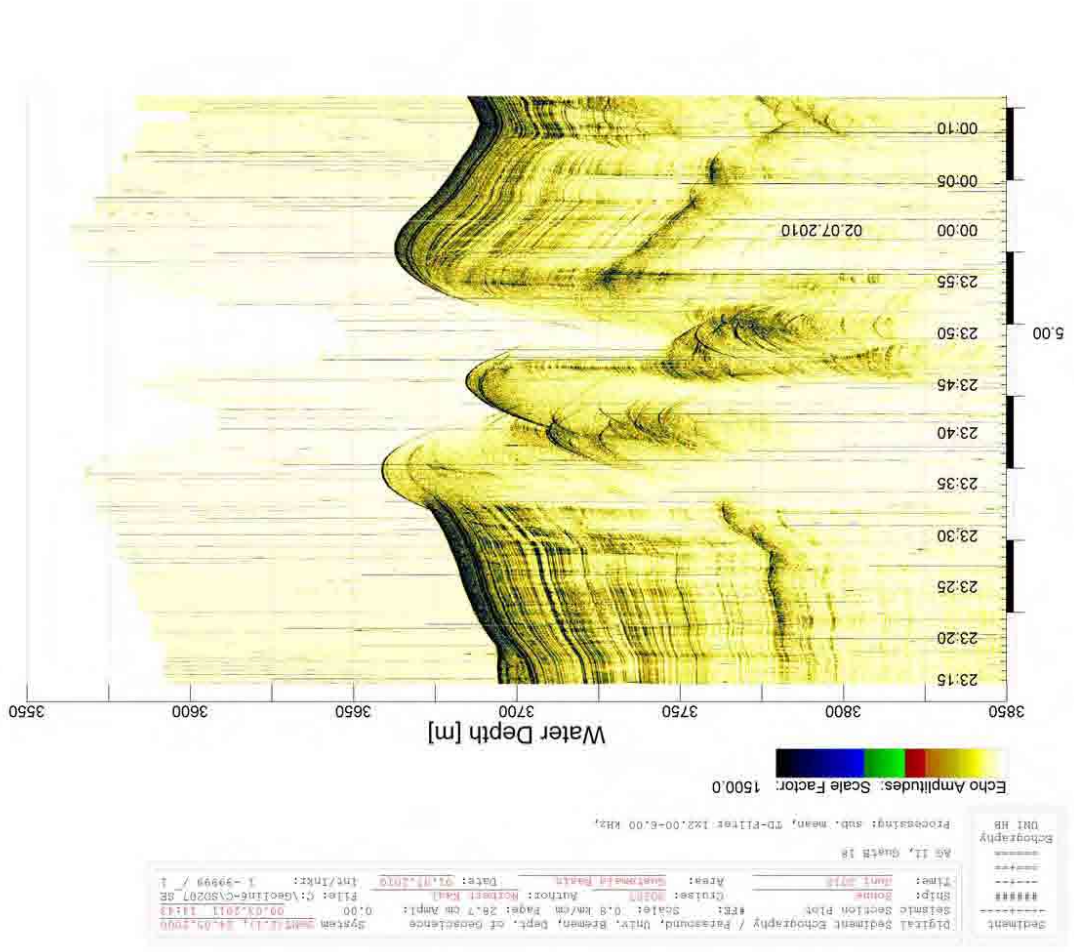

Figure 113: Parasound Profile GUATB18 in working area GUATB-02.

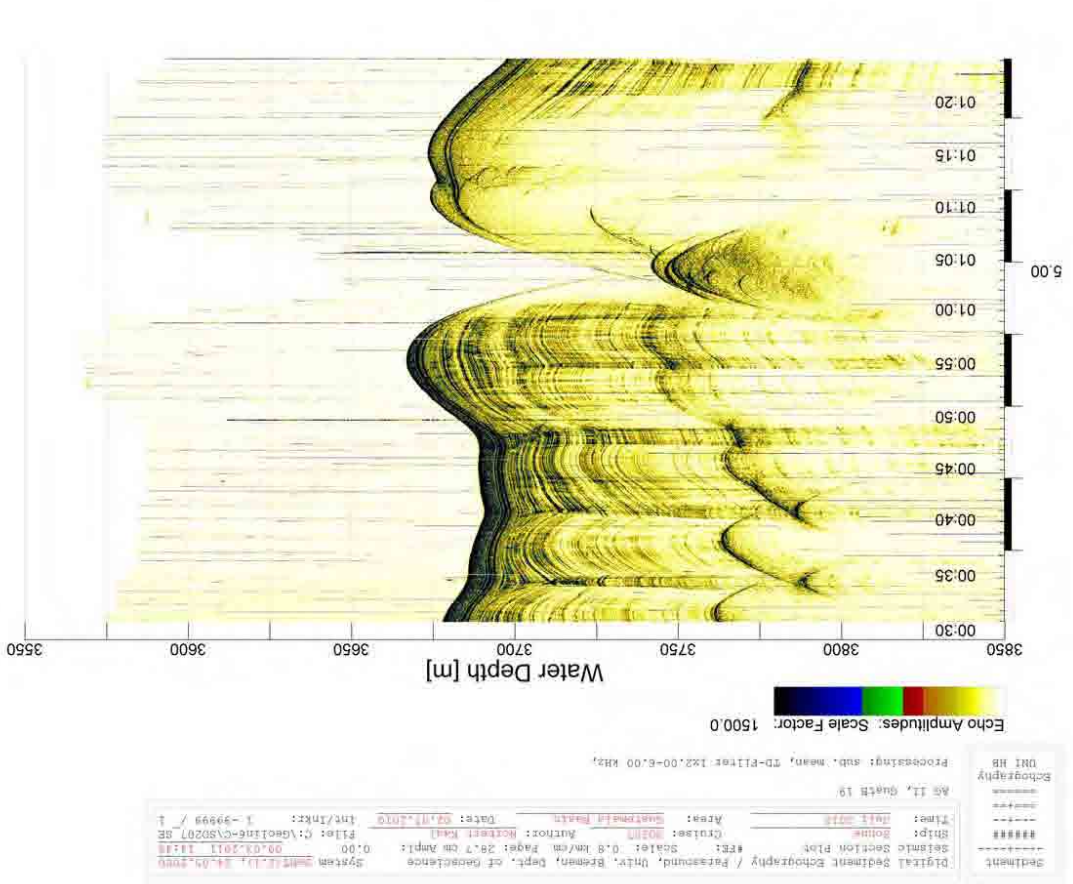

Figure 114: Parasound Profile GUATB19 in working area GUATB-02.

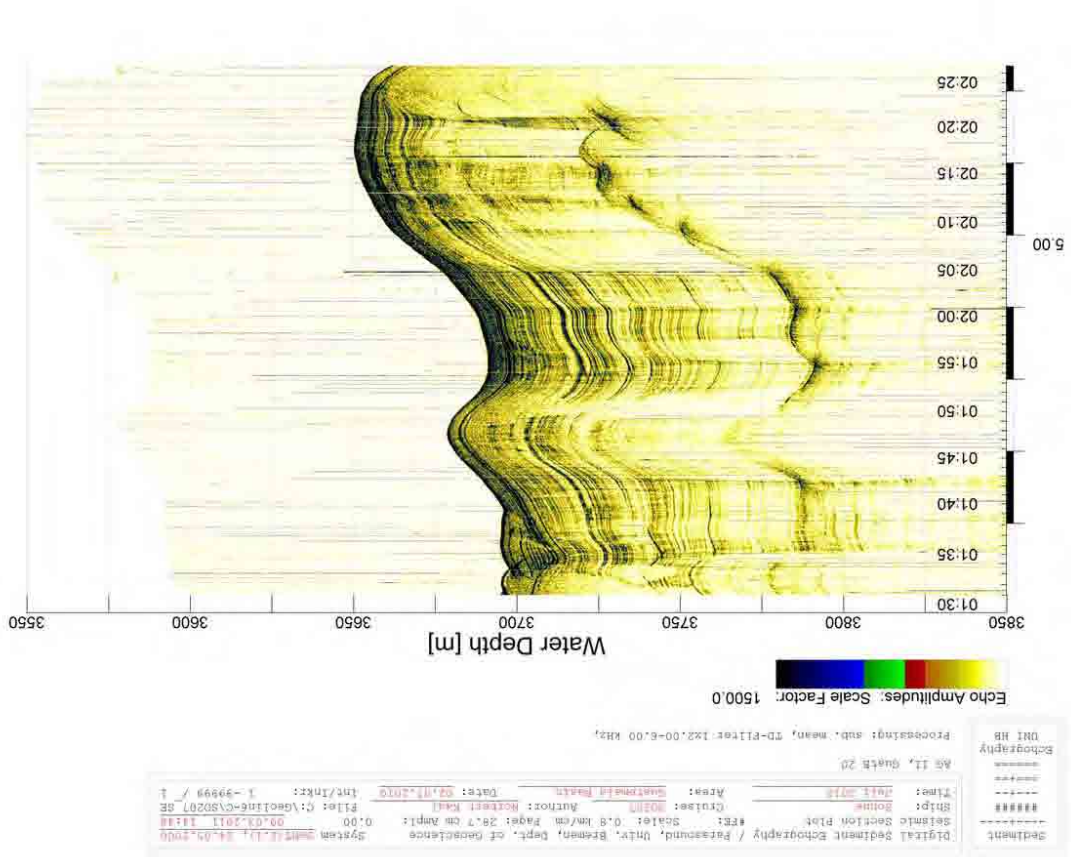

Figure 115: Parasound Profile GUATB20 in working area GUATB-02.

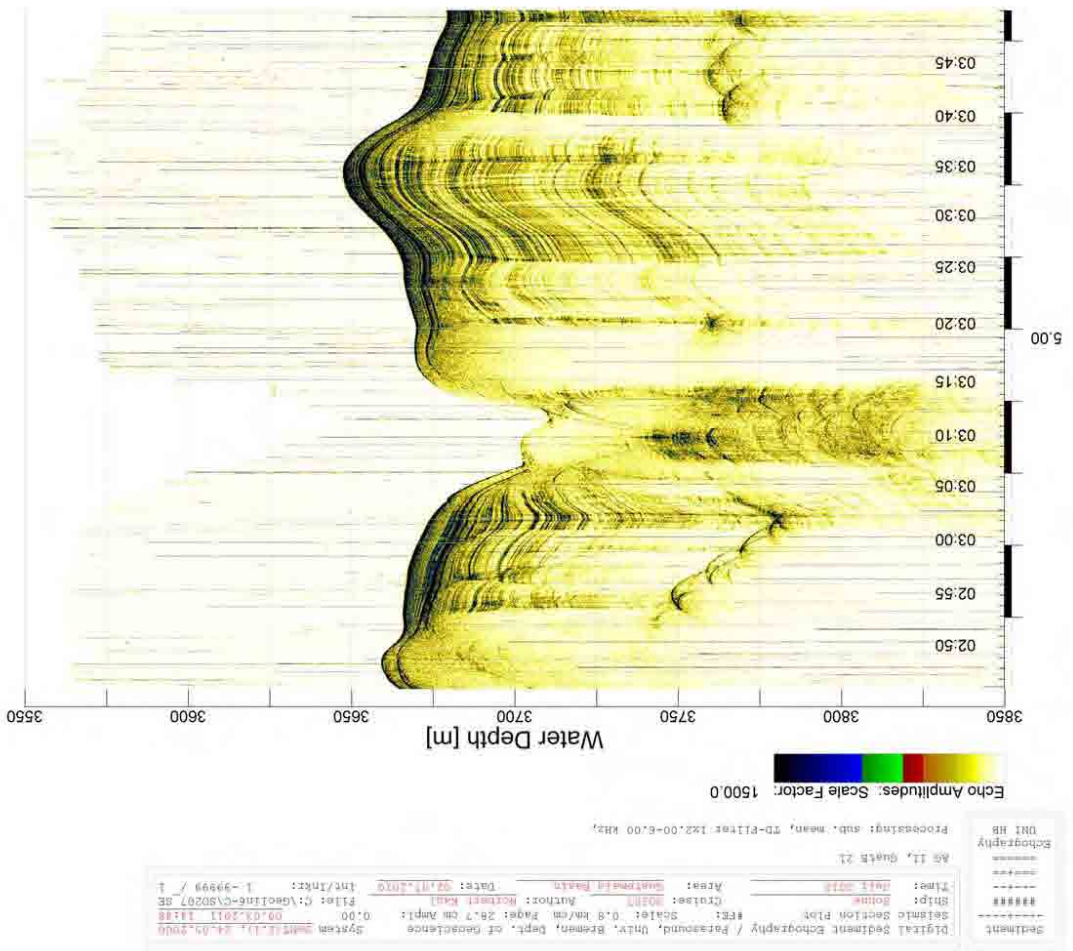

Figure 116: Parasound Profile GUATB21 in working area GUATB-02.

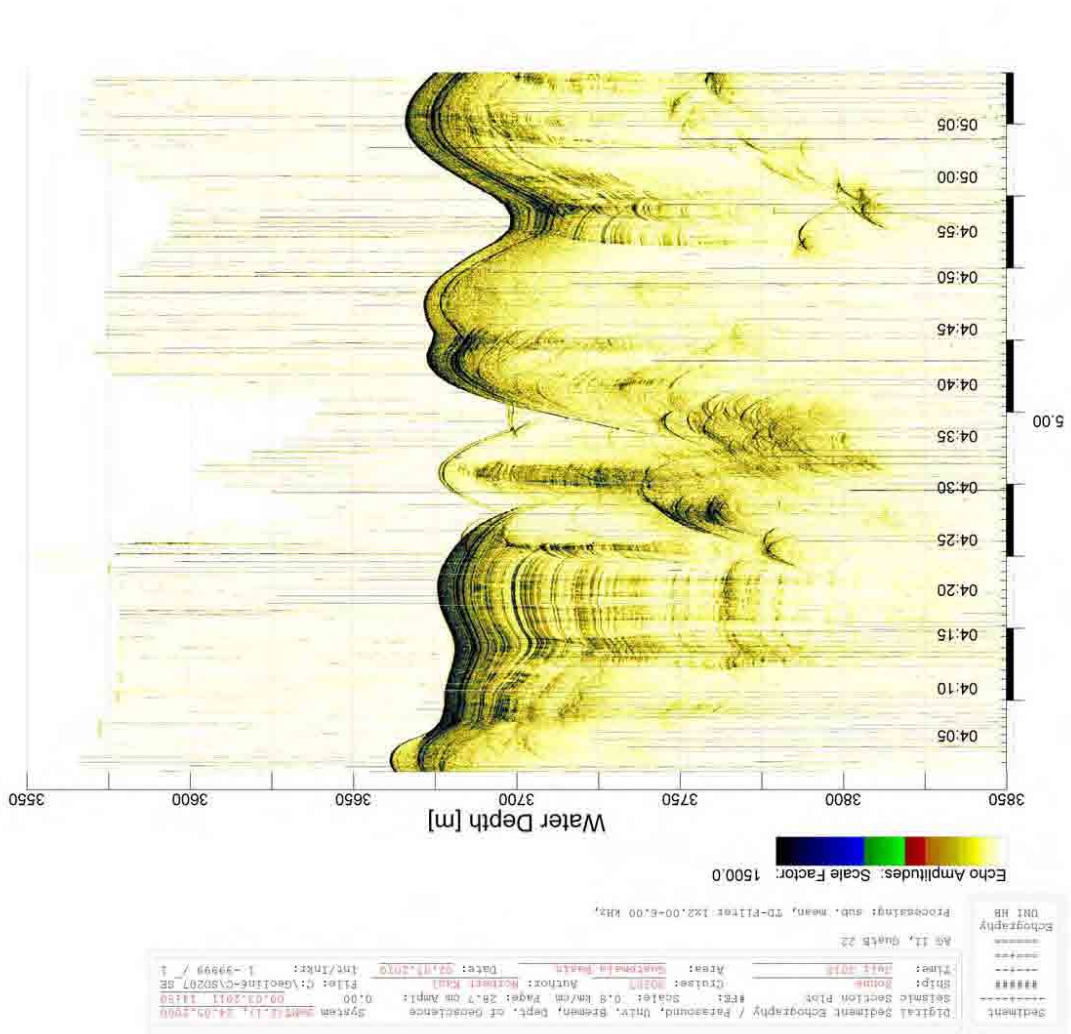

Figure 117: Parasound Profile GUATB22 in working area GUATB-02.

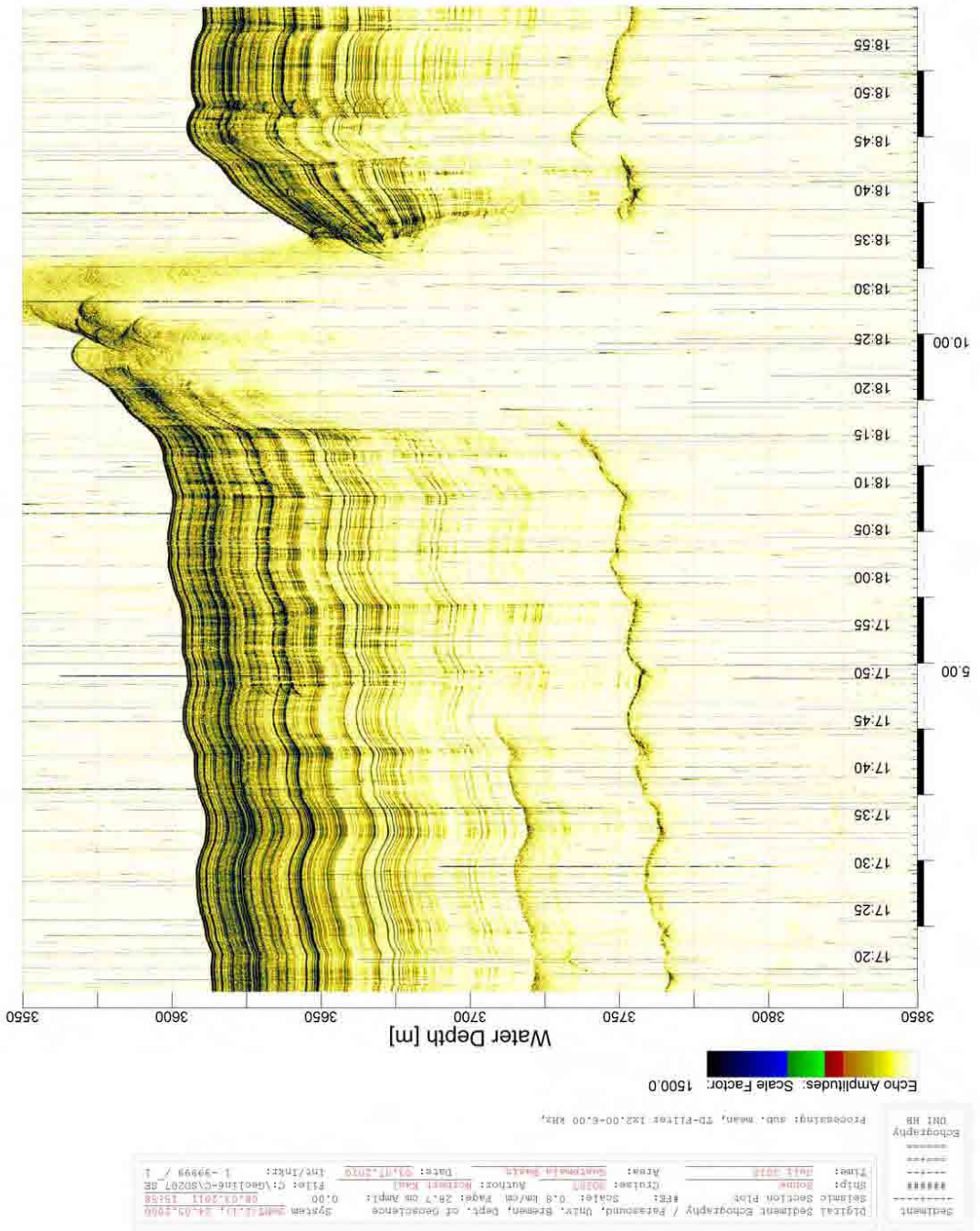

Figure 118: Parasound Profile GUATB24 in working area GUATB-03.

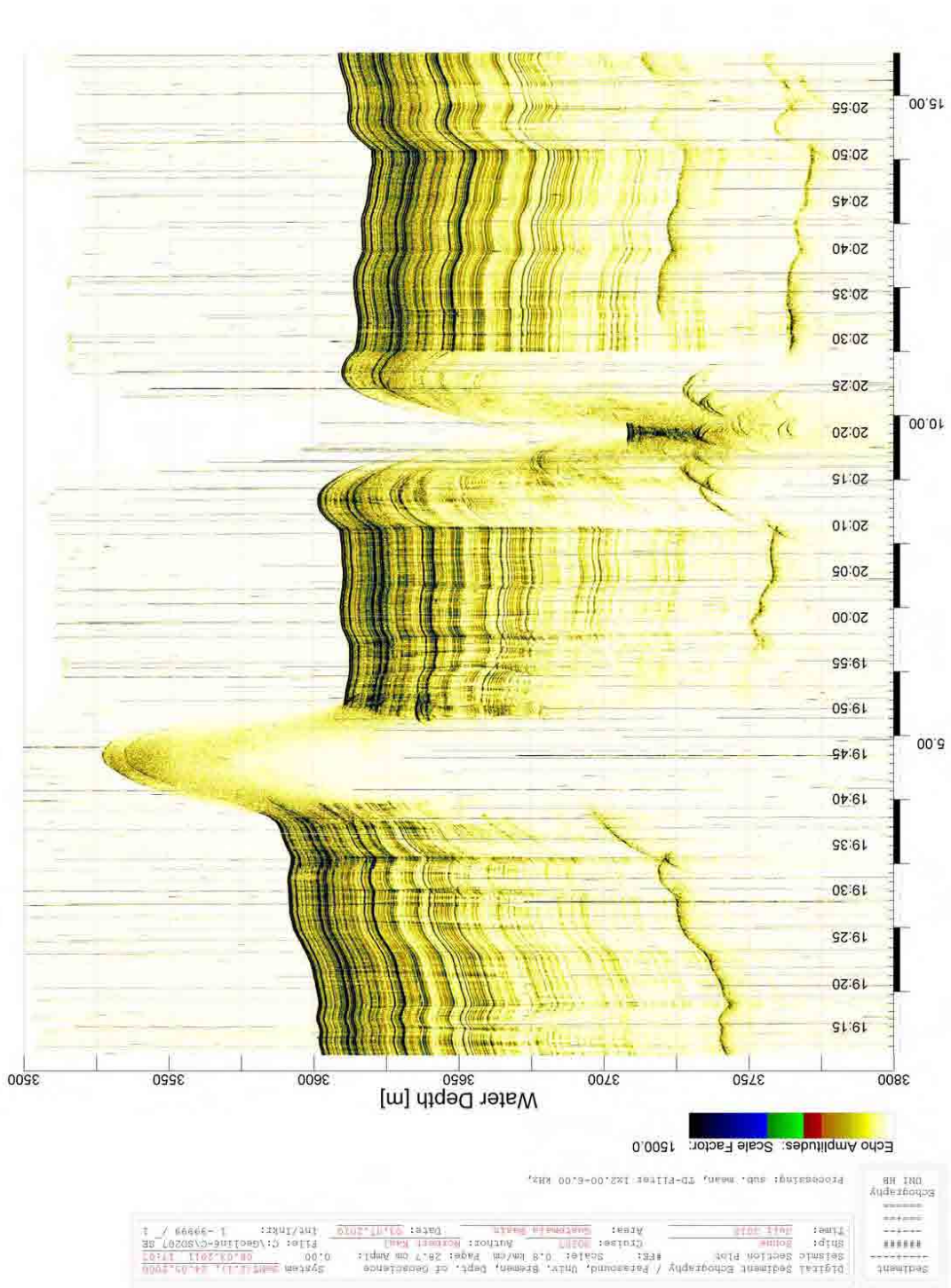

Figure 119: Parasound Profile GUATB25 in working area GUATB-03.

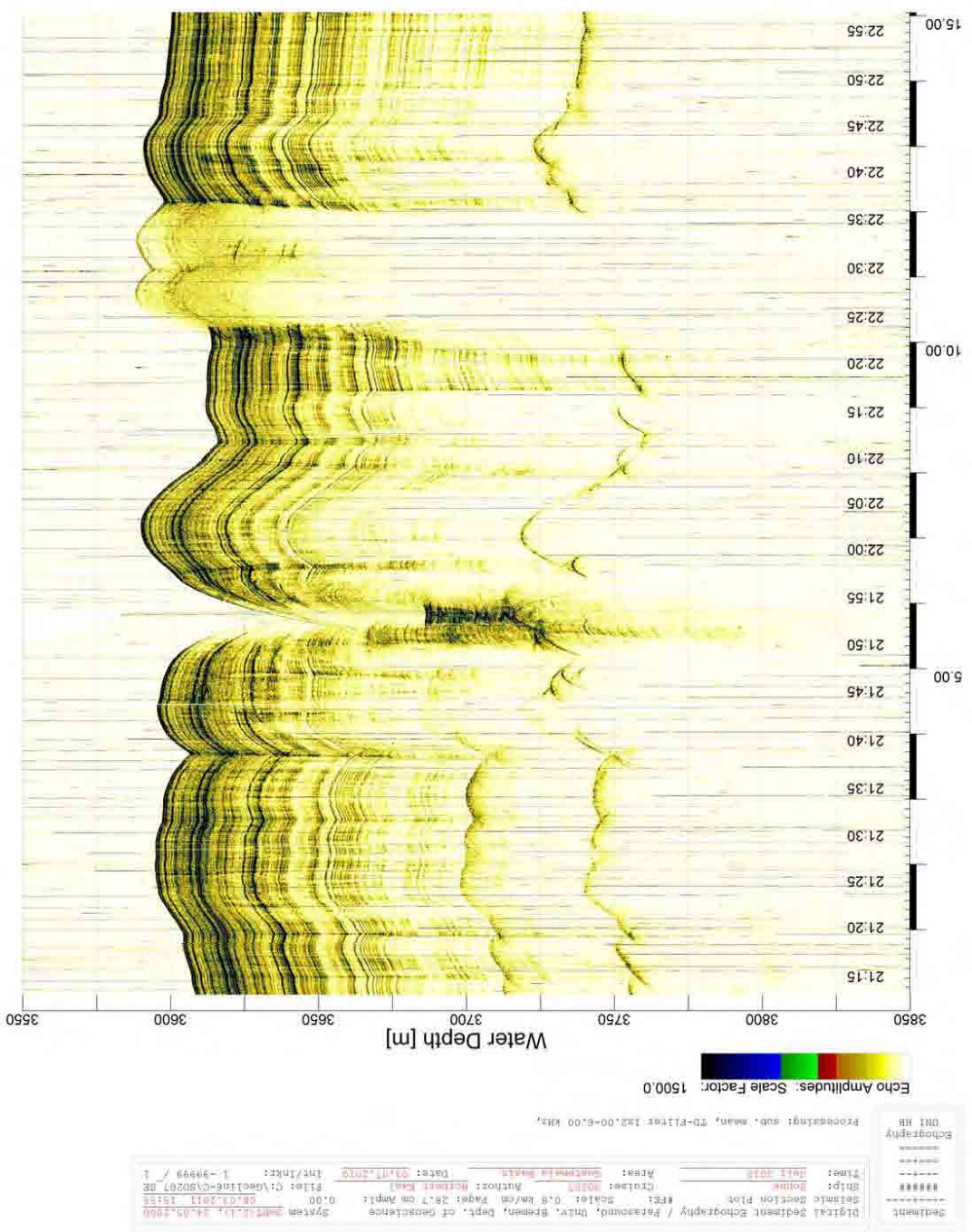

Figure 120: Parasound Profile GUATB26 in working area GUATB-03.

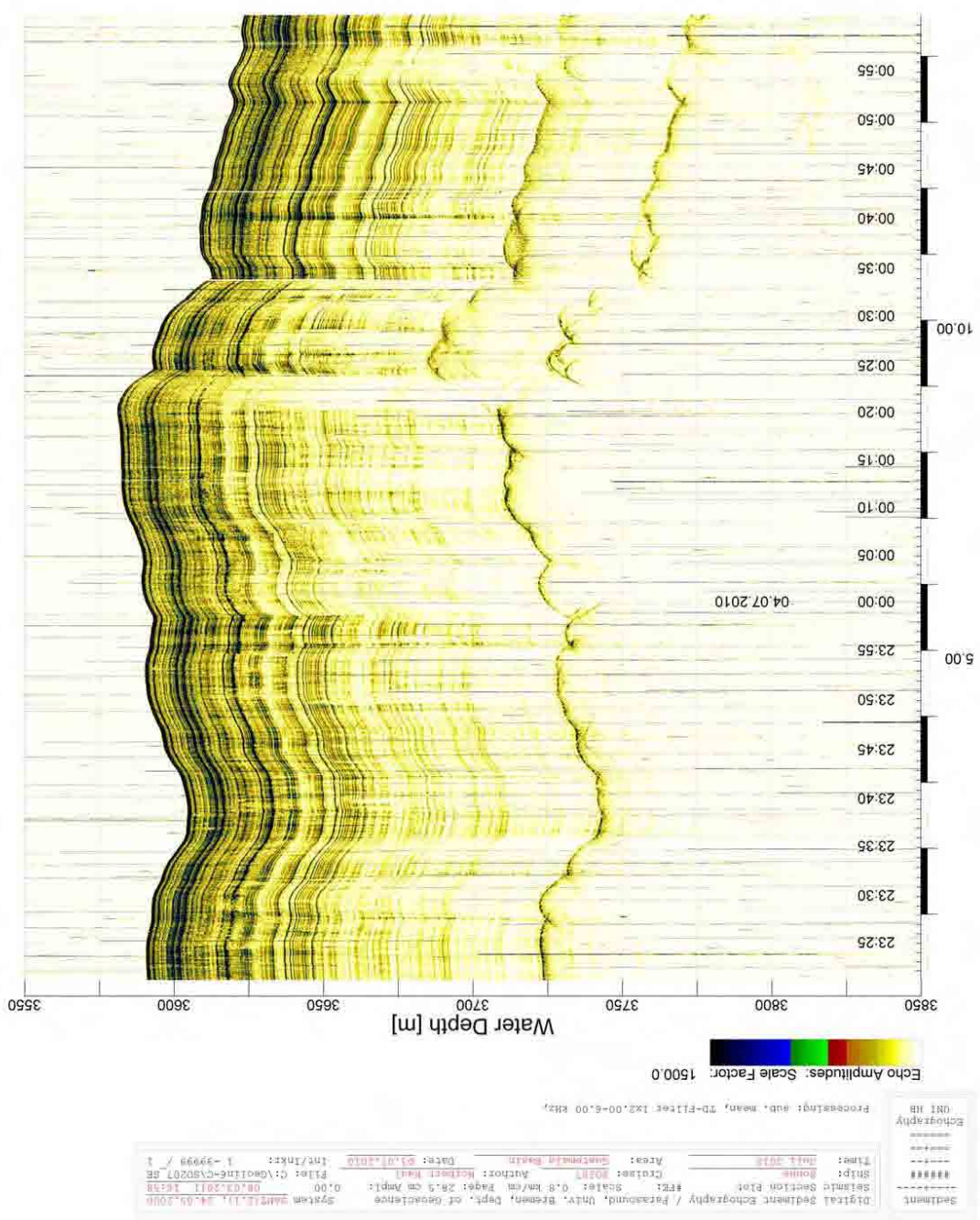

Figure 121: Parasound Profile GUATB27 in working area GUATB-03.

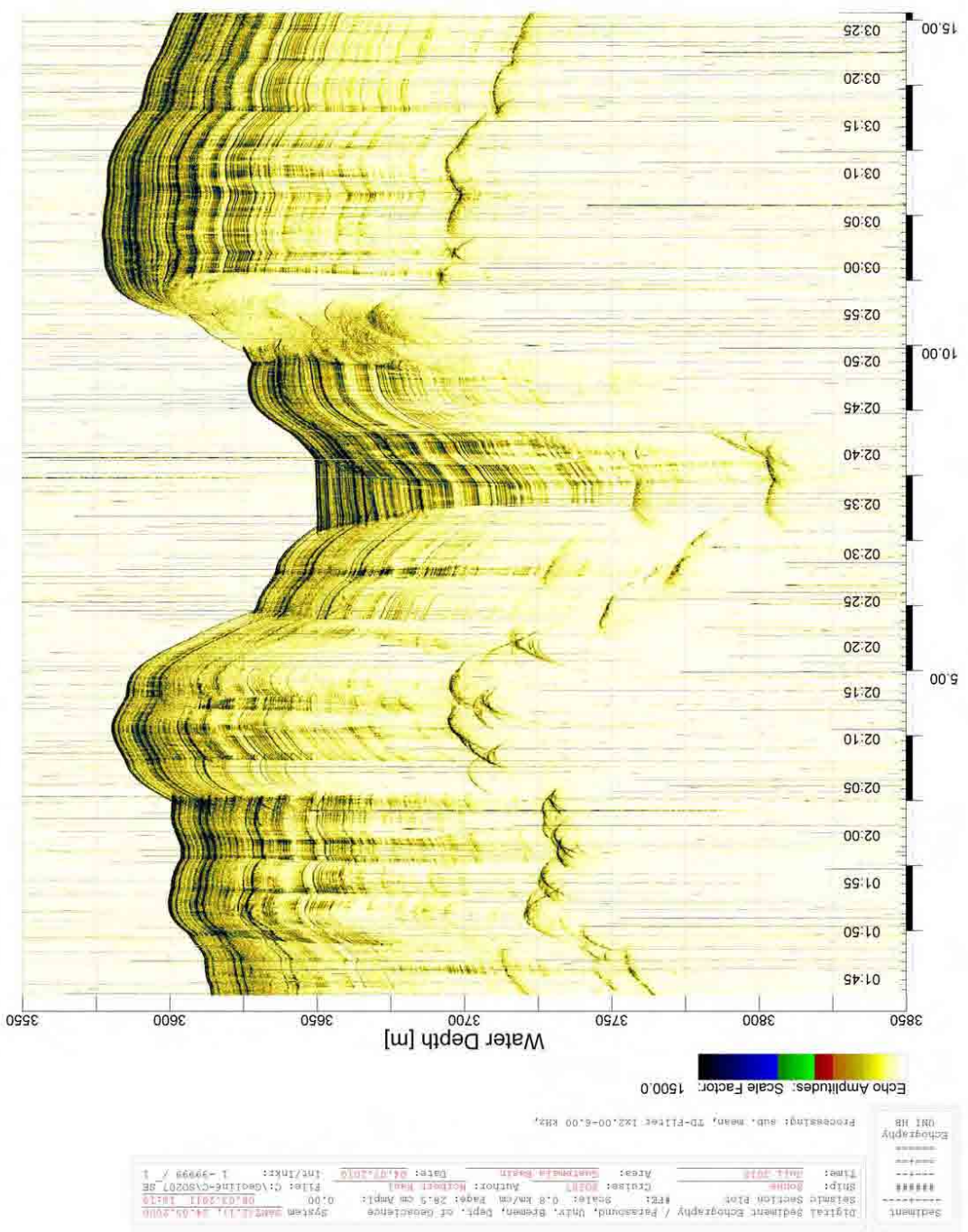

Figure 122: Parasound Profile GUATB28 in working area GUATB-03.

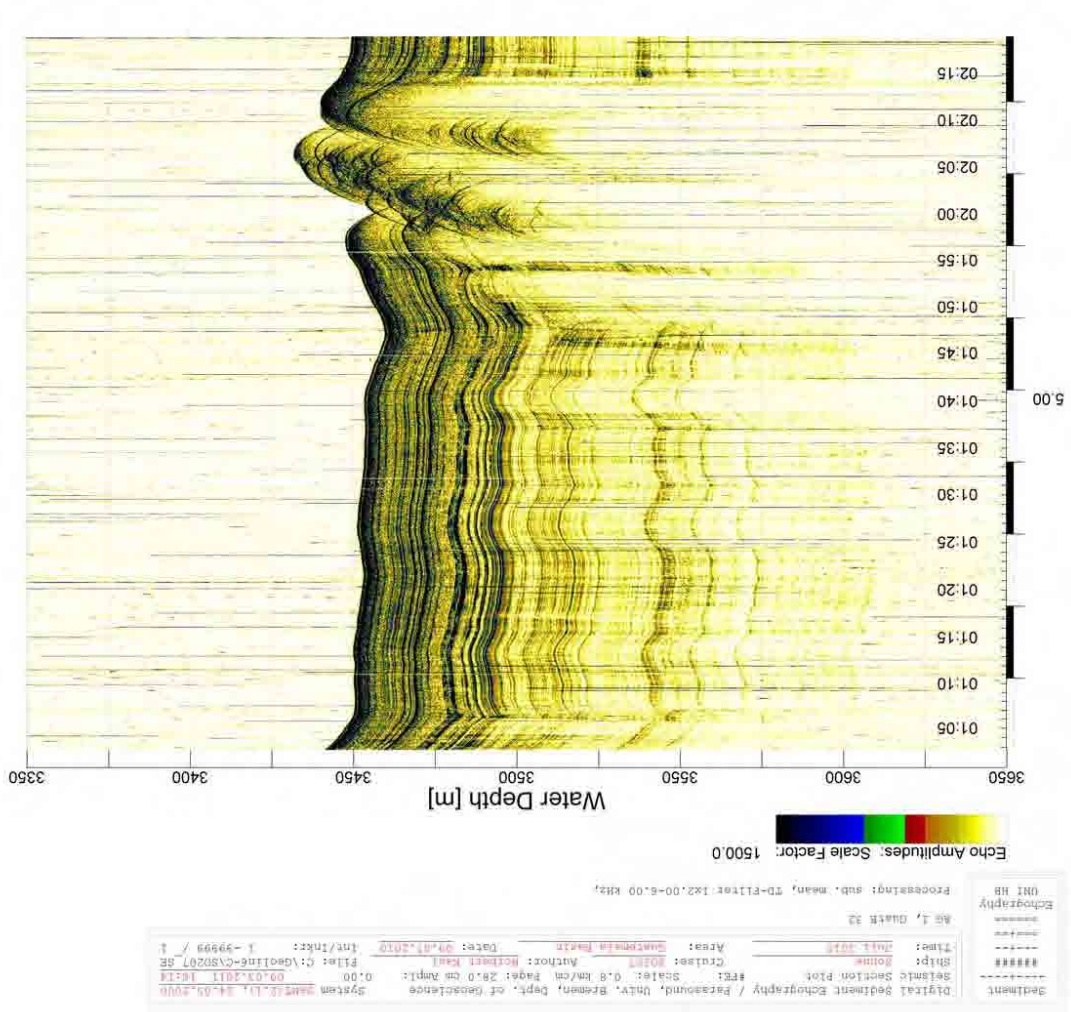

Figure 123: Parasound Profile GUATB32 in working area GUATB-01.

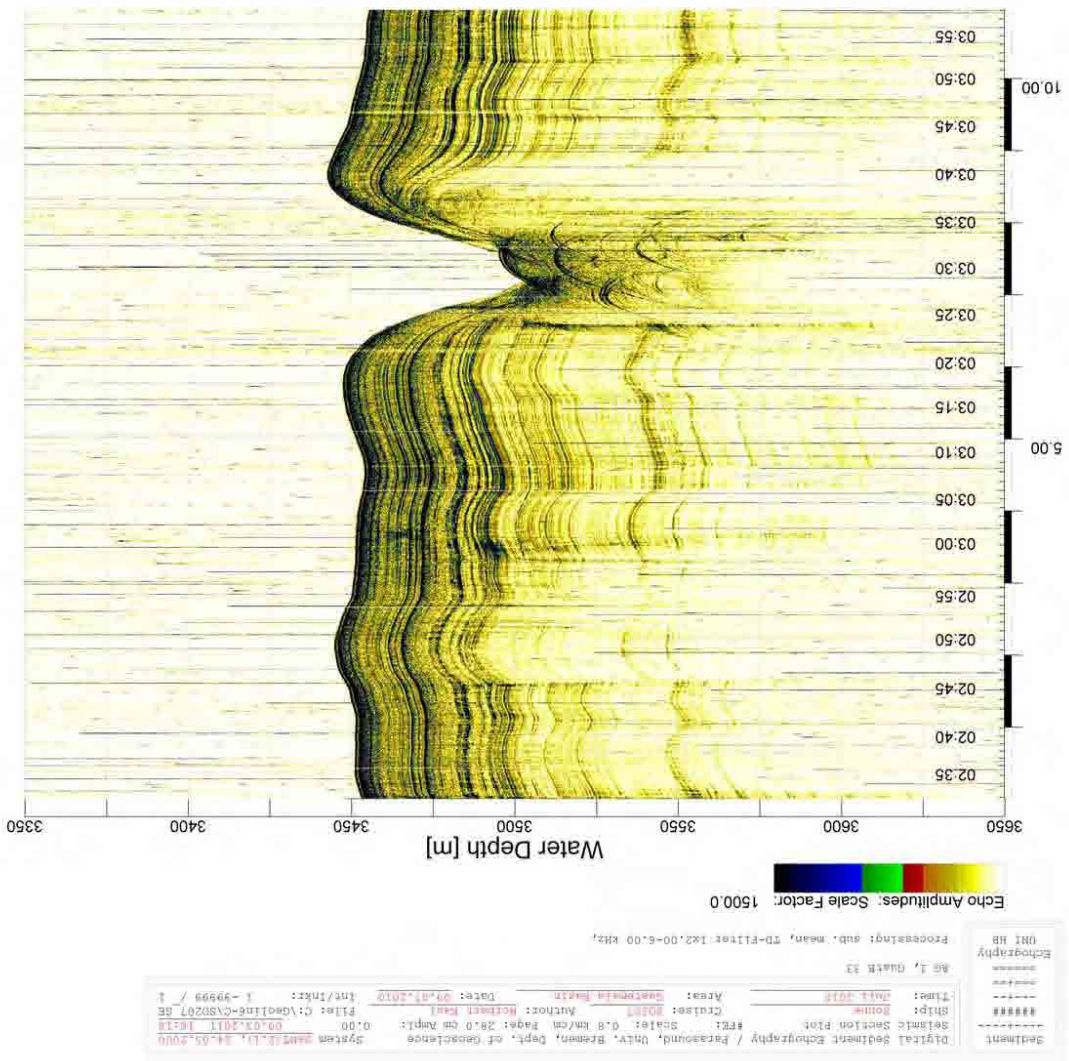

Figure 124: Parasound Profile GUATB33 in working area GUATB-01.

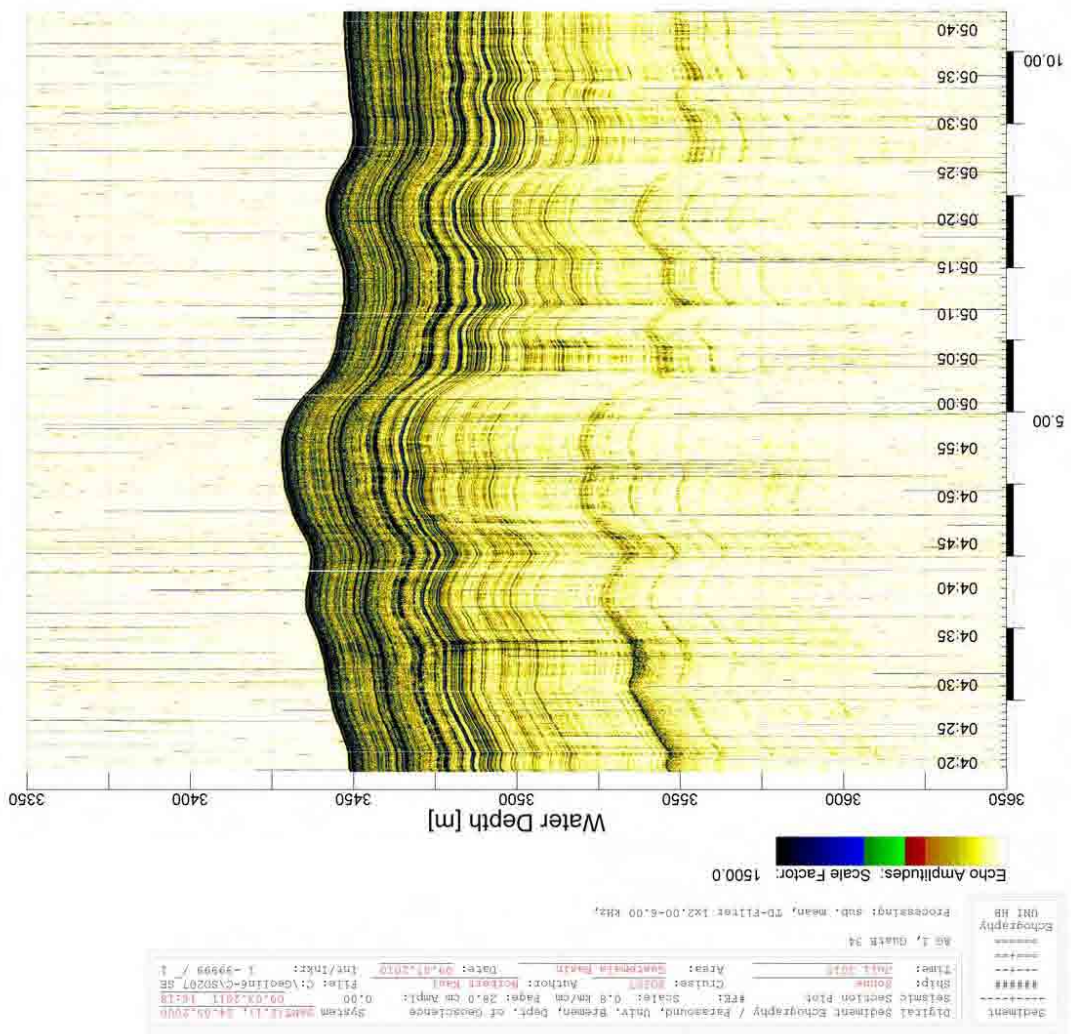

Figure 125: Parasound Profile GUATB34 in working area GUATB-01.

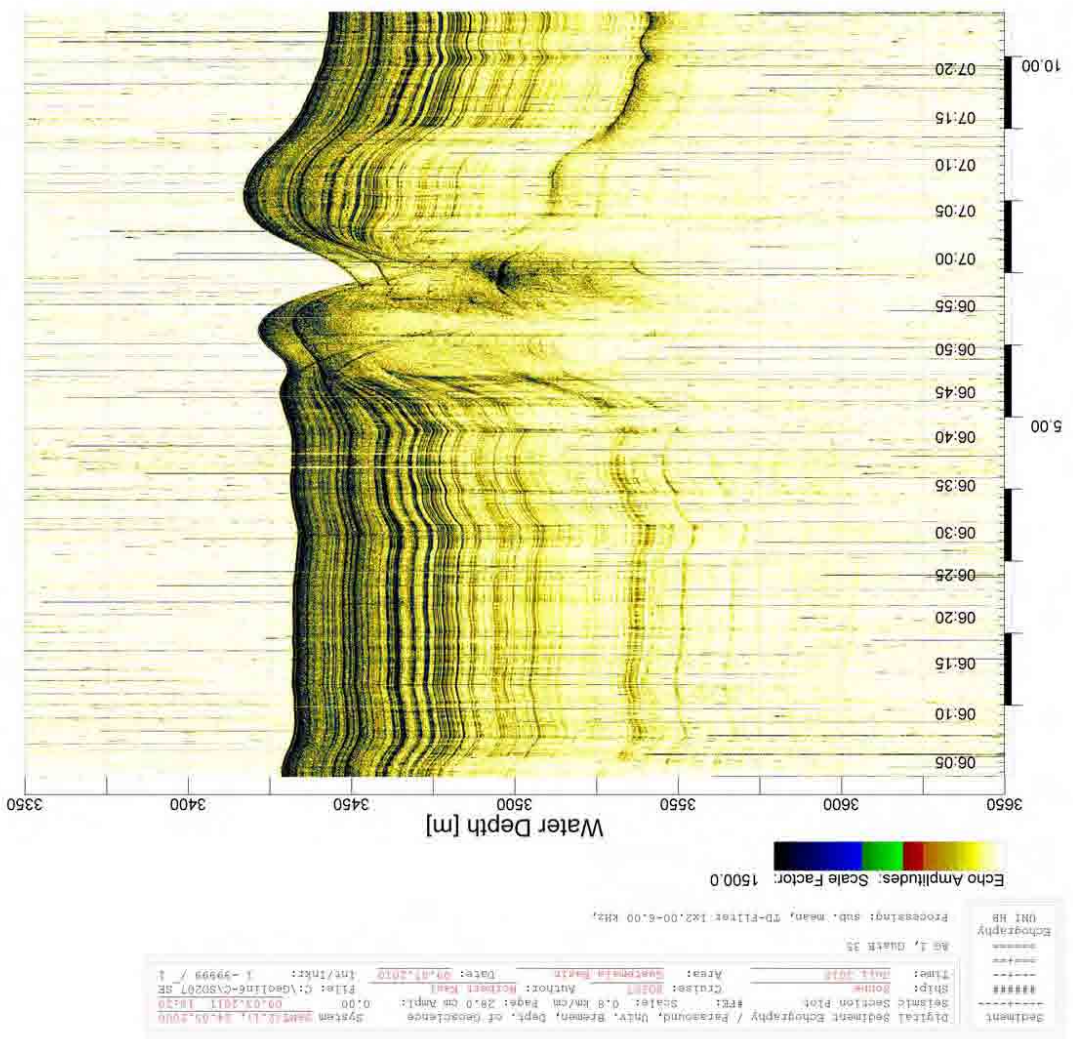

Figure 126: Parasound Profile GUATB35 in working area GUATB-01.

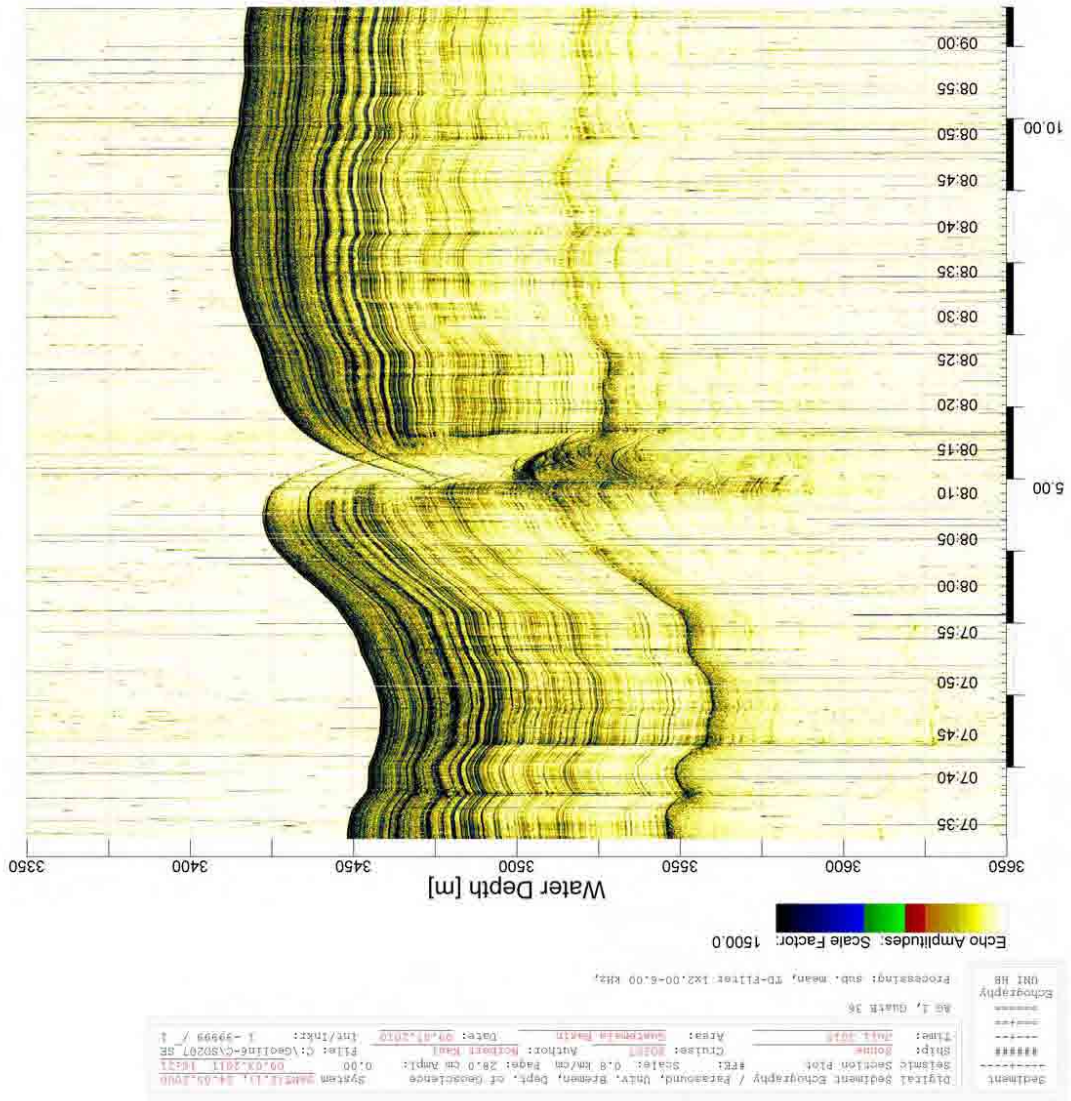

Figure 127: Parasound Profile GUATB36 in working area GUATB-01.

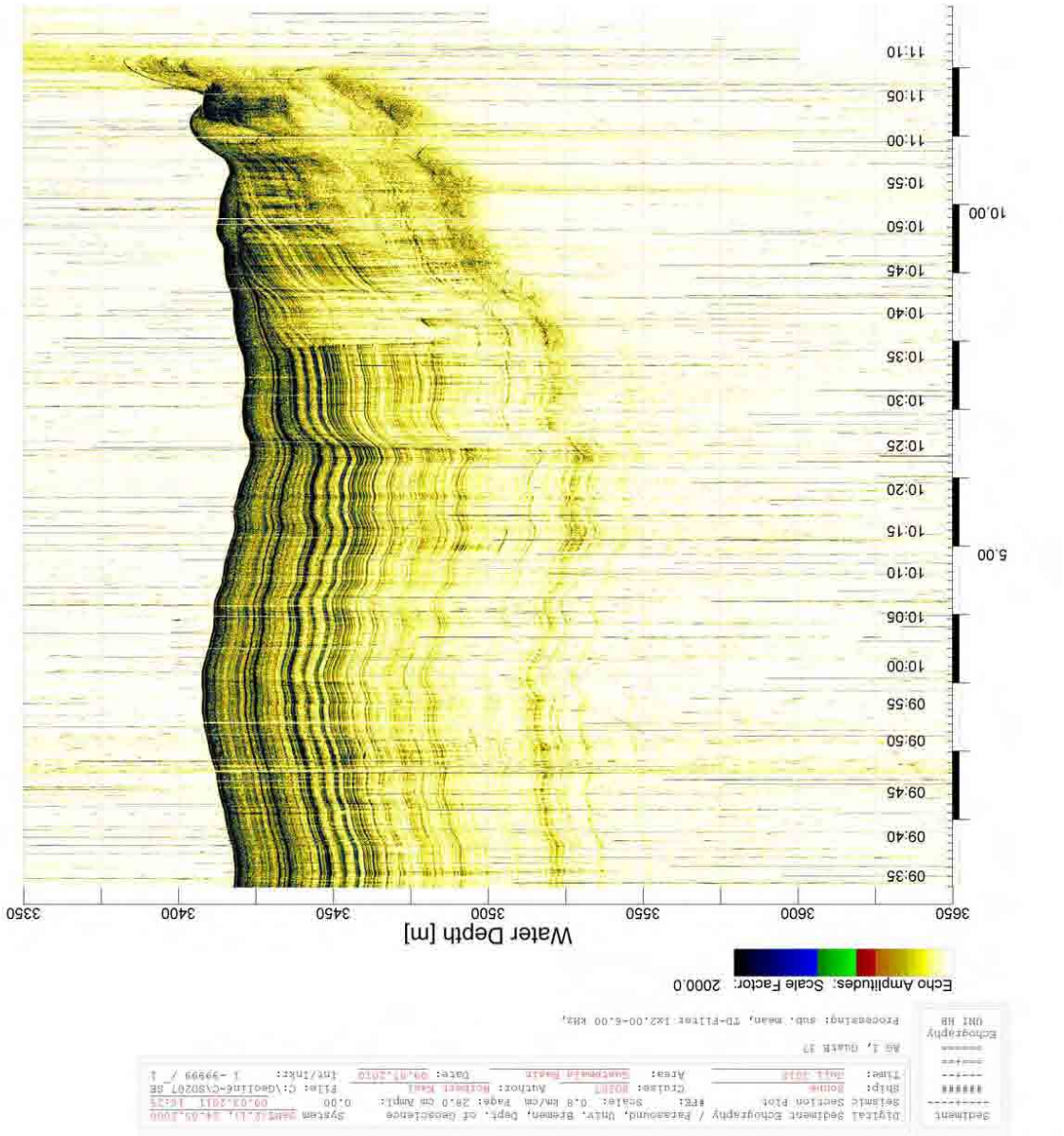

Figure 128: Parasound Profile GUATB37 in working area GUATB-01.

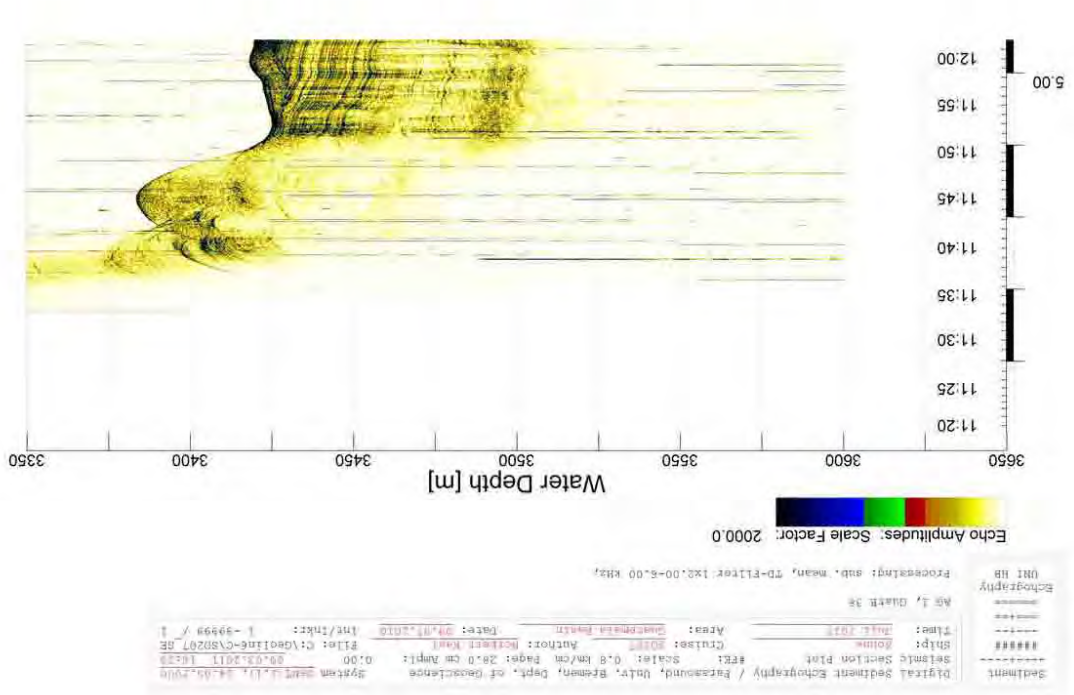

Figure 129: Parasound Profile GUATB38 in working area GUATB-01.

A.3 Heat Flow

Table 15: Overview of penetrations and their results for Heat Flow profile HF1030 in working area GUATB-01.

Number	Latitude	Longitude	Depth [m]	Date	Penetration Time	Heat Pulse Time	Used Sensors	TGrad [°C/km]	Mean TC [W/mK]	HF [mW/m²]
1	07 53.6037	-90 29.5214	3421	2010/06/24	23:05:30	NaN	21	21.13	NaN	16.5
2	07 53.9987	-90 29.8642	3428	2010/06/25	00:29:00	00:37:00	21	24.12	0.80	19.4
3	07 54.3136	-90 30.1847	3429	2010/06/25	01:51:25	NaN	21	28.46	NaN	22.2
4	07 54.5928	-90 30.5063	3466	2010/06/25	03:02:10	03:10:05	21	58.41	0.74	43.3
5	07 54.8615	-90 30.7679	3417	2010/06/25	04:23:00	NaN	21	39.12	NaN	30.5
6	07 55.1211	-90 31.0246	3502	2010/06/25	05:40:00	05:48:05	21	101.20	0.78	79.4
7	07 55.4144	-90 31.3111	3427	2010/06/25	07:10:50	NaN	21	43.09	NaN	33.6
8	07 55.6947	-90 31.5732	3426	2010/06/25	08:20:20	08:28:20	21	44.83	0.78	35.3
9	07 55.9132	-90 31.7382	3481	2010/06/25	09:40:25	NaN	21	166.87	NaN	130.2
10	07 56.1978	-90 32.0194	3428	2010/06/25	10:51:45	10:59:55	21	46.10	0.73	33.9
11	07 56.4383	-90 32.2718	3430	2010/06/25	12:04:35	NaN	21	47.39	NaN	37.0
12	07 56.6805	-90 32.5521	3432	2010/06/25	23:27:30	23:35:30	21	54.37	0.78	42.6
13	07 56.897	-90 32.7371	3431	2010/06/26	00:29:45	00:37:45	21	51.17	0.79	40.6
14	07 57.2452	-90 33.0862	3440	2010/06/26	01:51:40	NaN	21	63.02	NaN	49.2
15	07 57.5435	-90 33.3819	3466	2010/06/26	02:59:20	03:07:20	21	95.77	0.77	73.5
16	07 57.7191	-90 33.5789	3501	2010/06/26	21:12:45	NaN	21	171.38	NaN	133.7
17	07 57.7285	-90 33.5605	3501	2010/06/26	21:36:40	21:44:40	21	168.20	0.78	131.2
18	07 57.9723	-90 33.3745	3490	2010/06/26	22:44:25	NaN	21	137.02	NaN	106.9
19	07 57.9703	-90 33.7959	3500	2010/06/26	23:46:30	NaN	21	390.61	NaN	304.7
20	07 58.1421	-90 34.0574	3443	2010/06/27	00:48:30	NaN	21	93.47	NaN	72.9
21	07 58.3924	-90 34.2513	3448	2010/06/27	01:37:00	01:45:10	21	133.64	0.73	97.3
22	07 58.7007	-90 34.5472	3452	2010/06/27	02:51:30	NaN	21	154.02	NaN	120.1

Table 16: Overview of penetrations and their results for Heat Flow profile HF1038 in working area GUATB-01.

Number	Latitude	Longitude	Depth [m]	Date	Penetration Time	Heat Pulse Time	Used Sensors	TGrad [°C/km]	Mean TC [W/mK]	HF [mW/m²]
1	7 58.6484	-90 32.5608	3455	2010/07/09	23:54:23	NaN	21	57.24	NaN	44.7
2	7 58.5233	-90 32.7015	3455	2010/07/10	00:35:42	NaN	21	60.03	NaN	46.8
3	7 58.3874	-90 32.8647	3452	2010/07/10	01:20:36	01:27:42	21	66.28	0.79	53.0
4	7 58.263	-90 33.001	3456	2010/07/10	02:08:00	NaN	21	68.53	NaN	53.5
5	7 58.127	-90 33.1361	3457	2010/07/10	02:51:57	NaN	21	73.60	NaN	57.4
6	7 57.9023	-90 33.4322	3504	2010/07/10	03:46:00	03:53:05	21	237.02	0.81	193.9
7	7 58.014	-90 33.555	3508	2010/07/10	04:34:08	NaN	21	158.51	NaN	123.6
8	7 57.7612	-90 33.568	3495	2010/07/10	05:22:20	NaN	21	184.91	NaN	144.2
9	7 57.5476	-90 33.5784	3500	2010/07/10	06:06:50	NaN	21	145.79	NaN	113.7
10	7 57.6671	-90 33.6349	3502	2010/07/10	06:45:35	NaN	20	204.65	NaN	159.6
11	7 57.9172	-90 33.7474	3508	2010/07/10	07:48:10	07:55:15	21	262.71	0.78	204.9
12	7 57.8104	-90 33.7591	3496	2010/07/10	08:38:30	NaN	21	221.23	NaN	172.6
13	7 57.5672	-90 33.7361	3478	2010/07/10	09:35:23	NaN	21	162.82	NaN	127.0
14	7 57.2954	-90 34.0953	3448	2010/07/10	10:24:48	NaN	21	108.97	NaN	85.0
15	7 57.258	-90 34.1454	3447	2010/07/10	11:06:51	11:13:53	21	123.25	0.79	97.1
16	7 57.1076	-90 34.2982	3453	2010/07/10	11:53:34	NaN	21	140.54	NaN	109.6

Table 17: Overview of penetrations and their results for Heat Flow profile HF1039 in working area GUATB-01.

Number	Latitude	Longitude	Depth [m]	Date	Penetration Time	Heat Pulse Time	Used Sensors	TGrad [°C/km]	Mean TC [W/mK]	HF [mW/m²]
1	7 55.3093	-90 28.7832	3418	2010/07/10	21:37:06	NaN	17	15.76	NaN	12.3
2	7 55.3029	-90 28.7885	3418	2010/07/10	21:53:25	NaN	17	15.50	NaN	12.1
3	7 55.2973	-90 28.7756	3419	2010/07/10	22:09:00	NaN	19	14.70	NaN	11.5
4	7 54.9298	-90 28.7999	3421	2010/07/10	22:53:30	NaN	16	15.91	NaN	12.4
5	7 54.6097	-90 28.8002	3424	2010/07/10	23:50:06	NaN	17	13.68	NaN	10.7
6	7 54.2943	-90 28.7889	3428	2010/07/11	00:37:03	NaN	16	13.81	NaN	10.8
7	7 54.0442	-90 28.7941	3426	2010/07/11	01:16:57	NaN	17	11.79	NaN	9.2
8	7 53.6672	-90 28.8024	3419	2010/07/11	02:11:53	NaN	18	11.32	NaN	8.8
9	7 53.2936	-90 28.79	3415	2010/07/11	03:01:30	NaN	14	11.17	NaN	8.7
10	7 52.9595	-90 28.7906	3414	2010/07/11	03:54:03	NaN	13	8.40	NaN	6.6
11	7 52.6117	-90 28.7905	3412	2010/07/11	04:50:55	NaN	10	14.16	NaN	11.0
12	7 52.4173	-90 28.7889	3418	2010/07/11	05:33:00	05:40:03	10	13.61	0.82	11.2
14	7 52.2539	-90 28.7861	3421	2010/07/11	06:36:30	NaN	12	11.34	NaN	8.8
15	7 52.019	-90 28.7804	3419	2010/07/11	07:28:40	NaN	17	20.22	NaN	15.8
16	7 51.8136	-90 28.7723	3413	2010/07/11	08:20:43	08:27:57	20	16.84	0.79	13.3
17	7 51.6236	-90 28.8086	3412	2010/07/11	09:21:00	NaN	17	12.28	NaN	9.6

Table 18: Overview of penetrations and their results for Heat Flow profile HF1032 in working area GUATB-02.

Number	Latitude	Longitude	Depth [m]	Date	Penetration Time	Heat Pulse Time	Used Sensors	TGrad [°C/km]	Mean TC [W/mK]	HF [mW/m²]
1	07 16.0354	-91 15.5233	3690	2010/06/29	22:51:30	23:00:20	10	34.38	0.75	25.8
2	07 16.0433	-91 16.0469	3698	2010/06/30	00:10:30	NaN	10	33.16	NaN	25.9
3	07 16.0678	-91 16.5641	3674	2010/06/30	01:17:00	01:24:05	21	54.73	0.79	43.3
4	07 16.0602	-91 17.1342	3748	2010/06/30	02:32:20	02:39:25	21	197.38	0.78	154.3
5	07 16.0113	-91 17.4581	3717	2010/06/30	03:28:35	NaN	21	262.65	NaN	204.9
6	07 15.9985	-91 17.6758	3673	2010/06/30	04:14:40	NaN	21	80.46	NaN	62.8
7	07 16.1547	-91 18.1677	3654	2010/06/30	05:35:15	05:42:15	21	85.75	0.80	68.4
8	07 16.2489	-91 18.6706	3714	2010/06/30	07:06:30	07:13:35	21	78.50	0.79	62.5
9	07 16.0667	-91 18.6977	3771	2010/06/30	08:28:35	08:35:40	21	375.02	0.77	289.0
10	07 16.3216	-91 19.2613	3729	2010/06/30	10:13:00	10:20:05	21	187.09	0.77	144.9
11	07 16.6295	-91 19.6756	3680	2010/06/30	21:59:45	NaN	21	60.53	NaN	47.2
12	07 16.7933	-91 20.1964	3696	2010/06/30	23:18:50	23:25:55	21	56.32	0.79	44.4
13	07 17.1457	-91 20.8298	3724	2010/07/01	00:54:15	NaN	21	366.54	NaN	285.9
14	07 17.1133	-91 21.3642	3748	2010/07/01	01:56:40	NaN	21	228.69	NaN	178.4
15	07 17.2153	-91 21.8536	3693	2010/07/01	03:00:00	NaN	21	90.64	NaN	70.7
16	07 17.4615	-91 22.5828	3756	2010/07/01	04:20:25	04:27:35	21	184.24	0.78	143.8
17	07 17.6268	-91 22.5999	3733	2010/07/01	05:30:00	NaN	21	91.93	NaN	71.7
18	07 17.6602	-91 23.3012	3721	2010/07/01	07:06:15	NaN	21	155.38	NaN	121.2
19	07 17.6933	-91 23.8704	3657	2010/07/01	08:29:45	08:36:50	10	79.56	0.79	62.2
20	07 17.9081	-91 24.245	3711	2010/07/01	09:54:33	10:01:37	21	213.40	0.79	168.2
21	07 18.1275	-91 24.8348	3641	2010/07/01	11:31:11	NaN	20	67.39	NaN	52.6
22	07 18.2721	-91 25.4212	3624	2010/07/01	12:46:23	12:53:28	21	63.14	0.80	50.8

Table 19: Overview of penetrations and their results for Heat Flow profile HF1037 in working area GUATB-02.

Number	Latitude	Longitude	Depth [m]	Date	Penetration Time	Heat Pulse Time	Used Sensors	TGrad [°C/km]	Mean TC [W/mK]	HF [mW/m²]
1	7 23.2719	-91 25.6746	3652	2010/07/07	20:44:35	NaN	18	7.92	NaN	6.2
2	7 22.9436	-91 25.3115	3643	2010/07/07	21:40:32	NaN	9	10.91	NaN	8.5
3	7 22.5082	-91 24.9457	3657	2010/07/07	22:32:25	NaN	19	8.21	NaN	6.4
4	7 22.1172	-91 24.5955	3655	2010/07/07	23:28:30	NaN	6	4.05	NaN	3.2
5	7 21.7291	-91 24.2208	3670	2010/07/08	00:32:20	NaN	9	10.73	NaN	8.4
6	7 21.3339	-91 23.8939	3654	2010/07/08	01:34:41	01:41:46	21	10.48	0.79	8.3
7	7 20.9388	-91 23.5263	3653	2010/07/08	02:37:58	NaN	20	12.20	NaN	9.5
8	7 20.5533	-91 23.1947	3676	2010/07/08	03:44:55	NaN	20	33.21	NaN	25.9
9	7 20.1269	-91 22.8125	3688	2010/07/08	04:38:09	NaN	20	26.52	NaN	20.7
10	7 19.7425	-91 22.4532	3687	2010/07/08	05:36:40	NaN	20	22.81	NaN	17.8
11	7 19.3657	-91 22.0958	3685	2010/07/08	07:00:23	NaN	20	22.85	NaN	17.8

Table 20: Overview of penetrations and their results for Heat Flow profile HF1033 in working area GUATB-02.

Number	Latitude	Longitude	Depth [m]	Date	Penetration Time	Heat Pulse Time	Used Sensors	TGrad [°C/km]	Mean TC [W/mK]	HF [mW/m²]
1	7 15.1919	-91 26.16	3659	2010/07/02	07:56:22	NaN	21	81.97	NaN	63.9
2	7 15.1096	-91 26.206	3667	2010/07/02	08:30:25	08:37:34	21	78.03	0.79	62.1
3	7 15.0287	-91 26.2969	3720	2010/07/02	09:03:47	NaN	21	80.27	NaN	62.6
4	7 14.9348	-91 26.3415	3764	2010/07/02	09:30:05	NaN	21	138.15	NaN	107.8
5	7 14.8878	-91 26.3974	3762	2010/07/02	09:53:05	10:00:10	21	292.41	0.78	228.7
6	7 14.8304	-91 26.4546	3755	2010/07/02	10:25:25	NaN	21	445.12	NaN	347.2
7	7 14.7746	-91 26.5192	3747	2010/07/02	10:50:55	NaN	21	407.14	NaN	317.6
8	7 14.7164	-91 26.5525	3744	2010/07/02	11:11:05	11:18:15	21	400.14	0.78	312.8
9	7 14.645	-91 26.624	3714	2010/07/02	11:41:23	NaN	21	264.24	NaN	206.1
10	7 14.5935	-91 26.6646	3667	2010/07/02	12:00:40	NaN	21	217.32	NaN	169.5
11	7 14.5266	-91 26.7274	3633	2010/07/02	12:24:10	NaN	20	84.64	NaN	66.0
12	7 14.4614	-91 26.7574	3617	2010/07/02	12:56:05	NaN	20	115.02	NaN	89.7
13	7 14.4041	-91 26.8196	3608	2010/07/02	13:18:40	NaN	7	119.62	NaN	93.3

Table 21: Overview of penetrations and their results for Heat Flow profile HF1036 in working area GUATB-02.

Number	Latitude	Longitude	Depth [m]	Date	Penetration Time	Heat Pulse Time	Used Sensors	TGrad [°C/km]	Mean TC [W/mK]	HF [mW/m²]
1	7 13.8647	-91 19.0103	3720	2010/07/07	01:46:18	01:53:25	21	176.90	0.78	139.3
2	7 13.5445	-91 19.3615	3731	2010/07/07	02:54:03	NaN	21	180.56	NaN	140.8
3	7 13.2284	-91 19.7119	3727	2010/07/07	03:56:00	NaN	21	179.54	NaN	140.0
4	7 12.902	-91 20.0808	3720	2010/07/07	05:00:50	05:07:57	21	179.41	0.79	141.8
5	7 12.6638	-91 20.3562	3694	2010/07/07	06:09:15	NaN	21	174.66	NaN	136.2
6	7 12.3686	-91 20.6655	3692	2010/07/07	07:14:35	NaN	21	200.13	NaN	156.1
7	7 12.067	-91 21.0663	3660	2010/07/07	08:29:28	NaN	21	183.13	NaN	142.8
8	7 11.764	-91 21.3847	3696	2010/07/07	09:49:15	09:56:22	21	186.43	0.78	146.1
9	7 11.448	-91 21.7176	3718	2010/07/07	11:00:50	NaN	21	185.91	NaN	145.0

Table 22: Overview of penetrations and their results for Heat Flow profile HF1034 in working area GUATB-03.

Number	Latitude	Longitude	Depth [m]	Date	Penetration Time	Heat Pulse Time	Used Sensors	TGrad [°C/km]	Mean TC [W/mK]	HF [mW/m²]
1	6 39.466	-91 53.1856	3623	2010/07/04	06:18:20	NaN	21	169.87	NaN	132.5
2	6 39.1205	-91 53.4325	3618	2010/07/04	07:19:20	NaN	21	157.44	NaN	122.8
3	6 38.754	-91 53.832	3616	2010/07/04	08:22:45	08:29:48	21	114.97	0.79	91.2
4	6 38.6429	-91 54.0975	3624	2010/07/04	09:21:40	NaN	21	76.68	NaN	59.8
5	6 38.5564	-91 54.1364	3673	2010/07/04	09:45:33	NaN	20	72.48	NaN	56.5
6	6 38.4334	-91 54.2156	3215	2010/07/04	10:20:30	10:27:38	21	145.85	0.78	113.9
7	6 38.277	-91 54.3379	3709	2010/07/04	10:57:10	11:04:18	21	142.77	0.78	112.2
8	6 38.2503	-91 54.4367	3646	2010/07/04	11:41:42	NaN	21	140.06	NaN	109.3
10	6 37.8331	-91 54.8488	3538	2010/07/04	13:09:57	13:17:00	12	49.69	0.78	38.8
11	6 37.3954	-91 55.3142	3615	2010/07/05	01:20:48	NaN	20	12.74	NaN	9.9
12	6 37.0952	-91 55.7378	3611	2010/07/05	02:18:05	NaN	19	2.21	NaN	1.7
13	6 36.9485	-91 55.9154	3560	2010/07/05	02:59:25	NaN	21	40.05	NaN	31.2
14	6 36.842	-91 56.0333	3520	2010/07/05	03:46:17	NaN	21	19.54	NaN	15.2
16	6 36.5983	-91 56.3099	3586	2010/07/05	04:57:20	NaN	20	7.45	NaN	5.8
17	6 36.3022	-91 56.6544	3595	2010/07/05	05:55:38	06:02:40	21	20.45	0.79	16.2
18	6 35.9336	-91 57.0449	3603	2010/07/05	07:18:08	NaN	21	34.33	NaN	26.8
19	6 35.5346	-91 57.5511	3608	2010/07/05	08:27:25	NaN	13	36.07	NaN	28.1
20	6 35.1842	-91 57.8663	3605	2010/07/05	09:26:00	09:33:05	21	46.75	0.81	37.9
21	6 34.7916	-91 58.2619	3610	2010/07/05	10:47:50	NaN	21	56.03	NaN	43.7

Table 23: Overview of penetrations and their results for Heat Flow profile HF1035 in the transition from working area GUATB-03 to GUATB-02.

Number	Latitude	Longitude	Depth [m]	Date	Penetration Time	Heat Pulse Time	Used Sensors	TGrad [°C/km]	Mean TC [W/mK]	HF [mW/m²]
1	7 1.58882	-91 31.8202	3660	2010/07/06	01:48:15	01:55:19	21	39.82	0.79	31.7
2	7 1.40595	-91 32.0233	3662	2010/07/06	02:41:55	NaN	21	49.10	NaN	38.3
3	7 1.23192	-91 32.2046	3657	2010/07/06	03:33:28	NaN	21	62.23	NaN	48.5
4	7 1.08883	-91 32.3973	3654	2010/07/06	04:13:05	NaN	21	81.79	NaN	63.8
5	7 0.88316	-91 32.6281	3649	2010/07/06	05:20:55	NaN	21	113.74	NaN	88.7
6	7 0.72483	-91 32.7915	3661	2010/07/06	06:18:52	NaN	21	123.94	NaN	96.7
7	7 0.510402	-91 33.0121	3652	2010/07/06	07:21:05	NaN	21	57.09	NaN	44.5
8	7 0.322195	-91 33.2258	3637	2010/07/06	08:16:27	08:23:34	21	26.50	0.79	21.1
9	7 0.236434	-91 33.3603	3644	2010/07/06	09:02:17	NaN	9	37.72	NaN	29.4
10	7 0.130105	-91 33.494	3590	2010/07/06	09:36:55	NaN	21	46.79	NaN	36.5
11	6 59.4049	-91 34.2412	3420	2010/07/06	11:16:38	11:23:47	18	15.56	0.86	13.4
12	6 59.4151	-91 34.236	3424	2010/07/06	11:38:20	NaN	19	16.70	NaN	13.0

A.4 Thermal Conductivity

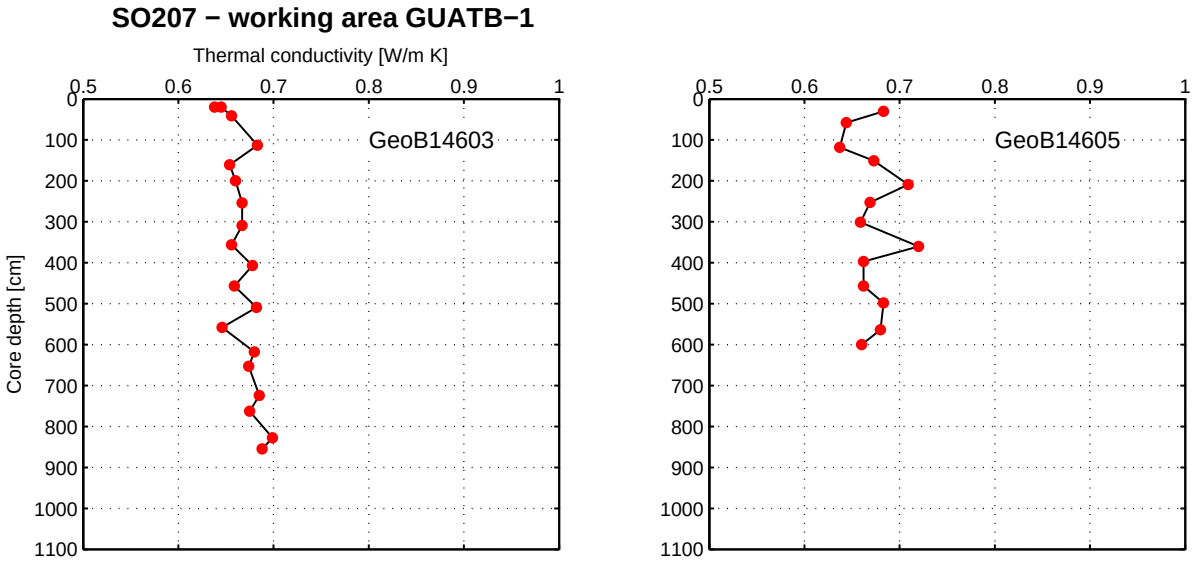

Figure 130: Results of thermal conductivity measurements in working area GUATB-01 on cores GeoB14603 and GeoB14605.

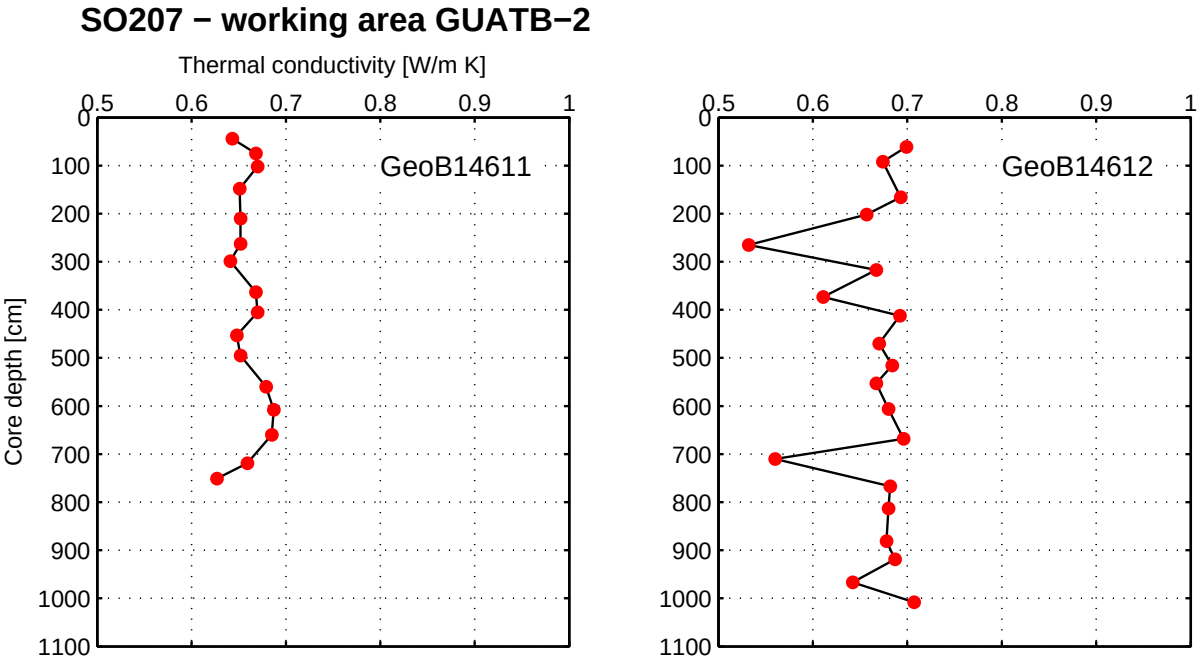

Figure 131: Results of thermal conductivity measurements in working area GUATB-02 on cores GeoB14611 and GeoB14612.

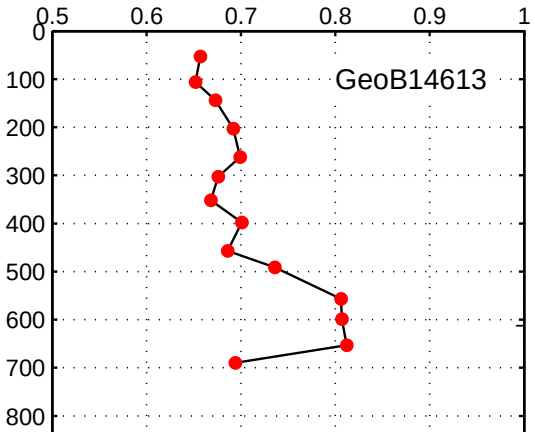

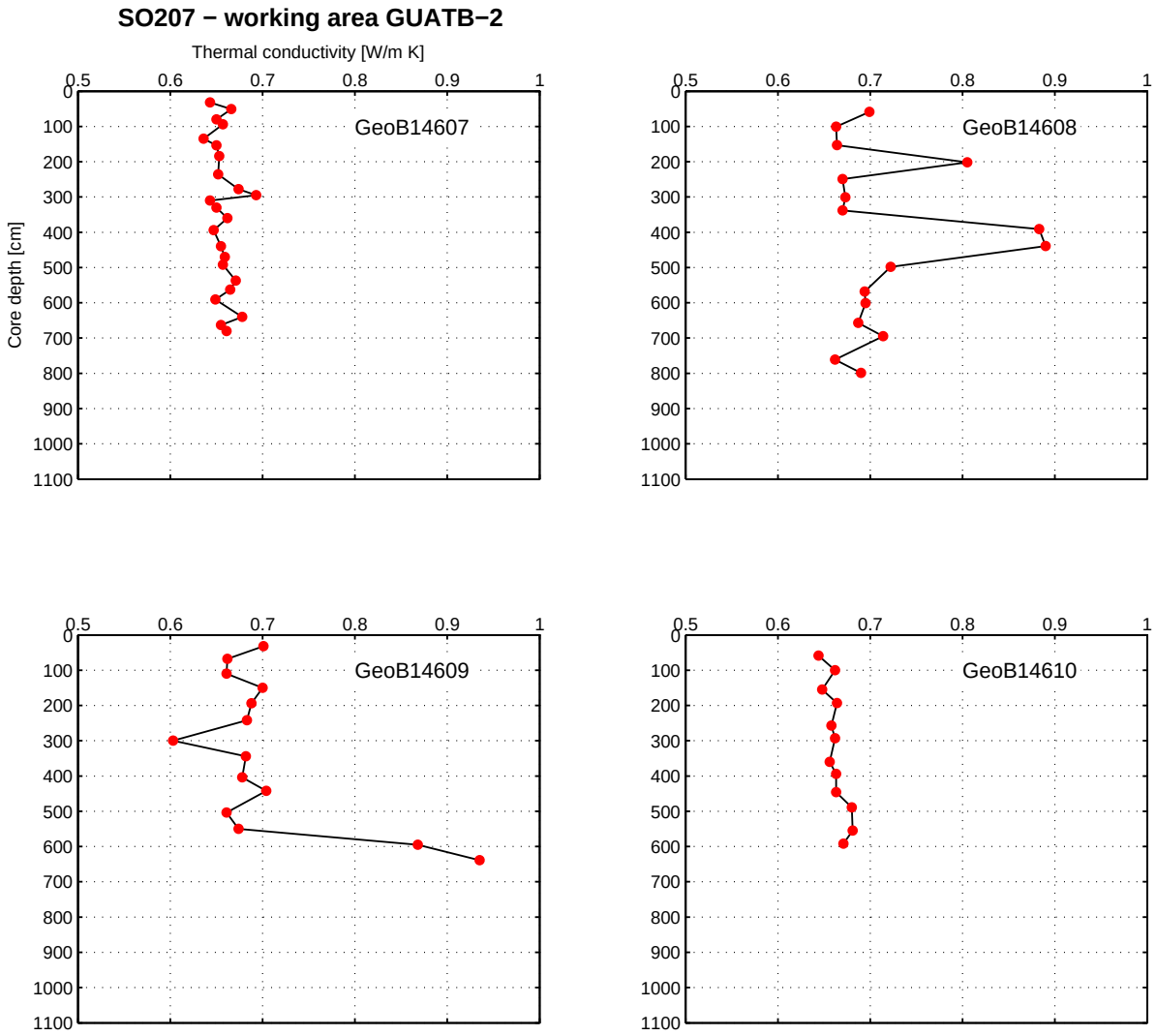

Figure 132: Results of thermal conductivity measurements in working area GUATB-02 on cores GeoB14607, GeoB14608, GeoB14609 and GeoB14610.

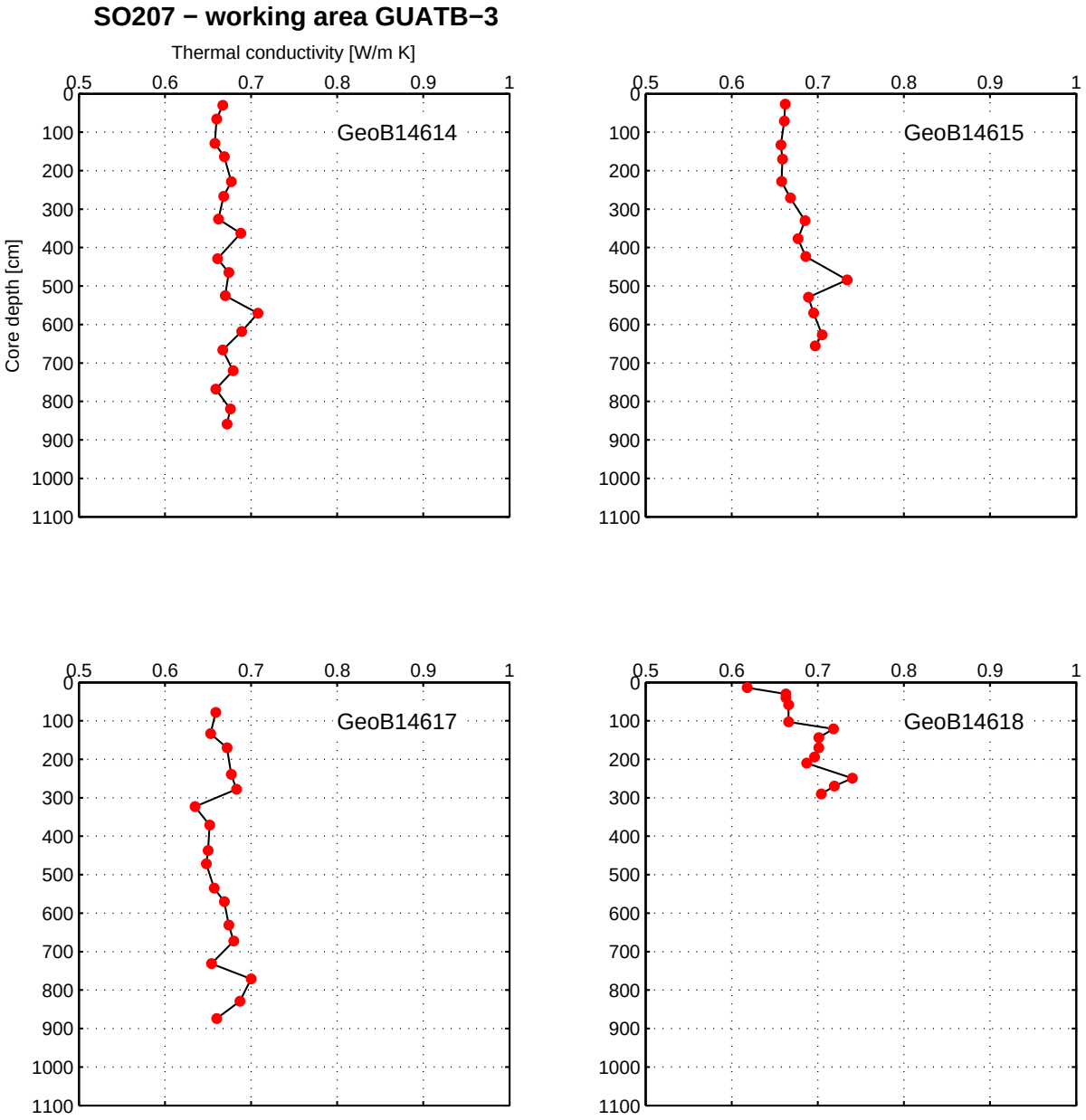

Figure 133: Results of thermal conductivity measurements in working area GUATB-03 on cores GeoB14614, GeoB14615, GeoB14617 and GeoB14618.

B Appendix Geochemistry

B.1 Core Logs

Complete listing of all gravity cores, which were taken onboard the RV Sonne during the Seamountflux Cruise (SO 207). The core descriptions were done on the archive half directly after finishing the pore water and sediment sampling on the working half. For details see legend below.

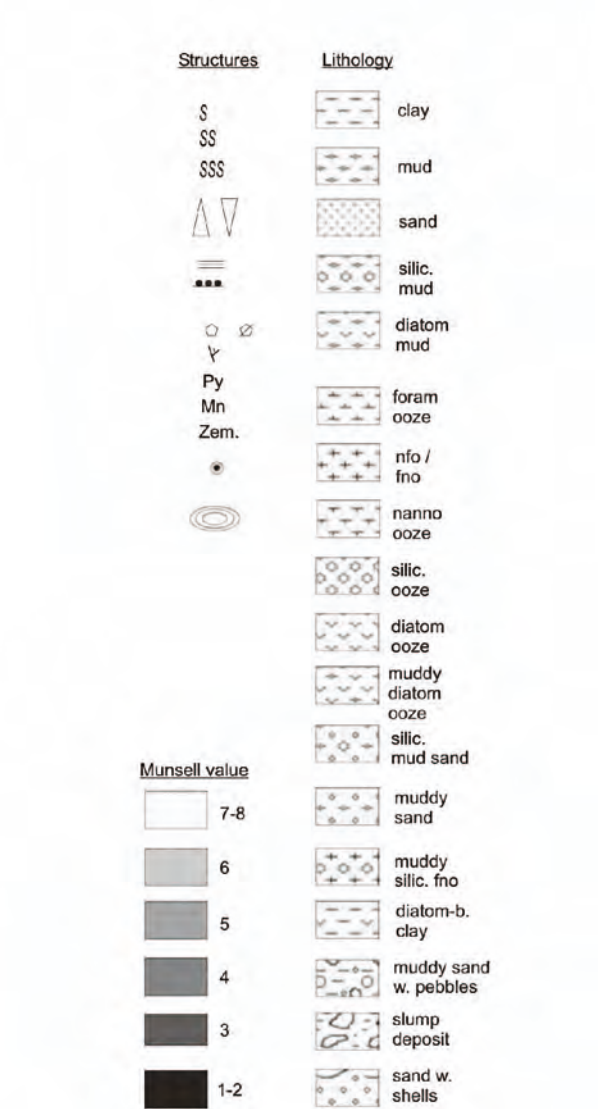

Figure 134: Legend for core logs

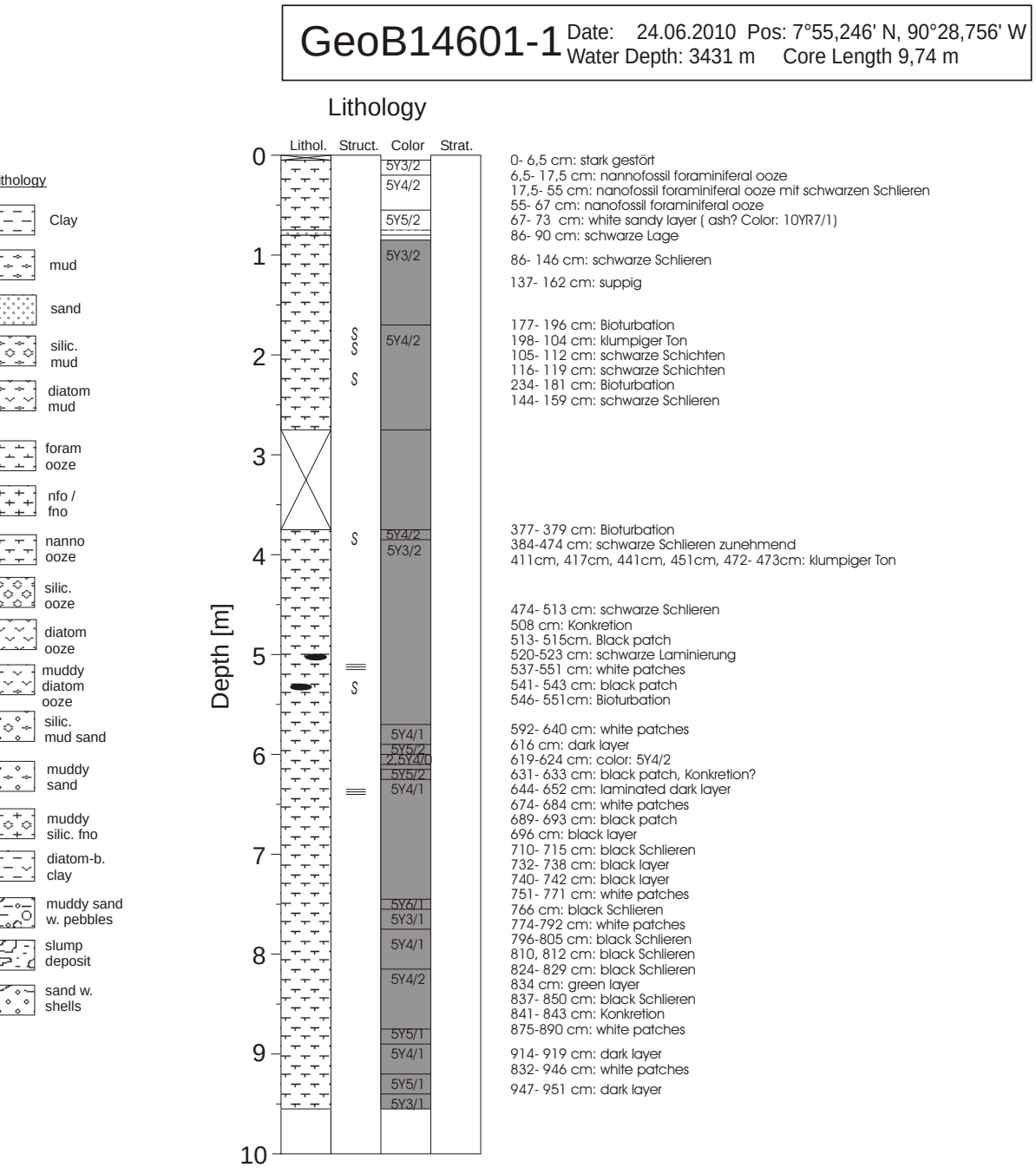

Figure 135: Core log of GeoB14601

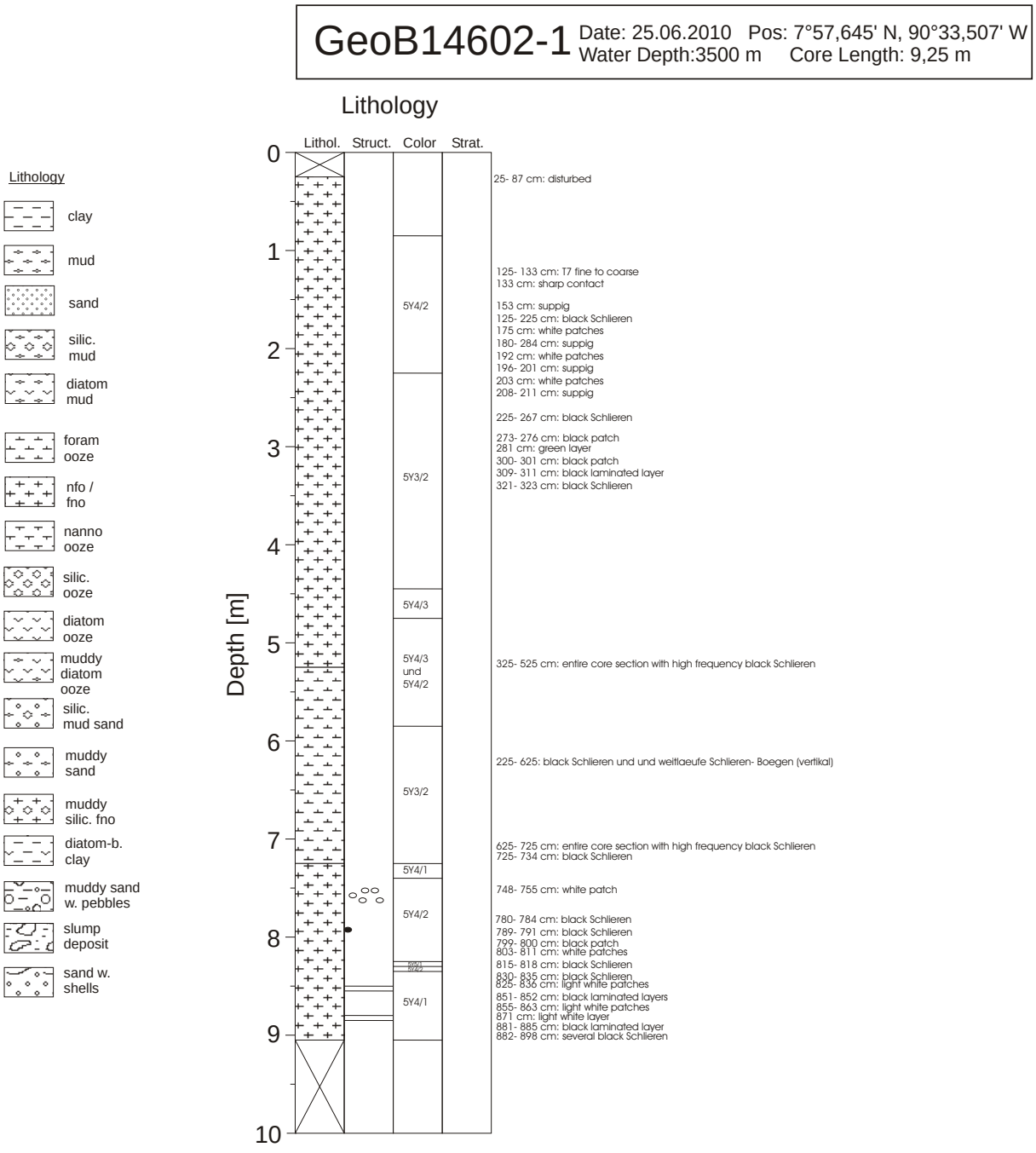

Figure 136: Core log of GeoB14602

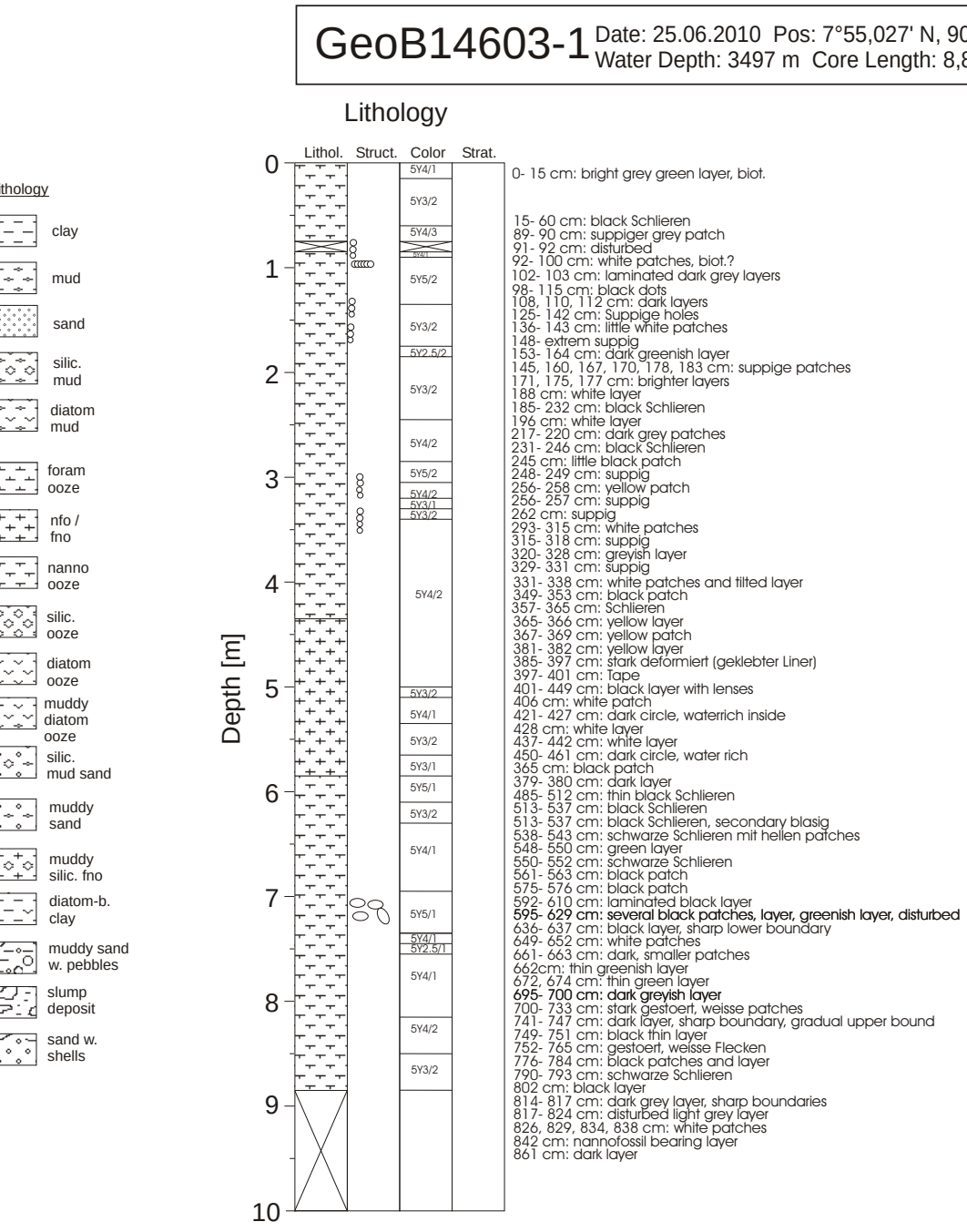

Figure 137: Core log of GeoB14603

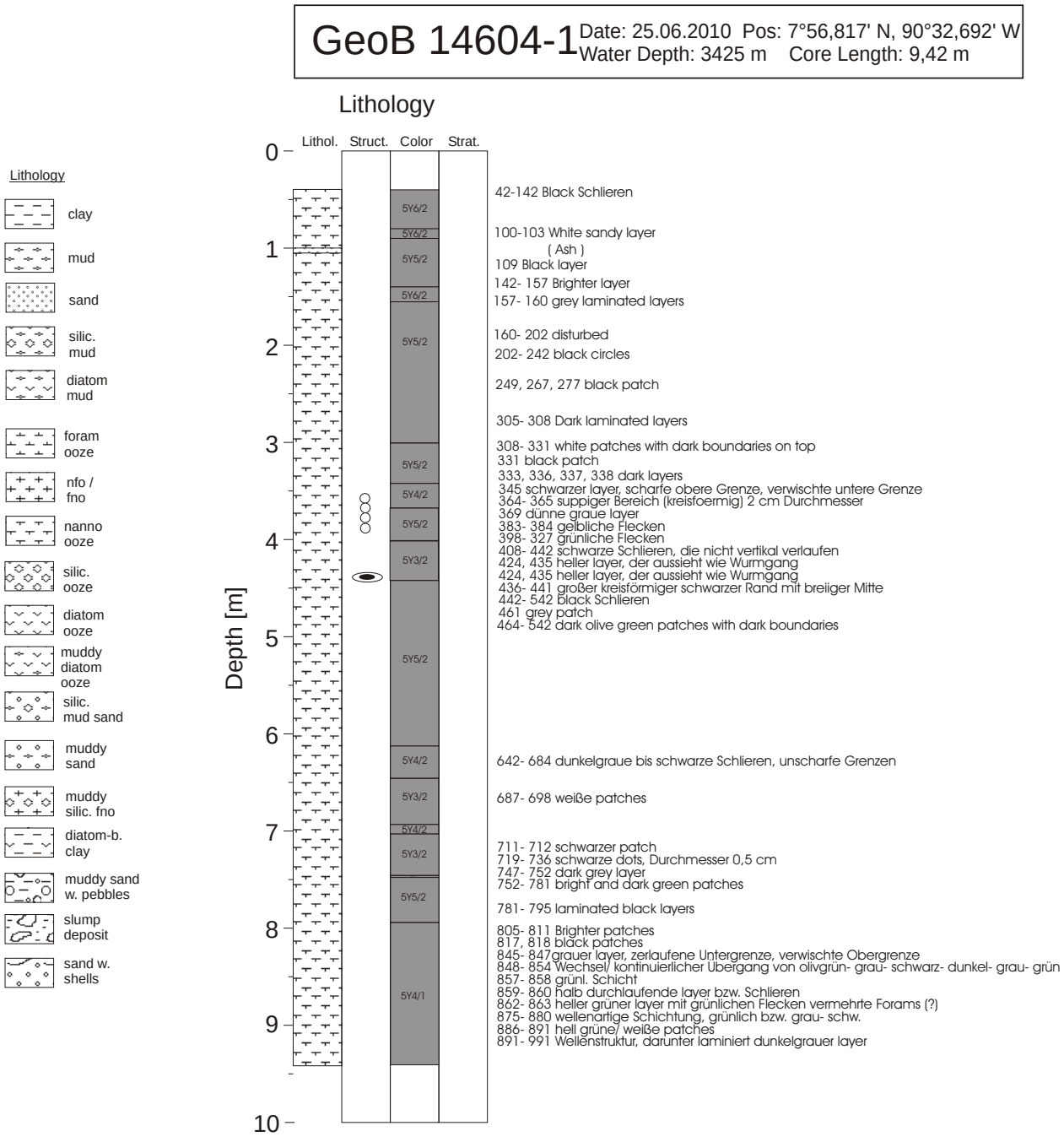

Figure 138: Core log of GeoB14604

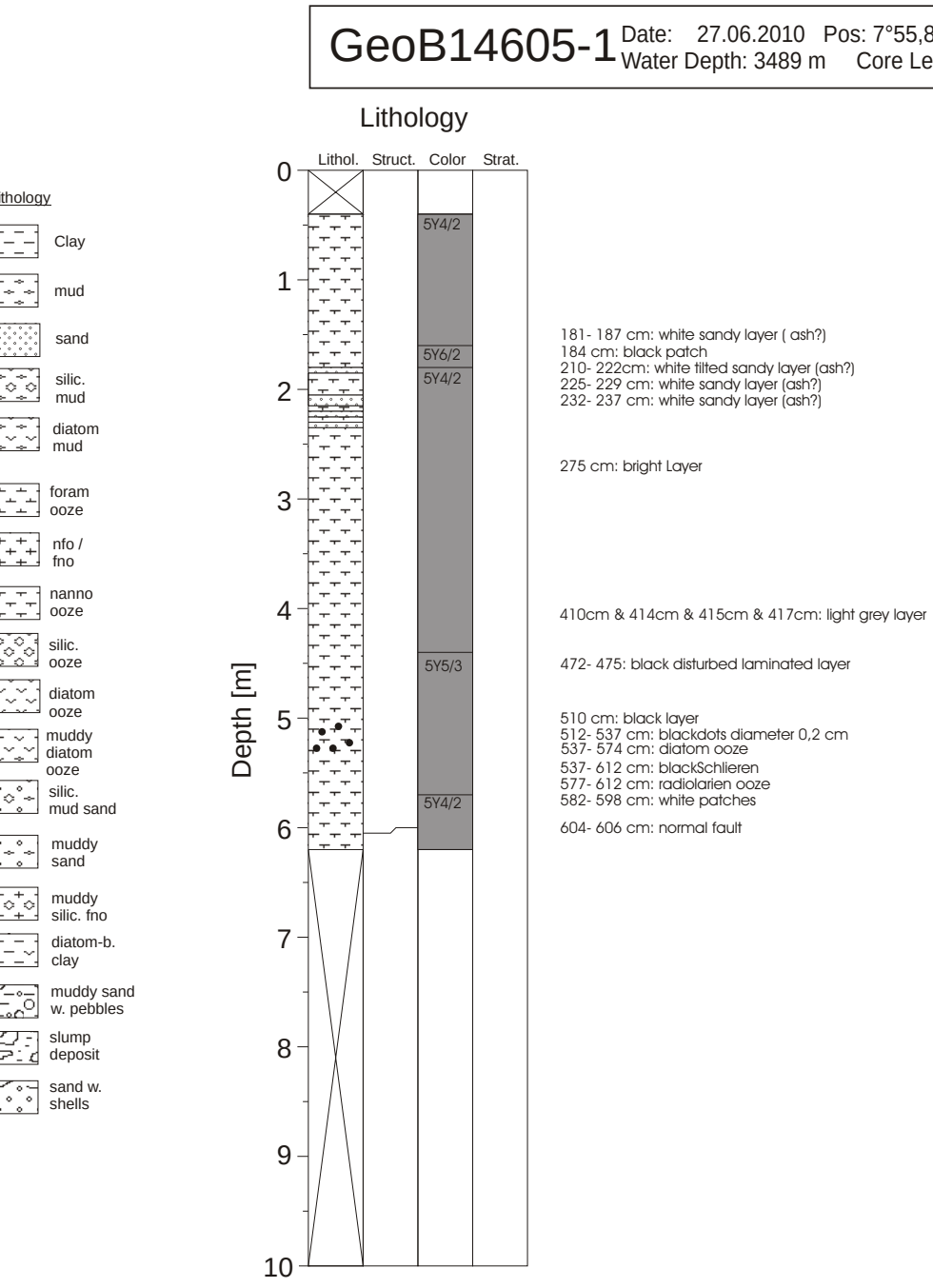

Figure 139: Core log of GeoB14605

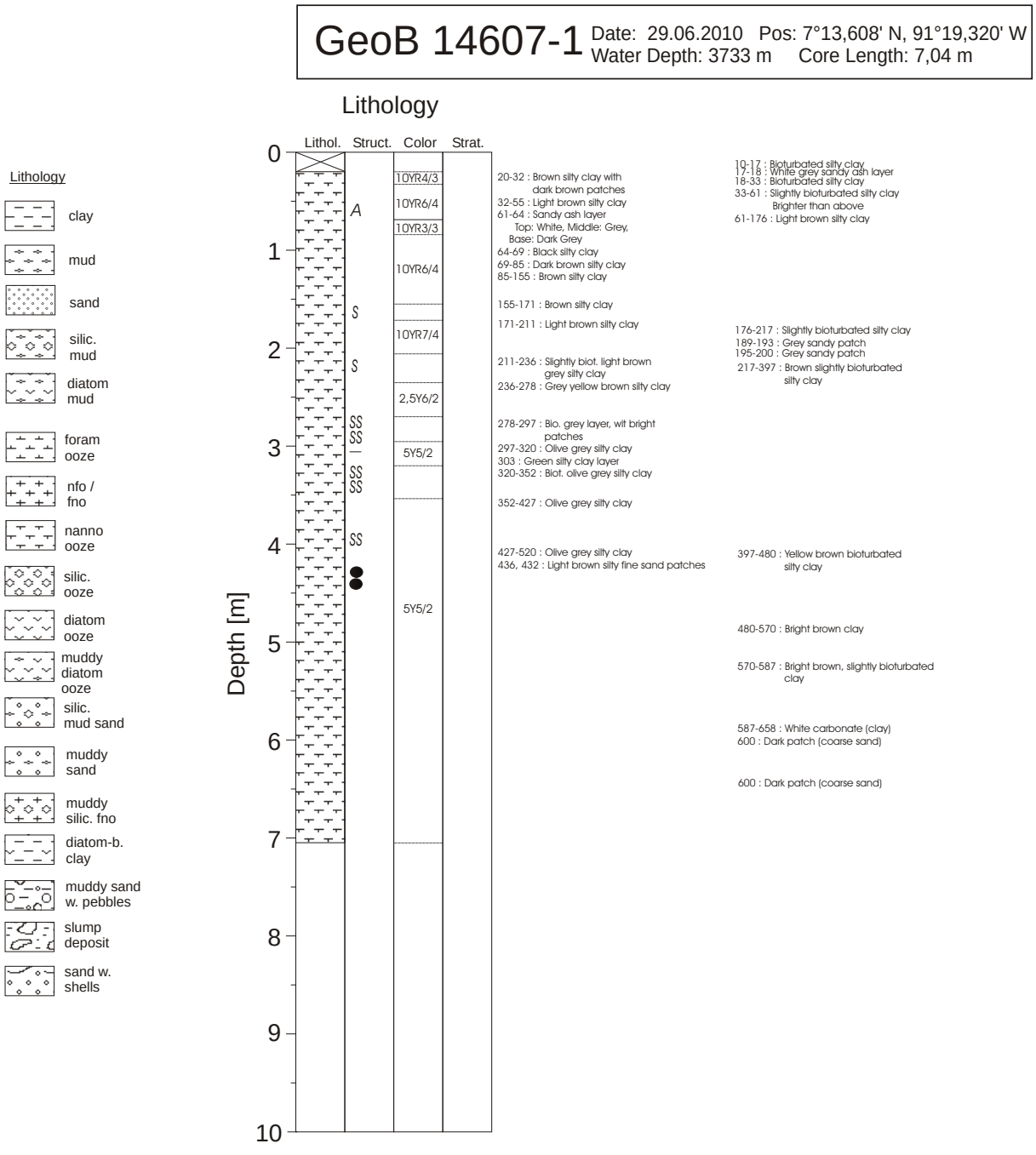

Figure 140: Core log of GeoB14607

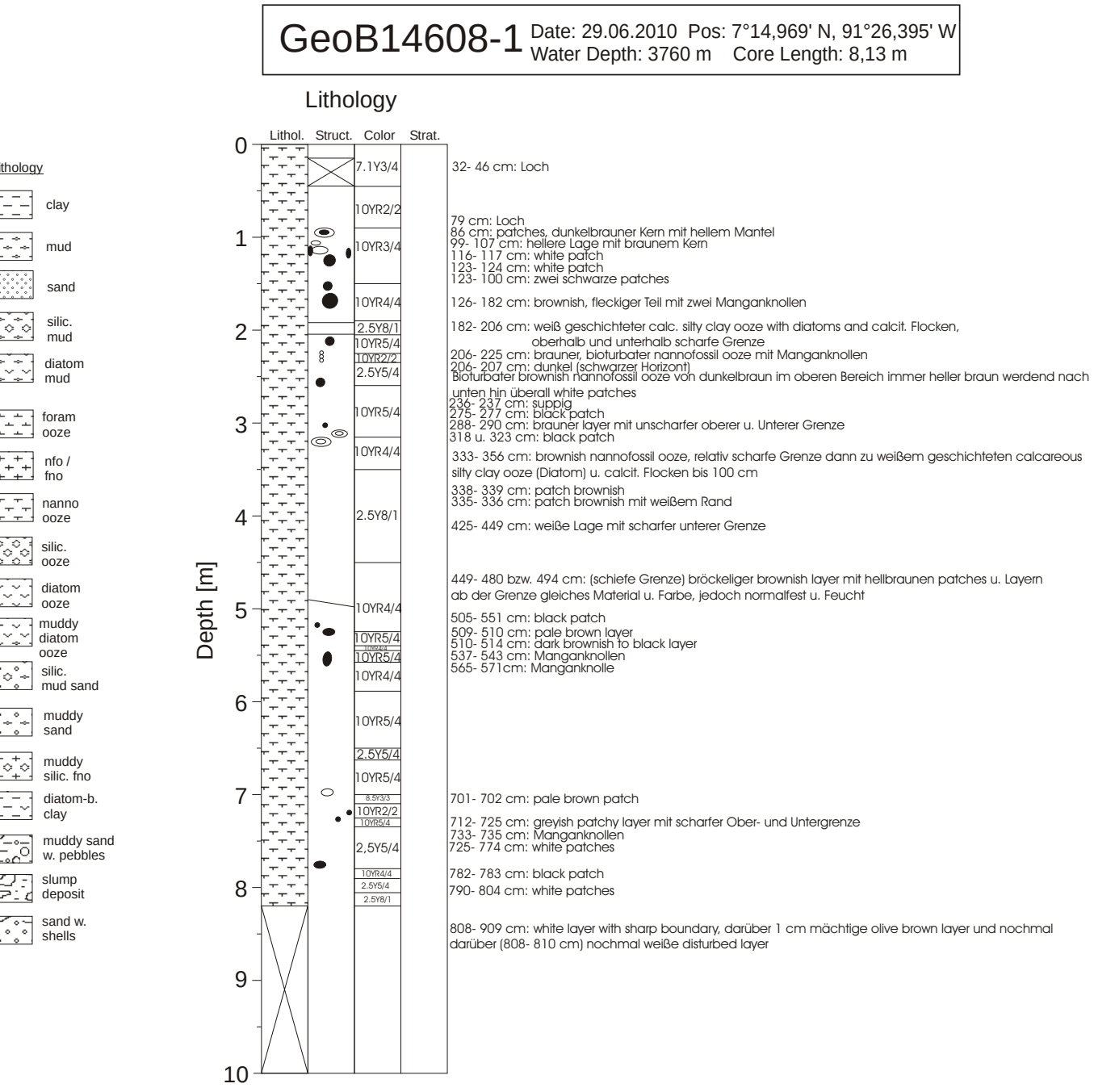

Figure 141: Core log of GeoB14608

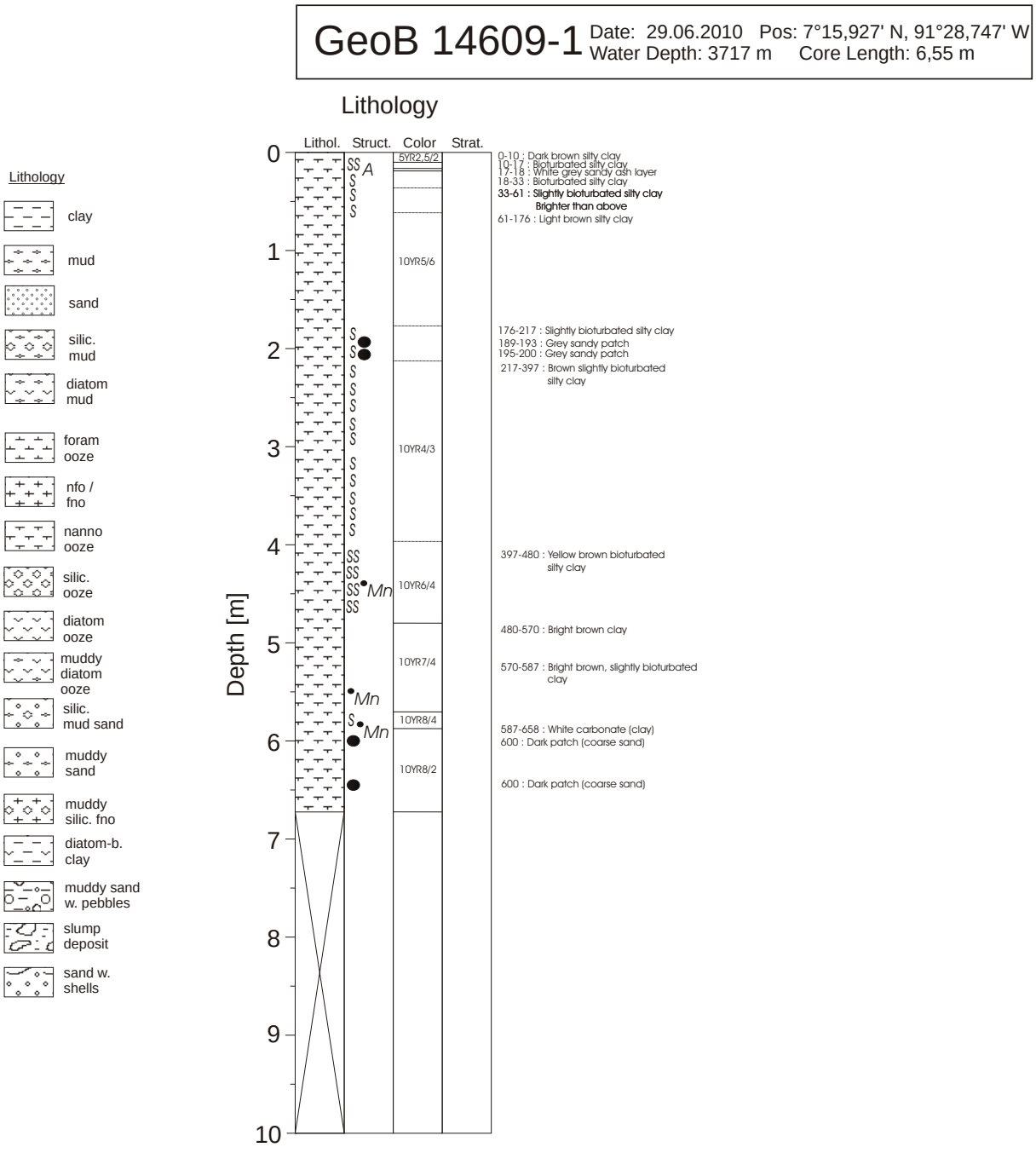

Figure 142: Core log of GeoB14609

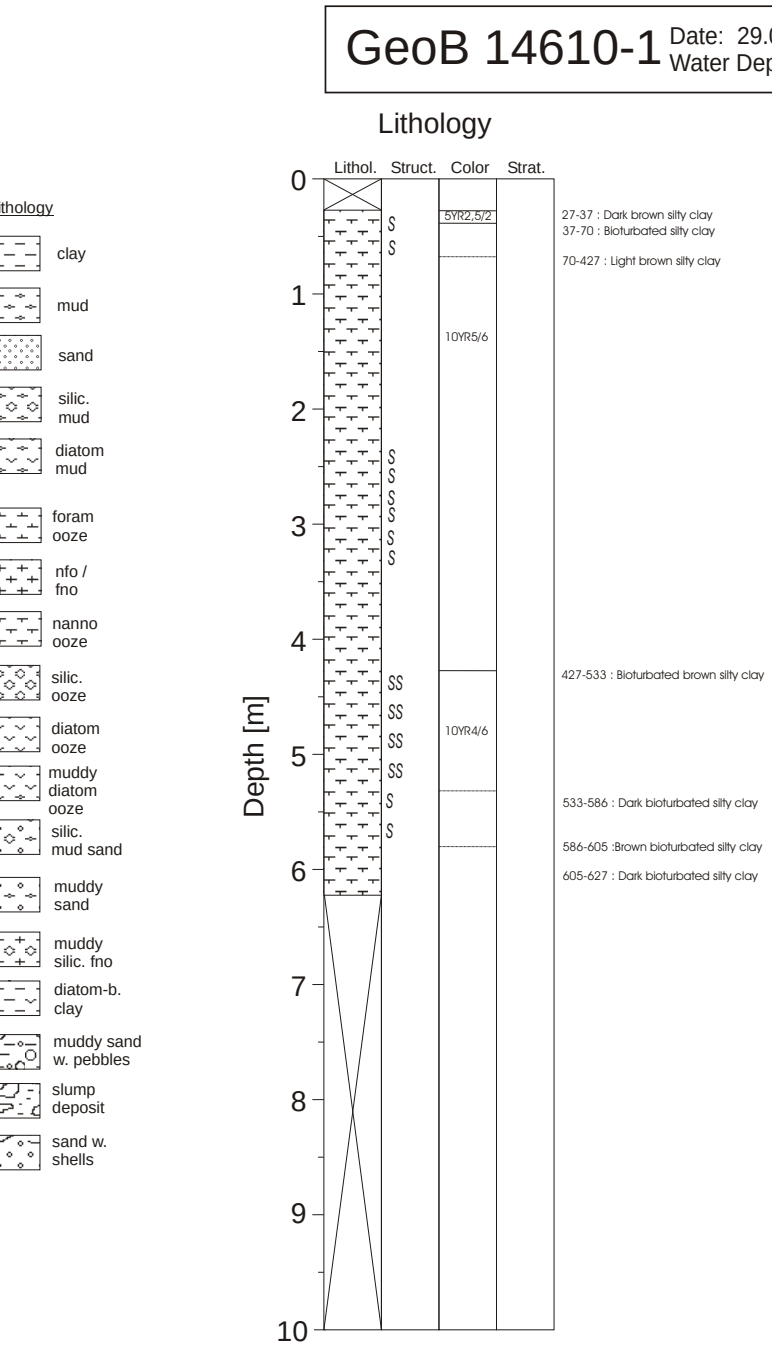

Figure 143: Core log of GeoB14610

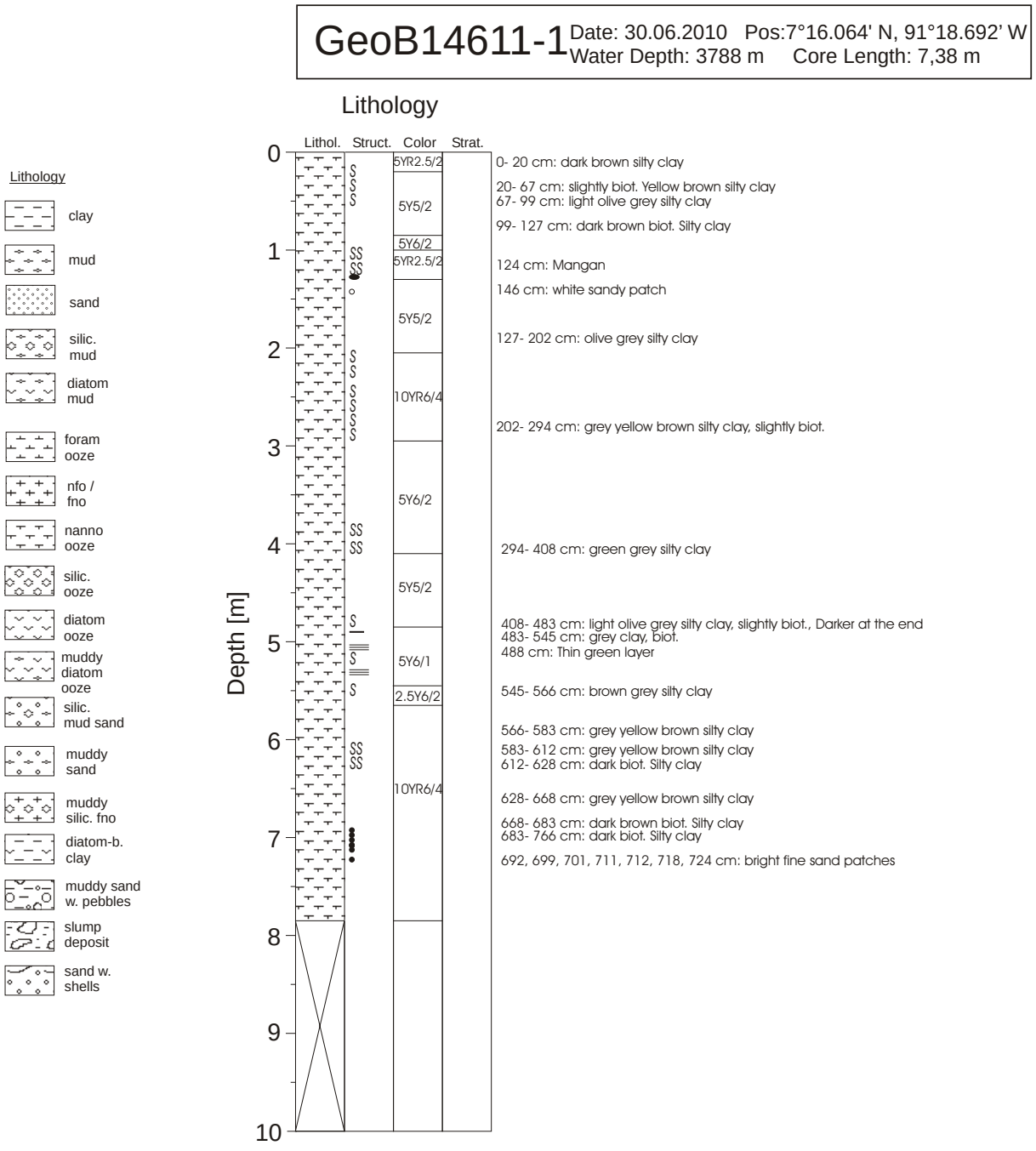

Figure 144: Core log of GeoB14611

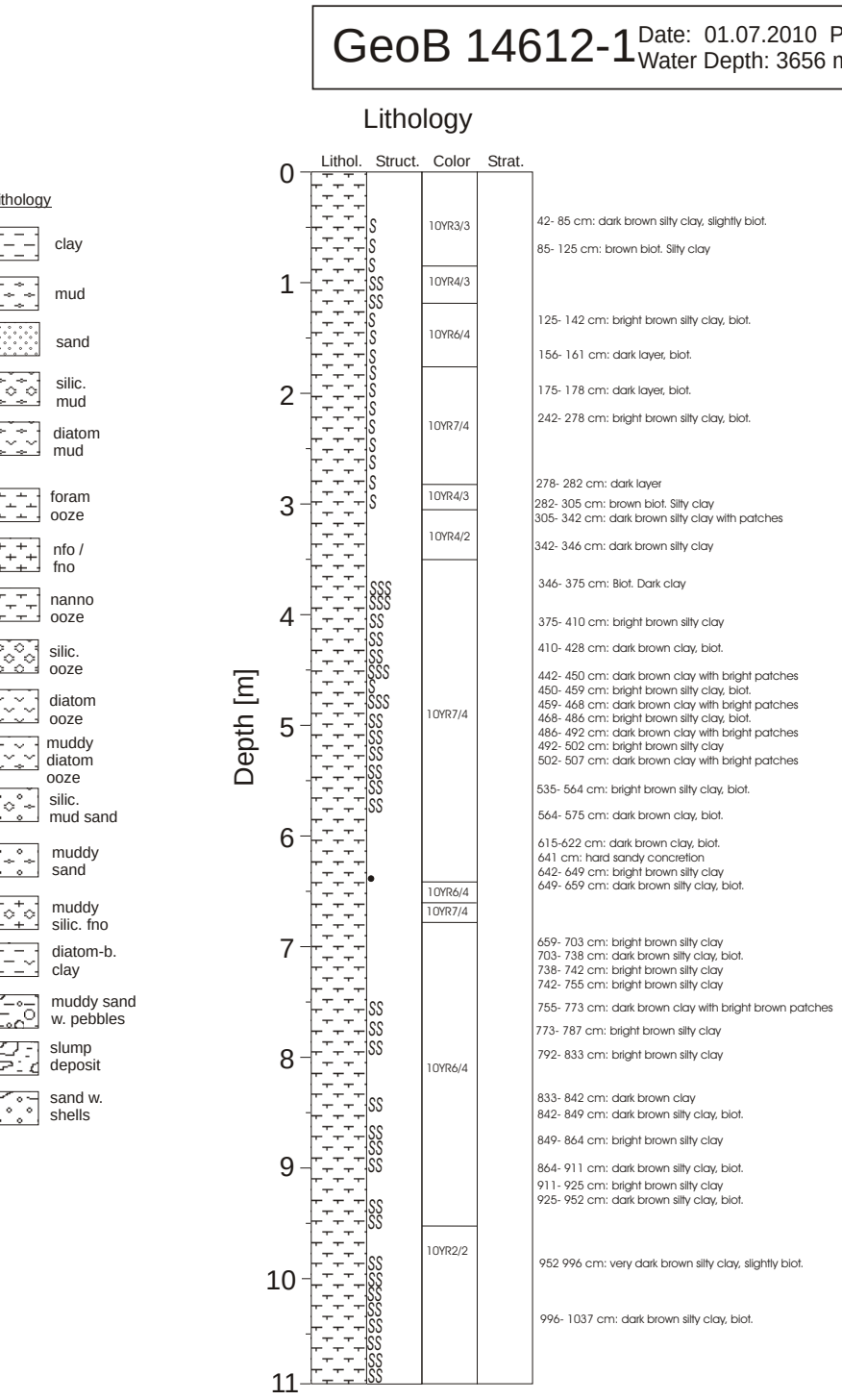

Figure 145: Core log of GeoB14612

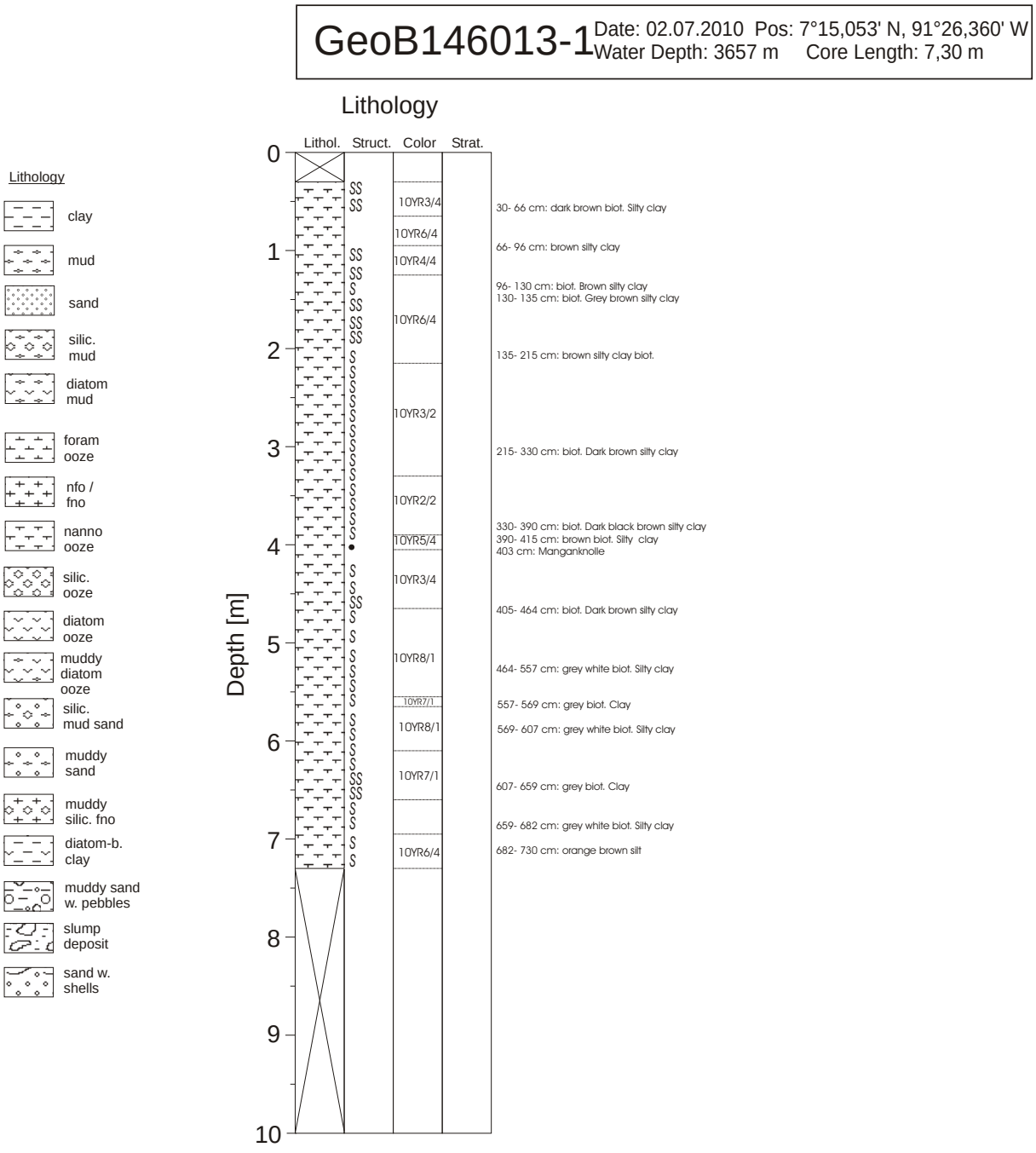

Figure 146: Core log of GeoB14613

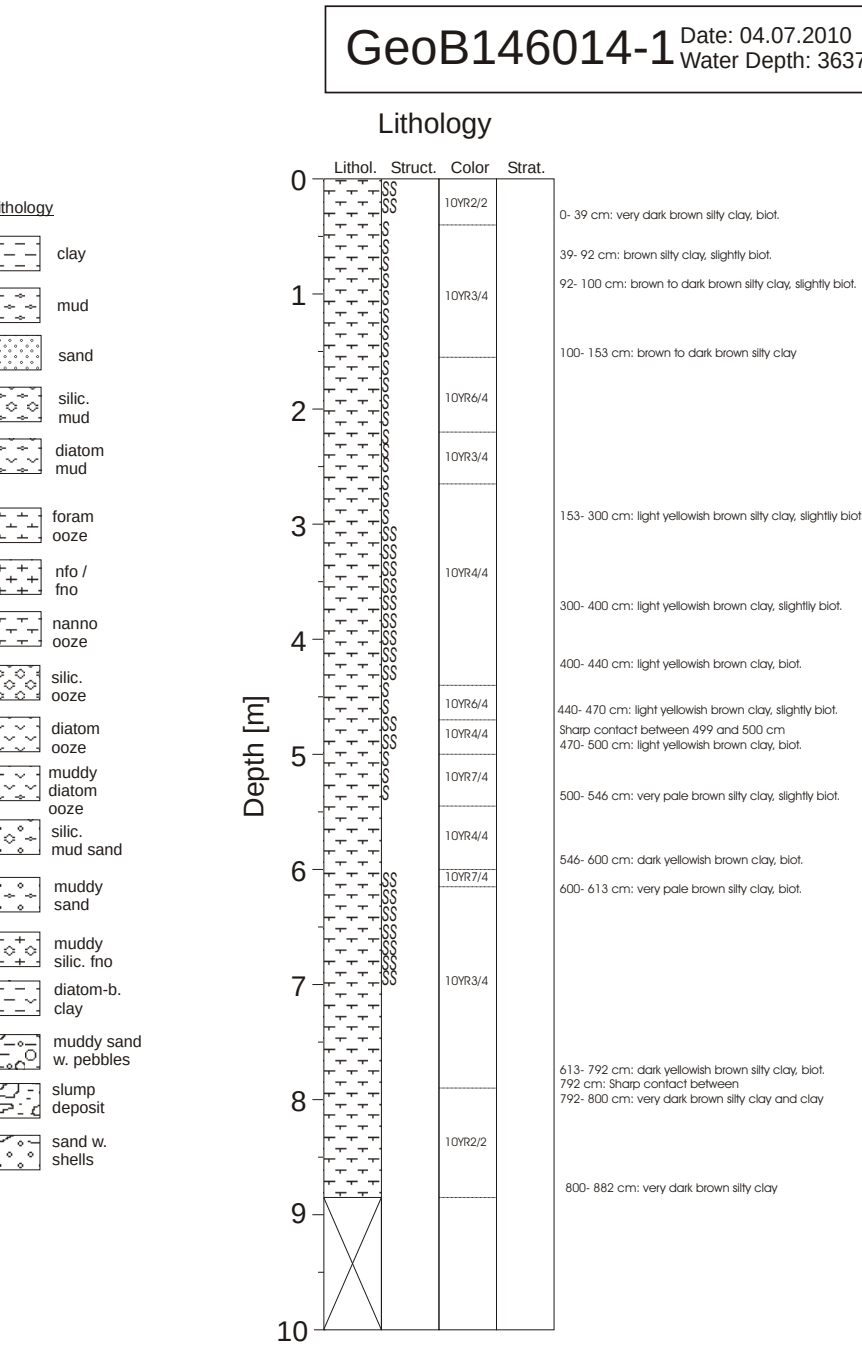

Figure 147: Core log of GeoB14614

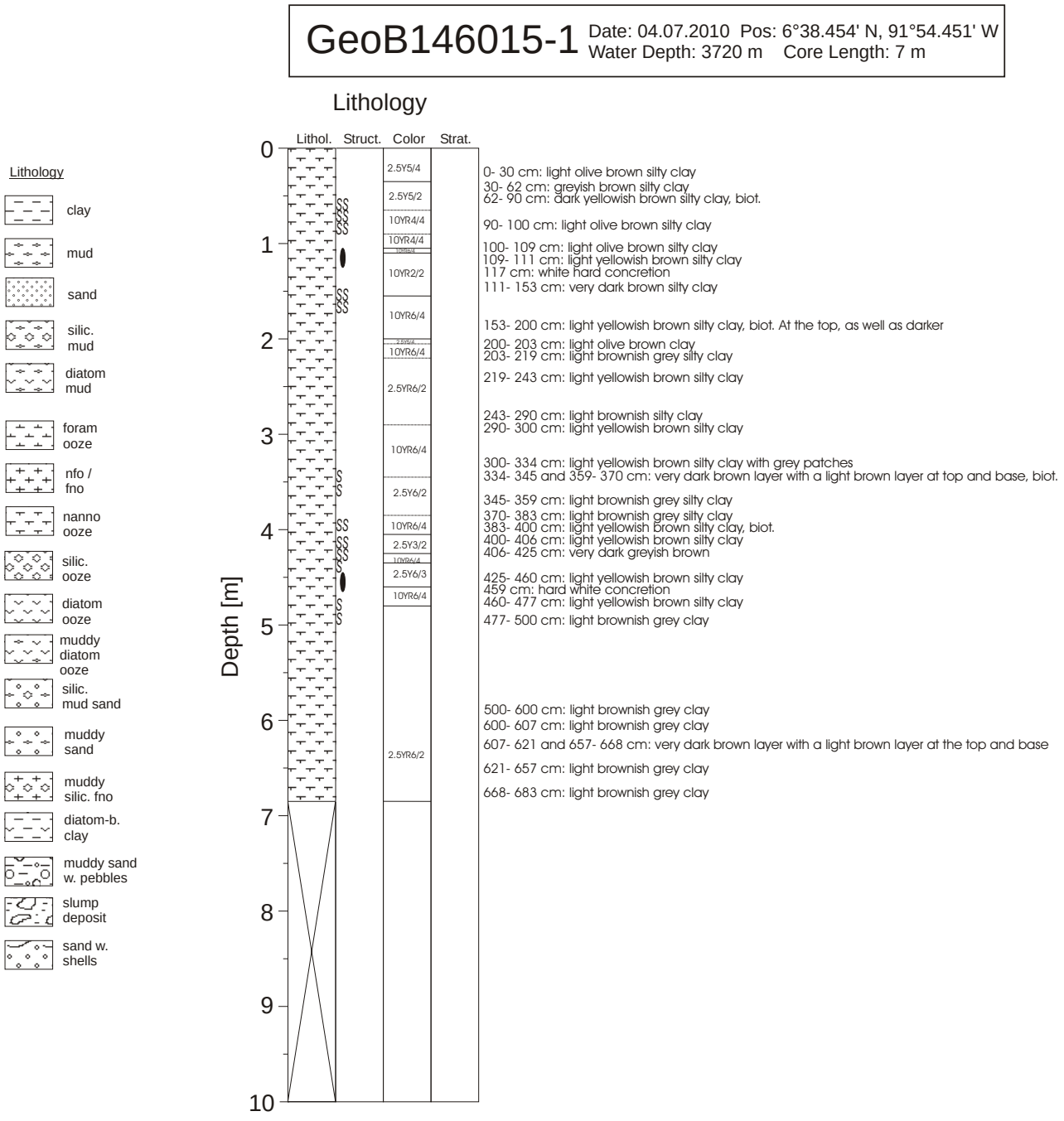

Figure 148: Core log of GeoB14615

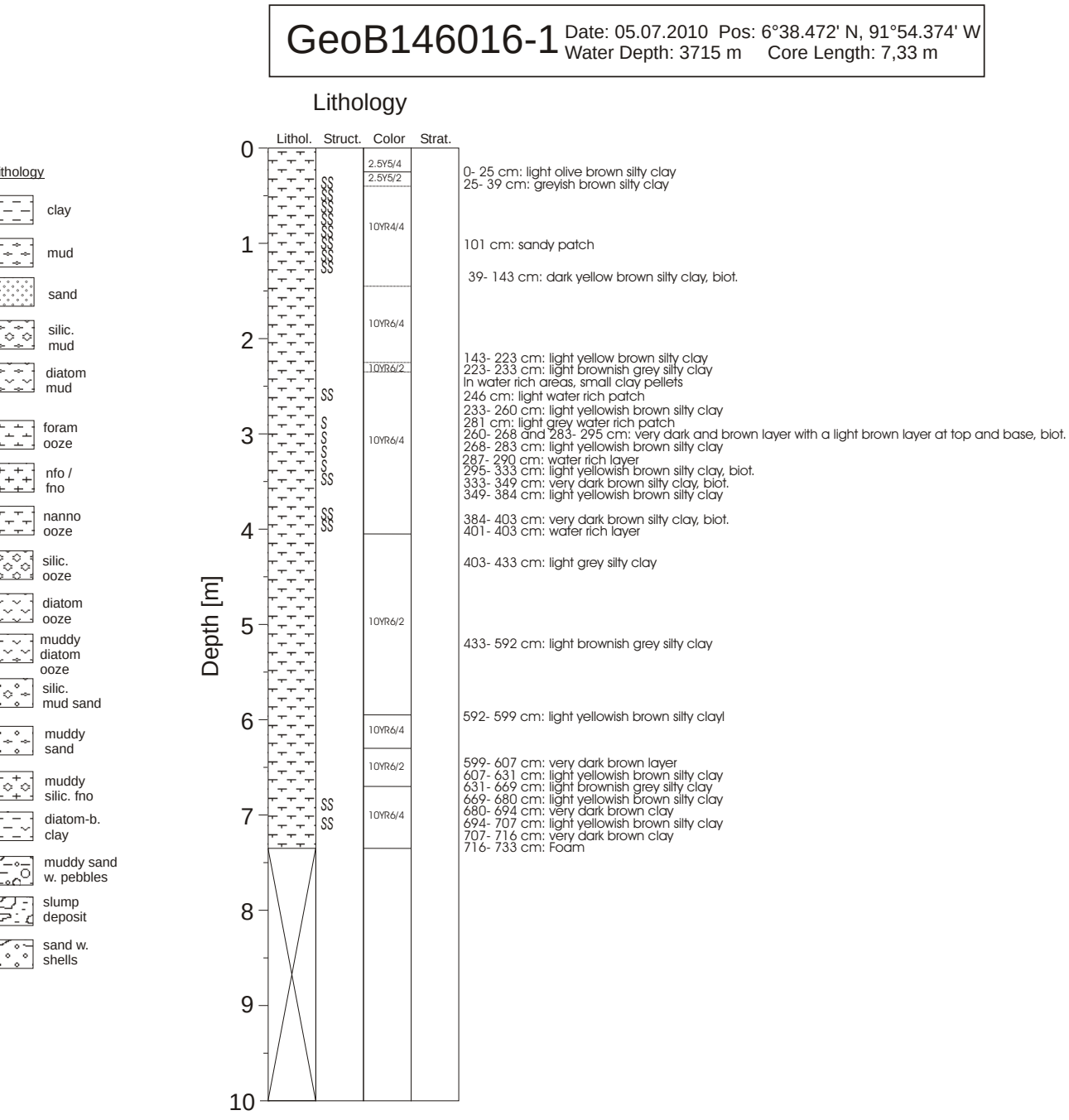

Figure 149: Core log of GeoB14616

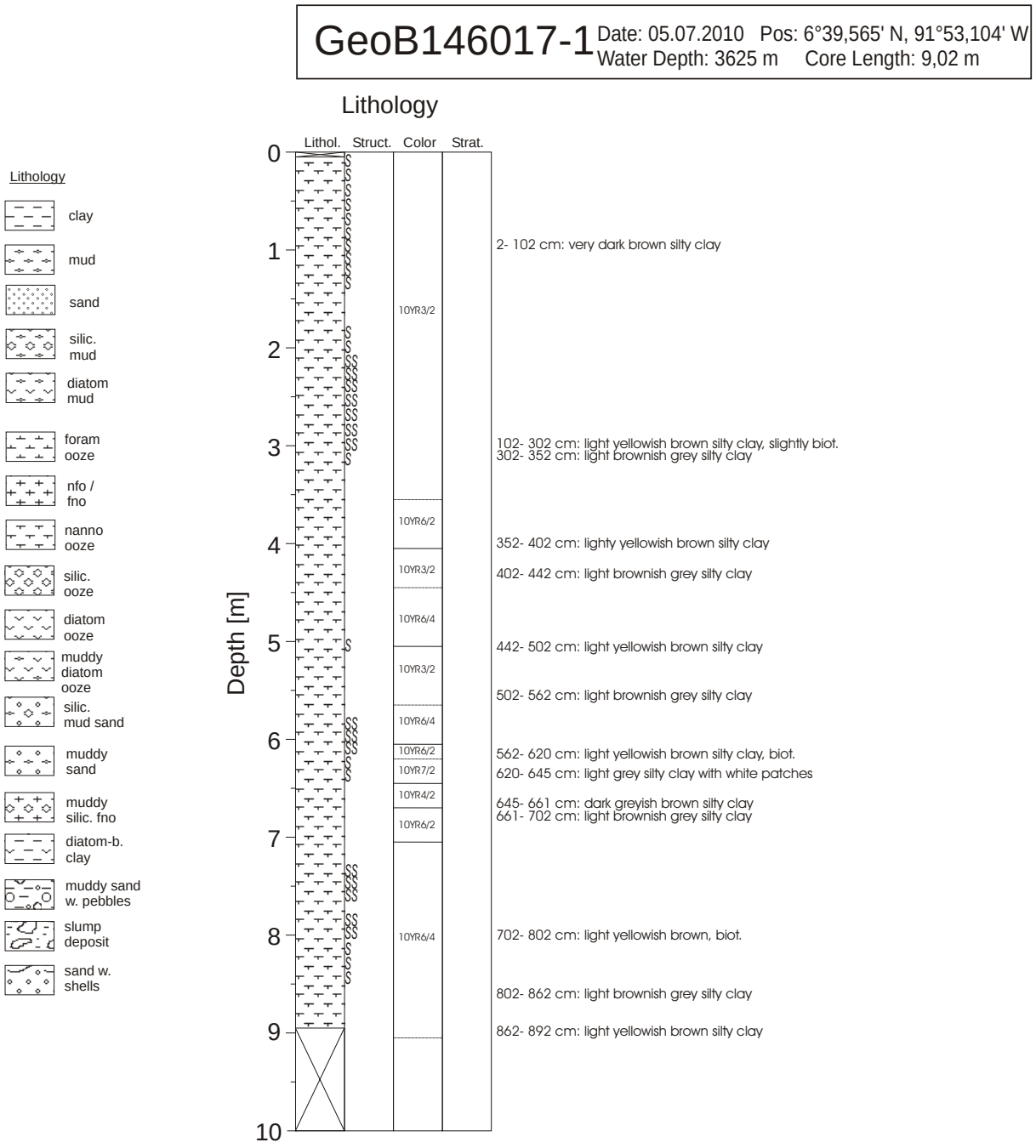

Figure 150: Core log of GeoB14617

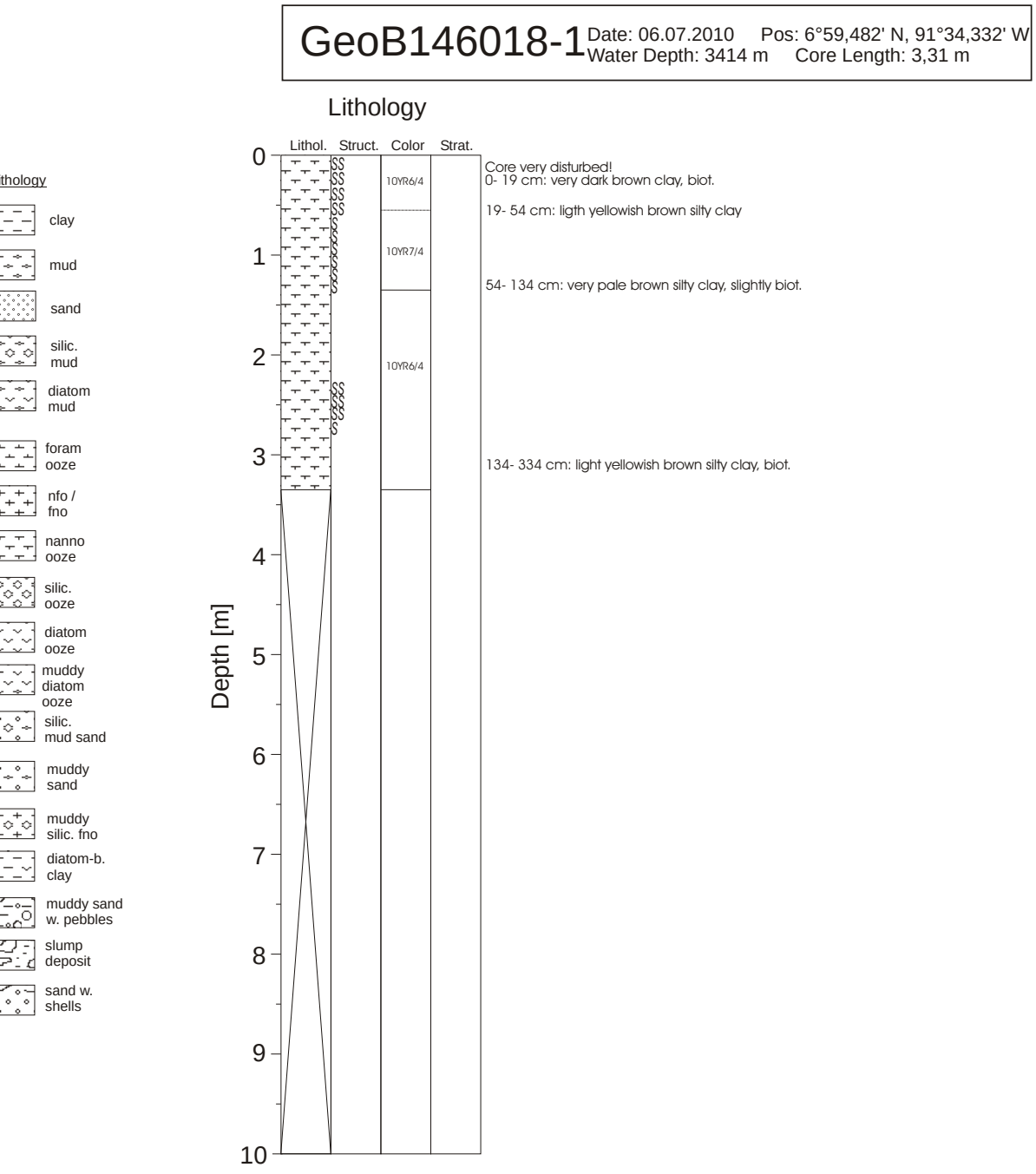

Figure 151: Core log of GeoB14618

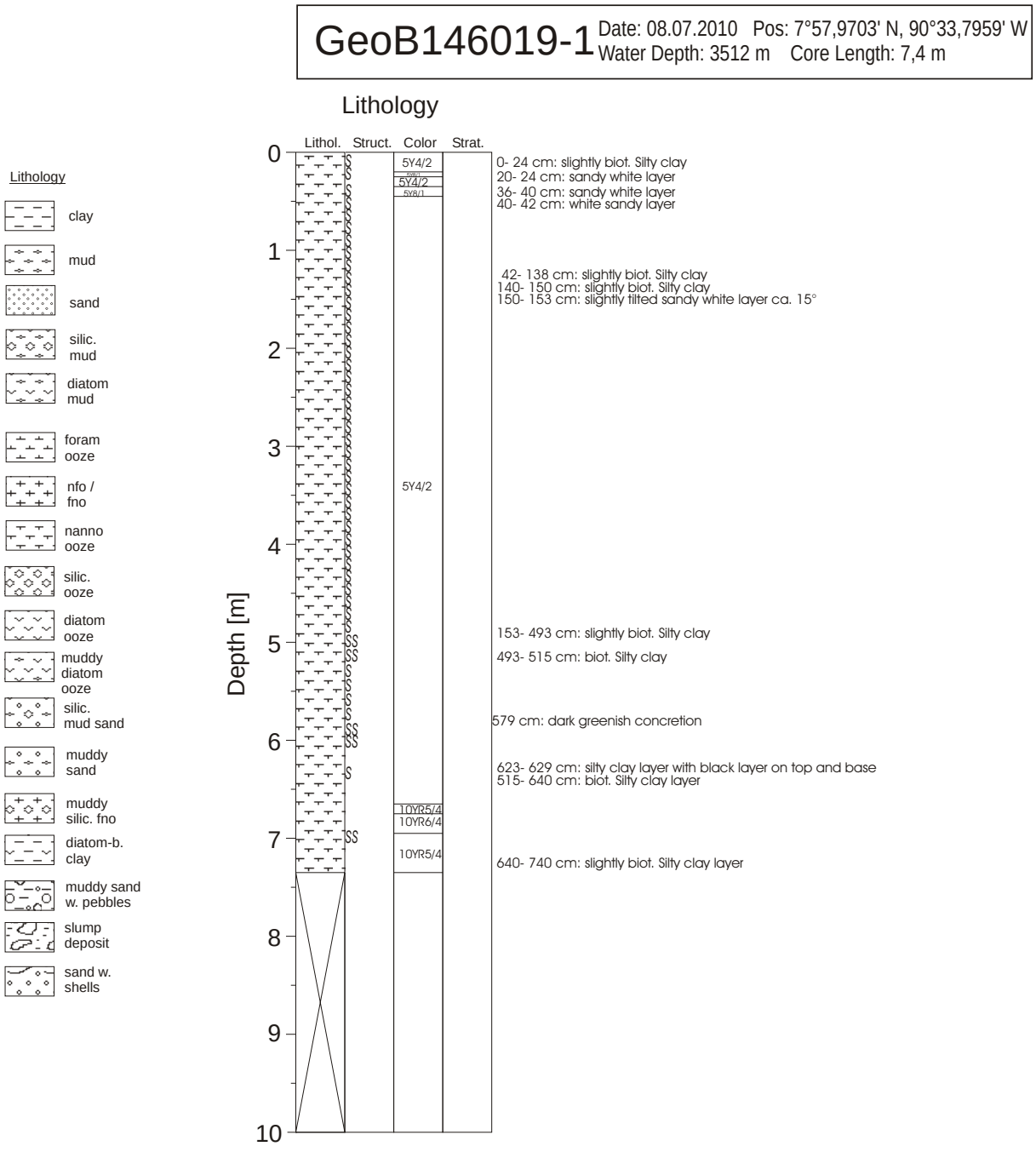

Figure 152: Core log of GeoB14619

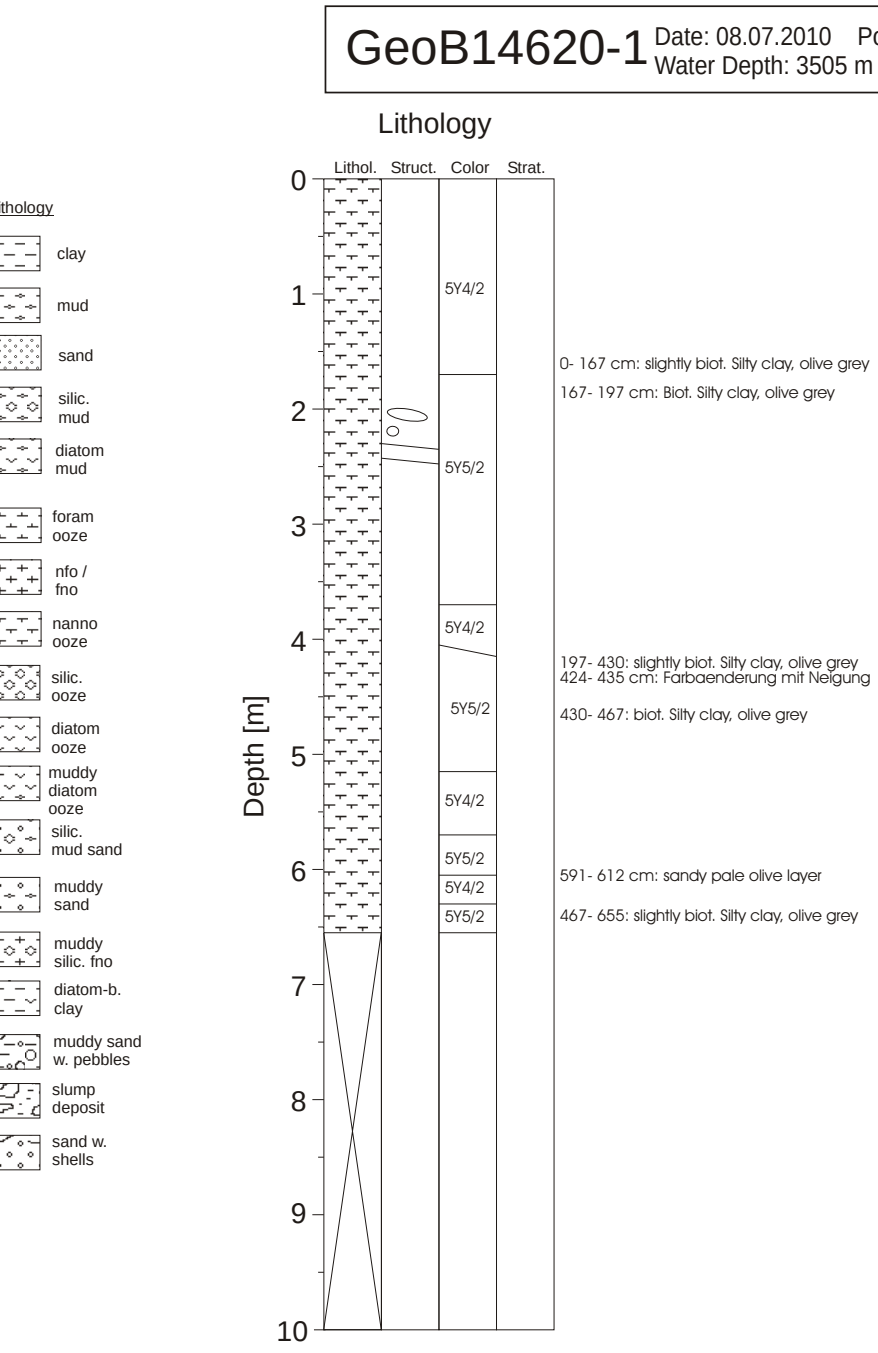

Figure 153: Core log of GeoB14620

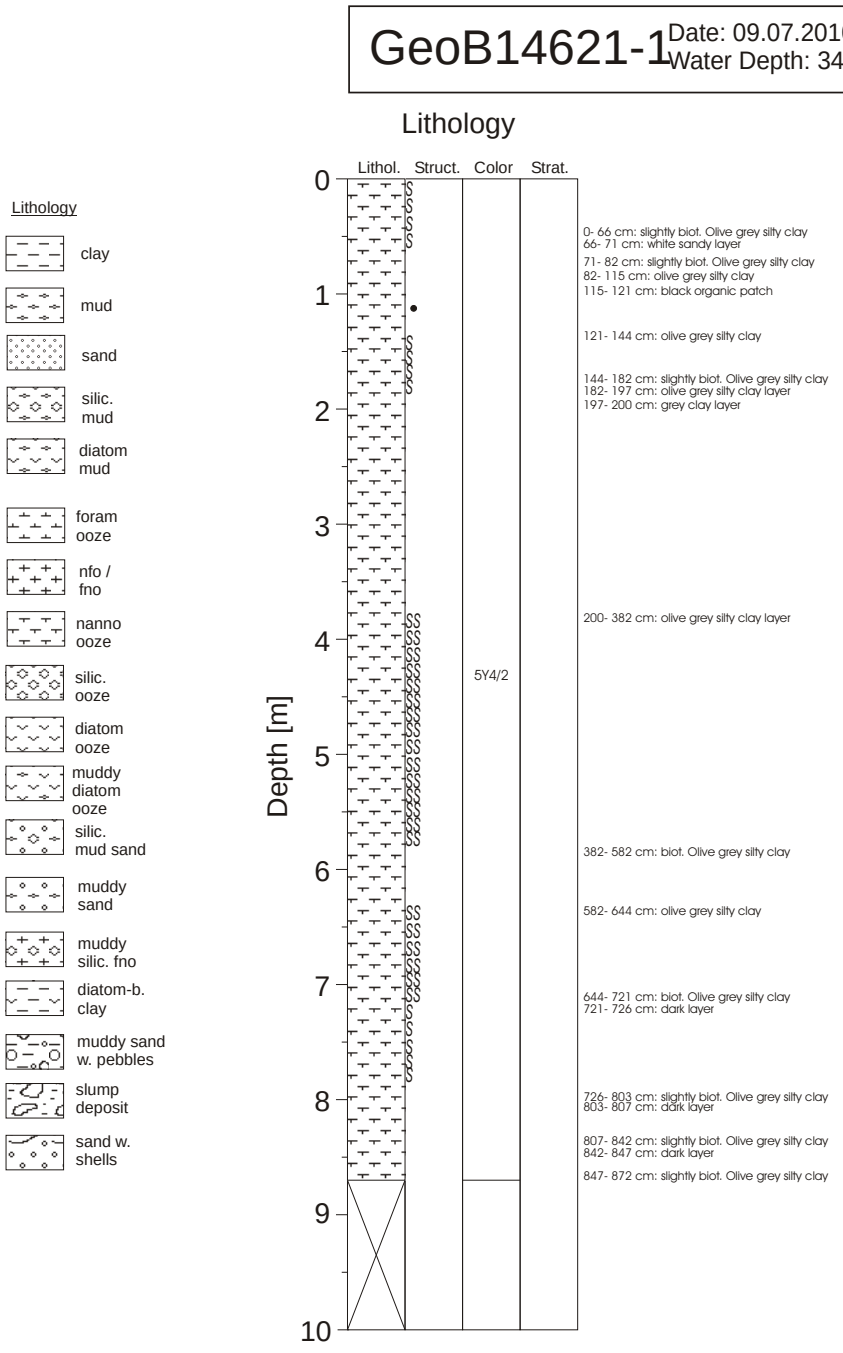

Figure 154: Core log of GeoB14621

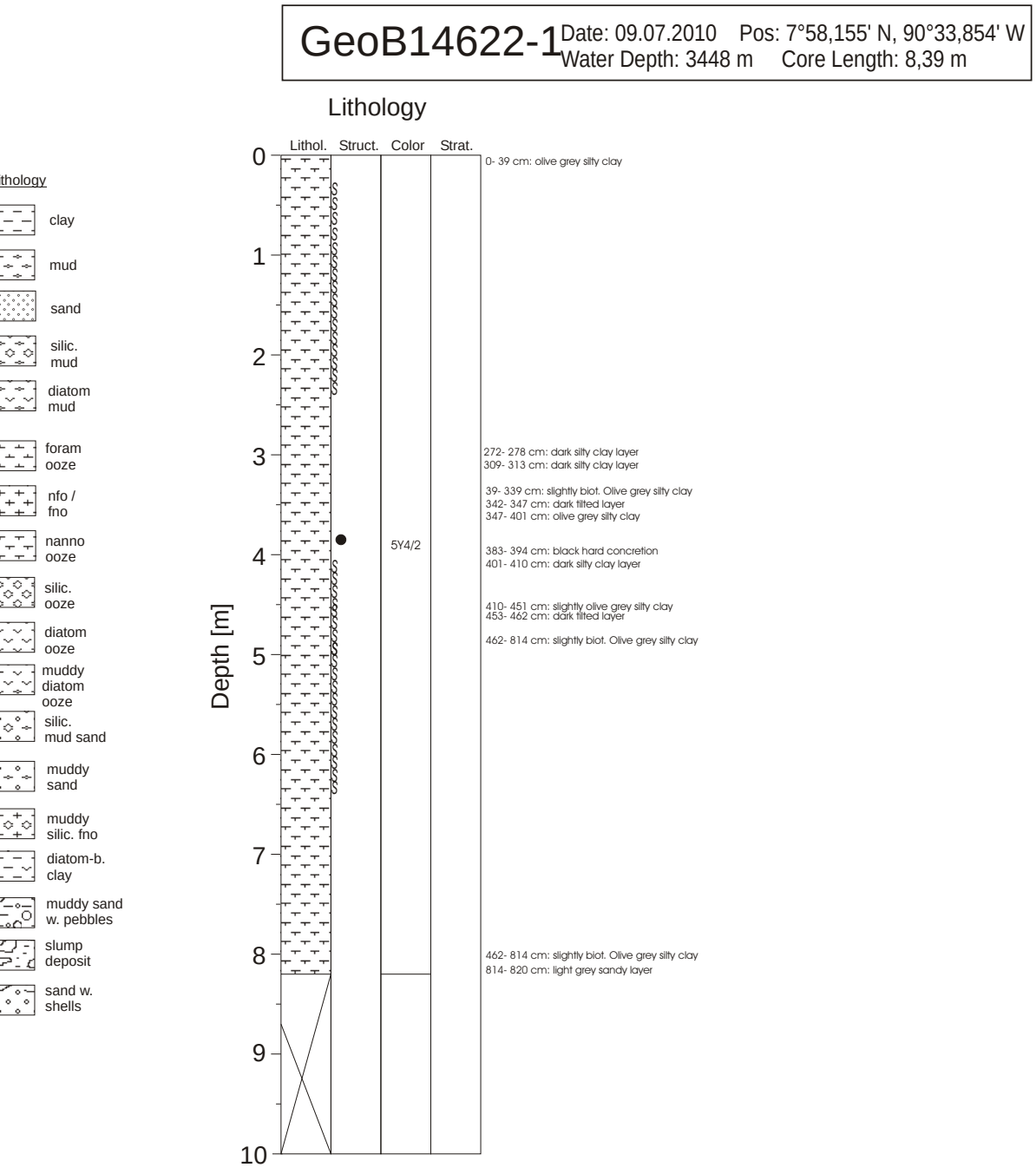

Figure 155: Core log of GeoB14622

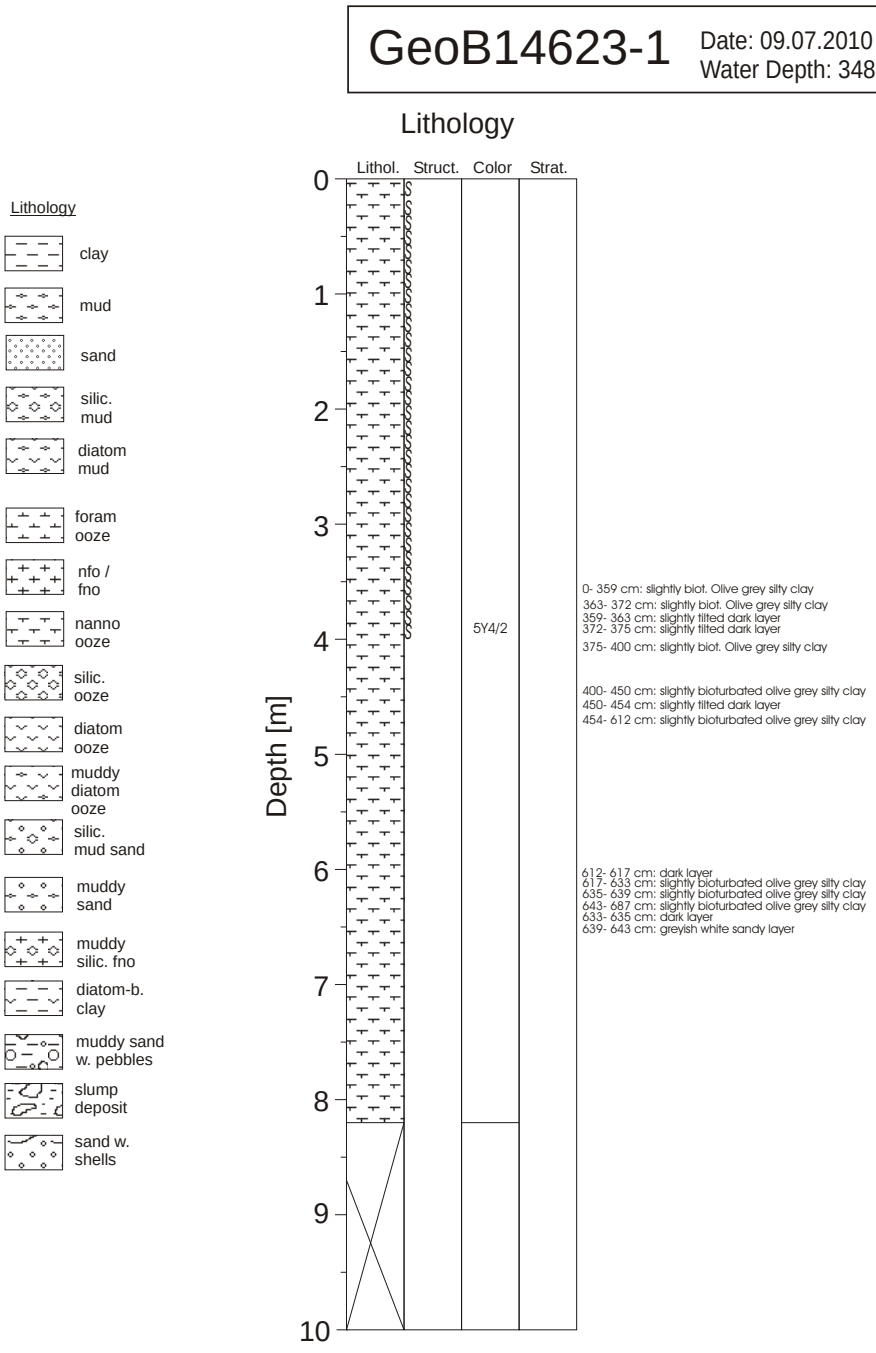

Figure 156: Core log of GeoB14623

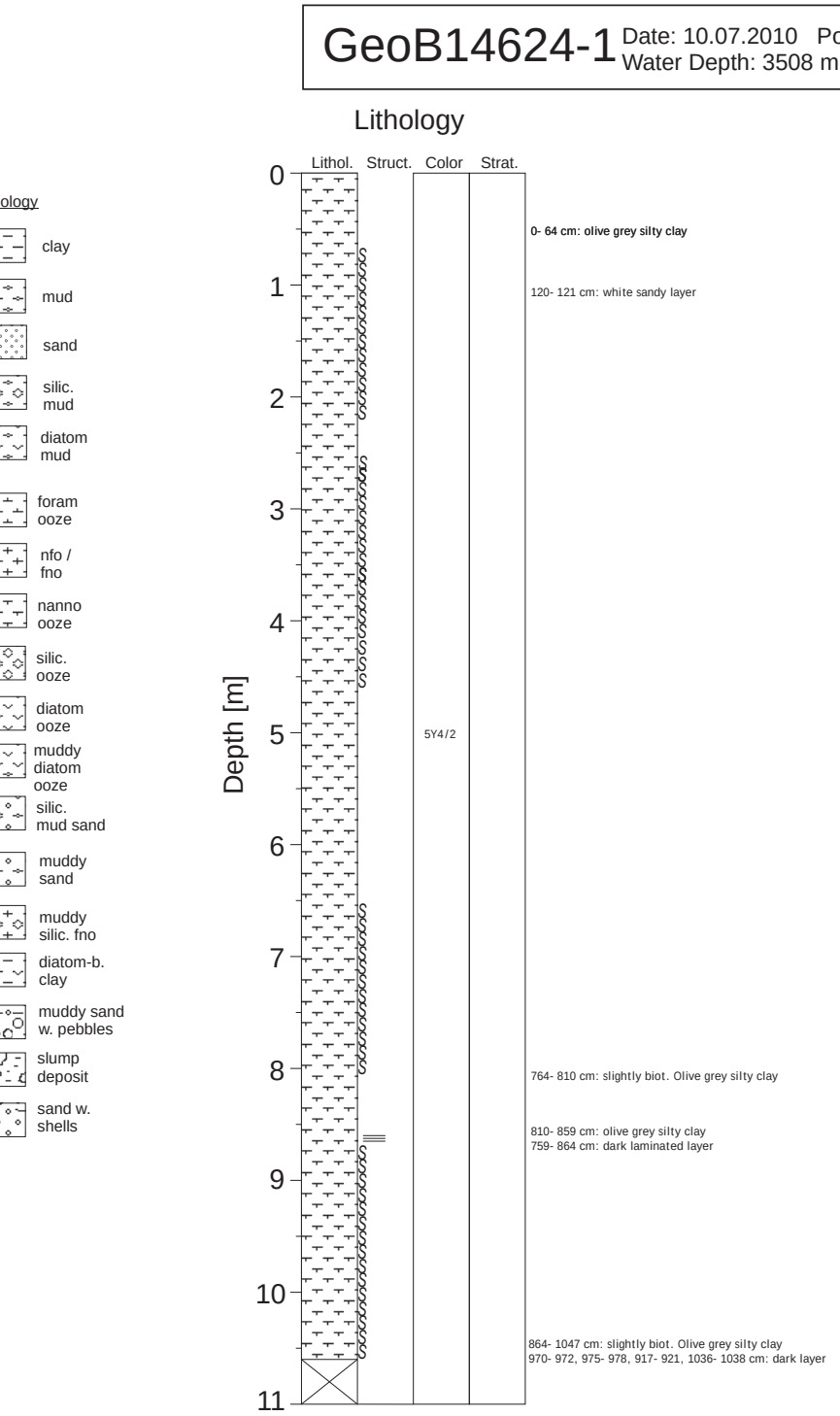

Figure 157: Core log of GeoB14624

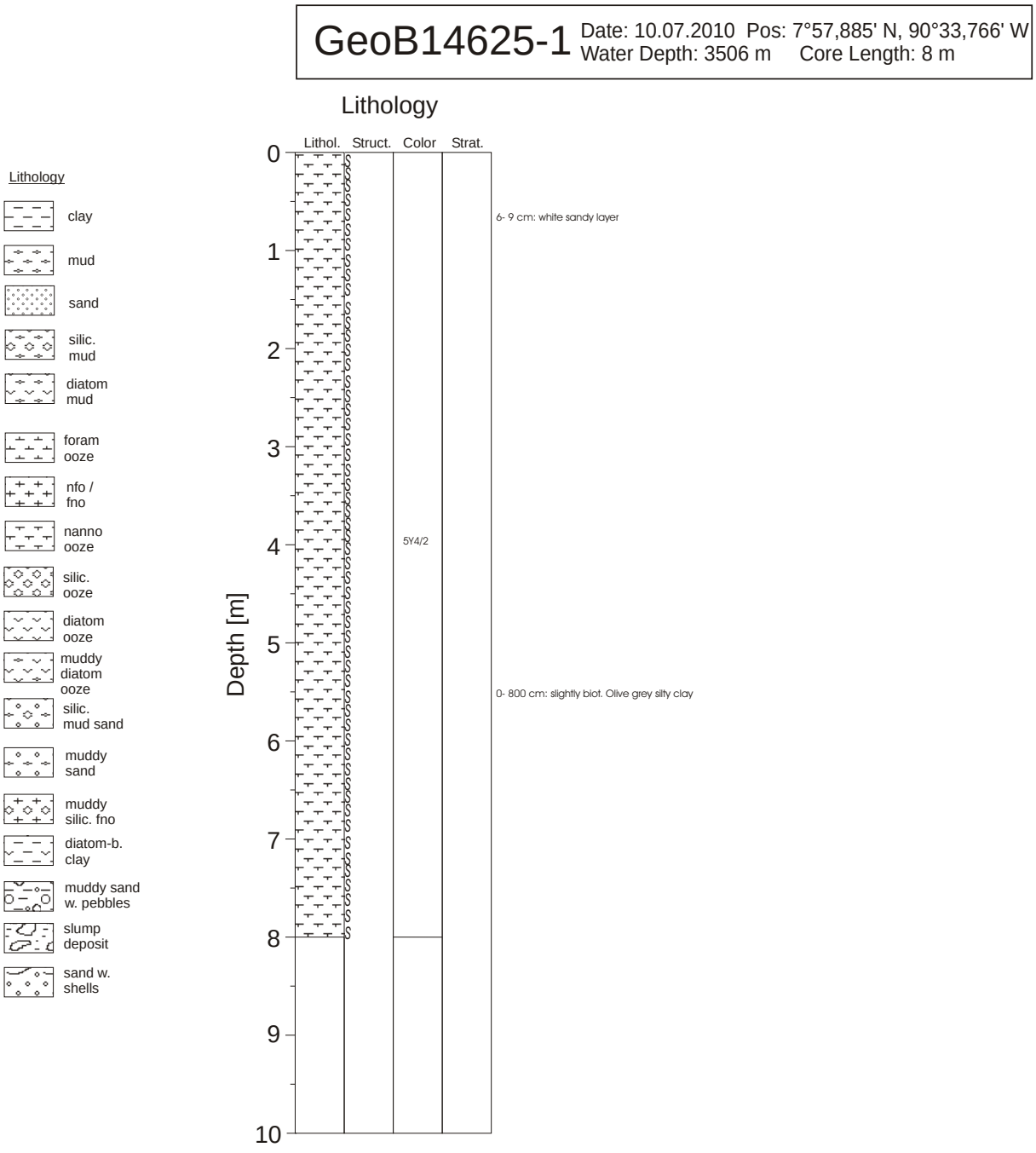

Figure 158: Core log of GeoB14625

B.2 Visual Seafloor Survey

Complete listing of all noteworthy observations made during the deployment of RV Sonne s Oceanfloor Oberservation System (OFOS) in GUATB-1. The goal was to carry out a video survey across pit bottom, pit slope, pit to normal seafloor transition and the seafloor between two pits. To achieve this a transect was established starting at (7° 14.292 N, 91° 27.190 W) and finishing at (7° 15.598 N, 91° 25.738 W).

Table 24: Protocol of the cisual seafloor survey with the OFOS. Page 1 of 2.

Universität Bremen Fachbereich 5 - Geowissenschaften				Datum:	6/27/10
OFOS - Protokoll					
Expedition:	**SO 207**				
Gerät:	**OFOS**				
Stationsnummer:	**GeoB14606-1**				
Tiefe [m]	Breite	Länge	Uhrzeit	Foto-Nr.	Bemerkungen
3496	7° 55,8820 N	90° 31,7560 W	18:20	8	Bodensicht
-	7° 55,8770 N	90° 31,7782 W	18:25	10	fischartiges Tier (Lanze?)
-	7° 55,9290 N	90° 31,8290 W	18:43	24	
-	7° 55,9350 N	90° 31,8290 W	18:44	25	evtl. Seegurke
-			18:45	26	Krabbe am li. Bildrand
-			18:46	27	Seeigel, Weichtier
-			18:46	28	Röhrengebilde
-	7° 55,9460 N	90° 31,8478 W	18:47	29/30	weiße Flecken (Bakterienmatten?)
-			18:50	34	Garnele
-	7° 55,9690 N	90° 31,8802 W	18:55	36/37	weiße Flecken (Bakterienmatten?)
-			18:56	38	Krabbe
-	7° 55,9910 N	90° 31,9060 W	19:00	39	weiße Flecken (Bakterienmatten?)
-	7° 55,9910 N	90° 31,9060 W	19:00	40	weiße Flecken (Bakterienmatten?)
-			19:01	41/42	kleine Löcher/ Boden sieht anders aus
-	7° 55,9970 N	90° 31,9199 W	19:03	45	kleine Löcher/ Boden sieht anders aus
3477*	7° 56,0120 N	90° 31,9388 W	19:07	48	weiße Flecken (Bakterienmatten?)
3463			19:10	52	weiße Flecken (Bakterienmatten?)
3455	7° 56,0340 N	90° 31,9671 W	19:11	54	weiße Flecken (Bakterienmatten?)
3443	7° 56,0470 N	90° 31,9802 W	19:14	57	weiße Flecken (Bakterienmatten?)
3440	7° 56,0570 N	90° 31,9900 W	19:16	59	weiße Flecken (Bakterienmatten?)
3425	7° 56,0970 N	90° 32,0400 W	19:24		
3423	7° 56,1980 N	90° 32,1408 W	19:40		
**3388	7° 56,3220 N	90° 32,2470 W	19:55		
3424	7° 56,4480 N	90° 32,3720 W	20:10		
3397***	7° 56,4680 N	90° 32,4900 W	20:25		
3417	7° 56,7460 N	90° 32,6052 W	20:40	61	Schlangenstern
3423				62	Qualle
3423			20:52		
3422	7° 56,8600 N	90° 32,7490 W	20:55		
3424	7° 56,9600 N	90° 32,8748 W	21:10		
3428	7° 57,0760 N	90° 32,9859 W	21:25		
3433	7° 57,1740 N	90° 33,0949 W	21:40	64/65	
3429	7° 57,2860 N	90° 33,1822 W	21:55	66-68	
*	350 m vom WP entfernt				
**	Fehlerhafte Tiefenanzeige, wahrscheinliche Tiefe: 3424 m				
***	Fehlerhafte Tiefenanzeige				

Table 25: Protocol of the cisual seafloor survey with the OFOS. Page 2 of 2.

Expedition:	SO 207	
Gerät:	OFOS	Stationsende: 23:32 h
Stationsnummer:	GeoB14606-1	

Tiefe [m]	Breite	Länge	Uhrzeit	Foto-Nr.	Bemerkungen
3438	7° 57,3800 N	90° 33,2899 W	22:07		*Test: Boden etwas härter
3440	7° 57,3950 N	90° 33,3018 W	22:09	72	weiße Flecken (Bakterienmatten?)
3442	7° 57,4150 N	90° 33,3162 W	22:11	73	weiße Flecken (Bakterienmatten?)
3444	7° 57,4290 N	90° 33,3301 W	22:13	74	fischartiges Tier, * Test: Boden noch fest
3453	7° 57,4670 N	90° 33,3572 W	22:17	75	weiße Flecken (Bakterienmatten?)
3458			22:26	80	blaues fischartiges Tier, * Test: Boden noch fest
3473	7° 57,5680 N	90° 33,4481 W	22:30		
3495	7° 57,6050 N	90° 33,5039 W	22:37	81	weiße Flecken (Bakterienmatten?)
	7° 57,6140 N	90° 33,6270 W	22:37	82	Häufigkeit weiße Flecken (Bakterienmatten?) nimmt zu
3491	7° 57,7150 N	90° 33,6039 W	22:48	83/84	weiße Flecken (Bakterienmatten?)
	7° 57,7530 N	90° 33,6268 W	22:51	85	ausgeprägtere weiße Flecken (Bakterienmatten?)
3491	7° 57,7490 N	90° 33,6629 W	22:52	86	weiße Flecken (Bakterienmatten?)
3489	7° 57,7540 N	90° 33,6510 W	22:54	87	Schwamm?/Bakterienmatten?
3489	7° 57,7540 N	90° 33,6711 W	22:55		* Test: Boden noch fest
3493	7° 57,8010 N	90° 33,6912 W	22:58		Häufigkeit weiße Flecken (Bakterienmatten?) nimmt zu
3492	7° 57,8090 N	90° 33,7141 W	22:59		* Test: Boden noch fest
3491	7° 57,8230 N	90° 33,7289 W	23:02	88/89	ausgeprägtere weiße Flecken (Bakterienmatten?)
3494	7° 57,8640 N	90° 33,7858 W	23:07	91	weiße Flecken (Bakterienmatten?)
			23:15-17		Loch im Meeresboden gesichtet
	7° 57,9910 N	90° 33,8989 W		92	weiße Flecken (Bakterienmatten?)
***3456	7° 58,0560 N	90° 33,9670 W	23:27	93	weiße Flecken (Bakterienmatten?)
***3452	7° 58,0590 N	90° 33,9698 W	23:28	94	weiße Flecken (Bakterienmatten?)
	7° 58,0810 N	90° 33,9910 W	23:30		*Test: Boden etwas weicher
			23:32	95	Survey beendet

*	Test bei dem ein Gewicht in auf dem Meerenboden fallen gelassen wird
**	Bakterienmatten ausgeprägter und etwas häufiger in Richtung der Ränder der Pits
***	Fehlerhafte Tiefenanzeige

B.3 Pore Water Chemistry

Complete listing of all chemical parameters which were measured onboard the RV Sonne during the Seamountflux Cruise (SO 207). Eh and pH measurements were done directly by inserting probes into the sediment. All other parameters were measured following extraction of pore water using rhizons.

Table 26: Summary of measured chemical parameters on core GeoB14601 and their results.

Station :		GeoB 14601				
Core number:		GeoB 14601-1				
Depth/cm	**pH**	**Eh/mV**	**Alk_T/mmol L^{-1}**	**NH_4^+/mg L^{-1}**	**Fe^{2+} /mg L^{-1}**	**PO_4^{3-} /mg L^{-1}**
4	7,69	-78	3,28	<0.1	0,07	0,45
24	7,65	-125	3,29	<0.1	0,13	0,54
44	7,64	-131	3,38	<0.1	0,19	0,58
64	7,55	122	3,09	<0.1	0,23	0,72
84	7,52	-123	2,98	<0.1	0,39	0,56
128	7,45	-140	3,67	<0.1	0,38	0,59
168	7,47	-200	3,67	<0.1	0,37	0,57
218	7,42	-214	3,38	<0.1	0,31	0,53
268	7,47	-238	3,38	0,18	0,28	0,49
318	7,44	-206	3,48	0,18	0,33	0,50
368	7,42	-163	3,28	0,25	0,15	0,40
418	7,47	-219	3,38	0,20	0,35	0,50
468	7,37	-107	3,58	0,24	0,25	0,49
522	7,44	-192	3,48	0,29	0,36	0,48
568	7,60	-101	3,68	0,24	0,31	0,44
618	7,38	-170	3,58	0,23	0,33	0,45
668	7,52	-178	3,58	0,25	0,26	0,44
718	7,37	-203	4,06	0,29	0,35	0,43
768	7,47	-127	3,58	0,22	0,36	0,37
818	7,47	-55	3,38	0,31	0,36	0,40
868	7,36	-120	3,58	0,27	0,33	0,36
880	7,48	-127	3,38	0,32	0,32	0,40
937	7,52	-170	3,68	0,31	0,30	0,34

Table 27: Summary of measured chemical parameters on core GeoB14602 and their results.

Station :		GeoB 14602				
Core number:		GeoB 14602-1				
Depth/cm	**pH**	**Eh/mV**	**Alk_T/mmol L^{-1}**	**NH_4^+/mg L^{-1}**	**Fe^{2+} /mg L^{-1}**	**PO_4^{3-} /mg L^{-1}**
5	7,62	-45	3,19	<0.1	n.d.	0,38
20	7,46	-89	3,09	<0.1	n.d.	0,59
35	7,52	-95	2,99	<0.1	n.d.	0,74
95	7,67	-150	3,39	0,41	n.d.	0,64
110	7,64	-150	3,19	0,43	n.d.	0,66
131	8,10	104	3,29	0,43	n.d.	0,67
160	7,59	-201	3,59	0,52	n.d.	0,59
188	7,56	-135	3,19	0,43	n.d.	0,56
235	7,63	-145	3,67	0,47	n.d.	0,54
285	7,69	-140	3,39	0,52	n.d.	0,48
335	7,67	-22	3,29	0,49	n.d.	0,45
385	7,57	-201	3,49	0,50	n.d.	0,43
435	7,63	-150	3,58	0,47	n.d.	0,39
485	7,55	-213	3,49	0,55	n.d.	0,41
535	7,60	-221	3,68	0,55	n.d.	0,38
585	7,57	-232	3,58	0,48	n.d.	0,36
635	8,00	-224	3,78	0,47	n.d.	0,36
685	7,52	-235	3,58	0,41	n.d.	0,36
735	7,68	-158	3,58	0,46	n.d.	0,35
785	7,62	-113	3,68	0,45	n.d.	0,32
835	7,74	-158	3,58	0,43	n.d.	0,32
885	7,69	-136	3,97	0,43	n.d.	0,27
937	7,52	-170	3,68	0,31	0,3	0,34

n.d. : not determined

Table 28: Summary of measured chemical parameters on core GeoB14603 and their results.

Station :		GeoB 14603				
Core number:		GeoB 14603-1				
Depth/cm	**pH**	**Eh/mV**	**Alk_T/mmol L^{-1}**	**NH_4^+/mg L^{-1}**	**Fe^{2+} /mg L^{-1}**	**PO_4^{3-} /mg L^{-1}**
3	7,58	97	2,99	<0.1	<0.05	0,41
28	7,72	10	3,09	<0.1	0,21	0,53
53	7,57	-104	3,18	<0.1	0,35	0,54
90	7,65	-37	3,19	<0.1	0,45	0,55
143	7,66	-125	3,19	<0.1	0,51	0,55
190	7,61	-110	3,09	<0.1	0,51	0,60
243	7,72	-123	3,19	<0.1	0,44	0,57
290	7,60	-130	3,59	<0.1	0,45	0,55
343	7,61	-189	3,19	<0.1	0,43	0,53
390	7,96	-184	3,09	0,40	0,36	0,50
443	7,86	-141	3,48	0,37	0,32	0,49
490	7,51	-2	3,28	0,41	0,16	0,39
543	7,58	-142	3,39	0,42	0,34	0,46
590	7,53	-120	3,58	0,40	0,38	0,42
643	7,60	-157	3,58	0,43	0,35	0,41
690	8,01	-135	3,58	0,44	0,26	0,35
743	7,57	-118	3,58	0,47	0,29	0,34
790	7,70	-160	3,58	0,40	0,25	0,33
815	7,60	-158	3,29	0,41	0,32	0,32
840	7,57	-117	3,58	0,40	0,30	0,36
870	n.d.	n.d.	3,78	0,43	n.d.	0,30

n.d. : not determined

Table 29: Summary of measured chemical parameters on core GeoB14604 and their results.

Station :		GeoB 14604				
Core number:		GeoB 14604-1				
Depth/cm	**pH**	**Eh/mV**	**Alk_T/mmol L^{-1}**	**NH_4^+/mg L^{-1}**	**Fe^{2+} /mg L^{-1}**	**PO_4^{3-} /mg L^{-1}**
5	7,51	144	2,82	<0.1	<0.05	0,37
35	7,64	-37	3,04	<0.1	0,19	0,54
96	8,07	146	3,07	<0.1	0,17	0,58
130	7,59	-90	3,09	0,38	0,36	0,57
180	7,63	-110	3,15	0,43	0,33	0,69
230	7,76	-110	3,18	0,39	0,33	0,60
280	7,65	-123	3,20	<0.1	0,29	0,49
330	7,66	-176	3,23	0,63	0,28	0,54
382	7,62	-170	3,24	0,49	0,32	0,53
430	7,78	-142	3,21	0,53	0,27	0,53
480	7,81	-55	3,31	0,52	0,28	0,55
530	7,63	-140	3,31	0,58	0,27	0,49
580	7,70	-156	3,31	0,52	0,31	0,47
630	7,58	-10	3,31	0,53	0,19	0,47
680	7,66	-8	3,38	0,55	0,32	0,46
730	7,65	-1	3,37	0,58	0,27	0,43
780	7,56	38	3,36	0,56	0,31	0,42
830	7,57	-200	3,34	0,54	0,32	0,41
880	7,57	-290	3,42	0,55	0,28	0,39
930	7,76	100	3,39	0,58	0,31	0,30

Table 30: Summary of measured chemical parameters on core GeoB14605-1 and their results.

Station :		GeoB 14605				
Core number:		GeoB 14605-1				
Depth/cm	**pH**	**Eh/mV**	**Alk_T/mmol L^{-1}**	**NH_4^+/mg L^{-1}**	**Fe^{2+} /mg L^{-1}**	**PO_4^{3-} /mg L^{-1}**
30	7,46	-101	3,13	<0.1	0,17	0,69
68	7,91	-110	3,20	0,48	0,20	0,80
97	7,80	-108	3,28	0,61	0,26	0,88
125	7,71	-111	3,35	0,74	0,29	0,98
164	7,88	-140	3,42	0,93	0,25	1,05
185	7,93	151	3,52	0,92	0,16	1,17
199	7,75	-145	3,50	1,46	0,10	0,72
215	7,70	159	3,53	1,31	0,09	0,84
221	7,58	-120	3,44	1,40	0,12	0,64
227	7,78	148	3,51	1,28	0,09	0,76
235	7,87	150	3,58	1,26	<0.05	0,74
240	7,63	-119	3,42	0,95	0,09	0,50
270	7,58	-136	3,31	1,19	0,08	0,49
320	7,50	-150	3,33	1,11	<0.05	0,38
370	7,50	21	3,25	1,05	<0.05	0,42
420	7,61	-172	3,28	0,97	<0.05	0,41
470	7,84	-160	3,22	0,90	<0.05	0,35
520	7,61	-168	3,20	0,81	<0.05	0,35
570	7,53	-239	3,15	0,90	<0.05	0,33
620	7,58	-255	3,15	0,72	<0.05	0,36

Table 31: Summary of measured chemical parameters on MIC GeoB14605-2 and their results.

Station :		GeoB 14605				
Core number:		GeoB 14605-2				
Depth/cm	**pH**	**Eh/mV**	**Alk_T/mmol L^{-1}**	**NH_4^+/mg L^{-1}**	**Fe^{2+} /mg L^{-1}**	**PO_4^{3-} /mg L^{-1}**
BW	7,84	213	2,72	<0.1	<0.05	0,23
8	n.d.	n.d.	2,82	<0.1	<0.05	0,36
18	7,48	203	3,00	<0.1	0,05	0,55
26	7,63	-65	2,19	<0.1	0,31	0,76

n.d. : not determined

Table 32: Summary of measured chemical parameters on core GeoB14607 and their results.

Station :		GeoB 14607				
Core number:		GeoB 14607-1				
Depth/cm	**pH**	**Eh/mV**	**Alk_T/mmol L^{-1}**	**NH_4^+/mg L^{-1}**	**Fe^{2+} /mg L^{-1}**	**PO_4^{3-} /mg L^{-1}**
10	7,35	177	2,94	<0.1	<0.05	0,35
24	7,29	241	2,94	<0.1	<0.05	0,39
47	7,35	234	2,96	<0.1	<0.05	0,40
57	7,35	243	3,01	<0.1	<0.05	0,44
60	7,41	260	3,00	<0.1	<0.05	0,45
63	7,50	240	2,99	<0.1	<0.05	0,49
68	7,50	208	3,02	<0.1	<0.05	0,45
70	7,52	180	3,13	<0.1	<0.05	0,46
75	7,52	197	3,03	<0.1	<0.05	0,45
86	7,55	229	2,96	<0.1	<0.05	0,46
103	7,61	150	2,98	<0.1	<0.05	0,47
140	7,52	125	3,02	<0.1	<0.05	0,49
174	7,51	124	3,05	<0.1	<0.05	0,51
205	7,51	115	3,04	<0.1	<0.05	0,52
232	7,53	15	3,05	<0.1	<0.05	0,50
254	7,54	87	3,05	<0.1	<0.05	0,52
272	7,59	-80	3,10	<0.1	<0.05	0,52
286	7,64	-57	3,09	<0.1	<0.05	0,54
304	7,61	-77	3,13	<0.1	0,17	0,49
350	7,61	-94	3,10	<0.1	0,39	0,48
450	7,62	-149	3,18	<0.1	0,45	0,39
550	7,84	-58	3,14	0,35	0,38	0,40
650	7,74	-150	3,19	0,37	0,22	0,39
704	7,78	n.d.	3,22	0,39	<0.05	0,33

n.d. : not determined

Table 33: Summary of measured chemical parameters on core GeoB14608-1 and their results.

Station :		GeoB 14608				
Core number:		GeoB 14608-1				
Depth/cm	**pH**	**Eh/mV**	**Alk_T/mmol L^{-1}**	**NH_4^+/mg L^{-1}**	**Fe^{2+} /mg L^{-1}**	**PO_4^{3-} /mg L^{-1}**
12	7,32	226	2,80	<0.5	<0.05	0,33
43	7,55	123	2,92	<0.5	<0.05	0,36
80	7,54	197	2,94	<0.5	<0.05	0,38
125	7,57	175	2,94	<0.5	<0.05	0,34
176	7,99	205	2,94	<0.5	<0.05	0,31
193	7,95	220	2,76	<0.5	<0.05	0,27
213	7,60	182	2,98	<0.5	<0.05	0,30
280	7,56	200	2,95	<0.5	<0.05	0,28
348	7,58	185	3,12	<0.5	<0.05	0,25
365	8,02	196	3,20	<0.5	<0.05	0,22
405	7,90	216	3,78	<0.5	<0.05	0,23
445	8,00	219	2,73	<0.5	<0.05	0,20
453	7,68	206	2,99	<0.5	<0.05	0,21
506	7,59	208	2,92	<0.5	<0.05	0,22
538	7,62	185	3,00	<0.5	<0.05	0,24
580	7,62	231	2,94	<0.5	<0.05	0,21
638	7,62	156	2,96	<0.5	<0.05	0,31
701	7,60	208	2,93	<0.5	<0.05	0,20
706	7,64	245	2,94	<0.5	<0.05	0,20
711	7,58	262	2,90	<0.5	<0.05	0,19
733	7,62	250	2,92	<0.5	<0.05	0,18
809	7,83	227	2,76	<0.5	<0.05	0,17

Table 34: Summary of measured chemical parameters on MIC GeoB14608-2 and their results.

Station :		GeoB 14608				
Core number:		GeoB 14608-2				
Depth/cm	**pH**	**Eh/mV**	**Alk_T/mmol L^{-1}**	**NH_4^+/mg L^{-1}**	**Fe^{2+} /mg L^{-1}**	**PO_4^{3-} /mg L^{-1}**
BW	n.d.	n.d.	2,67	<0.5	<0.05	0,25
6	7,24	354	2,68	<0.5	<0.05	0,28
12	7,37	272	2,73	<0.5	<0.05	0,33
18	7,45	228	2,79	<0.5	<0.05	0,35
24	7,51	207	2,82	<0.5	<0.05	0,36
30	7,53	181	2,84	<0.5	<0.05	0,36

n.d. : not determined

Table 35: Summary of measured chemical parameters on core GeoB14609 and their results.

Station :		GeoB 14609				
Core number:		GeoB 14609-1				
Depth/cm	**pH**	**Eh/mV**	**Alk_T/mmol L^{-1}**	**NH_4^+/mg L^{-1}**	**Fe^{2+} /mg L^{-1}**	**PO_4^{3-} /mg L^{-1}**
9	7,45	217	2,81	<0.5	<0.05	0,40
16	7,55	232	2,87	<0.5	<0.05	0,37
54	7,55	200	2,87	<0.5	<0.05	0,34
100	7,58	167	2,93	<0.5	<0.05	0,32
156	7,59	183	2,93	<0.5	<0.05	0,28
201	7,62	174	2,93	<0.5	<0.05	0,26
254	7,56	170	2,97	<0.5	<0.05	0,26
321	7,58	174	2,97	<0.5	<0.05	0,20
422	7,58	214	2,98	<0.5	<0.05	0,18
478	7,49	174	2,94	<0.5	<0.05	0,17
522	7,71	148	2,99	<0.5	<0.05	0,15
580	7,53	242	2,79	<0.5	<0.05	0,17
649	7,58	175	2,76	<0.5	<0.05	0,14

Table 36: Summary of measured chemical parameters on core GeoB14610 and their results.

Station :		GeoB 14610				
Core number:		GeoB 14610-1				
Depth/cm	**pH**	**Eh/mV**	**Alk_T/mmol L^{-1}**	**NH_4^+/mg L^{-1}**	**Fe^{2+} /mg L^{-1}**	**PO_4^{3-} /mg L^{-1}**
10	7,45	213	2,86	<0.5	<0.05	0,34
33	7,54	172	2,87	<0.5	<0.05	0,36
52	7,59	197	2,88	<0.5	<0.05	0,35
72	7,57	176	2,91	<0.5	<0.05	0,34
93	7,59	210	2,93	<0.5	<0.05	0,32
111	7,57	202	2,91	<0.5	<0.05	0,32
144	7,63	215	2,91	<0.5	<0.05	0,30
177	7,58	185	2,93	<0.5	<0.05	0,31
209	7,56	200	2,94	<0.5	<0.05	0,29
247	7,62	119	2,93	<0.5	<0.05	0,27
277	7,62	160	n.d.	<0.5	<0.05	0,26
311	7,59	210	2,95	<0.5	<0.05	0,25
347	7,63	137	2,92	<0.5	<0.05	0,24
381	7,63	172	2,90	<0.5	<0.05	0,23
413	7,58	192	2,93	<0.5	<0.05	0,22
462	7,60	174	2,92	<0.5	<0.05	0,20
511	7,60	175	2,93	<0.5	<0.05	0,18
562	7,58	198	2,96	<0.5	<0.05	0,16
611	7,53	237	2,93	<0.5	<0.05	0,16

n.d. : not determined

Table 37: Summary of measured chemical parameters on core GeoB14611 and their results.

Station :		GeoB 14611				
Core number:		GeoB 14611-1				
Depth/cm	**pH**	**Eh/mV**	**Alk_T/mmol L^{-1}**	**NH_4^+/mg L^{-1}**	**Fe^{2+} /mg L^{-1}**	**PO_4^{3-} /mg L^{-1}**
10	7,49	180	2,88	<0.5	<0.05	0,45
41	7,57	140	2,89	<0.5	<0.05	0,50
75	7,73	-82	2,95	<0.5	0,08	0,54
113	7,59	169	2,96	<0.5	<0.05	0,55
160	7,62	-66	2,96	<0.5	0,05	0,55
193	7,69	-14	2,97	<0.5	<0.05	0,53
243	7,62	75	2,93	<0.5	<0.05	0,49
301	7,59	185	2,95	<0.5	<0.05	0,46
349	7,58	138	2,94	<0.5	<0.05	0,41
393	7,58	169	3,04	<0.5	<0.05	0,39
430	7,59	169	2,97	<0.5	<0.05	0,37
463	7,73	169	3,02	<0.5	0,06	0,35
505	7,72	-58	3,06	<0.5	0,07	0,34
524	n.d.	n.d.	3,00	<0.5	<0.05	0,36
541	7,75	-77	3,00	<0.5	<0.05	0,30
574	7,59	168	3,01	<0.5	<0.05	0,26
634	7,51	196	2,96	<0.5	<0.05	0,24
691	7,52	308	2,94	<0.5	<0.05	0,22
697	7,52	295	2,98	<0.5	<0.05	0,23
703	7,60	273	2,97	<0.5	<0.05	0,25
710	7,47	284	2,95	<0.5	<0.05	0,22
717	7,60	278	2,90	<0.5	<0.05	0,20
766	7,55	244	2,90	<0.5	<0.05	0,18

n.d. : not determined

Table 38: Summary of measured chemical parameters on core GeoB14612 and their results.

Station :		GeoB 14612				
Core number:		GeoB 14612-1				
Depth/cm	**pH**	**Eh/mV**	**Alk_T/mmol L^{-1}**	**NH_4^+/mg L^{-1}**	**Fe^{2+} /mg L^{-1}**	**PO_4^{3-} /mg L^{-1}**
26	7,46	215	2,84	<0.5	<0.05	0,27
76	7,51	203	2,89	<0.5	<0.05	0,28
126	7,57	206	2,91	<0.5	<0.05	0,26
176	7,58	216	2,91	<0.5	<0.05	0,25
226	7,57	215	2,96	<0.5	<0.05	0,25
276	7,54	220	2,93	<0.5	<0.05	0,25
326	7,64	183	2,97	<0.5	<0.05	0,23
376	7,64	195	2,94	<0.5	<0.05	0,21
426	7,64	212	2,96	<0.5	<0.05	0,21
476	7,65	235	3,00	<0.5	<0.05	0,21
526	7,59	189	2,94	<0.5	<0.05	0,19
576	7,65	182	3,02	<0.5	<0.05	0,21
626	7,62	150	3,00	<0.5	<0.05	0,19
676	7,62	176	3,01	<0.5	<0.05	0,17
726	7,58	202	3,04	<0.5	<0.05	0,18
778	7,59	214	3,01	<0.5	<0.05	0,18
824	7,60	197	3,01	<0.5	<0.05	0,17
876	7,63	240	3,00	<0.5	<0.05	0,16
936	7,61	264	3,01	<0.5	<0.05	0,16
976	7,55	239	3,01	<0.5	<0.05	0,15
1026	7,66	250	3,00	<0.5	<0.05	0,14

Table 39: Summary of measured chemical parameters on core GeoB14613 and their results.

Station :		GeoB 14613				
Core number:		GeoB 14613-1				
Depth/cm	**pH**	**Eh/mV**	**Alk_T/mmol L^{-1}**	**NH_4^+/mg L^{-1}**	**Fe^{2+} /mg L^{-1}**	**PO_4^{3-} /mg L^{-1}**
10	7,33	223	2,86	<0.5	<0.05	0,32
60	7,48	237	2,85	<0.5	<0.05	0,31
90	7,50	199	2,91	<0.5	<0.05	0,30
120	7,51	246	2,93	<0.5	<0.05	0,29
180	7,51	248	2,91	<0.5	<0.05	0,27
283	7,49	225	2,93	<0.5	<0.05	0,26
383	7,53	256	2,98	<0.5	<0.05	0,23
450	7,55	250	3,00	<0.5	<0.05	0,21
499	7,41	251	2,80	<0.5	<0.05	0,21
577	7,64	245	2,77	<0.5	<0.05	0,19
673	7,64	202	2,76	<0.5	<0.05	0,17

Table 40: Summary of measured chemical parameters on core GeoB14614 and their results.

Station :		GeoB 14614				
Core number:		GeoB 14614-1				
Depth/cm	**pH**	**Eh/mV**	**Alk_T/mmol L^{-1}**	**NH_4^+/mg L^{-1}**	**Fe^{2+} /mg L^{-1}**	**PO_4^{3-} /mg L^{-1}**
15	7,61	189	3,00	<0.5	<0.05	0,36
80	7,66	205	2,99	<0.5	<0.05	0,35
180	7,70	160	3,07	<0.5	<0.05	0,32
280	7,71	241	3,08	<0.5	<0.05	0,29
380	7,70	145	3,05	<0.5	<0.05	0,26
480	7,71	154	3,11	<0.5	<0.05	0,25
580	7,67	218	3,11	<0.5	<0.05	0,24
680	7,63	220	3,11	<0.5	<0.05	0,20
780	7,62	250	3,10	<0.5	<0.05	0,19
880	7,64	225	3,10	<0.5	<0.05	0,20

Table 41: Summary of measured chemical parameters on core GeoB14615 and their results.

Station :		GeoB 14615				
Core number:		GeoB 14615-1				
Depth/cm	**pH**	**Eh/mV**	**Alk_T/mmol L^{-1}**	**NH_4^+/mg L^{-1}**	**Fe^{2+} /mg L^{-1}**	**PO_4^{3-} /mg L^{-1}**
17	7,68	147	3,05	<0.5	<0.05	0,43
24	n.d.	129	n.d.	n.d.	n.d.	n.d.
28	n.d.	121	n.d.	n.d.	n.d.	n.d.
30	n.d.	90	n.d.	n.d.	n.d.	n.d.
32	n.d.	0	n.d.	n.d.	n.d.	n.d.
34	n.d.	-20	n.d.	n.d.	n.d.	n.d.
37	n.d.	-32	n.d.	n.d.	n.d.	n.d.
53	7,81	-74	3,06	<0.5	0,05	0,48
79	7,74	132	3,04	<0.5	<0.05	0,54
105	7,80	50	2,98	<0.5	<0.05	0,51
142	7,73	138	3,01	<0.5	<0.05	0,57
185	7,71	141	2,97	<0.5	<0.05	0,58
251	7,71	101	2,93	<0.5	<0.05	0,57
354	7,67	75	2,92	<0.5	<0.05	0,55
415	7,63	171	2,94	<0.5	<0.05	0,54
442	7,73	106	2,89	<0.5	<0.05	0,52
470	7,62	156	2,90	<0.5	<0.05	0,50
550	7,72	-55	2,93	<0.5	0,30	0,46
604	7,78	136	2,93	<0.5	<0.05	0,37
613	7,58	160	2,88	<0.5	<0.05	0,37
618	7,62	197	2,94	<0.5	<0.05	0,40
631	7,70	83	2,86	<0.5	<0.05	0,36
677	7,65	72	2,92	<0.5	<0.05	0,29

n.d. : not determined

Table 42: Summary of measured chemical parameters on core GeoB14616 and their results.

Station :		GeoB 14616				
Core number:		GeoB 14616-1				
Depth/cm	**pH**	**Eh/mV**	**Alk_T/mmol L^{-1}**	**NH_4^+/mg L^{-1}**	**Fe^{2+} /mg L^{-1}**	**PO_4^{3-} /mg L^{-1}**
15	7,74	73	3,07	<0.5	<0.05	0,47
40	7,90	27	3,05	<0.5	<0.05	0,50
105	7,75	172	3,03	<0.5	<0.05	0,55
186	7,74	150	2,98	<0.5	<0.05	0,58
259	7,72	159	3,00	<0.5	<0.05	0,56
326	7,67	144	2,88	<0.5	<0.05	0,51
397	7,60	182	2,89	<0.5	<0.05	0,48
407	7,74	127	2,89	<0.5	<0.05	0,47
485	7,72	63	2,86	<0.5	<0.05	0,44
544	7,77	-12	2,83	<0.5	<0.05	0,40
610	7,60	168	2,83	<0.5	<0.05	0,39
659	7,75	77	2,88	<0.5	<0.05	0,34
710	7,67	201	2,87	<0.5	<0.05	0,32

Table 43: Summary of measured chemical parameters on core GeoB14617 and their results.

Station :		GeoB 14617				
Core number:		GeoB 14617-1				
Depth/cm	**pH**	**Eh/mV**	**Alk_T/mmol L^{-1}**	**NH_4^+/mg L^{-1}**	**Fe^{2+} /mg L^{-1}**	**PO_4^{3-} /mg L^{-1}**
35	7,65	147	3,05	<0.5	<0.05	0,37
81	7,68	161	3,09	<0.5	<0.05	0,43
155	7,75	80	3,10	<0.5	<0.05	0,53
255	7,75	150	3,11	<0.5	<0.05	0,44
353	7,69	117	3,06	<0.5	<0.05	0,38
428	7,76	122	3,05	<0.5	<0.05	0,32
485	7,62	130	3,02	<0.5	<0.05	0,31
523	7,68	41	3,03	<0.5	<0.05	0,31
587	7,65	191	3,01	<0.5	<0.05	0,30
621	7,64	133	3,04	<0.5	<0.05	0,29
688	7,63	139	3,04	<0.5	<0.05	0,27
747	7,63	127	3,00	<0.5	<0.05	0,25
819	7,67	123	3,03	<0.5	<0.05	0,24
882	7,59	168	3,03	<0.5	<0.05	0,22

Table 44: Summary of measured chemical parameters on core GeoB14618 and their results.

Station :		GeoB 14618				
Core number:		GeoB 14618-1				
Depth/cm	**pH**	**Eh/mV**	**Alk_T/mmol L^{-1}**	**NH_4^+/mg L^{-1}**	**Fe^{2+} /mg L^{-1}**	**PO_4^{3-} /mg L^{-1}**
4	7,64	158	3,00	<0.5	<0.05	0,29
53	7,66	128	2,85	<0.5	<0.05	0,28
106	7,68	132	2,91	<0.5	<0.05	0,26
172	7,65	140	2,86	<0.5	<0.05	0,25
282	7,64	131	2,88	<0.5	<0.05	0,21

Table 45: Summary of measured chemical parameters on core GeoB14619 and their results.

Station :		GeoB 14619				
Core number:		GeoB 14619-1				
Depth/cm	**pH**	**Eh/mV**	**Alk_T/mmol L^{-1}**	**NH_4^+/mg L^{-1}**	**Fe^{2+} /mg L^{-1}**	**PO_4^{3-} /mg L^{-1}**
8	7,59	-168	2,90	<0.5	0,24	0,24
32	7,63	-88	2,85	<0.5	0,13	0,16
38	8,09	137	2,84	<0.5	0,16	0,20
46	7,70	-270	2,80	<0.5	0,12	0,16
83	7,60	-300	2,78	<0.5	<0.05	0,15
118	7,69	-262	2,79	<0.5	<0.05	0,15
145	7,69	-199	2,81	<0.5	0,07	0,15
151	7,88	139	2,80	<0.5	0,07	0,19
166	7,75	-283	2,77	<0.5	0,10	0,14
218	7,75	-300	2,77	<0.5	0,10	0,14
258	7,94	-265	2,76	<0.5	0,10	0,14
294	7,75	-262	2,76	<0.5	0,11	0,12
325	7,72	-254	2,74	<0.5	0,11	0,13
358	7,95	-239	2,73	<0.5	0,10	0,13
394	7,81	-219	2,73	<0.5	0,09	0,12
428	7,82	-207	2,73	<0.5	<0.05	0,14
467	7,82	-162	2,73	<0.5	0,08	0,13
531	7,88	-110	2,58	<0.5	<0.05	0,15
567	7,85	-87	2,72	<0.5	0,07	0,12
632	7,75	-58	2,69	<0.5	<0.05	0,13
657	7,86	-72	2,75	<0.5	<0.05	0,11
671	7,67	94	2,70	<0.5	<0.05	0,11
732	7,66	43	2,69	<0.5	<0.05	0,11

Table 46: Summary of measured chemical parameters on core GeoB14620 and their results.

Station :		GeoB 14620				
Core number:		GeoB 14620-1				
Depth/cm	**pH**	**Eh/mV**	**Alk_T/mmol L^{-1}**	**NH_4^+/mg L^{-1}**	**Fe^{2+} /mg L^{-1}**	**PO_4^{3-} /mg L^{-1}**
5	7,58	-77	3,05	<0.5	0,16	0,71
20	7,68	-140	3,10	<0.5	0,08	0,76
50	7,65	-117	3,26	<0.5	0,16	0,91
81	7,70	-160	3,34	0,69	0,19	0,90
114	7,71	-185	3,43	0,81	0,16	0,94
149	7,77	-198	3,50	0,95	0,14	0,92
181	7,73	-203	3,54	1,04	0,13	0,87
214	7,74	-256	3,54	1,09	0,13	0,84
249	7,84	-215	3,56	1,17	0,13	0,85
281	7,77	-238	3,57	1,26	0,15	0,81
314	7,74	-250	3,55	1,27	0,19	0,85
349	7,68	-271	3,41	1,36	0,22	0,57
381	7,81	-270	3,43	1,30	0,22	0,55
414	7,80	98	3,38	1,29	0,22	0,49
449	7,78	-141	3,38	1,24	0,22	0,47
481	7,75	-198	3,29	1,16	0,23	0,43
514	7,62	-247	3,31	1,11	0,23	0,42
549	7,69	-264	3,25	1,02	0,20	0,38
581	7,71	-260	3,27	0,97	0,14	0,33
614	7,88	-242	3,17	0,86	0,14	0,29
649	7,73	-215	3,15	0,70	0,14	0,23
681	7,66	-199	3,02	0,57	0,11	0,20
714	7,66	-208	3,01	<0.5	0,09	0,18
749	7,63	-115	2,88	<0.5	0,05	0,16

Table 47: Summary of measured chemical parameters on core GeoB14621 and their results.

Station :		GeoB 14621	
Core number:		GeoB 14621-1	
Depth/cm	**pH**	**Eh/mV**	**Alk_T/mmol L^{-1}**
20	7,68	-131	3,07
68	7,97	168	3,15
114	7,71	-154	3,09
164	7,66	-192	3,18
214	7,69	-212	3,20
264	7,60	-210	3,19
314	7,65	-236	3,23
364	7,59	-242	3,26
414	7,65	-272	3,31
464	7,65	-138	3,25
514	7,67	-266	3,36
564	7,62	-268	3,29
614	7,70	-266	3,32
664	7,69	-199	3,35
714	7,68	-210	3,31
764	7,80	-185	3,37
814	7,66	-162	3,38
864	7,63	-228	3,35

Table 48: Summary of measured chemical parameters on core GeoB14622 and their results.

Station :	GeoB 14622		
Core number:	GeoB 14622-1		
Depth/cm	**pH**	**Eh/mV**	**Alk_T/mmol L^{-1}**
16	7,54	-39	2,66
29	7,55	105	2,67
64	7,65	-112	2,65
114	7,63	-159	2,90
164	7,62	-175	2,94
214	7,62	-147	3,00
264	7,75	-91	2,87
314	7,75	-165	3,02
364	7,62	-91	3,03
414	7,62	-216	3,07
464	7,62	-221	3,13
514	7,74	-186	3,15
564	7,67	-213	3,12
614	7,69	-221	3,18
664	7,70	-198	3,18
714	7,95	-176	3,28
764	7,84	-135	3,08
814	7,87	-79	3,19
817	8,02	233	3,26

Table 49: Summary of measured chemical parameters on core GeoB14623 and their results.

Station :	GeoB 14623		
Core number:	GeoB 14623-1		
Depth/cm	**pH**	**Eh/mV**	**Alk_T/mmol L^{-1}**
4	7,59	-86	3,03
77	7,62	-156	3,04
127	7,66	-204	3,07
177	7,64	-174	3,06
227	7,65	-214	3,13
277	7,63	-185	3,11
327	7,69	-194	3,13
377	7,71	-207	3,12
427	7,69	-190	3,08
477	7,67	-205	3,13
527	7,80	-215	3,00
577	7,91	-165	3,09
627	7,70	-152	3,09
640	n.d.	n.d.	3,19
677	7,73	-136	3,05

n.d. : not determined

Table 50: Summary of measured chemical parameters on core GeoB14624 and their results.

Station :	GeoB 14624		
Core number:	GeoB 14624-1		
Depth/cm	**pH**	**Eh/mV**	**Alk_T/mmol L^{-1}**
44	7,67	-105	2,90
84	7,74	-185	2,83
117	7,75	-180	2,85
144	7,69	-205	2,85
194	7,68	-220	2,83
244	7,72	-140	2,81
294	7,95	-265	2,78
344	7,74	-315	2,78
394	7,73	-300	2,77
444	7,76	-333	2,78
494	7,69	-330	2,69
544	7,85	-335	2,82
594	7,77	-339	2,77
644	7,71	-328	2,73
694	7,74	-313	2,81
744	7,75	-274	2,79
794	7,75	-292	2,73
844	7,74	-303	2,80
894	7,84	-273	2,74
944	7,84	-232	2,75
994	7,87	-235	2,71
1024	7,84	-220	2,75

Table 51: Summary of measured chemical parameters on core GeoB14625 and their results.

Station :		GeoB 14625	
Core number:		GeoB 14625-1	
Depth/cm	**pH**	**Eh/mV**	**Alk_T/mmol L^{-1}**
30	7,56	-173	3,04
80	7,56	-165	3,14
108	7,69	152	3,16
130	7,76	-313	3,21
180	7,61	-305	3,17
230	7,69	-278	3,20
280	7,66	-290	3,16
330	7,70	-270	3,19
380	7,68	-298	3,06
430	7,72	-310	3,15
480	7,61	-310	3,14
530	7,61	-324	3,14
580	7,64	-239	3,10
630	7,74	-218	3,05
680	7,70	-221	3,08
730	7,79	-188	3,10
780	7,67	-75	3,04